MULTIPHASE FLOW OF OIL, WATER AND GAS IN HORIZONTAL PIPES

by

Andrew Robert William Hall

A thesis submitted in partial fulfillment of the requirements
for the degree of Doctor of Philosophy

Imperial College of Science, Technology and Medicine,
University of London

October 1992

THIS IS A BLANK PAGE

ABSTRACT

This thesis describes an experimental and theoretical study of the multiphase flow of two immiscible liquid phases (oil and water) and a gas phase. The experimental study has been carried out using a new high pressure multiphase flow facility. Known as WASP (Water, Air, Sand, Petroleum), this facility has a main test section of length 42 m and diameter 78 mm and can operate at pressures up to 50 bar. Experimental studies concentrated on the measurement of pressure gradient and holdup and the observation of flow patterns for flows of water, air and a light lubricating oil. These experiments have provided new data in an area for which there is little published work in the scientific literature.

The theoretical studies have been based on the concept of a three-fluid model of horizontal stratified three-phase flow, based on similar models for two-phase (gas-liquid) flow. This basic model was tested against a numerical solution of the steady-state momentum equations, making use of bipolar coordinate grids to match the geometry of a circular pipe with planar interfaces, for both laminar flows and turbulent flows (using a Prandtl-mixing length approach to give an effective turbulent viscosity). The stratified flow model has been tested against published experimental data for stratified three-phase flows and has been used as a basis for modelling the transition from stratified to intermittent flows. Combination with empirical correlations from the literature has allowed modelling of the separation of oil and water in three-phase slug flows. A simple model for three-phase slug flow has been developed from similar work for gas-liquid flows, taking into account the effect of the second liquid phase. Calculations of pressure gradient and holdup from this model were compared with experimental data.

Empirical correlations for pressure gradient in two-phase flows have been adapted for use in three-phase flows, by particularly considering the correct effective viscosity which should be used. Equations for the calculation of the viscosity of oil-water dispersions have been used and the results compared both with previously-published data and with new data from the experimental studies.

CONTENTS

ABSTRACT 3

LIST OF FIGURES 9

LIST OF TABLES 14

ACKNOWLEDGMENTS 15

CHAPTER 1 INTRODUCTION 17

CHAPTER 2 LITERATURE REVIEW 21

2.1 INTRODUCTION 21

2.2 EXPERIMENTAL STUDIES OF THREE-PHASE FLOWS IN PIPES 22

2.3 EXPERIMENTAL STUDIES OF OIL-WATER FLOWS IN PIPES 25

2.4 EMPIRICAL TOOLS FOR TWO-PHASE FLOW 27

2.4.1 Correlations for frictional pressure gradient 27

2.4.2 Flow pattern maps 29

2.4.3 Correlations for slug frequency 31

2.4.4 Rheology of liquid-liquid mixtures 32

2.5 ANALYTICAL STUDIES OF TWO-PHASE FLOWS 34

2.5.1 Pressure gradient and holdup 34

2.5.2 Stratified to slug flow transition 37

2.6 PRACTICAL EXAMPLES FROM THE OIL INDUSTRY 39

2.7 SUMMARY 40

CHAPTER 3 EMPIRICAL PRESSURE GRADIENT CALCULATION METHODS 43

3.1 INTRODUCTION 43

3.2 PRESSURE GRADIENT CALCULATION 44

3.2.1 Introduction 44

3.2.2 Calculation of frictional pressure gradient from homogeneous model 45

3.2.3 Calculation of frictional pressure gradient from the separated flow model 45

3.3 LIQUID MIXTURE VISCOSITY 46

3.3.1 Liquid mixture viscosity equations 46

3.3.2 Comparison of experimental data with Brinkman's equation 47

3.3.3 Inversion point 48

3.4 ANALYSIS OF EXPERIMENTAL DATA 50

3.4.1 Malinowsky 50

3.4.2 Laflin & Oglesby 52

3.4.3 Sobocinski 54

3.4.4 Stapelberg 56

3.5 ANALYSIS OF FIELD DATA 56

3.5.1 Fayed & Otten 56

3.5.2 UK National Multiphase Flow Database 57

3.6 SUMMARY 58

CHAPTER 4		**SIMPLE MODELS FOR STRATIFIED THREE-PHASE FLOW**	**61**
4.1		INTRODUCTION	61
4.2		SOLUTIONS FOR LAMINAR FLOWS BETWEEN FLAT PLATES	63
	4.2.1	Single phase flow	63
	4.2.2	Two-phase flow	66
	4.2.3	Three-phase flow	69
	4.2.4	Solution of systems of non-linear equations (Newton's method)	73
4.3		TAITEL & DUKLER TWO-FLUID MODEL FOR STRATIFIED GAS-LIQUID FLOW IN PIPES	74
4.4		TWO-FLUID MODEL FOR STRATIFIED OIL-WATER FLOW	75
4.5		THREE-FLUID MODEL OF STRATIFIED OIL-WATER-GAS FLOW IN PIPES	77
	4.5.1	Model derivation	77
	4.5.2	Model solution	80
4.6		COMPARISON WITH EXPERIMENTAL DATA FOR THREE-PHASE STRATIFIED FLOW	81
4.7		SUMMARY	83
CHAPTER 5		**NUMERICAL MODELLING OF STRATIFIED THREE-PHASE FLOW**	**85**
5.1		INTRODUCTION	85
5.2		MODELLING OF STRATIFIED TWO-PHASE FLOW	86
	5.2.1	Bipolar coordinate system	86
	5.2.2	Navier-Stokes equations	87
	5.2.3	Finite difference scheme	88
	5.2.4	Turbulence modelling	89
	5.2.5	Solution	91
5.3		CALCULATIONS FOR OIL-WATER FLOWS	91
	5.3.1	Comparison of models	91
	5.3.2	Experimental results from the WASP Facility	93
	5.3.3	Experimental results from Russell, Hodgson & Govier	94
	5.3.4	Experimental results from Stapelberg & Mewes	95
	5.3.5	Experimental results from Charles	97
5.4		MODELLING OF STRATIFIED THREE-PHASE FLOW	98
5.5		CALCULATIONS FOR OIL-WATER-GAS FLOWS	100
	5.5.1	Stapelberg & Mewes	100
	5.5.2	Sobocinski	101
	5.5.3	Nuland	102
5.6		SUMMARY	103

CHAPTER 6 FLOW PATTERN TRANSITIONS IN THREE-PHASE FLOW 105

6.1 INTRODUCTION 105

6.2 TRANSITION FROM STRATIFIED TO INTERMITTENT FLOW USING STEADY-STATE (KELVIN-HELMHOLTZ) THEORY 106

6.2.1 Kelvin-Helmholtz instability in a two-dimensional channel 106

6.2.2 Taitel & Dukler transition model for flow in a pipe 107

6.2.3 Taitel & Dukler transition model applied to oil-water-gas flow: separate oil and water layers 107

6.2.4 Taitel & Dukler transition model applied to oil-water-gas flow: dispersed oil and water layers 109

6.3 TRANSITION FROM STRATIFIED TO INTERMITTENT FLOW USING LINEAR STABILITY THEORY: TWO-DIMENSIONAL CHANNELS 110

6.3.1 Conditions for neutral stability for a turbulent-turbulent gas-liquid flow in a two–dimensional channel 110

6.3.2 Conditions for neutral stability for turbulent-gas laminar-liquid flow in a two-dimensional channel 113

6.3.3 Reduction to the Kelvin-Helmholtz instability 115

6.3.4 Application of two-phase linear stability analysis to three-phase flow in a two-dimensional channel 115

6.3.5 Comparison of two-dimensional models 118

6.4 TRANSITION FROM STRATIFIED TO INTERMITTENT FLOW USING LINEAR STABILITY THEORY: FLOWS IN PIPES 120

6.4.1 Conditions for neutral stability for a turbulent-turbulent gas-liquid flow in a pipe (Lin & Hanratty) 120

6.4.2 Application of Lin & Hanratty two-phase analysis to three-phase flow in a pipe 124

6.4.3 Reduction of three-phase flow equations to two-phase flow equations for zero water flow 129

6.4.4 Comparison of models 129

6.4.5 Comparisons with experimental data 130

6.5 SEPARATION OF WATER PHASE IN THREE-PHASE PIPE FLOWS 131

6.6 OIL-WATER INTERFACE MIXING (TRANSITION FROM STRATIFIED TO WAVY FLOW) 134

6.7 SUMMARY 136

CHAPTER 7 SIMPLE MODELS FOR THREE-PHASE SLUG FLOWS 137

7.1 INTRODUCTION 137

7.2 DUKLER & HUBBARD MODEL FOR TWO-PHASE SLUG FLOWS 137

7.3 MODIFICATIONS FOR THREE-PHASE FLOWS 140

7.3.1 Acceleration zone 140

7.3.2 Slug body 142

7.3.3 Film region 143

7.4 SUMMARY 144

CHAPTER 8 HIGH PRESSURE MULTIPHASE FLOW FACILITY 145

8.1 DESCRIPTION OF WASP FACILITY 145

8.1.1 History 145

8.1.2 Layout and design 146

8.2		CONTROL & INSTRUMENTATION	147
	8.2.1	Control system	147
	8.2.2	Flow metering	148
	8.2.3	Pressure drop measurement	149
	8.2.4	Liquid tank levels	149
	8.2.5	Flow visualisation	150
	8.2.6	Holdup measurement	150
8.3		OIL SELECTION	151
	8.3.1	Flammability properties	152
	8.3.2	Health and environment	153
	8.3.3	Physical properties	153
	8.3.4	Practical features	153
	8.3.5	Summary	154
8.4		OIL PROPERTIES	154
	8.4.1	Separation from water	154
	8.4.2	Viscosity	154
	8.4.3	Density	155
	8.4.4	Growth of micro-organisms	155
CHAPTER 9		**EXPERIMENTAL INVESTIGATION OF THREE-PHASE OIL-WATER-GAS FLOWS**	**157**
9.1		EXPERIMENTAL PROGRAMME	157
9.2		RESULTS	158
	9.2.1	Pressure gradient	158
	9.2.2	Holdup	161
	9.2.3	Flow visualisation	164
9.3		SUMMARY	167
CHAPTER 10		**CONCLUSIONS**	**169**
10.1		CONCLUSIONS	169
	10.1.1	Pressure gradient correlations	169
	10.1.2	Multi-fluid stratified flow models	169
	10.1.3	Numerical stratified flow models	170
	10.1.4	Flow pattern transitions in three-phase flows	170
	10.1.5	Simple models for three-phase slug flows	171
	10.1.6	Experimental studies of three-phase flows	171
10.2		RECOMMENDATIONS FOR FURTHER WORK	171
	10.2.1	Further analysis	171
	10.2.2	Further experimental data	171
REFERENCES			**173**

NOMENCLATURE 179

FIGURES 183

APPENDIX A SUMMARY OF PRESSURE GRADIENT CORRELATION EQUATIONS 245

A.1 Common Calculations 245
A.2 McAdams-Homogeneous 245
A.3 Schlichting 246
A.4 Friedel 247
A.5 Lockhart & Martinelli 248
A.6 Beggs & Brill 249
A.7 Dukler 252
A.8 Theissing 253

APPENDIX B FINITE DIFFERENCE SOLUTION FOR STRATIFIED TWO-PHASE FLOW USING BIPOLAR COORDINATES 255

B.1 Finite difference equations for the upper phase 255
B.2 Listing of the source code for the bipolar solution 256

APPENDIX C TABLES OF EXPERIMENTAL DATA POINTS 269

APPENDIX D WASP EXPERIMENTAL DATA POINTS (THREE-PHASE FLOW) 273

LIST OF FIGURES

Figure 2.1 Guzhov oil-water flow pattern map 185

Figure 2.2 Guzhov pressure gradient in oil-water flow 185

Figure 2.3 Flow pattern map for oil-water equal density flow 186

Figure 2.4 Charles & Lilleleht pressure gradient correlation for oil-water flow 186

Figure 2.5 Schneider gas-liquid flow pattern map 187

Figure 2.6 Baker gas-liquid flow pattern map 187

Figure 2.7 Mandhane gas-liquid flow pattern map 188

Figure 2.8 Taitel & Dukler gas-liquid flow pattern map 188

Figure 2.9 Arirachakaran oil-water flow pattern map 189

Figure 2.10 Stapelberg & Mewes oil-water flow pattern map 189

Figure 2.11 Thistle Field production profile 190

Figure 2.12 North West Hutton Field production 190

Figure 3.1 Pseudo liquid viscosity by Malinowsky back-calculation 191

Figure 3.2 Comparison of Woelflin data with Brinkman equation 191

Figure 3.3 Analysis of Malinowsky data with Beggs & Brill correlation: comparison of ϕ_{inv} 192

Figure 3.4 Analysis of Malinowsky data with Beggs & Brill correlation: comparison of viscosity calculations 192

Figure 3.5 Analysis of Malinowsky data with Beggs & Brill correlation: comparison of k 193

Figure 3.6 Analysis of Malinowsky data: comparison of correlations using Brinkman equation ($k = 2.5$, $\phi_{inv} = 0.46$) 193

Figure 3.7 Analysis of Malinowsky data: comparison of correlations using Brinkman equation ($k = 2.5$, $\phi_{inv} = 0.46$) 194

Figure 3.8 Analysis of Laflin & Oglesby data with Beggs & Brill correlation: comparison of ϕ_{inv} 194

Figure 3.9 Analysis of Laflin & Oglesby data with Beggs & Brill correlation: comparison of viscosity calculations 195

Figure 3.10 Analysis of Laflin & Oglesby data with Beggs & Brill correlation: comparison of k 195

Figure 3.11 Analysis of Laflin & Oglesby data: comparison of correlations using Brinkman equation ($k = 2.5$, $\phi_{inv} = 0.46$) 196

Figure 3.12 Analysis of Laflin & Oglesby data: comparison of correlations using Brinkman equation ($k = 2.5$, $\phi_{inv} = 0.46$) 196

Figure 3.13 Analysis of Sobocinski data: linear viscosity 197

Figure 3.14 Analysis of Sobocinski data: location of inversion point 197

Figure 3.15 Comparison of Stapelberg data with Beggs & Brill correlation 198

Figure 3.16 Comparison of measured pressure gradients with correlations for Fayed & Otten 12 and 16″ data 198

Figure 3.17 Pressure gradients for Fayed & Otten 6″ data 199

Figure 4.1 Solution for lower phase height in laminar-laminar flow between flat plates200

Figure 4.2 Dependence of the liquid height on Martinelli parameter for two-phase turbulent-turbulent stratified flow 200

Figure 4.3 Gas-liquid flow between flat plates: comparison of exact solution with two-fluid model 201

Figure 4.4 Oil-water flow between flat plates: comparison of exact solution with two-fluid model 201

Figure 4.5 Gas-liquid flow in a pipe: comparison of exact solution with two-fluid model202

Figure 4.6 Oil-water flow in a pipe: comparison of exact solution with two-fluid model202

Figure 4.7 Comparison water layer height with three-fluid model for Sobocinski stratified and ripple data 203

Figure 4.8 Comparison of oil layer height with three-fluid model for Sobocinski stratified and ripple data 203

Figure 4.9 Comparison of liquid layer heights with three-fluid model for Stapelberg stratified flow data 204

Figure 5.1 Pressure gradient calculation (WASP) 205

Figure 5.2 Holdup calculation (WASP) 205

Figure 5.3 Oil shear stress calculation (WASP) 206

Figure 5.4 Water shear stress calculation (WASP) 206

Figure 5.5 Interfacial shear stress calculation (WASP) 207

Figure 5.6 Comparison of WASP oil-water pressure gradient with models (Oil superficial velocity 0.15 m/s) 207

Figure 5.7 Comparison of WASP oil-water pressure gradient with models (Oil superficial velocity 0.26 m/s) 208

Figure 5.8 Comparison of WASP oil-water pressure gradient with models (Oil superficial velocity 0.55 m/s) 208

Figure 5.9 Comparison of WASP oil-water pressure gradient with models (Oil superficial velocity 0.87 m/s) 209

Figure 5.10 Comparison of WASP oil-water holdup ratio with models (Oil superficial velocity 0.15 m/s) 209

Figure 5.11 Comparison of WASP oil-water holdup ratio with models (Oil superficial velocity 0.26 m/s) 210

Figure 5.12 Comparison of WASP oil-water holdup ratio with models (Oil superficial velocity 0.55 m/s) 210
Figure 5.13 Pressure gradient calculation (Russell) 211
Figure 5.14 Holdup calculation (Russell) 211
Figure 5.15 Water shear stress calculation (Russell) 212
Figure 5.16 Oil shear stress calculation (Russell) 212
Figure 5.17 Interfacial shear stress calculation (Russell) 213
Figure 5.18 Pressure gradient calculation (Stapelberg) 213
Figure 5.19 Pressure gradient calculation (Charles 1.04″ line) 214
Figure 5.20 Pressure gradient calculation (Charles 2.45″ line) 214
Figure 5.21 Bipolar-rectangular-bipolar coordinate grid for three-phase stratified flow 215
Figure 5.22 Numerical calculation of Stapelberg & Mewes laminar three-phase flow 215
Figure 5.23 Comparison of Sobocinski measured oil height with numerical solution 216
Figure 5.24 Comparison of Sobocinski measured water height with numerical solution 216
Figure 5.25 Comparison of Sobocinski measured three-phase holdup with numerical solution 217
Figure 5.26 Comparison of Sobocinski measured three-phase pressure gradient with numerical solution 217
Figure 5.27 Three-phase holdup prediction (Nuland et al) 218
Figure 5.28 Three-phase holdup prediction (Nuland et al) 218
Figure 6.1 Stratified-intermittent transition (Separate oil and water layers) 219
Figure 6.2 Stratified-intermittent transition (Dispersed oil and water phases) 219
Figure 6.3 Calculated transition lines for Lin & Hanratty test cases 220
Figure 6.4 Transition lines presented by Lin & Hanratty 220
Figure 6.5 Comparison of Taitel & Dukler correction with inviscid Kelvin-Helmholtz theory 221
Figure 6.6 Predicted transition line for three-phase flow in a channel, compared with two-phase transitions 221
Figure 6.7 Effect of varying water fraction on predicted transition for three-phase channel flow 222
Figure 6.8 Three-phase stratified-intermittent flow transition (flow in a pipe: 30% and 50% water) 222
Figure 6.9 Three-phase stratified-intermittent flow transition (flow in a pipe: 30% and 70% water) 223
Figure 6.10 Comparison of Sobocinski data with transition prediction 223
Figure 6.11 Comparison of Stapelberg data with transition prediction 224

Figure 6.12 Prediction of water separation 224

Figure 6.13 Oil-water-gas interfacial stability (Oil-gas interface) 225

Figure 6.14 Oil-water-gas interfacial stability (Oil-water interface) 225

Figure 7.1 Physical model for slug flow (Dukler & Hubbard) 226

Figure 8.1 Development of the WASP Consortium 227

Figure 8.2 Typical oil-water-gas flow conditions 227

Figure 8.3 Schematic diagram of the WASP facility 228

Figure 8.4 Overall view of the WASP facility 229

Figure 8.5 Mixer section and liquid storage tanks 229

Figure 8.6 WASP test section 231

Figure 8.7 Slug catcher and visualisation section 231

Figure 8.8 Drawing of the test section 233

Figure 8.9 Rise in upstream pressure due to actuation of quick-closing valves 234

Figure 8.10 Viscosity of clean and used Shell Tellus 22 oil (strain rate dependence) 234

Figure 8.11 Viscosity of clean and used Shell Tellus 22 oil (Temperature dependence) 235

Figure 9.1 Comparison of WASP three-phase flow pressure gradient with Beggs & Brill correlation: linear and Brinkman liquid viscosities 236

Figure 9.2 Comparison of WASP pressure gradient with Beggs & Brill correlation: two-phase and three-phase data 236

Figure 9.3 Error in WASP three-phase flow pressure gradient calculations vs oil fraction: linear and Brinkman liquid viscosities 237

Figure 9.4 WASP three-phase flow calculated/measured pressure gradient vs oil fraction: linear and Brinkman liquid viscosities 237

Figure 9.5 Effective liquid viscosity in WASP three-phase flow: linear and Brinkman liquid viscosities 238

Figure 9.6 Comparison of correlations with WASP three-phase flow pressure gradient data: Beggs & Brill, McAdams, Schlichting and Dukler 238

Figure 9.7 Comparison of correlations with WASP three-phase flow pressure gradient data: Beggs & Brill, Friedel and Lockhart & Martinelli 239

Figure 9.8 Comparison of WASP pressure gradient data with slug flow model 239

Figure 9.9 Comparison of WASP pressure gradient data with slug flow model and Beggs & Brill correlation 240

Figure 9.10 Variation of WASP three-phase flow oil holdup measurements with input oil/water ratio 240

Figure 9.11 Variation of WASP three-phase flow water holdup measurements with input oil/water ratio 241

Figure 9.12 Comparison of WASP three-phase flow oil holdup measurements with slug flow model 241

Figure 9.13 Comparison of WASP three-phase flow water holdup measurements with slug flow model 242

Figure 9.14 WASP three-phase flow slug frequency data: slug frequency vs total liquid superficial velocity 242

Figure 9.15 WASP three-phase flow slug frequency data: comparison of measured frequencies with correlations 243

Figure 9.16 Prediction of water separation in WASP three-phase water-continuous flows243

Figure 9.17 Comparison of WASP three-phase water continuous separated slug flow data with transition prediction from linear stability theory 244

Figure 9.18 WASP three-phase flow slug transition prediction: comparison with slug frequency data 244

LIST OF TABLES

Table 3.1	Monson emulsion viscosity data	48
Table 3.2	Comparison of inversion point with equation (3.13)	49
Table 3.3	UKNMFD three-phase flow points	58
Table 4.1	Comparison of three-fluid model with Sobocinski stratified flow data	82
Table 4.2	Comparison of three-fluid model with Sobocinski ripple flow data	82
Table 4.3	Comparison of three-fluid model with Stapelberg stratified flow data	83
Table 5.1	WASP pipeline properties	92
Table 5.2	Russell experimental parameters	94
Table 5.3	Stapelberg experimental parameters	95
Table 5.4	Effect of moving the interface position on prediction of Stapelberg pressure gradient results	97
Table 5.5	Results of numerical calculations with Stapelberg three-phase data	101
Table 8.1	Factors influencing choice of oil	152
Table 9.1	Ranges of parameters in WASP three-phase experiments	157
Table 9.2	Errors in pressure gradient calculations from correlations using Brinkman viscosity	159
Table 9.3	Errors in pressure gradient calculations using the Beggs & Brill correlation	159
Table 9.4	Errors in pressure gradient calculations using the adapted Dukler & Hubbard slug flow model	161
Table 9.5	Errors in slug frequency calculations	166
Table C.1	Sobocinski (University of Oklahoma, 1955)	269
Table C.2	Stapelberg (University of Hannover, 1991)	270
Table D.1	WASP measured quantities	274
Table D.2	WASP physical properties	278
Table D.3	WASP holdup measurements	282
Table D.4	Stratified flow equilibrium holdup and slug frequency	283
Table D.5	Stratified-slug transition boundaries	286
Table D.6	Pressure gradient calculations (linear liquid viscosity)	287
Table D.7	Pressure gradient calculations (Brinkman liquid viscosity)	294

ACKNOWLEDGMENTS

I must open by thanking my supervisor, Professor Geoff Hewitt, without whom this work would not have been possible. He introduced to me the subject of multiphase flow with his unique interest and enthusiasm. Ideas, solutions and good advice never ceased to be forthcoming throughout the past three years. To all his present and future students — you are very fortunate.

This work would also not have been possible without the financial support of the UKAEA through AEA Petroleum Services. I am therefore particularly grateful to Dr Lawrence Daniels and Stephen Davies at Harwell for enabling this support to continue, but also many others who have helped in many ways with this work.

At Imperial College, Dr Alcina Mendes-Tatsis has been a tower of strength, for both practical and pastoral assistance. Sid Fisher has been a great help in the experimental programme, as manager of the WASP facility in recent months. The Mechanical Workshops, under Bob King and the Electrical Workshops under Malcolm Dix showed flexibility and understanding in getting the work done. There are many others, too numerous to list, each of whom played their part, and whose help is gratefully remembered.

For advice and help with some of the analytical work I must thank Dr Sreenivas Jayanti, and for experimental work of their own, Professor Dick Lahey and Dr Heinrich Stapelberg.

For good friendship, Daren Austin, Tim and Vicky Lockett cannot be thanked enough, and I wish you the best of everything in the future.

And finally to my mother and father, for all they have done for me, to whom this work is dedicated.

Libera animas omnium fidelium defunctorum de pœnis inferni et de profundo lacu, de morte transire ad vitam.
Requiem æternam dona eis Domine: et lux perpetua luceat eis.

Chapter 1:
INTRODUCTION

This thesis describes a study of the three-phase flow of a gas phase and two immiscible liquid phases in a horizontal pipe. Despite the great economic importance of this topic in the petroleum industry and the extensive study of multiphase flows over the last few decades, there is little published work on three-phase flows. Most of the work has taken the form of experimental studies, with only very rudimentary analytical treatment. The description of three-phase flows is complex, due to the uncertainty in predicting the form of both the gas-liquid and oil-water interfaces and the coupling between them. The work described here may be considered as progressing the basic foundations of the subject of three-phase flow, opening up new avenues which may be explored by future workers.

Three-phase oil-water-gas flows occur in the petroleum recovery industry, since reservoirs of oil and gas almost invariably contain water. Also, as the natural pressure of an oil reservoir decreases with production, water is often injected to boost the pressure. Due to the greater mobility of the water than the oil through the pores of the rock, water is usually found to enter the production wells soon after injection starts. The resulting three-phase mixture may then be required to flow vertically up to a platform, or horizontally along a sub-sea pipeline for transport to central processing facilities. This latter situation is of increasingly common occurrence in North Sea fields where satellite fields are developed around existing production platforms as a way of boosting production from declining fields.

Many features of three-phase flows are important in the design of pipelines and ultimately in the economic operation of mature oil fields, and highlight the growing interest in the subject. In inclined and vertical pipes, the holdup of each phase has an important influence on the hydrostatic component of the pressure gradient and hence the possible production rate. The flow pattern, in particular the distribution of the two liquid phases, has a strong influence on the frictional pressure gradient and on the possible corrosion of the pipeline. Intermittent flows can lead to large fluctuations in pressure and volumetric throughput of liquid, which must be accommodated in the

design; the prediction of the region of intermittent flow is therefore of key importance. The flow history of the fluids along a pipeline may also influence the separation of the oil and water phases; clearly with the limited space available on an offshore platform, this can have an important bearing on the economics of a project.

There are other consequences of the presence of water in an oil recovery system which are due to chemical and temperature factors. Two examples are the formation of highly corrosive hydrogen sulphide due to the interaction of sulphur-reducing bacteria in sea water and the sulphur present in the hydrocarbon reservoir, and the formation of waxy 'hydrates' from the interaction between low molecular weight hydrocarbons and water as the temperature falls. While these subjects are not covered here, the hydrodynamics of the flow may have an important influence on the design of systems to avoid these problems.

The objective of this project has been to try to develop both simple correlations or design tools and more detailed and mechanistic models of processes. Extensive use has been made of a small number of studies of three-phase flow from the literature to provide experimental data, but there are shortcomings in this data. For this reason considerable time has been spent using the new High Pressure Multiphase Flow facility in the Department of Chemical Engineering at Imperial College to obtain new data for three-phase flow of oil, water and air. This data complements and extends the existing databank for three-phase flow and has formed a key support of the development of models for three-phase flows.

The structure of the thesis roughly follows the chronological order of the work, starting with a review of the literature on three-phase oil-water-gas flow and a short consideration of the literature on oil-water flow, with particular emphasis on pressure drop reduction. Empirical correlations for the calculation of frictional pressure gradient are then considered, with an examination of the methods for calculation of the correct effective liquid viscosity to modify existing two-phase correlations. A comparison is then made between these methods and the data points obtained from the literature.

The following chapter begins the presentation of the new analytical material, starting with simple models for stratified three-phase flow. Although the interfacial geometry is simple in this case, the interaction with the circular pipe geometry already makes the algebra complicated. Thus a solution is developed in stages, starting with that for one-dimensional laminar flows between flat plates, which provides insight into the relationship between the flow of and channel fraction occupied by the phases, and the shear stresses between them and the channel walls. An averaging method making use of equivalent diameters and friction factors is then used to describe both the one-dimensional and circular systems. These averaged solutions are compared with experimental oil and water holdup data for three-phase oil-water-air flow.

The analysis of stratified flow of two phases in a circular pipe is assisted greatly by the use of *bipolar* coordinates which describe the geometry of a plane intersecting a circle. For laminar flow of two phases, solutions may be obtained in terms of Fourier integrals, which may be easily evaluated numerically. For turbulent flow of either phase, a numerical solution of the Navier-Stokes equations using a finite difference grid is required, with the introduction of the uncertainties associated with turbulence models. For three-phase flow, the approach of using bipolar coordinates was maintained in the water and gas phases, but with the introduction of rectangular coordinates to fit the oil phase. The simplest model of turbulence, based on the concept of a mixing length, was used and comparisons made with the available stratified flow data and the averaging method mentioned earlier.

The next chapter describes the analysis of some of the possible flow pattern transitions which may occur in three-phase flows. The approach has been to try to extend existing methods for gas-liquid flows by taking into account the effects of the second liquid phase. The most important transition is that between the stratified and slug flow regimes which is considered first by adaptation of simple Kelvin-Helmholtz theory, and then by a more comprehensive stability analysis.

The final chapter describing modelling of three-phase flows is concerned with the slug flow regime. A relatively simple model for gas-liquid slug flow has been adapted for description of three-phase slug flow, principally by taking into account the changed

physical properties which arise from the addition of a second liquid phase. This model allows the calculation of pressure gradient and the average holdup (of oil and of water) in a flow where the oil and water form separate layers in the film region between slugs.

The next two chapters are concerned with the experimental investigation of three-phase flows. The design, operation and instrumentation of the High Pressure Multiphase Flow facility is described, together with details of the properties of the oil used in the experiments. Then the experimental results are described in detail and compared with the analytical methods presented in the earlier chapters.

In the final chapter the main conclusions of the preceding chapters are summarised, together with a discussion of possible future areas of work.

Chapter 2:
LITERATURE REVIEW

2.1 INTRODUCTION

The literature on multiphase flows has been reviewed during this study in order to collect experimental data and to consider methods for the analysis of multiphase flow phenomena. Experimental data from other workers is important for comparison with proposed models and to highlight deficiencies which may be addressed by new experiments. Methods of analysis of multiphase flows cover empirical correlations, numerical solutions of the hydrodynamic equations, averaging methods and detailed physical models of flow mechanisms which have been reviewed in order to provide the most appropriate tools for the analysis of three-phase flows.

In this review experimental studies of three-phase oil-water-gas flows in pipes are considered first, followed by a discussion of experimental investigations of oil-water flows, which provide useful insight into the interaction between the two liquid phases. Much of the data obtained from the oil-water flow experiments can be used in the development of analytical methods for three-phase flows.

A number of empirical tools have been drawn from the literature on two-phase gas-liquid and oil-water flows and used in the development of three-phase flow models. These include correlations for frictional pressure gradient, flow pattern maps, correlations for slug frequency and determination of the rheology of liquid-liquid mixtures.

In addition to empirically-based correlations and models, a number of analytical studies of two-phase flows have been used as foundations for developing three-phase flow analysis. These are primarily methods for evaluating pressure gradient and holdup in laminar-laminar flows, and methods for the study of instability leading to the transition between stratified and slug flows.

Finally, a number of examples have been drawn from the literature to illustrate the practical importance of some of the issues discussed here.

2.2 EXPERIMENTAL STUDIES OF THREE-PHASE FLOWS IN PIPES

The first published study of three-phase oil-water-air flow in a horizontal pipe was presented by Sobocinski & Huntington[1] and the tabulated data points may be found in the thesis by Sobocinski[2]. The experiments were conducted in a clear plastic tube of 3″ diameter using air, water and diesel oil with a viscosity of 3.8 mPas at 24°C. Pressure drop was measured using manometers, holdup using quick-closing valves, and using a transparent pipe meant that films could be taken of the flow patterns. Flows were generally in the stratified-smooth, stratified-wavy and semi-annular flow regimes, with a varying degree of mixing or even partial emulsification of the oil and water depending on the flowrates. Pressure drop was found to increase with the air velocity as expected, but showed a maximum at a water/oil mass ratio of about 4.0, corresponding to the transition from a dispersion of oil in water to a dispersion of water in oil. Holdup varied qualitatively as expected, with a lower *in-situ* ratio of oil to water than the input oil/water ratio in stratified flow, and almost equality of the *in-situ* and input oil/water ratios where the oil and water were dispersed. This work is significant as the only source of experimental data for three-phase stratified flows giving both pressure gradient and holdup, although the viscosity of the oil phase is only slightly greater than that of the water phase.

Studies from the University of Tulsa by Malinowsky[3] and by Laflin & Oglesby[4]considered dispersed flow of oil, water and air in a horizontal pipe. The test section of their facility was a transparent acrylic pipe of 1.5″ internal diameter. The oil was a diesel oil with a viscosity ranging from 3 mPas at 40°C to 8 mPas at 5°C. Some experiments were performed by Malinowsky on oil-water systems, where the flow pattern was categorised as separated or dispersed, and pressure gradient was measured. In a few cases the holdup was also measured, but the measurements were found to be unsatisfactory in most cases, including all the oil-water-air tests (due to the large fluctuations in measured holdup in slug flow) and the holdup data was consequently not recorded in the thesis. In all the three-phase tests the oil and water were dispersed, and the main focus of the study was on back-calculation of an effective viscosity by using the Beggs & Brill[5] correlation. This approach was continued by Laflin & Oglesby agreeing well with Malinowsky's work, showing the

large peak in effective viscosity in the region where the inversion from a dispersion of water in oil to a dispersion of oil in water occurs.

Two earlier studies also concerned dispersed flow of oil, water and gas, but in vertical oil wells. Data from the US Bureau of Mines and Phillips Petroleum Company was correlated by Poettmann[6] using a graphical approach. Much of the effort in this correlation was directed at the treatment of the PVT behaviour of the well fluids, which is very significant in a well where, due to the large hydrostatic pressure loss, the ratio of gas to liquid increases significantly both by increase in the volume of gas due to pressure decrease and by release of gas dissolved in the oil phase. Tek[7] correlated the multiphase friction factor for the same data in a much simpler way than Poettmann, but this work has little relevance to the subject of three-phase flows, since due to the high temperatures in the oil wells, the effect of the water phase on the properties of the mixture was likely to be small.

These older papers from the United States demonstrate that the presence of water in oil and gas production has been significant for many years, and this reflects the maturity of the oil fields in the region, since water is generally produced in increasing quantities as an oilfield ages. The same has been true of oilfields in the Soviet Union where gradual appearance of water in production from older fields had been observed. Guzhov[8] pointed out that while established methods for calculation of the pressure loss in multiphase flow pipelines took no account of any effect the water may have on the liquid viscosity, it was well known that in an emulsion of oil and water, the viscosity increased sharply at a water content above about 25%. However, it was recognised that properties of stable water-oil emulsions may not apply to the temporary emulsions formed in pipelines and with the presence of a gas phase. It was shown that the actual pressure loss could be much greater (by a factor of two or three times) than the pressure loss calculated ignoring the effect of the water phase, with a maximum corresponding to the point of inversion from water-continuous to oil-continuous flow.

Shakirov[9] described an experimental programme to investigate the effect of the addition of water to oil-gas flows. An experimental facility was built with a number

of horizontal pipes with diameters from 40 to 102 mm and a measurement section of length 75 m, and connected to the discharge line from an oil-gas well. Water was introduced at measured flowrates through an atomizer with 1 mm holes, giving water fractions between 0 and 70%, and always leading to water-in-oil emulsions in this facility. A correlation was developed for the frictional resistance coefficient in terms of the various parameters which could be varied. An emulsion viscosity was used to represent the combined viscosity of the two liquid phases.

The subject of three-phase oil-water-gas flow has become of increasing interest in the context of the North Sea oilfields, with the maturity of the fields and their increasing water production. An important feature of mature North Sea development is the operation of satellite wells which are 'tied back' to existing production platforms by means of subsea multiphase pipelines, which may be up to 20 km in length. The multiphase mixture, which may consist of oil, gas, water and sand is then separated at the platform for transmission of the oil and gas via the existing pipeline systems and disposal of the water and sand. A good understanding of flows of oil-water-gas mixtures in pipelines is of crucial importance in the economic design and operation of these systems.

Stapelberg *et al*[10] have studied the flow of gas, water and a white mineral oil of viscosity 31 mPas in a test loop with diameters of 23.8 mm and 59.0 mm. The flows were in the stratified and slug regimes and results were obtained for pressure gradient and slug characteristics (slug frequency, slug length, etc); some measurements were also reported of holdup and information given on flow visualisation. These experiments have provided new data and physical information and have demonstrated the inadequacy of current methods for calculation of pressure gradient, particularly in stratified three-phase flows.

Nuland *et al*[11] developed a dual-energy gamma densitometer for the measurement of holdup in three-phase flow. This was compared with the quick-closing valve method for measurement of holdup for a three-phase air/oil/water flow in a 32 mm internal diameter pipe; the oil viscosity in these experiments was 1.75 mPas at 20°C. Reasonable agreement was obtained between the phase fractions obtained using the

gamma densitometer and those using the quick-closing valves. In those cases where significant discrepancies occurred, the disagreement was due to the assumption of a stratified flow geometry for the calculation of holdup from the gamma densitometer readings, when the interfaces were in reality curved.

Açikgöz *et al*[12] investigated three-phase flows of air, water and mineral oil (viscosity 116.4 mPas at 25°C) in a pipe of 19 mm. The main objective of the experiments so far has been to observe and classify the flow patterns, which has been done in terms of the basic two-phase flow patterns together with a description of the nature of the liquid phase (oil- or water-continuous and separated or dispersed). The small pipe diameter may have a significant effect on the flow patterns in this system, and in particular the region of stratified flow was found to be very restricted.

2.3 EXPERIMENTAL STUDIES OF OIL-WATER FLOWS IN PIPES

The flow of two immiscible liquids, oil and water, is in itself an important subject. Water may be present in oil pipelines, either introduced deliberately to reduce frictional pressure gradient or produced with the oil as undesired emulsified water. In the analysis of three-phase oil-water-gas flows, the interaction between the two liquid phases may be as important as the interaction between the gas and liquid phases. Thus, a good understanding of the behaviour of oil-water systems is important.

One of the earliest studies of horizontal flow of oil and water was that of Russell *et al*[13]. The experiments were performed in a 20 mm pipe using a oil with a viscosity 20 times that of water, and covered a very wide range of oil and water superficial velocities. Flow patterns ranging from stratified to drop and 'mixed' flows were observed, and pressure gradient and holdup were measured, the latter using quick-closing valves. Only very limited analysis of the results was presented, but the data has been made available, and can therefore be analysed further.

A similar study was performed by Charles *et al*[14], but there was particular interest in these experiments in producing an oil-in-water concentric flow pattern, rather than stratified flow patterns. This was achieved by adding carbon tetrachloride to commercial oils in order to increase their density to match that of the water. Three oils were used with viscosities of 7.0, 18.8 and 72.7 times that of water, in a test line

with an internal diameter of 26.4 mm. As expected, the greatest pressure gradient reductions were observed where the oil flowed inside a water annulus. Holdup was also measured, but noting the difficulties that Russell *et al* had experienced in recovering the liquids from the test section, a system was designed where a 'pig', which closely fitted the internal surface of the pipe, could be introduced and forced through by air pressure, thus recovering all the liquid.

Guzhov *et al*[15] studied the flow of transformer oil and water in a 39.4 mm pipe. The purpose of the experiments was to examine emulsification during laminar-turbulent flow of oil and water, which was of interest in the flow from water-flooded oil wells. Unlike the experiments of Russell, Charles and co-workers described above, where water was considered in the context of deliberate addition in order to reduce the pressure gradient, this was an investigation of the effects of water produced with the oil and the problems it could lead to. Results were presented in the form of a flow pattern map and a graph of pressure drop, both in terms of mean velocity and the water fraction, as shown in Figures 2.1 and 2.2.

Stapelberg & Mewes[16] considered oil-water flow to be an important boundary condition in the study of three-phase flow. The viscosity ratio of the oil and water was 31, and experiments were conducted in tubes of 23.8 mm and 59 mm diameter. The flowrates were relatively small, and thus a much narrower range of flow patterns was covered than, for example, by Guzhov. The results for pressure gradient are interesting, showing both a reduction in pressure gradient when water is added to a pure oil flow and a further reduction corresponding to the transition from a stratified flow to a flow of oil drops in water.

A comprehensive study of oil-water flows was performed by Arirachakaran *et al*[17] who combined results from the work of Oglesby[18] in a 1.5″ test facility with that of Arirachakaran[19] in a 1″ test facility. This allowed the full range of flow patterns from separated to dispersed flows to be analysed over a range of oil viscosities. Calculation of pressure gradient was considered, together with the construction of flow pattern maps. In addition, the relationship between the water fraction required

for inversion from a continuous water phase to a continuous oil phase and the oil viscosity was considered.

The flow of oil inside a water annulus, which was considered by Charles *et al* was the subject of a study by Oliemans *et al*[20]. The oil used had a viscosity of 3000 mPas, while the densities of the oil and water were almost equal; to aid the establishment of an annular flow pattern, the water contained an additive which made the pipe wall oil-repellant. Observations were made in a transparent 5 cm diameter pipe, and a model using lubrication theory was derived to take into account the turbulence in the water phase, allowing excellent agreement with the experimental data. Considerable reduction was obtained in the pressure gradient (compared to the oil flowing alone) but this was less than the theoretical maximum derived for concentric laminar oil and water flow, due to the turbulence in the water phase and the effect of waves on the oil-water interface.

A further application of experimental studies of liquid-liquid systems is in the simulation of zero-gravity two-phase flow, for example by Fujii *et al*[21]. The flow of air and water at zero-gravity was simulated by experiments with water and silicone oil as the 'gas' and 'liquid' phases respectively. The densities of the liquids were equal, thereby eliminating the effect of gravity, while the ratio of viscosities was the same as that of air and water. Flow patterns observed in these experiments were therefore all axisymmetric, as illustrated by Figure 2.3.

2.4 EMPIRICAL TOOLS FOR TWO-PHASE FLOW

2.4.1 Correlations for frictional pressure gradient

One of the first and most widely used correlations for frictional pressure gradient in two-phase flow is that of Lockhart & Martinelli[22]. This correlation takes no account of flow pattern, except that slug flow is excluded, and has limited accuracy, but is redeemed by its simplicity. Essentially the two-phase frictional pressure gradient was related to the pressure gradient for one of the phases (which would result if it was flowing alone in the pipe) by a multiplier, ϕ_g or ϕ_ℓ:

$$-\frac{dp_F}{dz} - \frac{\tau_w S}{A} - \phi_g^2\left(\frac{dp_F}{dz}\right)_g - \phi_\ell^2\left(\frac{dp_F}{dz}\right)_\ell \qquad (2.1)$$

where the multipliers ϕ_g^2 and ϕ_ℓ^2 were given graphically as functions of the parameter:

$$X^2 = \left(\frac{dp_F}{dz}\right)_\ell \div \left(\frac{dp_F}{dz}\right)_g \tag{2.2}$$

which is commonly referred to as the 'Lockhart-Martinelli' parameter. The multipliers were related to X by Chisholm[23] by the following equations, which, while simple in form, where found to fit the original correlation extremely well:

$$\phi_\ell^2 = 1 + \frac{C}{X} + \frac{1}{X^2} \tag{2.3}$$

and

$$\phi_g^2 = 1 + CX + X^2 \tag{2.4}$$

where C is a dimensionless parameter, dependent on the nature (turbulent or laminar) of the gas and liquid phases. For the most common situation where both phases are turbulent, $C = 20$.

Schlichting[24] modified the Lockhart-Martinelli correlation for oil-water-gas flows, particularly where the oil viscosity was very high (10 to 6000 mPas) in the form:

$$\phi_\ell^2 - C_1 + \frac{C_2}{X} \tag{2.5}$$

where

$$C_1 = \frac{1 + 0.65\left(\frac{\mu_\ell}{\mu_g} \times 10^4\right)^{0.8}}{(1 - \varepsilon_{fw})} \tag{2.6}$$

and

$$C_2 = 6.0 + 7.5\left(\frac{\mu_\ell}{\mu_g} \times 10^4\right)^{0.5} \tag{2.7}$$

However, despite the title of the paper, it would appear that this correlation is intended for dispersed three-phase flows, where mixture properties are used to characterise the combined oil and water phases. The data from which the correlation was derived is not given in the paper, and the correlation would appear to be of relatively little general application.

A similar analysis to that of Lockhart & Martinelli was performed by Charles & Lilleleht[25] for pressure gradient in oil-water flows in a variety of geometries, in terms of the parameters:

$$\phi_\ell^2 = \left(\frac{dp_F}{dz}\right)_{tp} \div \left(\frac{dp_F}{dz}\right)_w \tag{2.8}$$

and

$$X^2 = \left(\frac{dp_F}{dz}\right)_o \div \left(\frac{dp_F}{dz}\right)_w \tag{2.9}$$

All the data fell onto one single line, of similar form to the Lockhart-Martinelli curve, but considerably displaced from it, as shown in Figure 2.4. Theissing[26], by considering the density and viscosity of the two fluids in the Lockhart-Martinelli and Charles-Lilleleht correlations, produced a more general correlation, claimed to be valid for any combination of two fluids.

By comparison with a data bank of 25000 data points, Friedel[27] produced a general correlation for the parameter ϕ_{lo}^2 which is the ratio of the two-phase frictional pressure gradient to the pressure gradient which would result if the whole mass flow of the two-phase mixture were liquid. This has been a more successful correlating parameter than ϕ_l^2 and a widely-used correlation was also proposed by Chisholm[28]. However, all these correlations generally give poor predictions when compared to a wide range of data, and this seems to be particularly so for horizontal flows.

Some correlations for pressure gradient try to take into account the flow pattern in the pipe. The most notable example of this is the correlation of Beggs & Brill[5] which divides the commonly identified flow patterns in horizontal two-phase flow into three categories, namely:

1.	**Segregated**	Stratified, Wavy and Annular flows
2.	**Intermittent**	Plug and Slug flows
3.	**Dispersed**	Bubble and Mist flows

These flow categories are then used to calculated the liquid holdup, which is combined with a two-phase friction factor to give an overall frictional pressure gradient. The correlation was extensively tested against data for horizontal and inclined pipes for many flow conditions.

2.4.2 Flow pattern maps

Flow pattern maps have long been used in the study of multiphase flows to present the regions of different flow regimes and the transitions between them. One of the earliest was published by Schneider *et al*[29] for the flow of kerosene and natural gas

in horizontal pipes, as shown in Figure 2.5. This map was drawn in terms of the gas and liquid flowrates, and no account was taken of the fluid properties. Baker[30] produced a map showing similar regions, but plotted in terms of the gas mass velocity divided by λ and the liquid/gas ratio multiplied by $\lambda\psi$, where:

$$\lambda = \left[\left(\frac{\rho_g}{\rho_a}\right)\left(\frac{\rho_\ell}{\rho_w}\right)\right]^{\frac{1}{2}} \tag{2.10}$$

and

$$\psi = \left(\frac{\sigma_w}{\sigma}\right)\left[\frac{\mu_\ell}{\mu_w}\left(\frac{\rho_w}{\rho_\ell}\right)^2\right]^{\frac{1}{3}} \tag{2.11}$$

This map is shown in Figure 2.6. A thorough study was performed of flow patterns by Mandhane *et al*[31] using a large data bank of flow pattern observations. This resulted in the map in Figure 2.7, which is plotted in terms of gas and liquid superficial velocities. Perhaps the most useful study, however, was that of Taitel & Dukler[32]. This was a series of theoretical models for the main flow regime transitions, with some empirical adjustments. The basis of the models was a one-dimensional stratified flow model to give the equilibrium liquid height from which the flow pattern transitions were developed. The flow map was plotted in terms of dimensionless parameters, as shown in Figure 2.8. Different physical properties, pipe inclination and pipe diameter can in principle be accommodated by this method, but it should be noted that the empirical correction factors were largely determined from air-water flows at low pressures in small diameter pipes.

There has been much less study of the flow patterns in oil-water systems, and in general the number of possible flow regimes is greater. Guzhov *et al*[15] studied the flow of a transformer oil and water in a 39.4 mm diameter pipe. The viscosity of the oil was about 23 times that of the water. Eight flow regimes were identified, as shown in Figure 2.1. Arirachakaran *et al*[17] collected a large number of experimental observations from various sources, and arrived at the following five flow pattern categories:

1.	**Stratified**	(S)	Possibly with some mixing at the interface
2.	**Mixed**	(MO, MW)	With separated layers of a dispersion and a "free" phase
3.	**Annular**	(AO,AW)	Core of one phase within the other phase
4.	**Intermittent**	(IO,IW)	Phases alternately occupying the pipe as a free phase or as a dispersion
5.	**Dispersed**	(DO,DW)	Homogeneous mixture

The second letter of the abbreviations (O or W) refers to the *continuous* or predominantly continuous phase. The flow pattern maps were found to depend on the physical properties, particularly the oil viscosity, and Figure 2.9 shows the flow pattern map for an oil viscosity of 84 mPas at 21°C

Stapelberg & Mewes[16] presented a few results for flow of an oil of viscosity 31 mPas and water in pipes of 23.8 and 59 mm diameter. These results are shown in Figure 2.10 and cover just the S, MO and MW regions described above.

Unlike gas-liquid flows, there has been no attempt to produce a generalised method for predicting flow patterns in oil-water flows. The flow patterns in any particular liquid-liquid system are very strongly dependent on the physical properties of the two liquids, and some flow patterns which occur in one system may not appear at all in another — particularly the annular and intermittent flows.

2.4.3 Correlations for slug frequency

The frequencies of liquid slugs in gas-liquid slug flow were measured by Gregory & Scott[33] for the system of carbon dioxide and water flowing in a 0.75″ pipe. Noticing that there was a minimum in the slug frequency at a slug velocity of about 6 m/s, the data was correlated by assuming a velocity dependence of the form:

$$\omega = \frac{A}{U_s} + BU_s + C \tag{2.12}$$

leading finally to the equation:

$$\omega - 0.0226\left[\frac{U_\ell}{gD}\left(\frac{19.75}{u_{ns}} + u_{ns}\right)\right]^{1.2} \tag{2.13}$$

where u_{ns} is defined as the no-slip velocity, which is the sum of the gas and liquid superficial velocities. This correlation, however, does not take into account the physical properties of the fluids in the system.

A more recent correlation, recommended by Stapelberg *et al*[10] for use in three-phase flow systems is that by Tronconi[34]. It was assumed that the slug frequency is half of the frequency of the unstable wave precursors to slugs, as determined by analysis of finite amplitude waves in conduits. This led to the equation for slug frequency:

$$\omega - 0.61\frac{\rho_g}{\rho_\ell}\frac{u_g}{h_g} \tag{2.14}$$

Stapelberg found that better correlation was obtained with three-phase flow data by assuming a correction factor of one quarter rather that one half, giving a coefficient of 0.305 in the above equation. It should be noted, however, that very accurate correlation of slug frequencies is generally not possible, due to the large variations in measured values of slug frequency.

2.4.4 Rheology of liquid-liquid mixtures

A distinction must first be drawn between *mixtures* of liquids, for example alcohol and water and *dispersions* of one liquid in another, for example oil and water. A lot of error has been introduced into methods of calculating frictional pressure gradient in oil-water or oil-water-gas systems by attempting to use a mixture viscosity calculated as if the two liquids were miscible. The simplest such equation is a volume average:

$$\mu_{mix} = \phi\mu_A + (1-\phi)\mu_B \tag{2.15}$$

Other equations for the calculation of the viscosity of liquid-liquid mixtures were given by Bingham[35]:

$$\mu_{mix} = \left[\frac{\phi}{\mu_A} + \frac{(1-\phi)}{\mu_B}\right]^{-1} \tag{2.16}$$

and by Arrhenius[36]:

$$\mu_{mix} = \mu_A^{\phi}\mu_B^{1-\phi} \tag{2.17}$$

where, in all three equations, ϕ is the volume fraction of component A. It should be readily apparent that these equations are not necessarily true for a dispersion of

one immiscible liquid within another, particularly noting that none of the equations predict a maximum in the mixture viscosity as a function of volume fraction.

Einstein[37] derived an equation to represent the viscosity increase for a *dilute* suspension of spherical solid particles ($\phi \lesssim 0.01$):

$$\mu_\phi = \mu_0(1 + k\phi) \tag{2.18}$$

where k was 2.5 for a suspension of solid particles in a liquid phase. Taylor[38] showed that for emulsions, the factor k would be given by:

$$k = 2.5\left(\frac{\mu_{\text{disp}} + 0.4\mu_{\text{cont}}}{\mu_{\text{disp}} + \mu_{\text{cont}}}\right) \tag{2.19}$$

which for a dispersion of a viscous oil in water gives k as virtually 2.5. Brinkman[39] assumed that adding one particle to a solution already containing n particles would increase the solution viscosity by the ratio given by Einstein's equation, and thus derived an integral expression which led to the final result:

$$\mu_{\text{mix}} = \frac{\mu_{\text{cont}}}{(1 - \phi)^k} \tag{2.20}$$

Richardson[41] obtained the expression:

$$\mu_{\text{mix}} = \mu_{\text{cont}} \exp(k\phi) \tag{2.21}$$

while Hatschek[42] gave:

$$\mu_{\text{mix}} = \frac{\mu_{\text{cont}}}{1 - \sqrt{\phi}} \tag{2.22}$$

for emulsions with a high volume fraction ($\phi > 0.50$) of the dispersed phase. Equations (2.20) to (2.22) were extensively compared with experimental measurements and were found to give similar results. In particular, the large viscosity of an emulsion around the point of 'inversion' is predicted by all three equations.

Viscosities of petroleum-in-water emulsions were measured by Monson[43] and Woelflin[44] and the values compare well with the above equations. Woelflin classified emulsions as *loose*, *medium* or *tight* according to the particle size of the dispersed phase. As might be expected, tight emulsions gave higher viscosities for the same volume fraction of dispersed phase than medium or loose emulsions. This behaviour can be accommodated in the Brinkman and Richardson equations by adjustment of the parameter k.

2.5 ANALYTICAL STUDIES OF TWO-PHASE FLOWS

2.5.1 Pressure gradient and holdup

Considerable insight into the behaviour of three-phase flows may be gained by consideration of the simplest flow configurations. Exact analyses are often possible for two-phase flows in simple geometries where the fluids are both in the laminar flow regime.

Russell & Charles[45] considered the flow of two immiscible liquids in two geometries, namely between flat plates and concentrically in a pipe, with a view to explaining the phenomenon of pressure gradient reduction which had been observed when water was injected into oil pipelines. Thus equations were developed to express the volumetric flowrates of each phase in terms of the pressure gradient and holdup, and by differentiation, the minimum pressure gradient for a given oil flowrate could be determined. For flow between flat plates, the maximum pressure gradient reduction factor, even for very viscous oils, was 3–4. For concentric flow, however, the maximum predicted pressure gradient reduction factor was given by:

$$\left(\frac{dp}{dz}\right)_{full} \div \left(\frac{dp}{dz}\right)_{min} - \frac{\mu_o^2}{(2\mu_o - \mu_w)\mu_w} \qquad (2.23)$$

and thus for very viscous oils, the pressure gradient reduction factor could be substantial. This was not observed in the experiments cited by Russell & Charles, presumably because, in the experiments, the water did not form a complete annulus around the oil phase.

Similar treatments to that by Russell & Charles can be found in the fluid mechanics textbooks by Bird, Stewart & Lightfoot[46] and Denn[47]. In the former, the solution was for a holdup equal to half the channel depth, while Denn derived a solution for the holdup of the water phase, $\tilde{h}$ (= h/H), in terms of the volumetric flowrates and viscosities of the two phases:

$$\frac{Q_w}{Q_o} = \left(\frac{\mu_o}{\mu_w}\right)\left[\frac{\tilde{h}^4\left(\frac{\mu_o}{\mu_w}\right) + \tilde{h}^2\left(3+\tilde{h}\right)\left(1-\tilde{h}\right)}{\tilde{h}\left(4-\tilde{h}\right)\left(1-\tilde{h}\right)^2\left(\frac{\mu_o}{\mu_w}\right) + \left(1-\tilde{h}\right)^2}\right] \qquad (2.24)$$

When a stratified flow in a circular pipe is considered, such straightforward derivations are not possible. An analytical solution for laminar flow of the two phases may be

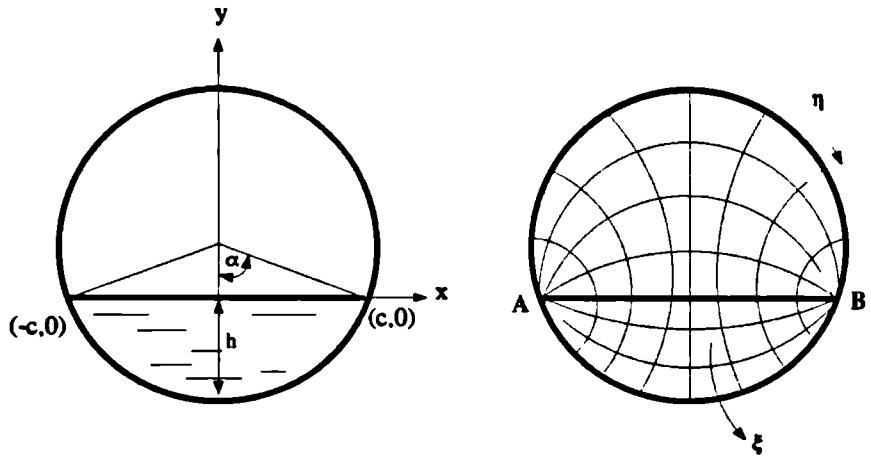
obtained if bipolar coordinates are employed. This coordinate system was discussed by Bateman[48] in the context of the classical problem of the effect of a mound or ditch on an electric potential.

In the geometry of the cross-section of a stratified two-phase pipe flow shown below, bipolar coordinates (ξ, η) are defined by:

$$x - \frac{\sin\alpha \sinh\xi}{\cosh\xi - \cos\eta} \tag{2.25}$$

and

$$y - \frac{\sin\alpha \sin\eta}{\cosh\xi - \cos\eta} \tag{2.26}$$



Such a coordinate system was used by Ranger & Davis[49] who by the use of Fourier cosine transforms were able to express the volumetric flow rate factor of oil (defined as the ratio of the volumetric flowrate of oil when the interface subtends an angle 2α at the centre of the pipe to the volumetric flowrate for oil filling the pipe) as follows:

$$V_o - \frac{Q_o(\alpha)}{Q_o(0)} - \frac{1}{\pi}\left(\pi - \alpha + \frac{2}{3}\sin 2\alpha + \frac{1}{12}\sin 4\alpha\right)$$
$$-16\sin^3\alpha \int_0^\infty \frac{k^2 \cosh k\alpha[k \sin\alpha \cosh k(\pi-\alpha) + \cos\alpha \sinh k(\pi-\alpha)]dk}{[\lambda \sinh k\pi + \sinh k(\pi - 2\alpha)]\sinh^2 k\pi} \tag{2.27}$$

where λ is defined by:

$$\lambda - \frac{\mu_o + \mu_w}{\mu_w - \mu_o} \tag{2.28}$$

and for oil filling the pipe with a pressure gradient (dp/dz):

$$Q_o(0) = \frac{\pi}{8\mu_o}\left(\frac{dp}{dz}\right) \tag{2.29}$$

The integral in equation (2.27) may be easily evaluated using Simpson's rule to any required precision, and thus this may be viewed as an exact solution for laminar-laminar stratified flow in a pipe. This solution is useful later in validating the numerical solution for stratified flow, but it is clear that the manipulation of the algebra is difficult, even for such relatively simple examples.

More complex situations were considered by Bentwich[50] for the cases with an eccentric circular interface and a circular arc-segment interface, confirming the above view that the algebra becomes extremely complicated.

Two early papers describing the application of numerical analyses to stratified laminar pipe flows using rectangular coordinates were those of Gemmell & Epstein[51] and Charles & Redberger[52]. Both the resolution of the computational grid and the convergence of the solutions were limited by the available computer power. Gemmell & Epstein performed calculations using a desk calculator, rejecting the alternative of using a contemporary digital computer because the storage capacity was too limited for direct matrix inversion, while the iterative scanning time was of the order of hours. Comparisons were made with the experimental data points of Russell *et al*[13] showing good agreement when the flow of both phases was laminar. Charles & Redberger concentrated on calculating velocity profiles and pressure gradient reduction factors for a range of oil/water viscosity ratios from 4 to 1500, showing that for stratified flow in a pipe, there is a maximum pressure gradient reduction factor of about 1.3. Greater reduction factors than this were observed for flows of crude oil and water in pipelines, for example by Charles[53], and must therefore have been caused by the water wetting a greater portion of the pipe walls than would be the case with a flat interface.

With the advent of more powerful computing resources, numerical solutions have been produced for stratified flows where both phases are turbulent. Shoham & Taitel[54] assumed that the gas phase could be treated as a uniform flow in a closed

duct bounded by the pipe wall and the interface, and thus needed to provide a correlation for interfacial shear stress. The flow in the liquid phase was simulated using the Prandtl mixing length theory to calculate an effective turbulent viscosity, employing the bipolar coordinate system described above to fit the computational grid to the pipe walls and the interface. One particular feature predicted by Shoham & Taitel was regions of reverse flow in upward inclined stratified flow. This result was disputed by Issa[55] who solved for the velocity profiles in both the gas and the liquid phases, using a k-ϵ model for turbulence. Issa found much better agreement with the one-dimensional model of Taitel & Dukler[32] than with Shoham & Taitel, particularly at high values of Martinelli parameter. The treatment of the gas-liquid interface in such calculations remains an area of some difficulty.

2.5.2 Stratified to slug flow transition

As discussed in Section 2.4.2, a semi-theoretical flow pattern map was presented by Taitel & Dukler[32]. The basis of this method was a model for smooth, equilibrium stratified flow derived from the momentum balances for the two phases:

$$-A_\ell\left(\frac{dp}{dz}\right) - \tau_\ell S_\ell + \tau_i S_i + \rho_\ell A_\ell g \sin\theta - 0 \tag{2.30}$$

and

$$-A_g\left(\frac{dp}{dz}\right) - \tau_g S_g - \tau_i S_i + \rho_g A_g g \sin\theta - 0 \tag{2.31}$$

The pressure gradient was eliminated between the two equations and the shear stresses evaluated conventionally using friction factors. In calculating the friction factors, hydraulic diameters were used. The gas phase was assumed to be a closed-duct flow and so:

$$D_g = \frac{4A_g}{S_g + S_i} \tag{2.32}$$

while the liquid phase was assumed to be an open-channel flow:

$$D_\ell - \frac{4A_\ell}{S_\ell} \tag{2.33}$$

All lengths were non-dimensionalised by dividing by tube diameter, D (eg $\tilde{S}_g = S_g/D$), all areas by dividing by D^2 (eg $\tilde{A}_g - A_g/D^2$) and both velocities by

dividing by the superficial velocity (i.e $\tilde{u}_\ell = u_\ell/U_\ell$ and $\tilde{u}_g = u_g/U_g$). The interfacial friction factor was assumed equal to the gas phase friction factor, and the final relation from which the liquid height may be calculated becomes:

$$X^2\left[\left(\tilde{u}_\ell\tilde{D}_\ell\right)^{-n}\tilde{u}_\ell^2\frac{\tilde{S}_\ell}{\tilde{A}_\ell}\right] - \left[\left(\tilde{u}_g\tilde{D}_g\right)^{-m}\tilde{u}_g^2\left(\frac{\tilde{S}_g}{\tilde{A}_g} + \frac{\tilde{S}_i}{\tilde{A}_\ell} + \frac{\tilde{S}_i}{\tilde{A}_g}\right)\right] - 4Y = 0 \qquad (2.34)$$

where X^2 is the Martinelli parameter and Y is an inclination parameter:

$$Y = \frac{(\rho_\ell - \rho_g)g\sin\theta}{\left(\frac{dP}{dz}\right)_g} \qquad (2.35)$$

All the dimensionless quantities in equation (2.34) may be expressed in terms of the liquid height, $\tilde{h}_\ell$ thus allowing the value of $\tilde{h}_\ell$ to be calculated for any combination of X and Y.

The transition between stratified and slug flow was modelled by Taitel & Dukler by modification of the Kelvin-Helmholtz theory to apply to a finite wave on stratified liquid in an inclined pipe. The Kelvin-Helmholtz theory dictates that a wave of infinitesimal amplitude will grow when:

$$u_g > \left[\frac{g(\rho_\ell - \rho_g)h_g}{\rho_g}\right]^{\frac{1}{2}} \qquad (2.36)$$

Neglecting the motion of the wave, the criterion for growth of a finite wave is a balance between the Bernoulli effect (drop in pressure above the wave due to increased gas velocity) and the gravity effect of an increased liquid level, leading to the expression:

$$u_g > C_1\left[\frac{g(\rho_\ell - \rho_g)h_g}{\rho_g}\right]^{\frac{1}{2}} \qquad (2.37)$$

where

$$C_1 = \left[\frac{2}{\frac{h_g}{h_g'}\left(\frac{h_g}{h_g'} + 1\right)}\right]^{\frac{1}{2}} \qquad (2.38)$$

and clearly, a finite disturbance is less stable than an infinitesimal disturbance, as C_1 is always less than unity. For a finite wave in a round, inclined pipe, Taitel & Dukler showed that:

$$u_g > C_2\left[\frac{(\rho_\ell - \rho_g)g\cos\theta A_g}{\rho_g\frac{dA_\ell}{dh_\ell}}\right]^{\frac{1}{2}} \qquad (2.39)$$

where

$$C_2 \simeq \frac{A'_g}{A_g} \tag{2.40}$$

and argued qualitatively that C_2 could be estimated by:

$$C_2 = 1 - \tilde{h}_\ell \tag{2.41}$$

One of the most important features of the Taitel & Dukler analysis was the assumption that the motion of the waves could be neglected. Lin & Hanratty[56] disputed this approach, arguing that the omission of time-dependent (inertial) effects meant that shear stresses at the gas-liquid interface and the component of pressure out of phase with the wave height were not considered. Including the inertial effects caused the wave velocity to be greater than the average liquid velocity at neutral stability, instead of being equal to it, as would be the case for Kelvin-Helmholtz instability. The effect of inertial terms is destabilising, causing the instability (and hence transition to slug flow) to occur at a lower gas velocity than predicted by the inviscid stability analysis.

Lin & Hanratty point out that good agreement between Taitel & Dukler's predicted transition boundary and their own analysis (assuming a smooth interface) is evidence that the correction factor, C_2 can be interpreted as a correction for the destabilising effect of liquid inertia, for air-water flow.

2.6 PRACTICAL EXAMPLES FROM THE OIL INDUSTRY

A number of papers were found to give some background information on specific issues in the oil production industry. Brand[57] discussed the engineering challenges of the Thistle field, which is one of the major North Sea oilfields. Thistle started production in 1978, and because of rapid pressure decline in the reservoir, water injection was started in 1979. Very soon after, water started to be produced with the oil, and the proportion of water has steadily risen to nearly 90%, as shown by Figure 2.11. This example demonstrates the importance of being able to handle a large production of water, and the final economics of operating this field may well be constrained by the engineering difficulties, for example those associated with separating oil from the produced water to a sufficient degree to satisfy environmental

controls. Laing[58] discussed the North West Hutton field, also in the North sea, which has shown a similar production profile to Thistle, as shown in Figure 2.12.

The influence of water injection on the design of a pipeline for the transport of viscous crude was investigated by Leach[59]. A 92-mile line was required to transport a viscous crude oil from a field in southern Venezuela to a refinery and terminal on the northern coast. Various options were considered including heating, insulating and burying the line, injecting water to reduce frictional losses, or diluting the crude with a lighter oil. Some pilot experiments showed that by injecting water, the frictional pressure drop was substantially reduced, thus allowing a pipeline of much lower cost to be built, compared to all other methods. In the end, however, an unheated overground 30″ pipeline was built rather than a water-lubricated pipeline, due to concerns about the technology of water injection, particularly concerning the formation of emulsions.

Wicks & Fraser[60] were concerned with explaining the onset of corrosion of crude oil pipelines where water was known to be present. They conducted experiments using kerosene and dyed water and were able to correlate the formation of a settled water layer with the total liquid velocity. Comparisons were made with experimental results for pipeline where corrosion had been observed with good agreement. Further comparison was made between this method and observations of corrosion from Bahrain by Duncan[61].

2.7 SUMMARY

Useful experimental data for three-phase flows was found in works by Sobocinski, Malinowsky, Laflin & Oglesby and Stapelberg. These experimental projects covered a variety of flow patterns in facilities with small pipe diameters operating at around atmospheric pressure. A number of other studies provided useful background to the subject.

Two-phase oil-water studies have been more extensive and results have been published for pressure gradient, holdup and flow patterns in a variety of oil-water systems. Of particular interest are studies by Russell, Charles and co-workers.

Empirical methods for the calculation of frictional pressure gradient, flow pattern transitions, slug frequency and liquid-liquid mixture viscosity were discussed. These methods will be used in later chapters for further development of methods applicable to three-phase systems.

Finally, methods of predicting pressure gradient, holdup and stratified-intermittent flow transition by analytical methods were outlined. These form a basis for the work presented in Chapters 3, 4 and 5 in the development of a model for three-phase stratified flow and transition from stratified to intermittent flow.

THIS IS A BLANK PAGE

Chapter 3:
EMPIRICAL PRESSURE GRADIENT CALCULATION METHODS

3.1 INTRODUCTION

It is often found in the petroleum production industry that the water content of a petroleum well increases with the life of the well. It is therefore important to be able to predict the variation in the properties of the flow, not only as a function of the total gas and liquid flowrates, but also of the oil/water ratio in the liquid phase.

One of the most important parameters in the design of pipeline systems is the pressure gradient. Pipeline design requires a balance to be made between the cost of material thickness for pipeline fabrication, the driving pressure available at the pipeline inlet, the length of the pipeline and the required flowrate through the pipeline. The pressure gradient is strongly affected by the oil/water ratio: at constant total liquid volume flowrate, as the water fraction increases, the effective viscosity increases and therefore the frictional pressure gradient is increased. Once the water fraction reaches the *inversion point*, there is a dramatic drop in the effective viscosity (and hence the frictional pressure gradient) due to the change from the continuous phase being oil to it being water. There is a further slight drop in viscosity if the water fraction increases from this point, due to decreasing oil content of the dispersion.

This phenomenon will occur in flows where the oil and water phases are well-mixed. In slug flow, which is commonly observed in petroleum pipelines, the dominant component of the pressure gradient is from the motion of the liquid slugs, where the oil and water are likely to be well-mixed irrespective of the nature of the flow in the regions between slugs.

The pressure gradient correlations encountered in the literature make no attempt to model the observed effects of the water fraction on the pressure gradient. The most common suggestion for liquid viscosity is a volume average of the oil and water viscosities. This leads to large errors in the prediction of the pressure gradient around the inversion point. Malinowsky[3], using the Beggs & Brill[5] correlation, adjusted the viscosity so that the pressure gradient prediction was correct. A plot of the

pseudo-viscosity against water fraction demonstrates the viscosity changes described above, as shown in Figure 3.1.

Assuming well-mixed oil and water phases, a number of equations are available to predict the viscosity of the dispersion. Improved agreement can be obtained between calculated and measured pressure drop, by recalculating the pressure gradient correlations using these predictions of viscosity.

3.2 PRESSURE GRADIENT CALCULATION

3.2.1 Introduction

Two approaches are generally used to derive conservation equations for two-phase flows, namely the homogeneous model, where the gas and liquid are combined to form a mixture behaving as a homogeneous fluid, and the separated flow model, where the two fluids are considered separately and interact through the interfacial shear stress. The conservation equations are given by Hewitt[62]. For steady-state flow in a duct of constant cross-section, for homogeneous flow:

$$-\left(\frac{dp}{dz}\right) - \frac{\tau_w S}{A} + \frac{d(\dot{m}^2/\rho_H)}{dz} + g\rho_H \sin\theta \qquad (3.1)$$

and for separated flow:

$$-\left(\frac{dp}{dz}\right) = \frac{\tau_w S}{A} + \dot{m}^2 \frac{d}{dz}\left[\frac{(1-x)^2}{\rho_\ell(1-\varepsilon_g)} + \frac{x^2}{\rho_g \varepsilon_g}\right] + g\rho_{TP} \sin\theta \qquad (3.2)$$

In both these equations the three terms on the right hand side represent the frictional, accelerational and gravitational components of the pressure gradient. The gravitational component is clearly important in non-horizontal flows, and the accelerational component is significant in cases where the pressure drop is sufficient to cause a significant change in the gas density, where gas is dissolved in the oil phase and comes out of solution as the pressure drops or where there is a phase change due to heat transfer. In this work, attention is focussed on calculation of the *frictional* component of pressure gradient, $\tau_w S/A$. Since this has an inverse dependence on the pipe diameter, the frictional pressure gradient is of most importance in smaller diameter pipes.

3.2.2 Calculation of frictional pressure gradient from homogeneous model

The wall shear stress in the first term of equation (3.1) can be replaced by a two-phase friction factor:

$$\left(\frac{dp_f}{dz}\right) - \frac{\tau_w S}{A} = \frac{2f_{tp}\dot{m}^2}{D\rho_H} \tag{3.3}$$

The two-phase friction factor may be calculated by the Blasius equation:

$$f_{tp} - 0.079(Re_{tp})^{-\frac{1}{4}} \tag{3.4}$$

where the two-phase Reynolds number is defined by:

$$Re_{tp} - \frac{\dot{m}D}{\mu_{tp}} \tag{3.5}$$

This has simply moved the problem to one of determining a suitable homogeneous viscosity, μ_{tp}. Of the variety of equations which have been tried, the most commonly used form is that of McAdams *et al*[63]:

$$\mu_{tp} - \left(\frac{x}{\mu_g} + \frac{1-x}{\mu_\ell}\right)^{-1} \tag{3.6}$$

where x is the *quality* (or gas mass flow fraction). It will be seen, however, that the homogeneous viscosity calculated from this equation is very insensitive to the liquid viscosity, and will not exhibit the correct variation with water fraction in the liquid phase, even if the liquid viscosity used is a liquid-liquid mixture viscosity. This proves to be the case when the homogeneous model is compared to experimental three-phase flow data.

3.2.3 Calculation of frictional pressure gradient from the separated flow model

Correlations for frictional pressure gradient for the separated flow model were discussed in Section 2.4.1. Five correlations were considered for analysis of three-phase flow data:

1. **Lockhart & Martinelli**[22] correlation fitted by **Chisholm**[23] equations. This correlation gives the pressure gradient multiplier, ϕ_ℓ^2 as a function of the Lockhart-Martinelli parameter, $X^2 - \left(\frac{dp_F}{dz}\right)_\ell \div \left(\frac{dp_F}{dz}\right)_g$

2. **Schlichting**[24] correlation gives a modified relationship between ϕ_ℓ^2 and X^2 for oil-water-gas flows where the oil viscosity is in the range 10 to 6000 mPas.
3. **Friedel**[27] general correlation for $\phi_{\ell o}^2$ produced by use of a data bank of 25000 data points. The standard deviation of this correlation, however, was particularly high for horizontal flows.
4. **Beggs & Brill**[5] correlation for determination of the flow regime, the holdup, the single-phase friction factor and a two-phase friction factor multiplier. The flow regimes were simplified into categories of segregated, intermittent and distributed flow, with a transition region between the segregated and intermittent regions.
5. **Dukler *et al***[64] correlation which is rather simpler than the Beggs & Brill correlation, consisting only of a calculation of single phase friction factor and a two-phase friction factor multiplier.

The equations used to calculate pressure gradient from each correlation are summarised in Appendix B.

3.3 LIQUID MIXTURE VISCOSITY

3.3.1 Liquid mixture viscosity equations

Most correlations for pressure gradient in three-phase flows suggest that the liquid viscosity should be calculated as a volume-fraction average of the oil and water viscosities. As discussed in Section 2.4.4 this may be appropriate for mixtures of miscible liquids, but not for the case of dispersions of oil and water phases. Another approach has been to just use the viscosity of the continuous liquid phase as the liquid mixture viscosity. While this may be satisfactory when one of the liquids forms only a small fraction of the liquid flow ($\phi \lesssim 0.1$), it does not explain the observed increase in liquid viscosity when there is a larger fraction of one liquid dispersed in the other. The viscosity under these conditions can be several times that of the more viscous phase. Three equations were discussed in Section 2.4.4 which express the liquid viscosity in terms of the viscosity of the continuous phase and the fraction of the dispersed phase, namely those of Richardson[41]:

$$\mu_{\text{mix}} = \mu_{\text{cont}} \exp(k\phi) \tag{3.7}$$

Hatschek[42]:

$$\mu_{\text{mix}} - \frac{\mu_{\text{cont}}}{1 - \sqrt[3]{\phi}} \tag{3.8}$$

and Brinkman[39]:

$$\mu_{\text{mix}} - \frac{\mu_{\text{cont}}}{(1 - \phi)^k} \tag{3.9}$$

The coefficient, k, for a dispersion of monosized solid spheres in a liquid phase was shown to be 2.5 by Einstein[37]. It is assumed that this will be approximately true for a dispersion of one liquid in another. The equations by Richardson and Hatschek were derived by fitting experimental data, while that of Brinkman was derived theoretically, as follows.

Consider a suspension containing n particles of volume v in a total volume V. Its viscosity is a function of the concentration n/V and will be indicated by $\mu(n/V)$. Consider now the effect of adding one more solute particle. If such a particle were added to a pure solvent of volume V, the viscosity would be multiplied by Einstein's factor, $(1 + kv/(V + v))$. If this *ratio* is assumed to hold when one particle is added to a suspension already containing n particles, the viscosity would be given by:

$$\mu\left(\frac{n+1}{V+v}\right) - \mu\left(\frac{n}{V}\right) \cdot \left(1 + \frac{kv}{V+v}\right) \tag{3.10}$$

which leads to:

$$\frac{\mathrm{d}\mu}{\mathrm{d}\phi} - \frac{k\mu}{(1-\phi)} \tag{3.11}$$

where ϕ is the volume fraction nv/V and by integration:

$$\mu = \frac{\mu^\circ}{(1-\phi)^k} \tag{3.12}$$

where μ° is the viscosity of the pure continuous phase.

3.3.2 Comparison of experimental data with Brinkman's equation

A few data points for the viscosity of emulsions of crude oil and water are given by Monson[43] and Woelflin[44] as viscosity ratios of the emulsion to the pure oil.

Monson's data in Table 3.1 can be best fitted by Brinkman's equation using the coefficient of $k = 2.76$.

Table 3.1: Monson emulsion viscosity data

ϕ	μ_{emul}/μ_{oil}
0.10	1.3
0.20	1.8
0.30	2.7
0.40	4.1

Woelflin's data is categorised into *loose*, *medium* and *tight* emulsions according to their stability. Generally the tighter the emulsion, the more shearing has occurred in its formation, and the smaller the drops of dispersed phase. The best fits to Brinkman's equation are given by coefficients of $k = 2.70$, 3.02 and 3.24 for loose, medium and tight emulsions respectively. The data points compared with these lines are shown in Figure 3.2. The reason that the coefficient is consistently higher than 2.5 for these experimental measurements is probably that there was a distribution of droplet sizes. This would increase the viscosity compared to a dispersion of the same volume fraction of monosized drops. However, the difference is small, and the value of 2.5 has been used throughout this work.

3.3.3 Inversion point

Even with a suitable relationship between viscosity and volume fraction, it is still necessary to know the emulsion inversion point, in order to determine the continuous phase at any volume fraction of water. This will obviously depend on a number of factors, for example viscosities of the two liquid phases, interfacial tension, degree of mixing, presence of surface-active agents and contaminants and the nature of the containing material. Many of these factors, or their effects are difficult to assess. In the absence of other forces, surface tension would cause inversion at a volume fraction of 50%, on the basis of minimum surface area. Alternatively, if the dispersed phase is made up of uniform spheres, coalescence may occur when the volume fraction is such that the spheres must touch. The closest packing possible results in a volume fraction of 74.02% of dispersed phase. Woelflin reports observations of brine in crude

oil emulsions with a volume fraction as high as 95% brine; this can only be achieved by having a distribution of drop sizes or if the drops are non-spherical. There is little possibility of predicting the inversion point with any accuracy from first principles.

Yeh *et al*[65] studied the relationship between inversion volume fraction and the viscosities of the two phases in a number of binary systems, leading to:

$$\frac{\phi_{inv}}{1-\phi_{inv}} - \sqrt{\frac{\mu_{disp}}{\mu_i}} \tag{3.13}$$

where μ_i is the viscosity of the interfacial phase, which would normally be that of the continuous phase (in the absence of surfactants).

In experimental investigations of oil-water-gas flows, there seems to be little agreement with equation (3.13), particularly at high oil viscosities, as shown in Table 3.2.

Table 3.2: Comparison of inversion point with equation (3.13)

Authors	Oil Viscosity	Observed Inversion Point	Inversion Point from Equation (3.13)
	mPas	(Water fraction)	(Water fraction)
Sobocinski[2]	3.83	0.77	0.66
Malinowsky[3]	6.0	0.50	0.71
Laflin & Oglesby[4]	6.0	0.50	0.71
Imperial College WASP	70	0.60	0.89

The method of determining the inversion point for sets of experimental data was to start from an inversion point at a water fraction of 50%. By comparing calculated pressure gradient with measured pressure gradient, this would generally result in large underprediction of some points (inversion point too high) or large overprediction of some points (inversion point too low). Thus, the correct inversion point can be easily determined. There are currently too many uncertainties and too little information to be able to produce improved methods of inversion prediction.

3.4 ANALYSIS OF EXPERIMENTAL DATA

3.4.1 Malinowsky[3]

a) Description of experiments

Malinowsky's thesis reports a study of flow patterns, void fractions and pressure gradients in oil-water and oil-water-air flows. The experimental facility consisted of a 30 m long by 38 mm internal diameter transparent pipe. The oil used was 'No.2 diesel fuel' from Continental Oil Co., which had the following properties at 13°C:

Density	855 kg/m^3
Viscosity	6 mPas

In the oil-water-air experiments, water content ranged from 25 to 80% of the liquid phase. The superficial gas velocities were in the range 1.6 to 4.4 m/s and the total superficial liquid velocities in the range 0.6 to 2.0 m/s. Slug flow was observed in all tests except at the highest air velocities, which resulted in a transitional region between slug and annular flow. Large pressure fluctuations were observed together with the formation of temporary liquid dispersions. Great difficulty was encountered with the measurement of liquid holdup, which was therefore not recorded.

b) Description of calculations

One of the conclusions from Malinowsky's work was that if a suitable effective liquid viscosity could be calculated, the pressure drop would be reasonably predicted by either the Beggs & Brill or Dukler correlations. The results of the calculations are shown in Figures 3.4 to 3.7; these graphs plot the measured pressure drop divided by the calculated pressure drop against the oil fraction, and the objective would therefore be to produce a straight line, parallel to the x-axis, passing through 1.0 on the y-axis. Four variables were investigated:

Inversion point: As discussed in Section 3.3.3, an initial estimate of 50% was used as the inversion point. Figure 3.3 shows that $\phi_{inv} - 0.46$ is a more accurate inversion point, eliminating the three stray points. Similar performance would also

be expected from either the Richardson or Hatschek equations in respect of inversion point location.

Choice of viscosity calculation: Figure 3.4 quite clearly demonstrates the deficiency of using a linear interpolation (based on volumetric phase fraction) to determine effective viscosity; however, in the region of where water was the continuous phase, $\phi_o < 0.4$, there is little difference between the linear method and the other three shown. In the oil-continuous region, the pressure drop is greatly underestimated by the linear method. The Richardson, Hatschek and Brinkman equations all give similar results, but the Brinkman equation gives the least scatter.

Brinkman phase fraction coefficient, k: In equation (3.9) for effective viscosity, k has quite a marked effect. The expected value of k, from Einstein's equation, would be 2.5 if the dispersed drops behaved as monosized spherical solid particles. Figure 3.5 shows a comparison using values of 1.5, 2.5 and 5.0 for k. The least scatter was obtained when k was 2.5. A value of 5.0 very clearly over-estimates the viscosity increase around the inversion point.

Choice of correlation: Estimating viscosity from Brinkman's equation with the parameters $k = 2.5$ and $\phi_{inv} = 0.46$ various frictional pressure drop correlations were used to estimate the pressure gradients for Malinowsky's data. The results from these calculations are given in Figures 3.6 and 3.7. Apart from those of Beggs & Brill and Dukler, most correlations do not perform well in the oil-continuous region. This may be due to using the correlations outside their intended region of applicability. Dukler's correlation gives slightly more scatter than Beggs & Brill as was also observed by Malinowsky.

c) Conclusions

The least scatter of calculated pressure drops compared to measured pressure drops was obtained by using the Beggs & Brill correlation using an effective liquid viscosity predicted by Brinkman's equation with $k = 2.5$ and $\phi_{inv} = 0.46$. However, it will be noticed that the average measured pressure drop is only 0.687 times the average

calculated pressure drop. The most likely cause of this overprediction is that the two-phase friction factor is too high.

More data is required to eliminate this problem and produce a good three-phase pressure drop prediction, by reformulating the two-phase friction factor equation to be valid as a three-phase friction factor.

3.4.2 Laflin & Oglesby[4]

a) Description of experiments

Laflin & Oglesby report a study of the effect of water fraction, fluid flowrates and gas/liquid ratio on the inversion point and apparent viscosity of oil-water-air mixtures. The experiments were performed with the same facility as used by Malinowsky, using the same oil but focused on a narrower range of oil/water ratios, around the inversion point. All the oil-water-air results were for slug flow, and considerable scatter was observed in the results. Some possible reasons for this are discussed later.

The liquid mixture velocity was found to have a significant effect on the apparent liquid viscosity for oil-water flow, but little effect for three-phase flow. The inversion point was not affected by the mixture velocity. The presence of a gas phase was found to shift the inversion point from a water fraction of approximately 0.4 in the oil-water system to approximately 0.5 in the oil-water-gas system.

b) Description of calculations

The same sequence of calculations as for the Malinowsky data was pursued. Since these results were from the same experimental facility and with the same fluids, similar performance would be expected.

Inversion Point: An estimate of 0.5 oil fraction was used as a starting point, and 0.46 gave the least scatter. Note from Figure 3.8 that in order to correct the vastly underpredicted points, some other points are consequently overpredicted. This may indicate that it is possible to have either water or oil as the continuous phase in the oil fraction range 0.46 to 0.50. A reason suggested by the authors was that if there was slip between the oil and water phases, the *in situ* ratio may be different to the

flowing ratio used for the calculations. Note also that there are a number of greatly underpredicted points in the oil-continuous region.

Choice of Viscosity Calculation: Figure 3.9 shows a comparison of the linear, Richardson, Brinkman and Hatschek equations. Despite the much greater scatter in this data than in Malinowsky's, the performance of the linear method is quite clearly worse than the other three. Looking at the values of mean and scatter shows this, with little to choose between the three mechanistic formulae.

Brinkman Phase Fraction Index: Figure 3.10 shows a comparison of values of k of 1.5, 2.5 and 5.0. Unfortunately due to the large number of points, and their scatter, it is difficult to see much from this graph, except that using a value of 5.0 quite clearly over-corrects for the viscosity effect in the region of the inversion point.

Choice of Correlation: Using the parameters $k = 2.5$ and $\phi_{inv} = 0.46$ in Brinkman's equation, the various correlations were used to estimate the pressure drop. The results from these calculations are given in Figures 3.11 and 3.12. Despite the scatter, it is quite clear that most correlations do not perform well in the oil-continuous region. Looking at the calculations of mean and scatter, there is little to choose between the Beggs & Brill or Dukler correlations, which are far superior to any of the other correlations.

c) Conclusions

There is considerably more scatter in this data than in Malinowsky's results. Three reasons for this were put forward by the authors:

1. Experimental errors in measurement of flowrates and pressure drop.
2. The use of input liquid fraction (ratio of flowrates at the inlet) instead of actual oil and water holdup. This may affect the inversion, as discussed above, but doesn't explain the scatter of points away from the region of the inversion point.
3. Range of temperatures among tests. The oil viscosity changed more with temperature than did the water viscosity over the range studied; however,

this factor should have been taken account of in calculating the individual viscosities.

The most likely cause of the scatter in the data is in the measurement of pressure drop, due to the fluctuations caused by the slug flow. However, the conclusions obtained from the analysis of Malinowsky's data were also found to hold for this data. Using the Beggs & Brill correlation with Brinkman's viscosity equation ($k = 2.5$ and $\phi_{inv} = 0.46$) gave one of the smallest scatters of calculated pressure gradients compared to measured values. The average measured pressure gradient was 0.73 times the average calculated pressure gradient, compared with a figure of 0.687 for Malinowsky. Unfortunately, this set of data points is not good enough to develop a three-phase fraction factor to refine the Beggs & Brill correlation, as discussed at the end of Section 3.4.1.

3.4.3 Sobocinski[2]

a) Description of experiments

Sobocinski's work was one of the first recorded experimental investigations of oil-water-gas flow. The experimental facility consisted of a horizontal test section of length 11.6 m and internal diameter 0.079 m. The oil used was diesel oil with a density of 841 kg/m^3 and viscosity of 3.83 mPas (at 75°F). The data covers a comprehensive range of flow conditions, although for a fairly limited number of oil/water ratios and total mass flowrates. Mixing between the oil and water phases was observed to occur as a result of increased gas velocity. At low gas velocities, three-layer stratified flow was observed and at the highest gas velocities the oil and water formed a temporary emulsion in a semi-annular flow. Between the two extremes it was observed that the oil-water interface was less easily disturbed than the air-oil interface. A maximum was observed in the frictional pressure drop at a water volume fraction of 0.77. At higher water fractions, the emulsions inverted to oil-in-water. Slug flow was not observed in these experiments, and Sobocinski's analysis used the ubiquitous 'linear' mixture viscosity calculation.

b) Description of calculations

Attempts to use the same analysis as with Malinowsky (Section 3.4.1) were unsuccessful with this data. This was because no correlation could cover the wide range of flow patterns observed, from stratified flow to emulsified semi-annular flow. The only analysis that was performed was to use the Beggs & Brill correlation to demonstrate that some improvement could be made by switching from the 'linear' to the Brinkman viscosity calculation.

Figure 3.13 shows the ratio of measured to calculated pressure drop against oil fraction, with viscosity calculated by the linear method. The points are very scattered, but there are a few clear observations which can be made:

1. There is a peak in the pressure drop ratio at an oil fraction of around 0.2. This agrees with Sobocinski's pressure drop maximum at a water fraction of approximately 0.77.
2. There is an overprediction of pressure drop at high oil fractions, which is probably due to the drag reduction effect of having a small amount of water in contact with the pipe walls.
3. There are a number of points with extremely low pressure drop ratios. These are mostly stratified or 'ripple' flow. The recorded pressure drops in these flow regimes were very much smaller than in other regimes (in some cases by a factor of 100). This is not predicted by any of the correlations available.

Figure 3.14 shows the pressure drop ratio as a function of oil fraction with viscosity calculated by the Brinkman method, for two assumed inversion points. The curve for $\phi_{inv} = 0.23$ is similar to that obtained by the linear viscosity method, with less scatter. However, there are still some points which are clearly oil-continuous in the region $\phi < 0.23$, leading to high pressure drop ratios. Assuming an inversion point $\phi_{inv} - 0.15$ almost removes this problem, but still leaves the other two problems raised earlier.

c) Conclusions

Sobocinski's work was a very interesting experimental project which provided important information on stratified and stratified-annular three-phase flows, which

are regimes not covered by other experimental studies. However, it is difficult to produce the kind of analysis done with the data from Malinowsky or from Laflin & Oglesby. In particular, the liquid viscosity calculations used in the other analyses are not valid for the whole range of Sobocinski's data. An alternative approach is required to analyse stratified flows and for flows where the introduction of a small quantity of water causes a large decrease in pressure gradient.

3.4.4 Stapelberg[66]

Stapelberg studied flow patterns and pressure gradient for oil-water and oil-water-air flows in a facility with two test sections of the following geometries:

Diameter	Entrance Length	Test Section Length
0.0238	3.75	10.0
0.0590	9.00	35.0

The oil used was a white mineral oil (Shell *Ondina 15*) with a viscosity of approximately 30 mPas and a density of 845 kg/m^3 at room temperature. Full details of the experiments are given by Stapelberg[67].

Figure 3.15 shows a comparison of pressure gradient calculated using the Beggs & Brill correlation with the Brinkman viscosity with the measured pressure gradient. Some of the data points were stratified flow and are overpredicted by the correlation, but the points in the slug flow regime are reasonably well calculated. All the slug flows had separated oil and water in the regions between slugs, with some dispersion in the liquid slug itself, and were all effectively water-continuous.

3.5 ANALYSIS OF FIELD DATA

3.5.1 Fayed & Otten

Fayed & Otten[68] compared pressure gradient measurements from 6, 12 and 16 inch pipelines with the correlations of Beggs & Brill[5] and Dukler[64]. For the 12 and 16 inch lines, which had oil-gas flow only, there was reasonable agreement between the correlations and the measurements, with the Dukler correlation overpredicting consistently and the Beggs & Brill correlation underpredicting the pressure gradient,

as shown in Figure 3.16. The six-inch line data points were for oil-water-gas flow, and agreement with the correlations was not so good. The Woelflin[44] method was used to estimate the mixture viscosity for some of the calculations with the Dukler correlation, with the result of greatly overpredicting the pressure gradient, Figure 3.17. This suggests that the water was not dispersed in the oil phase, but flowed as a separate phase, producing a drag-reduction effect compared to pure oil. This was particularly noticeable for the pipelines with 18% water fraction.

Without more information, which is not present in the paper, it is difficult to come to any firm conclusions. A lot of error in pressure drop calculations in industrial pipelines may be introduced by not considering the effect of gas coming out of solution as the pressure falls.

3.5.2 UK National Multiphase Flow Database

The UK National Multiphase Flow Database is a project operated by AEA Petroleum Services at Harwell, intended for the collection and examination of data for pipelines in the petroleum industry from different operators. Table 3.3 shows three points taken from the database, with values of pressure gradient calculated from the Beggs & Brill correlation with the Brinkman liquid viscosity correction. It can be seen that the calculated pressure gradient is more or less correct for two of these points, but greatly underpredicted for the third. Such a large underprediction probably arises due to a gravitational component to the pressure drop, but the information on the pipeline profile is not available. There is a large difference between the pressure gradient observed in the 16″ line compared to the 4″ line at similar fluid velocities, as expected due to the inverse relationship between frictional pressure gradient and pipe diameter.

Table 3.3: UKNMFD three-phase flow points

		Nigeria 05	Wytch 2	Nigeria 01
Operator	-	Mobil	BP	Mobil
Pipe Diameter	inches	16	4	16
Inlet Pressure	bar	25.83	21.37	20.32
Exit Pressure	bar	23.42	18.34	18.25
Length	m	5378	1990	13428
Pressure Drop	Pa/m	44.8	152.3	15.4
Oil Velocity	m/s	0.495	0.472	0.097
Oil Viscosity	mPas	10	10	8
Oil Density	kg/m^3	862	850	840
Water Velocity	m/s	0.055	0.081	0.014
Water Viscosity	mPas	0.678	0.7	0.76
Water Density	kg/m^3	995	995	995
Gas Velocity	m/s	1.884	0.932	0.808
Gas Viscosity	mPas	0.1	0.1	0.1
Gas Density	kg/m^3	19.5	15	15.3
Calculated Pressure Gradient	Pa/m	**42**	**160**	**4**

3.6 SUMMARY

In this chapter the aim was to develop correlations for frictional pressure gradient in three-phase flow. Correlations for pressure gradient in gas-liquid systems were amended by modifying the effective liquid viscosity to take account of the presence of oil and water phases. Suitable liquid mixture viscosity equations were discussed and compared with experimental data for emulsions of crude oil and water, and the calculation of the inversion point (oil-in-water to water-in-oil dispersion) was considered.

The correlations were compared with experimental data from Malinowsky, Laflin & Oglesby, Sobocinski and Stapelberg. The general conclusion was that the best overall prediction was given by the Beggs & Brill correlation with the effective liquid viscosity calculated from the Brinkman equation. The exception was the

Sobocinski data which was predominantly stratified or stratified-annular flow where none of the correlations considered was found to be applicable.

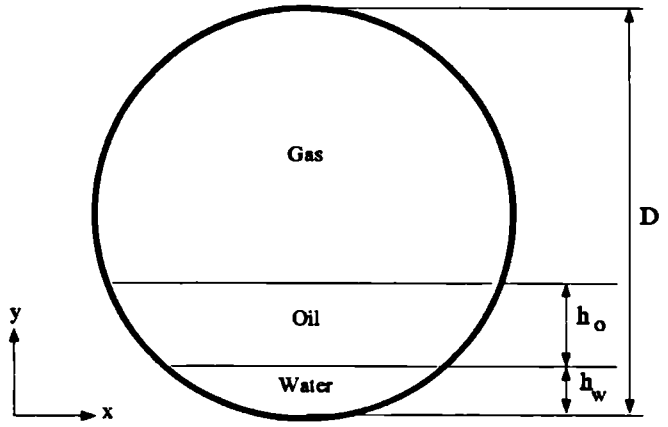
A limited number of calculations were possible with field data from Fayed & Otten and the UK National Multiphase Flow Database. The comparisons were generally favourable, but more complete data sets are required from operating pipelines to give a more thorough comparison.

THIS IS A BLANK PAGE

Chapter 4:
SIMPLE MODELS FOR STRATIFIED THREE-PHASE FLOW

4.1 INTRODUCTION

It was clear from the work reported in the previous chapter that a key area where improvement needs to be made to predictive capabilities is that of stratified three-phase flow. The objective of the work described in this chapter is to derive a method of calculation of the fractions of each phase in a three-phase stratified flow of gas, oil and water; the fractions may be expressed in terms of the heights of the liquid layers:



The geometry of the problem means that analytical solutions to the Navier-Stokes equations are not possible, and thus a solution is developed here from the Taitel & Dukler[32] two-fluid model for stratified flow. In Chapter 5, numerical models for this system are described.

Taitel & Dukler wrote momentum balances for the gas and liquid phases and eliminated pressure gradient between them, thus translating the problem into one of determining the three mean shear stresses, at the gas-wall, liquid-wall and gas-liquid interfaces. These shear stresses were calculated using friction factors based on equivalent diameters. The gas was treated as if it were flowing in a closed channel bounded by the pipe walls and the liquid phase; the liquid phase was treated as though it were an open channel flow, bounded only at its lower surface by the pipe walls. The interfacial friction factor was assumed equal to the gas phase friction factor. A unique relationship was derived between the gas and liquid superficial velocities, the physical properties and the liquid height.

In three-phase stratified flow, there are two interfacial shear stresses, between the gas and oil and between the oil and water phases, together with the three shear stresses between each phase and the pipe walls. The gas-wall, water-wall and gas-oil shear stresses may all be calculated as in Taitel & Dukler's model and the oil-wall shear stress may be calculated using an equivalent diameter involving only the oil-wall contacts. The oil-water interfacial shear stress presents the most difficulty, and it is proposed that it is replaced for algebraic convenience by the expression:

$$\tau_{ow} = \gamma \tau_o \tag{4.1}$$

where τ_o is the oil-wall shear stress. The factor γ must be less than unity, since the oil-water interfacial shear stress must be smaller than the oil-wall shear stress (due to smaller relative velocity). The difficulties of the three-fluid stratified flow model are therefore reduced to the problem of evaluating γ.

Analytical solutions may be obtained for stratified laminar flows between flat plates. Solutions for oil-water flows were given by Denn[47] and by Russell & Charles[45] and may be extended to three phases. The three-phase solution is algebraically complicated and the heights of the two liquid layers are given implicitly by two simultaneous non-linear equations, which must be solved numerically. The two-phase flat plate solution may be used to calculate the oil-wall shear stress in an oil-gas flow, where there is no oil-water interface, and the three-phase solution may be used to calculate the oil-water interfacial shear stress where there is no oil-wall interface. If these calculations are performed with appropriate flowrates and viscosities, an estimate can be made of γ for the three-phase pipe flow.

A solution can now be derived for the three-fluid stratified flow model. This is also algebraically complicated, and the liquid heights are once again given implicitly by two simultaneous non-linear equations, which now involve $\cos^{-1}$ terms.

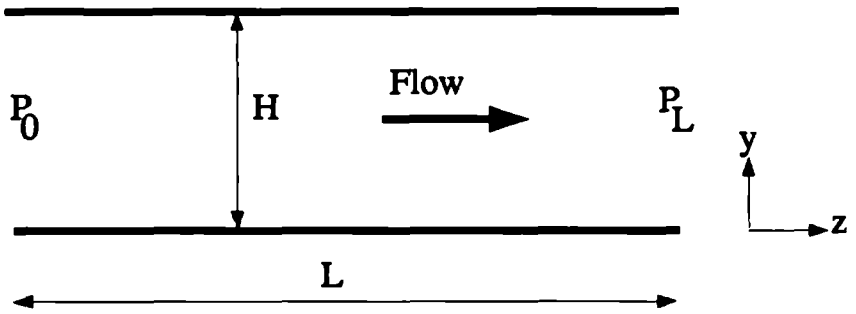
Finally, the values of holdup calculated from the three-fluid stratified flow model are compared with experimental data. The major source of data for three-phase stratified flow is the thesis of Sobocinski[2] for oil-water-air flow with an oil viscosity of 3.8 mPas, with some additional data from Stapelberg[66], where the oil viscosity was 31 mPas.

4.2 SOLUTIONS FOR LAMINAR FLOWS BETWEEN FLAT PLATES

4.2.1 Single phase flow

It is useful first to look at a single phase flow between flat plates, which introduces the simplifying assumptions which are common to the calculations for two- and three-phase flows between flat plates. There are two types of flow to consider: pressure-induced flow and drag-induced flow, which are explained by Richardson[69] and summarised below.

a) Pressure induced flow between parallel flat plates



The situation under consideration is the laminar flow of a single phase fluid between flat plates of separation H and infinite width under the action of a pressure difference $P_L - P_0$ acting over a length L, where $L \gg H$ so that entrance effects can be neglected. The flow is assumed to be *steady, fully-developed* and *incompressible.* Thus the equation for conservation of mass:

$$\underline{\nabla} \cdot \underline{u} - 0 \tag{4.2}$$

can be simplified to give:

$$\frac{\partial u_y}{\partial y} = 0 \tag{4.3}$$

since the assumption of fully developed flow makes $\partial u_z/\partial z - 0$ and the assumption of infinite width makes $\partial u_x/\partial x - 0$. Integration of (4.3), noting that there can be no flow through the plates, leads to:

$$u_y - 0 \tag{4.4}$$

and hence it follows that the only component of velocity is in the z-direction and varies only with the separation from the plate:

$$\underline{u} = u_z(y)\underline{i}_z \tag{4.5}$$

The equation for conservation of momentum:

$$\rho\frac{\partial \underline{u}}{\partial t} + \rho\underline{u}\cdot\underline{\nabla}\underline{u} - \rho\underline{g} - \underline{\nabla}p + \mu\Delta\underline{u} \tag{4.6}$$

becomes in the y-direction:

$$-\frac{\partial p}{\partial y} = 0 \tag{4.7}$$

and hence p, the pressure, is independent of y. In the z-direction:

$$0 = -\frac{\partial p}{\partial z} + \mu\frac{\partial^2 u_z}{\partial y^2} \tag{4.8}$$

The boundary conditions which must be applied to obtain a solution are that the velocity at the walls ($y = 0$ and $y = H$) is zero and because of the symmetry of the flow, the velocity gradient is zero along the centreline ($du_z/dy = 0$ at $y = H/2$). Thus equation (4.8) can be integrated to give:

$$y\frac{dp}{dz} = \mu\frac{du_z}{dy} + C_1 \tag{4.9}$$

where, from the first boundary condition:

$$C_1 - \frac{H}{2}\left(\frac{dp}{dz}\right) \tag{4.10}$$

and integrating again:

$$u_z = \frac{1}{\mu}\left(\frac{dp}{dz}\right)\left(\frac{y^2 - Hy}{2}\right) + C_2 \tag{4.11}$$

It follows from the second boundary condition that:

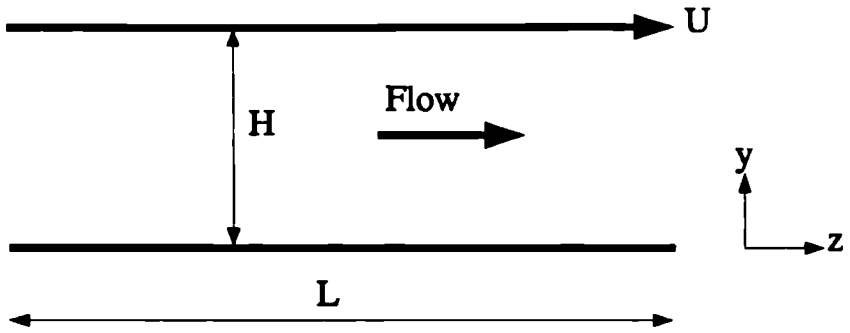
$$C_2 - 0 \tag{4.12}$$

Equation (4.11) may be more conveniently written as:

$$u_z = \frac{H^2}{2\mu}\left(-\frac{dp}{dz}\right)\frac{y}{H}\left(1 - \frac{y}{H}\right) \tag{4.13}$$

which is the equation of a parabolic velocity profile.

b) Drag induced flow between parallel flat plates



In this case the flow of the fluid is a result of the relative motion of the upper plate. The assumptions of the previous case hold, but because there is no pressure gradient in the x-direction, equation (4.8) becomes:

$$\frac{\partial^2 u_z}{\partial y^2} - 0 \tag{4.14}$$

subject to the boundary conditions that $u_z - U$ at $y - II$ and $u_z - 0$ at $y - 0$. Hence it may be shown that:

$$u_z - \frac{Uy}{II} \tag{4.15}$$

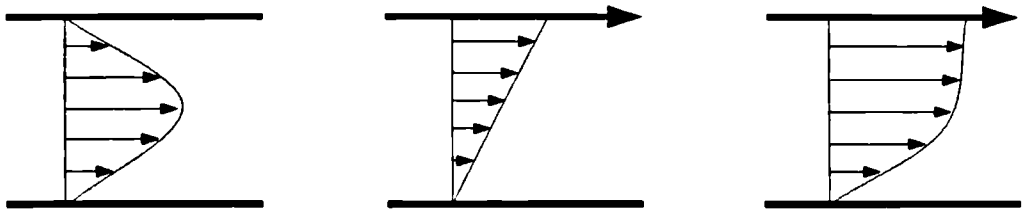
which is the equation of a linear velocity profile.

c) Combined pressure induced and drag induced flow between parallel flat plates

The two solutions obtained for the separate cases of pressure induced and drag induced flows, expressed by equations (4.13) and (4.15) respectively, can be added for the case of a flow under the combined effects of a pressure gradient and relative motion of the plates, giving:

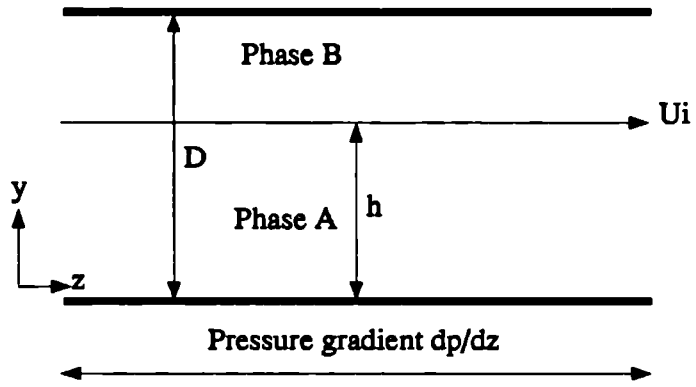
$$u_z - \frac{Uy}{II} - \frac{II^2}{2\mu}\left(\frac{dp}{dz}\right)\frac{y}{II}\left(1 - \frac{y}{II}\right) \tag{4.16}$$

The velocity profiles corresponding to the pressure-induced, drag induced and combined flows are shown below:



Two- and three-phase stratified flows may be considered as combinations of these types of flows, where phases are flowing between a fixed flat plate (the wall) and a moving flat plate (the interface), where the interfacial velocities are unknown. This deficiency is addressed by assuming continuity of velocity and of shear stress at the interface, which is true if the interface is smooth and flat.

4.2.2 Two-phase flow



The figure above shows the physical representation of a two-phase flow between flat plates. The phases are considered as the heavier 'A' phase and the lighter 'B' phase in this derivation, since it does not matter whether they are liquid and gas or liquid and liquid (The relative viscosities of the phases *will*, however, determine the direction of the interfacial shear stress in each phase and the location of the maximum in the velocity profile). The same assumptions are made as for single phase flow in this geometry, and thus for two-phase flow, the derivation can start from the simplified momentum equation given as equation (4.8). For phase A:

$$\mu_A \frac{d^2 u_A}{dy^2} - \frac{dp}{dz} \tag{4.17}$$

which integrates to give:

$$u_A = \frac{1}{2\mu_A}\left(\frac{dp}{dz}\right)y^2 + C_3 y + C_4 \tag{4.18}$$

Similarly for phase B:

$$u_B = \frac{1}{2\mu_B}\left(\frac{dp}{dz}\right)y^2 + C_1 y + C_2 \tag{4.19}$$

The boundary conditions are:

$u_B - 0$ at $y = II$	
$u_A = 0$ at $y = 0$	no slip at the walls
$u_B - u_A$ at $y = h$	no slip at the interface
$\mu_B \frac{du_B}{dy} = \mu_A \frac{du_A}{dy}$ at $y - h$	continuity of shear stress at the interface

The boundary conditions are then expressed in terms of equations (4.18) and (4.19):

$$0 = \frac{II^2}{2\mu_B}\left(\frac{dp}{dz}\right) + C_1 II + C_2 \tag{4.20}$$

$$C_4 - 0 \tag{4.21}$$

$$\frac{1}{2\mu_B}\left(\frac{dp}{dz}\right)h^2 + C_1 h + C_2 = \frac{1}{2\mu_A}\left(\frac{dp}{dz}\right)h^2 + C_3 h + C_4 \tag{4.22}$$

$$h\left(\frac{dp}{dz}\right) + \mu_B C_1 - h\left(\frac{dp}{dz}\right) + \mu_A C_3 \tag{4.23}$$

allowing the derivation of equations for the four constants of integration:

$$C_1 - \frac{-\left(\frac{dp}{dz}\right)\left[\mu_A(h^2 - II^2) - \mu_B h^2\right]}{2\mu_B(\mu_A(h - II) - \mu_B h)} \tag{4.24}$$

$$C_2 - \frac{hII(h - II)(\mu_A - \mu_B)\left(\frac{dp}{dz}\right)}{2\mu_B(\mu_A(h - II) - \mu_B h)} \tag{4.25}$$

$$C_3 = \frac{-\left(\frac{dp}{dz}\right)\left[\mu_A(h^2 - II^2) - \mu_B h^2\right]}{2\mu_A(\mu_A(h - II) - \mu_B h)} \tag{4.26}$$

$$C_4 - 0 \tag{4.27}$$

The velocity profile in the lower phase may therefore be expressed by:

$$u_A - \frac{-\left(\frac{dp}{dz}\right)y[\mu_A(h(h - y) - II(II - y)) - h\mu_B(h - y)]}{2\mu_A(\mu_A(h - II) - h\mu_B)} \tag{4.28}$$

and the mean velocity in the lower phase by:

$$\bar{u}_A = \frac{1}{h}\int_0^h u_A dy = \frac{-h\left(\frac{dp}{dz}\right)\left[\mu_A(h+3H)(h-H)-\mu_B h^2\right]}{12\mu_A(\mu_A(h-H)-\mu_B h)} \tag{4.29}$$

Similarly for the upper phase it can be shown that the velocity profile is given by:

$$u_B = \frac{\left(\frac{dp}{dz}\right)(H-y)[\mu_A(h-y)(h-H)-\mu_B h(h-H-y)]}{2\mu_B(\mu_A(h-H)-\mu_B h)} \tag{4.30}$$

and hence the mean velocity is given by:

$$\bar{u}_B = \frac{1}{(H-h)}\int_h^H u_B dy = \frac{-\left(\frac{dp}{dz}\right)(h-H)\left[\mu_A(h-H)^2-\mu_B h(h-4H)\right]}{12\mu_B(\mu_A(h-H)-\mu_B h)} \tag{4.31}$$

The ratio of mean velocities, obtained by dividing expression (4.29) by (4.31):

$$\frac{\bar{u}_A}{\bar{u}_B} = \frac{-h\mu_B\left[\mu_A(h+3H)(h-H)-\mu_B h^2\right]}{-(h-H)\mu_A\left[\mu_A(h-H)^2-\mu_B h(h-4H)\right]} \tag{4.32}$$

can be related to the ratio of the flowrates of the two phases by the expression:

$$\frac{Q_A}{Q_B} - \left(\frac{h}{H-h}\right)\frac{\bar{u}_A}{u_B} \tag{4.33}$$

hence giving:

$$\frac{Q_A}{Q_B} = \frac{-\mu_B h^2\left[\mu_A(h+3H)(h-H)-\mu_B h^2\right]}{\mu_A(h-H)^2\left[\mu_A(h-H)^2-\mu_B h(h-4H)\right]} \tag{4.34}$$

The quantities in equation (4.34) are made dimensionless, as follows:

$$\hat{Q} = Q_B/Q_A \tag{4.35}$$

$$\tilde{\mu} = \mu_B/\mu_A \tag{4.36}$$

and

$$\tilde{h} = h/H \tag{4.37}$$

and so the following expression can be obtained relating the height of the lower layer to the viscosity ratio and flowrate ratio of the two phases:

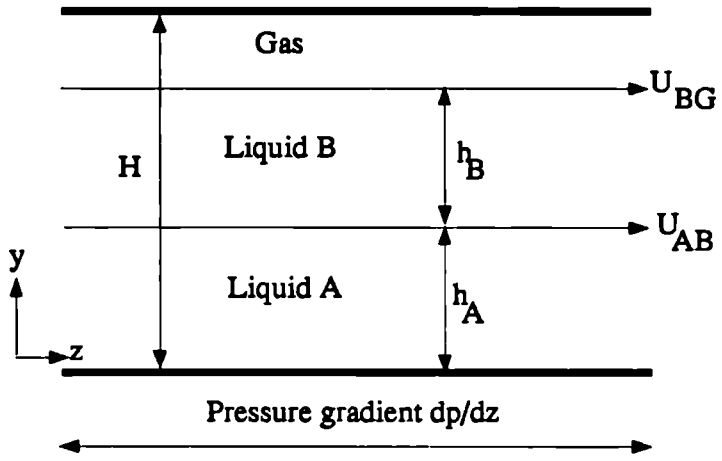
$$\tilde{h}^4\left[(1-\tilde{\mu})\left(\tilde{\mu}\hat{Q}+1\right)\right] + 2\tilde{h}^3\left[\tilde{\mu}\left(\hat{Q}+3\right)-2\right] - 3\tilde{h}^2\left[\tilde{\mu}\left(\hat{Q}+3\right)-2\right] + 4\tilde{h}(\tilde{\mu}-1)+1-0 \tag{4.38}$$

This equation may be easily solved using, for example, the Newton-Raphson method, and the solution as a function of $\tilde{Q}$ and $\tilde{\mu}$ is given in Figure 4.1. Note that if $\tilde{\mu} - 1$ and $\tilde{Q} = 1$ then equation (4.38) reduces to:

$$4\tilde{h}^3 - 6\tilde{h}^2 + 1 - 0 \tag{4.39}$$

of which the only solution which lies in the range $0 < \tilde{h} < 1$ is $\tilde{h} - \frac{1}{2}$. Once the height is calculated, the pressure gradient, interfacial velocity, shear stresses, etc, may be easily calculated using the velocity profile given in equations (4.28) and (4.30).

4.2.3 Three-phase flow



Three-phase flow between parallel flat plates is as shown in the figure above. The gas phase and the heavier liquid phase (A) flow between a flat plate and a moving interface, as in two-phase flow between flat plates. The lighter liquid phase (B) flows between the two moving interfaces. As for two-phase flow, the integrated momentum equations are:

$$u_g = \frac{1}{2\mu_g}\left(\frac{dp}{dz}\right)y^2 + C_1 y + C_2 \tag{4.40}$$

$$u_A - \frac{1}{2\mu_A}\left(\frac{dp}{dz}\right)y^2 + C_3 y + C_4 \tag{4.41}$$

and

$$u_B - \frac{1}{2\mu_B}\left(\frac{dp}{dz}\right)y^2 + C_5 y + C_6 \tag{4.42}$$

The boundary conditions are that there is no slip at the walls and the velocity and shear stress is continuous at both interfaces, thus:

$u_g = 0$ at $y = II$	no slip at the walls
$u_A = 0$ at $y = 0$	
$u_g = u_B$ at $y = h_A + h_B$	no slip at the interface
$u_B = u_A$ at $y = h_A$	
$\mu_g \frac{du_g}{dy} = \mu_B \frac{du_B}{dy}$ at $y = h_A + h_B$	continuity of shear stress at
$\mu_B \frac{du_B}{dy} = \mu_A \frac{du_A}{dy}$ at $y = h_A$	the interfaces

Hence, expressing the boundary conditions in terms of equations (4.40), (4.41) and (4.42), the following equations are obtained:

$$0 = \frac{II^2}{2\mu_g}\left(\frac{dp}{dz}\right) + C_1 II + C_2 \tag{4.43}$$

$$0 - C_4 \tag{4.44}$$

$$\begin{aligned} &\frac{1}{2\mu_B}\left(\frac{dp}{dz}\right)(h_A + h_B)^2 + C_5(h_A + h_B) + C_6 \\ &= \frac{1}{2\mu_g}\left(\frac{dp}{dz}\right)(h_A + h_B)^2 + C_1(h_A + h_B) + C_2 \end{aligned} \tag{4.45}$$

$$\frac{1}{2\mu_B}\left(\frac{dp}{dz}\right)h_A^2 + C_5 h_A + C_6 = \frac{1}{2\mu_A}\left(\frac{dp}{dz}\right)h_A^2 + C_3 h_A + C_4 \tag{4.46}$$

$$C_1\mu_g - C_5\mu_B \tag{4.47}$$

$$C_3\mu_A = C_5\mu_B \tag{4.48}$$

The velocity profiles are made dimensionless by dividing velocities by u_{As} (the superficial velocity of liquid A), viscosities by μ_A and distances by H. The volumetric

flowrate per unit width of channel, Q, of each phase is given by integrating the velocity over the height of the phase:

$$\tilde{Q}_g - \frac{Q_g}{Q_A} - \int_{\tilde{h}_A+\tilde{h}_B}^{1} \tilde{u}_g d\tilde{y} \tag{4.49}$$

$$\tilde{Q}_B - \frac{Q_B}{Q_A} = \int_{\tilde{h}_A}^{\tilde{h}_A+\tilde{h}_B} \tilde{u}_B d\tilde{y} \tag{4.50}$$

$$\tilde{Q}_A - 1 - \int_{0}^{\tilde{h}_A} \tilde{u}_A d\tilde{y} \tag{4.51}$$

and therefore, by substitution of the dimensionless velocity profiles into equations (4.49), (4.50) and (4.51):

$$\frac{\tilde{Q}_g}{\tilde{P}} - \frac{1 - \left(\tilde{h}_A + \tilde{h}_B\right)^3}{6\tilde{\mu}_g} + \frac{\tilde{C}_1}{2}\left(1 - \left(\tilde{h}_A + \tilde{h}_B\right)^2\right) + \tilde{C}_2\left(1 - \left(\tilde{h}_A + \tilde{h}_B\right)\right) \tag{4.52}$$

$$\frac{\tilde{Q}_B}{\tilde{P}} - \frac{\left(\tilde{h}_A + \tilde{h}_B\right)^3 - \tilde{h}_A^3}{6\tilde{\mu}_B} + \frac{\tilde{C}_5}{2}\left(\left(\tilde{h}_A + \tilde{h}_B\right)^2 - \tilde{h}_A^2\right) + \tilde{C}_6\tilde{h}_B \tag{4.53}$$

$$\frac{1}{\tilde{P}} - \frac{\tilde{h}_A^3}{6} + \frac{\tilde{C}_3\tilde{h}_A^2}{2} \tag{4.54}$$

where in these equations, the dimensionless pressure gradient is given by:

$$\tilde{P} - \frac{II^2}{\mu_A u_{As}}\left(\frac{dp}{dz}\right) \tag{4.55}$$

and the dimensionless constants of integration:

$$\tilde{C}_1 - C_1/\left(\frac{dp}{dz}\right) \tag{4.56}$$

can be derived from equations (4.43) to (4.48). This was done with the assistance of the algebra manipulation program *Derive*, giving:

$$\tilde{C}_1 - \frac{-\left[\tilde{\mu}_B\left(1 + \tilde{h}_A + \tilde{h}_B\right)\left(1 - \tilde{h}_A - \tilde{h}_B\right) + \tilde{\mu}_g\tilde{h}_B\left(2\tilde{h}_A + \tilde{h}_B\right) + \tilde{\mu}_g\tilde{\mu}_B\tilde{h}_A^2\right]}{2\tilde{\mu}_g\left[\tilde{\mu}_B\left(1 - \tilde{h}_A - \tilde{h}_B\right) + \tilde{\mu}_g\tilde{h}_B + \tilde{\mu}_B\tilde{\mu}_g\tilde{h}_A\right]} \tag{4.57}$$

$$\tilde{C}_2 = \frac{\left[\tilde{\mu}_B\left(\tilde{h}_A + \tilde{h}_B\right)\left(1 - \tilde{h}_A - \tilde{h}_B\right) - \tilde{\mu}_g\tilde{h}_B\left(1 - 2\tilde{h}_A - \tilde{h}_B\right) - \tilde{\mu}_g\tilde{\mu}_B\tilde{h}_A\left(1 - \tilde{h}_A\right)\right]}{2\tilde{\mu}_g\left[\tilde{\mu}_B\left(1 - \tilde{h}_A - \tilde{h}_B\right) + \tilde{\mu}_g\tilde{h}_B + \tilde{\mu}_B\tilde{\mu}_g\tilde{h}_A\right]} \tag{4.58}$$

$$\tilde{C}_3 = \frac{-\left[\tilde{\mu}_B\left(1 + \tilde{h}_A + \tilde{h}_B\right)\left(1 - \tilde{h}_A - \tilde{h}_B\right) + \tilde{\mu}_g\tilde{h}_B\left(2\tilde{h}_A + \tilde{h}_B\right) + \tilde{\mu}_g\tilde{\mu}_B\tilde{h}_A^2\right]}{2\left[\tilde{\mu}_B\left(1 - \tilde{h}_A - \tilde{h}_B\right) + \tilde{\mu}_g\tilde{h}_B + \tilde{\mu}_B\tilde{\mu}_g\tilde{h}_A\right]} \tag{4.59}$$

$$\tilde{C}_4 = 0 \tag{4.60}$$

$$\tilde{C}_5 = \frac{-\left[\tilde{\mu}_B\left(1 + \tilde{h}_A + \tilde{h}_B\right)\left(1 - \tilde{h}_A - \tilde{h}_B\right) + \tilde{\mu}_g\tilde{h}_B\left(2\tilde{h}_A + \tilde{h}_B\right) + \tilde{\mu}_g\tilde{\mu}_B\tilde{h}_A^2\right]}{2\tilde{\mu}_B\left[\tilde{\mu}_B\left(1 - \tilde{h}_A - \tilde{h}_B\right) + \tilde{\mu}_g\tilde{h}_B + \tilde{\mu}_B\tilde{\mu}_g\tilde{h}_A\right]} \tag{4.61}$$

$$\tilde{C}_6 = \frac{\tilde{h}_A\left[\tilde{\mu}_B\left(1 - \tilde{h}_A - \tilde{h}_B\left(\tilde{h}_A + \tilde{h}_B\right)\right) + \tilde{\mu}_g\tilde{h}_B\left(\tilde{h}_A + \tilde{h}_B\right)\right](1 - \tilde{\mu}_B)}{2\tilde{\mu}_B\left[\tilde{\mu}_B\left(1 - \tilde{h}_A - \tilde{h}_B\right) + \tilde{\mu}_g\tilde{h}_B + \tilde{\mu}_B\tilde{\mu}_g\tilde{h}_A\right]} \tag{4.62}$$

The pressure gradient can be eliminated between equations (4.52) and (4.54) and between (4.53) and (4.54) to give:

$$f_1\left(\tilde{h}_A, \tilde{h}_B\right) = \frac{\frac{1-\left(\tilde{h}_A+\tilde{h}_B\right)^3}{6\tilde{\mu}_g} + \frac{\tilde{C}_1}{2}\left(1 - \left(\tilde{h}_A + \tilde{h}_B\right)^2\right) + \tilde{C}_2\left(1 - \left(\tilde{h}_A + \tilde{h}_B\right)\right)}{\frac{\tilde{h}_A^3}{6} + \frac{\tilde{C}_3\tilde{h}_A^2}{2}} - \tilde{Q}_g = 0 \tag{4.63}$$

and

$$f_2\left(\tilde{h}_A, \tilde{h}_B\right) = \frac{\frac{\left(\tilde{h}_A+\tilde{h}_B\right)^3-\tilde{h}_A^3}{6\tilde{\mu}_B} + \frac{\tilde{C}_5}{2}\left(\left(\tilde{h}_A + \tilde{h}_B\right)^2 - \tilde{h}_A^2\right) + \tilde{C}_6\tilde{h}_B}{\frac{\tilde{h}_A^3}{6} + \frac{\tilde{C}_3\tilde{h}_A^2}{2}} - \tilde{Q}_B = 0 \tag{4.64}$$

These equations must be solved simultaneously to give the heights of the two liquid layers, $\tilde{h}_A$ and $\tilde{h}_B$ as a function of the ratios of flowrates $\tilde{Q}_g$ and $\tilde{Q}_B$ and viscosities $\tilde{\mu}_g$ and $\tilde{\mu}_B$. Since the equations are non-linear, this must be done numerically.

4.2.4 Solution of systems of non-linear equations (Newton's method)

The numerical solution of a system of non-linear equations may be tackled by the same approach used in the Newton-Raphson method for solution of a single non-linear equation. The equations are linearised by a Taylor expansion about the current estimate, $\underline{x}^{(0)}$ of the solution $\underline{x}^*$:

$$f_i(x_1 \ldots x_n) - f_i\left(x_1^{(0)} \ldots x_n^{(0)}\right) + \left(\frac{\partial f_i}{\partial x_1}\right)_{|\underline{x}^{(0)}} \cdot \left(x_1 - x_1^{(0)}\right) + \ldots + \left(\frac{\partial f_i}{\partial x_n}\right)_{|\underline{x}^{(0)}} \cdot \left(x_n - x_n^{(0)}\right) + \text{H.O.T.} \tag{4.65}$$

or in matrix notation:

$$\underline{f}(\underline{x}) \simeq \underline{f}\left(\underline{x}^{(0)}\right) + \underline{\underline{J}}\left(\underline{x}^{(0)}\right) \cdot \left(\underline{x} - \underline{x}^{(0)}\right) \tag{4.66}$$

where $\underline{\underline{J}}$ is the Jacobian matrix, defined as:

$$J_{ij}\left(\underline{x}^{(0)}\right) - \left(\frac{\partial f_i}{\partial x_j}\right)_{|\underline{x}\,0} \tag{4.67}$$

Although analytical derivatives could be derived from equations (4.63) and (4.64), it is probably easier to calculate the derivatives using finite difference approximations. This approach will be necessary when considering the solution for the three-fluid model of stratified oil-water-gas flow in a pipe in Section 4.5, for which analytical derivatives are intractable. The partial derivatives are therefore approximated by:

$$\left(\frac{\partial f_i}{\partial x_j}\right)_{|x\,k)} - \frac{f_i\left(x_1^{(k)} \ldots x_j^{(k)} + h_j \ldots x_n^{(k)}\right) - f_i\left(x_1^{(k)} \ldots x_j^{(k)} \ldots x_n^{(k)}\right)}{h_j} \tag{4.68}$$

where h_j is a small number. The next estimate of the solution, $\underline{x}^{(k+1)}$ can then be obtained by inverting the approximation to the Jacobian matrix:

$$\underline{x}^{(k+1)} - \underline{x}^{(k)} - \left[\underline{\underline{J}}^{(k)}\right]^{-1} \cdot \underline{f}\left(\underline{x}^{(k)}\right) \tag{4.69}$$

The iteration of the solution $\underline{x}^{(k+1)}$ is continued until the difference $\underline{x}^{(k+1)} - \underline{x}^{(k)}$ reaches a pre-determined small value $\underline{\varepsilon}$.

Note that only an approximation of the Jacobian matrix is *required*, since as the solution is approached, the difference $\underline{x}^{(k+1)} - \underline{x}^{(k)}$ approaches zero. Error in the magnitudes of the derivatives will simply affect the rate at which the solution is approached. The *signs* of the derivatives are important, however, in determining whether the iteration will converge or diverge.

4.3 TAITEL & DUKLER TWO-FLUID MODEL FOR STRATIFIED GAS-LIQUID FLOW IN PIPES

Taitel & Dukler[32] produced a simple model for stratified flow in a pipe from the momentum balances for the gas and liquid phases. The pressure gradient was eliminated between the two equations and the shear stresses replaced using friction factors based on hydraulic diameters. For the gas phase, the hydraulic diameter was based on flow in a closed duct bounded by the pipe walls and the gas-liquid interface, while for the liquid phase, the hydraulic diameter was based on flow in an open channel bounded only by the pipe walls. This method was discussed in Section 2.5.2, where the result:

$$X^2\left[\left(\tilde{u}_\ell\tilde{D}_\ell\right)^{-n}\tilde{u}_\ell^2\frac{\tilde{S}_\ell}{\tilde{A}_\ell}\right]-\left[\left(\tilde{u}_g\tilde{D}_g\right)^{-m}\tilde{u}_g^2\left(\frac{\tilde{S}_g}{\tilde{A}_g}+\frac{\tilde{S}_i}{\tilde{A}_\ell}+\frac{\tilde{S}_i}{\tilde{A}_g}\right)\right]-4Y=0 \qquad (4.70)$$

was presented. The parameter Y is an inclination parameter, proportional to $\sin\theta$ where θ is the angle of inclination to the horizontal, and is therefore zero for horizontal flows. X is the Lockhart-Martinelli parameter, defined by:

$$X^2=\left(\frac{dp}{dz}\right)_\ell \div \left(\frac{dp}{dz}\right)_g \qquad (4.71)$$

All the dimensionless quantities in equation (4.70) can be expressed in terms of the dimensionless liquid height, $\tilde{h}$:

$$\tilde{A}_\ell=0.25\left[\pi-\cos^{-1}\left(2\tilde{h}-1\right)+\left(2\tilde{h}-1\right)\sqrt{1-\left(2\tilde{h}-1\right)^2}\right]$$

$$\tilde{A}_g=0.25\left[\cos^{-1}\left(2\tilde{h}-1\right)-\left(2\tilde{h}-1\right)\sqrt{1-\left(2\tilde{h}-1\right)^2}\right]$$

$$\tilde{S}_i=\sqrt{1-\left(2\tilde{h}-1\right)^2}$$

$$\tilde{u}_g=\tilde{A}/\tilde{A}_g \qquad \tilde{D}_\ell=4\tilde{A}_\ell/\tilde{S}_\ell \qquad \tilde{S}_\ell=\pi-\cos^{-1}\left(2\tilde{h}-1\right)$$

$$\tilde{u}_\ell=\tilde{A}/\tilde{A}_\ell \qquad \tilde{D}_g=4\tilde{A}_g/\left(\tilde{S}_g+\tilde{S}_i\right) \qquad \tilde{S}_g-\cos^{-1}\left(2\tilde{h}-1\right)$$

This method is applicable to turbulent flows as well as laminar flows, and the constants m and n in (4.70) take the value of 1.0 for laminar flow or 0.2 for turbulent flow. There is a unique dependence of liquid height $\tilde{h}$ on the Martinelli parameter, as shown in Figure 4.2 for the case of turbulent flow of both phases.

4.4 TWO-FLUID MODEL FOR STRATIFIED OIL-WATER FLOW

The Taitel & Dukler approach can be extended to apply also to oil-water systems, but making the assumption that the upper phase is the more viscous phase. The behaviour of the two phases in the pipe is therefore geometrically the inverse of gas-liquid flow. By assuming that the interfacial shear stress is equal to the water-wall shear stress, it is possible to derive the expression:

$$X_{ow}^2\left[\left(\hat{u}_w\tilde{D}_w\right)^{-n}\hat{u}_w^2\left(\frac{\tilde{S}_w}{\hat{A}_w}+\frac{\tilde{S}_i}{\hat{A}_w}+\frac{\tilde{S}_i}{\hat{A}_o}\right)\right]-\left[\left(\hat{u}_o\hat{D}_o\right)^{-\ell}\hat{u}_o^2\frac{\tilde{S}_o}{\hat{A}_o}\right]-0 \qquad (4.72)$$

where X_{ow}^2 is defined by:

$$X_{ow}^2-\left(\frac{dp}{dz}\right)_w\div\left(\frac{dp}{dz}\right)_o \qquad (4.73)$$

and the dimensionless parameters are similar to those defined by Taitel & Dukler, except that the effective diameters of the two phases will be defined by:

$$\tilde{D}_w-\frac{4\hat{A}_w}{\left(\tilde{S}_w+\tilde{S}_i\right)} \qquad (4.74)$$

and

$$\hat{D}_o-\frac{4\tilde{A}_o}{\tilde{S}_o} \qquad (4.75)$$

Unlike gas-liquid systems where the gas viscosity is unlikely to be more than about 1/100th of the liquid viscosity, it is often the case for oil-water flows that the oil and water viscosities are relatively close. This means that the velocity profiles in the two phases are similar and this in turn has the consequence that the original assumptions in the Taitel & Dukler model, that the gas behaves as if it were flowing in a closed duct and the liquid as if it were flowing in an open channel are probably incorrect (and hence also the hydraulic diameters and shear stresses derived using this assumption are incorrect). Since analytical solutions are available for laminar flows

between flat plates, it was felt that a comparison of the calculated lower phase height should be made with a two-dimensional two-fluid model, to particularly illustrate the effect of the viscosity ratio of the two phases.

A two-fluid model for flow between flat plates may be derived from the equations for flow in a pipe, by taking into account the different geometrical parameters in the two-dimensional geometry, and using the relationship for fully developed laminar flow between flat plates of:

$$f = \frac{12}{Re} \tag{4.76}$$

For gas-liquid flow, equation (4.70) becomes:

$$\left(1-\hat{h}\right)^3 - \left(\frac{2}{X^2}\right)\tilde{h}^2\left(1+\hat{h}\right) = 0 \tag{4.77}$$

with the Martinelli parameter reducing to:

$$X^2 = \frac{1}{\hat{Q}\hat{\mu}} \tag{4.78}$$

while for oil-water flow, equation (4.72) gives:

$$2X_{ow}^2\left(1-\hat{h}\right)^2\left(2-\tilde{h}\right) - \hat{h}^3 = 0 \tag{4.79}$$

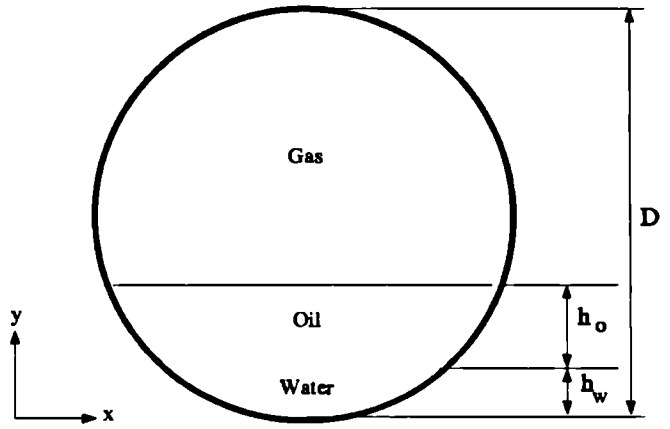
with the same Martinelli parameter as (4.78). The exact solution for the height of the liquid layer in a two-phase laminar flow between flat plates was given by equation (4.38) and it is therefore possible to compare the two-fluid model predictions with an exact value. This comparison is shown in Figures 4.3 and 4.4 for gas-liquid and oil-water flows respectively. In both cases there is excellent agreement when the viscosities of the phases differ by a ratio of more than about 100, but it is clear that for oil-water flows, where the viscosity ratio is likely to be of the order of 10, the two-fluid model leads to a large discrepancy in the calculation of the interfacial height.

Figures 4.5 and 4.6 show a similar comparison for three-dimensional flows in pipes. Here, the 'exact' values have been obtained numerically, by the method to be described in Chapter 5. The interesting feature of flows in pipes compared with flows between flat plates is that the exact values are much closer to the two-fluid model approximation over a wider range of viscosity ratio. It appears that for oil-water flow

in a pipe, the two-fluid model only becomes seriously in error as the viscosity ratio of the two liquid phases approaches the range from 1 to 10. Comparisons to be made with experimental data in later chapters confirm this conclusion.

4.5 THREE-FLUID MODEL OF STRATIFIED OIL-WATER-GAS FLOW IN PIPES

4.5.1 Model derivation



Following the arguments of the Taitel & Dukler two-fluid model for stratified gas-liquid flow, a three-fluid model for stratified oil-water-gas flow will now be developed. First, momentum balances are written for the three phases and the shear stresses are replaced with appropriate friction factor expressions. By eliminating pressure gradient and making variables dimensionless, two simultaneous equations are derived for the height of the water and oil layers, $\hat{h}_w$ and $\hat{h}_o$.

The momentum balances for the three phases are:

$$-A_g\frac{dp}{dz} - \tau_g S_g - \tau_{go} S_{go} - 0 \tag{4.80}$$

$$-A_o\frac{dp}{dz} - \tau_o S_o + \tau_{go} S_{go} - \tau_{ow} S_{ow} - 0 \tag{4.81}$$

$$-A_w\frac{dp}{dz} - \tau_w S_w - \tau_{ow} S_{ow} - 0 \tag{4.82}$$

The fluid-wall shear stresses are expressed by equations of the form:

$$\tau_\phi = C_\phi \left(\frac{D_\phi u_\phi \rho_\phi}{\mu_\phi} \right)^{-n} \frac{\rho_\phi u_\phi^2}{2} \tag{4.83}$$

where C and n take the values 16 and 1 for laminar flow and 0.046 and 0.2 for turbulent flows. By assuming that the gas-oil interfacial friction factor is equal to the gas-wall friction factor, and that the mean gas velocity is much greater than the mean oil velocity, it follows that:

$$\tau_{go} = \tau_g \tag{4.84}$$

For the oil-water interfacial shear stress, the simplifying assumption that the mean velocity of one phase is much greater than the other cannot be made, and the interfacial friction factor is difficult to estimate. For this reason, it is suggested that the oil-water interfacial shear stress is replaced by:

$$\tau_{ow} - \gamma \tau_o \tag{4.85}$$

The factor γ must lie in the range from τ_w/τ_o to 1, because (for a smooth interface) the limits of τ_{ow} are the water-wall shear stress (no oil) and the oil-wall shear stress (no water). As has been discussed earlier (Section 4.1), the value of γ will be estimated using the flat plate models derived earlier. One advantage of using this approximation is that it keeps the algebra as simple as possible. Substituting the shear stress expressions into the momentum balances (4.80), (4.81) and (4.82), eliminating the pressure drop and making variables dimensionless as before, leads to the following two equations:

$$\left(\tilde{D}_g \tilde{u}_g\right)^{-m} \tilde{u}_g^2 \left[\left(\tilde{S}_g + \tilde{S}_{go} \left(1 + \frac{\tilde{A}_g}{\tilde{A}_o} \right) \right) \right] + \frac{\tilde{A}_g}{\tilde{A}_o} X_{go}^2 \left(\tilde{D}_o \tilde{u}_o\right)^{-\ell} \tilde{u}_o^2 \left(\tilde{S}_o + \gamma \tilde{S}_{go} \right) - 0 \tag{4.86}$$

and

$$\left(\tilde{D}_g \tilde{u}_g\right)^{-m} \tilde{u}_g^2 \left(\tilde{S}_g + \tilde{S}_{go} \right) - \frac{\tilde{A}_g}{\tilde{A}_w} X_{gw}^2 \left(\tilde{D}_w \tilde{u}_w\right)^{-n} \tilde{u}_w^2 \tilde{S}_w$$
$$+ \frac{\tilde{A}_g}{\tilde{A}_w} X_{go}^2 \gamma \left(\tilde{D}_o \tilde{u}_o\right)^{-\ell} \tilde{u}_o^2 \tilde{S}_{ow} - 0 \tag{4.87}$$

These equations include Martinelli parameters, for consistency with the two-phase model, which are defined as:

$$X_{go}^2 = \left(\frac{dp}{dz} \right)_o \div \left(\frac{dp}{dz} \right)_g \tag{4.88}$$

and

$$X_{gw}^2 - \left(\frac{dp}{dz}\right)_w \div \left(\frac{dp}{dz}\right)_g \tag{4.89}$$

The dimensionless variables included in equations (4.86) and (4.87) can all be expressed in terms of the heights of the water and oil layers. The cross-sectional areas of the phases are:

$$\tilde{A}_g = \frac{1}{4}\left[\cos^{-1}\left(2\left(\tilde{h}_o + \tilde{h}_w\right) - 1\right) - \left(2\left(\tilde{h}_o + \tilde{h}_w\right) - 1\right)\sqrt{1 - \left(2\left(\tilde{h}_o + \tilde{h}_w\right) - 1\right)^2}\right] \tag{4.90}$$

$$\tilde{A}_w - \frac{1}{4}\left[\cos^{-1}\left(1 - 2\tilde{h}_w\right) - \left(1 - 2\tilde{h}_w\right)\sqrt{1 - \left(1 - 2\tilde{h}_w\right)^2}\right] \tag{4.91}$$

and

$$\tilde{A}_o - \tilde{A} - \tilde{A}_w - \tilde{A}_g \tag{4.92}$$

The dimensionless gas velocity is given by:

$$\tilde{u}_g - \tilde{A}/\tilde{A}_g \tag{4.93}$$

where $\tilde{A} - \pi/4$; similarly the oil and water velocities. The perimeter of pipe wall in contact with each phase is given by:

$$\tilde{S}_g = \cos^{-1}\left(2\left(\tilde{h}_o + \tilde{h}_w\right) - 1\right) \tag{4.94}$$

$$\tilde{S}_w - \cos^{-1}\left(1 - 2\tilde{h}_w\right) \tag{4.95}$$

$$\tilde{S}_o - \pi - \tilde{S}_w - \tilde{S}_g \tag{4.96}$$

and the lengths of the interfaces by:

$$\tilde{S}_{go} - \sqrt{1 - \left(2\left(\tilde{h}_o + \tilde{h}_w\right) - 1\right)^2} \tag{4.97}$$

and

$$\tilde{S}_{ow} - \sqrt{1 - \left(1 - 2\tilde{h}_w\right)^2} \tag{4.98}$$

The dimensionless hydraulic diameters of the three phases are given by:

$$\tilde{D}_g - \frac{4\tilde{A}_g}{\tilde{S}_g + \tilde{S}_{go}} \tag{4.99}$$

$$\hat{D}_o - \frac{4\hat{A}_o}{\hat{S}_o} \tag{4.100}$$

$$\hat{D}_w = \frac{4\hat{A}_w}{\hat{S}_w} \tag{4.101}$$

4.5.2 Model solution

To obtain a solution for the two liquid layer heights, it is necessary to evaluate the oil-water interfacial shear stress, from equation (4.85). The flow for which a solution is required has superficial velocities of the gas, oil and water phases of U_g, U_o and U_w with viscosities μ_g, μ_o and μ_w respectively.

Consider first a two-phase flow between flat plates, with the same gas/liquid ratio, but where the liquid has the oil viscosity. Thus the gas/liquid flowrate ratio would be:

$$\tilde{Q} = \frac{U_g}{(U_o + U_w)} \tag{4.102}$$

and the viscosity ratio:

$$\tilde{\mu} = \frac{\mu_g}{\mu_o} \tag{4.103}$$

The shear stress at the oil-wall contact is given by:

$$\tau_o = -\mu_o \left| \frac{du_o}{dy} \right|_{|y=0} \tag{4.104}$$

where the velocity, u_o, is obtained from equation (4.28). This gives the oil-wall shear stress in a case where there is no water.

Next, the oil-water interfacial shear stress, τ_{ow}, for a three-layer flow between flat plates can be calculated, using the velocity profile given by equation (4.41) and the dimensionless pressure gradient from equation (4.54), evaluated at $y = h_w$. This gives the oil-water interfacial shear stress in the case of no oil-wall contact. The proportionality factor, γ, for a flow with superficial velocities U_g, U_o and U_w is therefore calculated as the ratio of these two shear stresses.

The solution for the two liquid layer heights can now be obtained from equations (4.86) and (4.87) using the dimensionless parameters given by equations (4.88) to

(4.101) and the oil-water interfacial shear stress as described above. The two heights can only be obtained by simultaneous solution of (4.86) and (4.87), which can only be achieved numerically, due to the implicit nature of the equations. The same procedure is used as for the solution of the three-phase flat plate model in equations (4.63) and (4.64).

4.6 COMPARISON WITH EXPERIMENTAL DATA FOR THREE-PHASE STRATIFIED FLOW

The model presented in the preceding section can be compared with experimental data from two sources, namely the experiments of Sobocinski[2] and those of Stapelberg[66], both for stratified flow of oil, water and air. Sobocinski's experiments used diesel oil with a viscosity of 3.8 mPas and holdup was measured using a quick-closing valve system. The volumetric holdup values can be converted to liquid heights using equations (4.90) and (4.91). Data points from the 'stratified' and 'ripple' regimes have been used; in the ripple flow regime, slight ripples were observed on the gas-oil interface, while the oil-water interface remained smooth. Stapelberg used a white mineral oil with a viscosity of about 30 mPas and measured the liquid heights directly through the side of the tube.

The comparison between the three-fluid model and Sobocinski's stratified and ripple flow data is shown in Tables 4.1 and 4.2. The asterisks indicate points where the holdup was not measured. It will be seen that there is good agreement between the values of liquid heights derived from the measured holdup and the values calculated by the model. This is shown more clearly in Figures 4.7 and 4.8. It should be noted that the pressure drops measured in the experiments were very small, and are likely to include large errors and hence agreement between measured and calculated pressure gradient is less satisfactory.

Table 4.1: Comparison of three-fluid model with Sobocinski stratified flow data

	Velocities			Measured Values			Calculated Values			
No	U_o	U_w	U_g	$\tilde{h}_o$	$\tilde{h}_w$	$\frac{dp}{dz}$	$\tilde{h}_o$	$\tilde{h}_w$	$\frac{dp}{dz}$	γ
51	0.022	0.029	2.548	0.085	0.248	2.5	0.087	0.250	3.7	0.331
58	0.031	0.016	2.399	0.149	0.192	0.9	0.151	0.182	3.2	0.400
64	0.010	0.037	2.660	0.066	0.264	1.7	0.036	0.287	3.7	0.300
91	0.049	0.002	2.844	*	*	3.8	0.282	0.047	4.3	0.698
41	0.027	0.049	3.115	0.065	0.275	6.3	0.076	0.292	6.1	0.299
42	0.027	0.049	5.731	0.057	0.230	17.6	0.057	0.225	12.5	0.351
43	0.027	0.043	2.671	0.076	0.251	1.3	0.086	0.292	4.8	0.299
45	0.027	0.043	4.084	0.070	0.243	15.1	0.071	0.245	7.8	0.334
49	0.037	0.027	2.838	0.145	0.229	3.5	0.134	0.219	4.8	0.361
46	0.029	0.063	2.648	0.068	0.330	3.3	0.077	0.345	6.0	0.263

Table 4.2: Comparison of three-fluid model with Sobocinski ripple flow data

	Velocities			Measured Values			Calculated Values			
No	U_o	U_w	U_g	$\tilde{h}_o$	$\tilde{h}_w$	$\frac{dp}{dz}$	$\tilde{h}_o$	$\tilde{h}_w$	$\frac{dp}{dz}$	γ
52	0.022	0.029	3.811	0.075	0.226	8.2	0.072	0.210	6.0	0.365
61	0.033	0.014	3.444	0.125	0.219	3.3	0.140	0.143	5.0	0.446
92	0.051	0.010	2.844	*	*	5.0	0.228	0.119	4.7	0.494
93	0.051	0.008	4.095	*	*	11.5	0.204	0.089	7.1	0.548
50	0.037	0.027	4.174	0.128	0.251	12.6	0.112	0.187	7.6	0.392
71	0.016	0.051	3.862	0.068	0.258	3.8	0.041	0.279	7.2	0.306
47	0.029	0.063	4.007	0.060	0.289	11.3	0.064	0.295	9.2	0.296

The comparison between Stapelberg's stratified flow data and the stratified flow model is shown in Table 4.3 and Figure 4.9. The oil and water heights roughly agree with the model, but it should be noted that the experimental technique for measuring the liquid height was not very accurate. There could be errors due to distortion by the pipe walls and an uncertainty in the location of the exact top and bottom of the pipe. The heights measured were those of the water and air layers, and thus the greatest error would be expected in the oil height derived from them. Figure 4.9 shows that the errors in the water and oil heights are roughly complementary. As in the case of Sobocinski's results, there is broad agreement between the measured and calculated values of pressure gradient.

Table 4.3: Comparison of three-fluid model with Stapelberg stratified flow data

	Velocities			Measured Values			Calculated Values			
No	U_o	U_w	U_g	$\tilde{h}_o$	$\tilde{h}_w$	$\frac{dp}{dz}$	$\tilde{h}_o$	$\tilde{h}_w$	$\frac{dp}{dz}$	γ
3	0.042	0.065	0.386	0.580	0.252	42.7	0.451	0.348	40.4	0.027
10	0.032	0.051	0.604	0.496	0.336	30.2	0.396	0.343	26.4	0.036
30	0.035	0.037	0.386	0.580	0.252	21.8	0.481	0.290	26.4	0.038
31	0.035	0.051	0.386	0.538	0.294	26.8	0.437	0.339	28.0	0.032
32	0.035	0.065	0.386	0.496	0.336	28.3	0.400	0.380	29.6	0.029
33	0.035	0.037	0.495	0.538	0.252	27.9	0.455	0.294	24.7	0.043
34	0.035	0.051	0.495	0.496	0.336	28.1	0.409	0.344	26.0	0.037
35	0.035	0.037	0.604	0.454	0.252	28.3	0.432	0.297	23.5	0.047
36	0.035	0.051	0.604	0.433	0.315	30.5	0.386	0.347	24.7	0.041
37	0.035	0.037	0.714	0.496	0.210	30.0	0.414	0.298	22.7	0.051
38	0.035	0.051	0.714	0.433	0.315	30.2	0.369	0.349	24.1	0.044
39	0.035	0.037	0.823	0.370	0.252	34.0	0.399	0.299	22.3	0.055
40	0.035	0.051	0.823	0.370	0.294	31.4	0.355	0.349	23.8	0.047
44	0.027	0.051	0.823	0.370	0.294	31.4	0.332	0.362	21.3	0.041
45	0.027	0.065	0.386	0.496	0.336	28.3	0.368	0.401	25.0	0.026
47	0.027	0.051	0.604	0.433	0.315	30.5	0.358	0.364	21.4	0.036

The last column in each of the tables of results gives the value of γ, the ratio of oil-water interfacial shear stress to the oil-wall shear stress. Two observations may be made from these figures. Firstly, the ratio γ is clearly very closely related to the oil/water viscosity ratio, showing that the water phase has a much larger effect on the interfacial shear stress in the case where the oil viscosity is higher. Secondly, the ratio varies as expected with oil/water flowrate ratio, as shown particularly by point 91 in Table 4.1, where it is clear that as $U_w \rightarrow 0$ then $\tau_{ow} \rightarrow \tau_o$.

4.7 SUMMARY

This chapter described the development of a three-fluid model for stratified, three-phase oil-water-gas flow in a horizontal pipe.

To begin with, laminar flows between flat plates were considered for single phase, two-phase and three-phase flows, noting that a solution for the liquid heights in the three-phase case could only be obtained numerically.

The Taitel & Dukler two-fluid model for stratified gas-liquid flow in pipes was discussed and adapted for stratified oil-water flow. Here, it was found that the viscosity ratio of the two phases was important and is not considered in the Taitel & Dukler approach. The two-fluid model was found to be in serious error if the ratio of the viscosities of the two phases was less than about 10, often the case in oil-water systems.

A three-fluid model for stratified oil-water-gas flow in pipes was then developed, using a relationship for the oil-water interfacial shear stress from the flat plate models derived at the beginning of the chapter.

Comparisons were made with the experimental data of Sobocinski and of Stapelberg, showing reasonable agreement between measured oil and water heights and the calculated values from the three-fluid model.

Chapter 5:
NUMERICAL MODELLING OF STRATIFIED THREE-PHASE FLOW

5.1 INTRODUCTION

In the previous chapter, a three-fluid model for stratified oil-water-gas flow was derived, making a number of assumptions and approximations. In this chapter, numerical solutions for two- and three-layer stratified flows are developed. For laminar-laminar oil-water flows, this solution can be compared to the exact solution of Ranger & Davis[49] and the two-fluid model from Section 4.4. In oil-water flows it is often the case that the water phase is turbulent, and by including a simple turbulence model, comparisons can be made with the two-fluid model and experimental data, for example from Russell *et al*[13] and from Stapelberg[66]. Finally, for stratified three-phase flow, the numerical solutions can be compared to the data sources of Sobocinski[2] and Stapelberg and the three-fluid model, as discussed in Section 4.6.

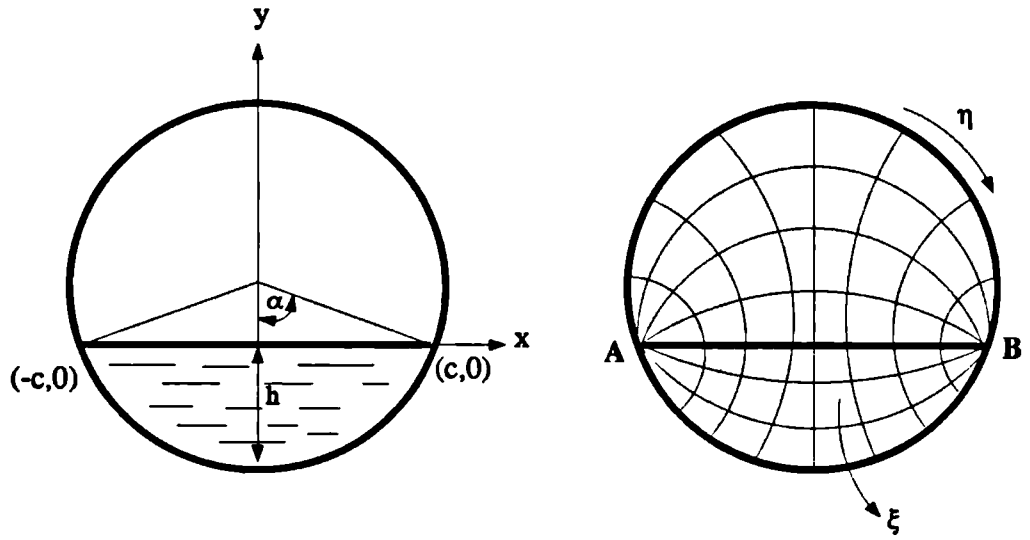
Early numerical solutions, for laminar-laminar stratified oil-water flows, for example by Charles & Redberger[52] and by Gemmell & Epstein,[51] used rectangular coordinate grids. Such grids are always unsatisfactory for stratified flow in a pipe, due to the mismatch of geometry. More recently, Shoham & Taitel[54] and Issa[55] have used bipolar coordinates, described by Bateman[48]. By using an initial guess of liquid height, the finite difference grid can be made to fit the pipe walls and the interface exactly, and the converged velocity profile can be used to give a new estimate of liquid height. Turbulence was accounted for by Shoham & Taitel with a mixing length model, and by Issa using a $k - \epsilon$ model.

One option considered for the extension of this methodology to stratified three-phase flows was to use two bipolar grids located on the gas-oil and oil-water interfaces, and matched so that grid nodes joined in the oil phase. However, this proved impractical, and the solution of using a rectangular grid in the oil phase was adopted. Since the oil phase is normally quite thin, the error of using a rectangular grid was thought to be small. The grids were computed so that lines of constant η in the gas and water

phases exactly matched lines of constant x in the oil phase. Thus, values of velocities at the interfaces could be passed easily between the grids.

5.2 MODELLING OF STRATIFIED TWO-PHASE FLOW

5.2.1 Bipolar coordinate system



The application of the bipolar coordinate system to a two-phase stratified flow in a pipe is illustrated in the figure above. The location of the interface A-B is defined uniquely by the dimensionless liquid height, $\tilde{h} = h/D$ which also defines the two parameters:

$$\frac{c}{R} = \sqrt{1 - \left(2\tilde{h} - 1\right)^2} \tag{5.1}$$

and

$$\alpha = \cos^{-1}\left(1 - 2\tilde{h}\right) \tag{5.2}$$

The transformation from the (x, y) plane to the (ξ, η) plane is defined by[48]:

$$x + iy = ic\cot\left[\frac{\xi + iy}{2}\right] \tag{5.3}$$

from which it follows that:

$$x = \frac{c\sinh\eta}{\cosh\eta - \cos\xi} \tag{5.4}$$

and

$$y = \frac{c\sin\xi}{\cosh\eta - \cos\xi} \tag{5.5}$$

The η-coordinate ranges from $-\infty$ to $+\infty$, with the normal mid-plane (y-axis) at $\eta = 0$ and the points A and B at $\eta = \pm\infty$. A value of $\eta - 5$ can be considered sufficiently close to infinity, particularly since at the points A and B, the velocity must be zero (because these points are on the pipe walls). The ξ-coordinate is an angle in the range $\gamma \leq \xi \leq \gamma + \pi$ with the interface (x-axis) located at $\xi - \pi$.

5.2.2 Navier-Stokes equations

The Navier-Stokes equations are simplified for this situation where the flow is assumed to be steady, fully-developed and horizontal, and using an effective viscosity to account for the turbulent behaviour. Hence for the lower phase, A:

$$\frac{\partial^2 u_A}{\partial \xi^2} + \frac{\partial^2 u_A}{\partial \eta^2} - \frac{1}{\mu_{A,eff}}\left(\frac{dp}{dz}\right)\frac{c^2}{(\cosh \eta - \cos \xi)^2} \tag{5.6}$$

where

$$\mu_{A,eff} = \mu_A + \mu_{A,\varepsilon} \tag{5.7}$$

with $\mu_{A,\varepsilon}$ the effective turbulent viscosity. Similarly for the upper phase, B:

$$\frac{\partial^2 u_B}{\partial \xi^2} + \frac{\partial^2 u_B}{\partial \eta^2} = \frac{1}{\mu_{B,eff}}\left(\frac{dp}{dz}\right)\frac{c^2}{(\cosh \eta - \cos \xi)^2} \tag{5.8}$$

Non-horizontal stratified flows could be treated by absorbing a gravitational pressure gradient term, $\rho g \sin \theta$, into the pressure gradient.

The boundary conditions in the bipolar coordinate system are:

(1)	$\xi - \gamma$	$u_B - 0$	*no slip at pipe walls*
	$\xi - \tau + \gamma$	$u_A - 0$	
(2)	$\xi - \pi$	$\mu_A \frac{\partial u_A}{\partial \xi} = \mu_B \frac{\partial u_B}{\partial \xi}$	*interfacial shear stress equal in both phases*
(3)	$\eta - 0$	$\frac{\partial u_A}{\partial \eta} - 0$	*symmetry*
		$\frac{\partial u_B}{\partial \eta} - 0$	
(4)	$\eta \rightarrow \infty$	$u_A - 0$	*no slip at wall-interface*
		$u_B - 0$	*junction*

Boundary condition (3) is a symmetry condition and implies that the computation need only be performed over half the pipe, ie over the range $0 \leq \eta \leq \infty$.

5.2.3 Finite difference scheme

The two phases are each covered by a (ξ,η) grid whose spacing is adjusted as required to give a close resolution in the region of the walls and the interface. Consider first the lower phase which is spanned by a grid of I+1 points in the η-direction and J+1 points in the ξ-direction, ie:

$$\xi_0 = \pi \twoheadrightarrow \xi_J = \pi + \gamma \tag{5.9}$$

and

$$\eta_0 = 0 \twoheadrightarrow \eta_I = \infty \ (\simeq 5) \tag{5.10}$$

Equation (5.6) can be expressed in finite difference form, for a variable grid spacing $\Delta\xi_j$ and $\Delta\eta_i$:

$$\frac{(u_{i,j+1} - u_{i,j})\Delta\xi_j - (u_{i,j} - u_{i,j-1})\Delta\xi_{j+1}}{\xi_d/2} + \frac{(u_{i+1,j} - u_{i,j})\Delta\eta_i - (u_{i,j} - u_{i-1,j})\Delta\eta_{i+1}}{\eta_d/2}$$

$$= \left(\frac{1}{\mu_{A,eff}}\right)\left(\frac{dp}{dz}\right)\frac{c^2}{(\cosh\eta_i - \cos\xi_j)^2} \tag{5.11}$$

where

$$\eta_d - \Delta\eta_i\Delta\eta_{i+1}(\Delta\eta_i + \Delta\eta_{i+1}) \tag{5.12}$$

and

$$\xi_d = \Delta\xi_j\Delta\xi_{j+1}(\Delta\xi_j + \Delta\xi_{j+1}) \tag{5.13}$$

Equation (5.11) can be rearranged to give:

$$u_{i,j} = P_1 u_{i,j-1} + P_2 u_{i+1,j} + P_3 u_{i,j+1} + P_4 u_{i-1,j} - P_5 \tag{5.14}$$

where

$$u_{i,j} = u_A(\xi_j, \eta_i) \tag{5.15}$$

$$P_1 = \frac{\Delta\xi_{j+1}\eta_d}{P_d} \tag{5.16}$$

$$P_2 = \frac{\Delta\eta_i\xi_d}{P_d} \tag{5.17}$$

$$P_3 - \frac{\Delta\xi_j \eta_d}{P_d} \tag{5.18}$$

$$P_4 - \frac{\Delta\eta_{i+1} \xi_d}{P_d} \tag{5.19}$$

$$P_5 - \left(\frac{dp}{dz}\right) \frac{\xi_d \eta_d}{2 P_d \mu_{A,eff}} \frac{c^2}{(\cosh \eta_i - \cos \xi_j)^2} \tag{5.20}$$

and

$$P_d - \eta_d(\Delta\xi_j + \Delta\xi_{j+1}) + \xi_d(\Delta\eta_i + \Delta\eta_{i+1}) \tag{5.21}$$

A similar set of equations can be derived for the upper phase and are given in Appendix B.1

5.2.4 Turbulence modelling

Because of the complex hydrodynamics of turbulent flow a rigorous solution cannot be obtained. One accepted approach is to use the concept of the eddy viscosity, where essentially the effects of turbulence are simplified into an effective turbulent viscosity. According to the Prandtl mixing length theory,

$$\mu_e(x, y) - \rho \ell_m^2 \left|\frac{du}{dn}\right| \tag{5.22}$$

and the problem is therefore to determine the mixing length ℓ_m. This is not straightforward and various correlations have been suggested, usually restricted to a certain region of the flow, based on the distance from the wall. Most common correlations for mixing length are given in 'wall coordinates' based on the frictional velocity, $u^* - \sqrt{\tau_w/\rho}$, which defines the dimensionless distance $y^+ - yu^*/\nu$. These correlations are generally for single-phase pipe flow where the mixing length is given in terms of the radial distance from the wall. As discussed by Shoham & Taitel, the use of a radial distance is not appropriate in a stratified flow due to the two-dimensional nature of the flow field, and they therefore proposed that the distance y should be measured along a line of constant η. Shoham & Taitel's suggestion was to use the Van Driest correlation:

$$\ell_m - ky\left[1 - \exp\left(-y^+/26\right)\right] \tag{5.23}$$

(where k = 0.4) near the wall and to apply a constant value for ℓ_m in the turbulent core, taken to be the value at $y^+ = 30$. The evaluation of the distance along a line of constant η proceeds as follows:

An arc length element along a line η = constant is given by:

$$d\ell_\xi = \frac{c}{\cosh\eta - \cos\xi} d\xi \tag{5.24}$$

and integrating between two points ξ_1 and ξ_2 gives:

$$\ell_\xi = \frac{2c}{\sqrt{B^2-1}} \left[\arctan\left(\sqrt{\frac{B+1}{B-1}} \tan\frac{\xi}{2} \right) \right]_{\xi_1}^{\xi_2} \tag{5.25}$$

where $B = \cosh\eta$. Note that at $\xi = \pi$,

$$\arctan\left(\sqrt{\frac{B+1}{B-1}} \tan\frac{\pi}{2} \right) - \frac{\pi}{2} \tag{5.26}$$

The dimensionless distance from the walls is then given by:

$$\ell_\xi^+ - \frac{1}{\nu_A}\left(\ell_\xi D \sqrt{\frac{\tau_{wA}}{\rho_A}} \right) \tag{5.27}$$

the mixing length by:

$$\ell_m = k\ell_\xi \left[1 - \exp\left(-\frac{\ell_\xi^+}{26} \right) \right] \tag{5.28}$$

and the turbulent viscosity by:

$$\mu_{A,e} = \ell_m^2 \left| \frac{\partial u_A}{\partial \xi} \frac{\cosh\eta - \cos\xi}{c} \right| \tag{5.29}$$

remembering that if $\ell_\xi^+ \geq 30$ to use the value of ℓ_m evaluated at $\ell_\xi^+ - 30$.

In the region of the interface, a point of some uncertainty is whether the mixing length should be measured from the interface or from the pipe wall. In the former case, the flow will be treated as if it were flowing in a rigid channel bounded by walls and interface, while measuring the mixing length from the pipe wall implies that the turbulent core extends to the interface. In comparisons with experimental data better agreement was obtained by using the latter method.

5.2.5 Solution

The liquid height and pressure gradient were estimated using the two-fluid model described in Section 4.4. From these a finite difference grid could be constructed to fit the estimated interface and the pipe walls. The velocity profile was taken to be converged when the change in the sum of all velocity components in each phase was less than $10^{-4}\%$ from one sweep of the grid to the next. The flowrate of each phase was calculated by summing the products of velocity and cell size over the area of the phase, for example, for the lower phase, A:

$$Q_A = 2c^2 \int_0^{\infty} \int_{\pi}^{\pi+\gamma} \frac{u_A d\xi d\eta}{(\cosh\eta - \cos\xi)^2} = 2c^2 \sum_{i=0}^{I} \sum_{j=0}^{J} \frac{u_{i,j} \Delta\xi_j \Delta\eta_i}{(\cosh\eta_i - \cos\xi_j)^2} \qquad (5.30)$$

This was then compared to the true flowrate, given by:

$$Q_A - \frac{\pi D^2 U_A}{4} \qquad (5.31)$$

to give a new estimate of the height of the lower layer (from the lower layer velocity) or the new pressure gradient (from the upper layer velocity). An arbitrary constraint was imposed of a maximum change in either parameter of 5% at each iteration, to prevent the solution from becoming unstable. This iteration process was repeated until the changes in both water height and pressure drop were less than 0.05% at each successive step.

The finite difference scheme (equations (5.12) to (5.21)), incorporating the turbulence model (equations (5.25) to (5.29)), grid generation and iteration processes was coded in the C language on a SUN Sparcstation IPC. The listing of this code is giving in Appendix B.2. A typical solution time for a laminar-laminar flow was 8 minutes and for a laminar-turbulent flow, 20 minutes.

5.3 CALCULATIONS FOR OIL-WATER FLOWS

5.3.1 Comparison of models

Before comparisons were made with experimental data some trial calculations were preformed to predict the possible pressure drop for oil/water flow operation of the WASP facility at Imperial College (Described in Chapter 8). This is characterised

by the fluid properties and geometry shown in Table 5.1. A range of 7 oil and 7

Table 5.1: WASP pipeline properties

Property	Units	Value
Oil density	kg/m^3	875
Water density	kg/m^3	998
Oil viscosity	mPas	60
Water viscosity	mPas	1.0
Diameter	m	0.0779
Oil superficial velocity	m/s	0 - 0.5
Water superficial velocity	m/s	0 - 0.5

water flowrates was covered to investigate the likely effects of different oil/water ratios. Pressure gradient, water height and shear stresses were calculated from the full numerical model and from the two-fluid model presented in Section 4.4. The pressure gradient was also calculated from the Theissing[26] correlation. There is good agreement between the three methods as shown in Figure 5.1 where pressure gradient is plotted against the Martinelli parameter, defined here by

$$X^2 - \left(\frac{dp}{dz}\right)_{oil} \div \left(\frac{dp}{dz}\right)_{water} \tag{5.32}$$

The holdup is best analysed by calculating the holdup ratio, defined by:

$$\text{holdup ratio} = \frac{\text{input oil/water volume ratio}}{\textit{in situ}\ \text{oil/water volume ratio}} = \frac{(U_o/U_w)_{inlet}}{(U_o/U_w)_{in\ situ}} \tag{5.33}$$

The *in-situ* oil/water ratio is normally larger than the input oil/water ratio when the oil is more viscous than the water due to the lower average velocity of the oil phase. The effect of increasing the water flowrate is shown in Figure 5.2. It will be seen that at higher water superficial velocities (i.e. $U_w \gtrsim 0.1 m/s$), the two-fluid model predicts much higher holdup ratio than the numerical solution.

Shear stresses for the numerical solution were compared with the values obtained from friction factor relationships. For the oil phase (which is laminar) there is good agreement between the two (Figure 5.3), using the oil cross-section and wetted perimeter to define the oil hydraulic diameter:

$$D_o = \frac{4A_o}{S_o} \tag{5.34}$$

In the case of the water phase, however, the shear stress calculated from the friction factor expression is greater than from the numerical solution (Figure 5.4). The interfacial shear stress is compared to the water-wall shear stress in Figure 5.5 where it will be seen that there is good correlation between the two shear stresses, and that they differ in magnitude by a factor of about 7. In the two-fluid model the interfacial shear stress is assumed to be *equal* to the water-wall shear stress, and this is the reason that higher water-wall shear stresses (and higher holdup ratios) are given, in disagreement with the numerical solution. This suggests that in the region where the two-fluid model predicts a much higher wall shear stress than the numerical solution (corresponding to the higher water flowrates), the stratified flow configuration would not be stable. This result is supported by the experimental work of Russell (Section 5.3.3).

5.3.2 Experimental results from the WASP Facility

Some data points for oil-water flows were obtained from the WASP facility by Shires *et al*[70]. The pressure gradient measurements from the experiments were compared with the two-fluid model, the numerical simulation and the Theissing correlation for the four ranges of oil superficial velocities studied. These comparisons are shown in Figures 5.6 to 5.9. It will be seen that at low oil and water superficial velocities, there is good agreement between the various methods and the experimental measurements, supporting the assumption of stratified flow. In Figures 5.6 and 5.7, the experimental measurements rise above the calculations at higher water velocities, as the flow departs from stratified and becomes mixed. In Figure 5.9, the experimental pressure drop is much smaller than the values calculated; this corresponds to dispersed flow, where the entire pipe circumference is water-wet. (Figure 2.9 shows the liquid-liquid flow patterns corresponding to these descriptions).

The holdup in the experiments was estimated by observing the velocity of oil drops in the water phase on video recordings of the flow. This gave the *in-situ* oil-water ratio, which thus allowed calculation of the holdup ratio. The observed values of holdup ratio were then compared with the predicted values from the two-fluid and numerical methods. Figure 5.10 shows the comparison for the smallest oil superficial velocity

range (0.11 to 0.16 m/s), with good agreement between the numerical calculation and the experimental data. This supports the observation of stratified flow for these points. Figure 5.11 shows a similar comparison for the next oil velocity range (0.24 to 0.29 m/s). The disagreement between the experimental results and the numerical model at lower Martinelli parameter (i.e. higher water velocity) corresponds to a departure from stratified flow and establishment of the mixed flow regime.

Figure 5.12 shows a comparison for experimental points which were firmly in the 'mixed' regime. Good agreement is obtained between these points and the two-fluid calculations; the odd point on this figure was for 'dispersed' flow, and it will be seen that the holdup ratio approaches 1, as would be expected.

5.3.3 Experimental results from Russell, Hodgson & Govier

The experiments by Russell *et al*[13] covered a number of liquid-liquid flow patterns, described as stratified, bubble and mixed. Comparisons have been made at two water flowrates, as detailed in Table 5.2. Calculations were performed in a similar way to those described in Section 5.3.2. The measured pressure gradient and the calculations

Table 5.2: Russell experimental parameters

Property	Units	Value
Oil density	kg/m^3	830
Water density	kg/m^3	995
Oil viscosity	mPas	18
Water viscosity	mPas	0.894
Diameter	m	0.02046
Oil superficial velocity	m/s	0.147 - 0.994
Water superficial velocity	m/s	0.219, 0.546

from the numerical solution are compared with the Theissing correlation in Figure 5.13 showing better agreement at the lower water flowrate than at the higher water flowrate. This is because the flow pattern was not smooth stratified at these higher water flowrates.

The holdup ratio from the experiments and the numerical calculations is compared in Figure 5.14. While there is good agreement at the lower water velocity, the holdup

ratio is considerably underpredicted for the higher water velocity. This is due to the mixing between the oil and water at these higher velocities, and as shown in Figure 5.15, the water-wall shear stress at the higher water flowrate is predicted by the friction factor calculations to be much higher than the numerical solutions. As may be seen from Figure 5.14, however, the two-fluid model produces much better predictions of holdup ratio at the higher water flowrate. The oil-wall shear stress from the numerical solutions was found to agree well with the expected values from friction factor (Figure 5.16) in agreement with the results in Section 5.3.2. Figure 5.17 shows a comparison between the interfacial shear stress and the water-wall shear stress, with the same behaviour as described in Section 5.3.2.

5.3.4 Experimental results from Stapelberg & Mewes

As part of their study of oil-water-air flows, Stapelberg & Mewes[71] investigated oil-water flows for the parameters given in Table 5.3. Pressure gradients in flows

Table 5.3: Stapelberg experimental parameters

Property	Units	Value
Oil density	kg/m^3	846.5
Water density	kg/m^3	996.3
Oil viscosity	mPas	28.6
Water viscosity	mPas	0.985
Diameter	m	0.0239
Oil superficial velocity	m/s	0.050 - 0.818
Water superficial velocity	m/s	0.062 - 1.113

which were described as stratified or stratified-wavy were compared to calculations from the Theissing correlation, the two-fluid model and the numerical simulation, and are shown in Figure 5.18. The three calculation methods gave results of similar form to those discussed in Sections 5.3.2 and 5.3.3. However, the experimentally measured pressure gradients were nearly always smaller (by about 10%) than all three calculated values. This is in contrast to the calculations for data from Russell (Section 5.3.3) where experimental pressure drop tended to be higher than predicted values.

The explanation proposed by Stapelberg[66] is that the oil-water interface was curved, so that a greater proportion of the wall was wet by water than would have been expected. This can occur in experiments using pipes of small diameters, where wall-wetting effects are important. It is interesting to note from Stapelberg & Mewes[71] that the pressure drop was higher (for the same Martinelli parameter) for stratified flow in a 2″ pipe than in the 1″ pipe, suggesting that these effects are less significant in larger pipes. Also, it is possible to have flows where the oil-wall contact is increased due to curvature in the opposite direction (Nuland *et al*[11]).

Bentwich[72] considered two-phase laminar flow with a naturally curved interface and showed that pressure drop reduction could be much greater if the water wets the surface preferentially than if the flow is horizontally stratified, as would be expected. With no fluid motion, the contact angle, γ, of the interface is given by:

$$\cos\gamma = \frac{\epsilon_{oil} - \epsilon_{water}}{\sigma} \tag{5.35}$$

where ϵ_i is the surface energy per unit solid surface wetted by phase i and σ is the interfacial tension.

One indication of the importance of surface tension effects is the Weber number,

$$We = \frac{U^2 \rho L}{\sigma} \tag{5.36}$$

which is the ratio of inertial to surface tension forces. It will be seen that for a particular oil (ρ, σ fixed), as the pipe diameter and velocity are increased, the effect of surface tension forces is diminished; thus the greatest effect of interface curvature would be expected at low velocities in the smaller pipe diameter.

Some numerical experiments were therefore tried, to simulate the effect of interface curvature. Referring back to Section 5.2.1, it is clear that this can be achieved by changing the value of the ξ-coordinate in the bipolar grid at which the interface is located. For a flat interface $\xi = \pi$, and this should be increased slightly to make the interface curve upwards towards the walls, thus increasing the water-wet perimeter. This method was tried for points which were labelled as stratified only, to avoid the complication caused by waves. Some results for a water superficial velocity of 0.062 m/s are shown in the top half of Table 5.4, where it will be seen that the

pressure drop predicted when the interface is slightly curved can be considerably smaller than for the same conditions with a flat interface. The angle, α, by which the interface position must be deviated (ie from $\xi = \pi$ to $\xi = \pi+\alpha$) is also recorded; smaller deviations are needed at higher oil velocities in accordance with the above discussion. In the second half of the table, results are given for a water superficial velocity of 0.117 m/s, where a minimum was found in pressure gradient as a function of α, but this was never as small as the measured pressure gradient. It must be concluded that at the higher water velocity, there must be a second mechanism for the reduction in measured pressure gradient.

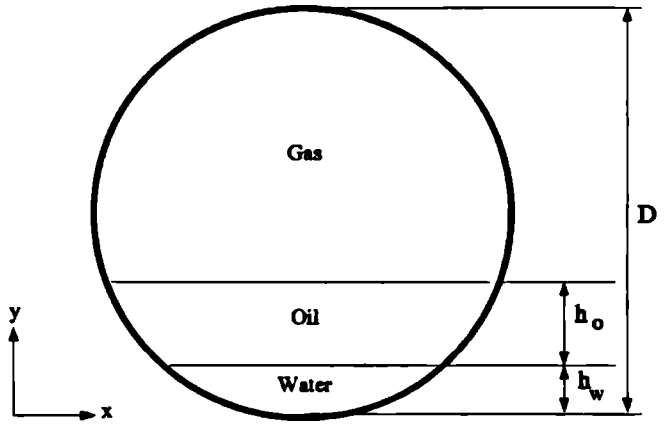
Table 5.4: Effect of moving the interface position on prediction of Stapelberg pressure gradient results

Point	U_o	U_w	$\left(\frac{dp}{dz}\right)_{meas}$	$\left(\frac{dp}{dz}\right)_{flat}$	$\left(\frac{dp}{dz}\right)_{\alpha}$	α
11	0.137	0.062	157.2 ±4.6	212.1	153.4	0.30
21	0.220	0.062	240.8 ±11.0	311.6	236.1	0.16
51	0.286	0.062	294.8 ±7.5	392.5	289.3	0.15
2	0.051	0.117	85.3 ±3.9	142.0	142.0	0.00
12	0.138	0.117	176.2 ±10.1	269.1	239.9	0.20
22	0.224	0.117	244.5 ±3.5	366.7	285.7	0.40

5.3.5 Experimental results from Charles

Charles[53] performed an experimental study of the flow of crude oil with water in a laboratory pipeline (1″ diameter) and a field-scale pipeline (2.45″ diameter). The viscosity of the oil was strongly dependent on the temperature, ranging from 0.124 to 0.910 Pas in the field line and 0.520 to 1.20 Pas in the laboratory. For this reason, all results are expressed as pressure gradient reduction factors. Experimental results are compared to calculations from the numerical solution and the Theissing correlation in Figures 5.19 and 5.20. It will be seen that the experimental pressure gradient reduction factors are much higher than those calculated. This suggests considerable deviation from a stratified flow, with water covering a much greater fraction of the pipe perimeter than would be the case for a stratified flow.

5.4 MODELLING OF STRATIFIED THREE-PHASE FLOW



The situation under consideration in this section is the stratified three-layer flow depicted in the above figure. A bipolar coordinate grid based on the gas-oil interface was used for the gas phase, a bipolar grid based on the oil-water interface for the water phase and a rectangular grid for the oil phase. The grid spacing in the η- and y-directions was arranged so that grid lines were continuous through the three phases, while the grid spacing in the ξ- and x-directions was arranged to give a fine resolution at the walls and the interfaces. The final grid is shown schematically in Figure 5.21. The discretised momentum equations are as given in equations (5.12) to (5.21) for the gas and water phases, and for the oil phase by:

$$\frac{\partial^2 u_o}{\partial x^2} + \frac{\partial^2 u_o}{\partial y^2} = \frac{1}{\mu_{o,eff}}\left(\frac{dp}{dz}\right) \tag{5.37}$$

The turbulence modelling is as for two-phase flow, described in Section 5.2.4, except that for the oil phase, the mixing length is measured along a line of constant x from the wall.

Once again, the difficulty of whether the turbulent core extends to the interfaces needs to be addressed. The solution adopted here, following the work done in Section 5.2, was to measure mixing length from the pipe walls only, with a turbulent core extending to the interfaces. For the water and gas phases this length was measured along lines of constant η while the normal distance was used in the oil phase. These assumptions were considered to be the most appropriate representation of the flow fields.

Starting with the superficial velocities of the three phases, and their physical properties, initial guesses for the water height, oil height and pressure gradient were obtained from the three-fluid model described in Chapter 4. Using these values, the velocity fields were considered to be converged when the convergence criterion that the change in the sum of all velocity components should be less than $10^{-4}\%$ between sweeps of the grids, for each phase, was satisfied. The flowrate of each phase was calculated (as in equation (5.30)) with the water flowrate used to update the water layer height, oil flowrate the oil height and gas flowrate the pressure gradient. These values were then used as initial guesses for a recalculation of the velocity profiles. This process was repeated until the flowrates of all three phases agreed with the original superficial velocities to better than 1%.

It was found that the number of iterations required to converge the velocity profile increased from several hundred (for a two-phase flow) to between 5000 and 10000 for a three-phase flow. This is due to the 'floating' oil layer: the necessity for a fine grid in the region of the two interfaces slows down the movement of numerical information from one part of the grid to another. The speed of calculation would be greatly increased in this case by using three parallel processors, one calculating for each phase. For a flow where all three phases were laminar, 20 to 40 iterations of the outer loop (liquid heights and pressure gradient) were required for convergence, with the number of iterations of the inner velocity profile loop reducing with each outer iteration. In a fully turbulent case, up to 80 outer iterations were required, mainly due to the under-relaxation of the eddy viscosity calculations to prevent numerical instability. Consequently, the solution time, on a SUN Sparcstation IPC ranged from 20 minutes for a laminar flow to 3 hours for a fully turbulent flow.

5.5 CALCULATIONS FOR OIL-WATER-GAS FLOWS

5.5.1 Stapelberg & Mewes

Stapelberg & Mewes[73] studied oil-water flow as a boundary condition to three-phase oil-water-air flows, as discussed in Section 5.3.4. It was observed that at constant oil flowrate, addition of a small flowrate of water caused a decrease in pressure gradient. The observed decrease was greater than that calculated from a stratified oil-water flow model, and it was explained in Section 5.3.4 that this was due (at least in part) to curvature of the oil-water interface. If a small gas flow was added to the oil-water flow, a *further* decrease in pressure gradient was caused. This was because the addition of the gas phase reduced the oil-wall contact at the top of the pipe. Further increase in the gas flowrate, however, caused the pressure gradient to increase (due to increased velocity).

The experimental results were compared by the authors to the Lockhart & Martinelli[22] correlation, by combining the two liquids into one homogeneous phase. Such an approach is clearly not applicable in a flow of this type where the oil and water are separate, and it was therefore not surprising that neither the qualitative behaviour not the absolute values of the pressure gradients were calculated.

Using the stratified flow model described in Section 4.5, the absolute values of the pressure gradient are predicted more closely, but have a maximum at $Re_w = 1000$ as shown in Table 5.5. At these very low flowrates, the flows are laminar, and the three-fluid model is not as accurate under these circumstances as it is for turbulent flows.

Using the numerical solution, the qualitative variation of the pressure gradient with gas flowrate is matched, and the absolute values are reasonable. The least accurate predictions are for oil-water flow for the reason discussed earlier. The results of the calculations are shown in Table 5.5 and Figure 5.22.

Table 5.5: Results of numerical calculations with Stapelberg three-phase data

Re_{oil}	Re_{water}	Re_{gas}	$\left(\frac{dp}{dz}\right)_{num}$	$\left(\frac{dp}{dz}\right)_{3f}$	$\left(\frac{dp}{dz}\right)_{meas}$
28	0	0	49.2	-	50.0
28	1000	0	43.2	-	31.2
28	1000	500	30.6	26.6	24.5
28	1000	1000	30.4	27.3	28.0
28	1000	1500	30.9	22.4	36.2
28	1400	0	45.7		32.4
28	1400	500	31.9	29.1	26.3
28	1400	1000	31.6	29.7	30.0
28	1400	1500	32.2	24.0	37.0

5.5.2 Sobocinski

The most important validation of the numerical calculations was against the experimental data of Sobocinski[2], which was for stratified flow of turbulent gas and laminar or turbulent liquids. This data was used to test the full simulation with gas, oil and water phases using the mixing length turbulence model. In the original thesis, the experimental data points were classified in terms of flow patterns. Of the many points, ten were listed as stratified flow and seven as 'ripple' flow (slight ripples on the air-oil interface). For most of these points, holdup as well as pressure drop was measured.

For the purpose of this study, the stratified and ripple points were taken together; there was no discernible difference in the results for either of these regimes. It was found that a grid of 25 points in each direction was necessary for the solution and that the change in turbulent viscosity had to be limited to a maximum of 5% at each iteration to prevent the solution from becoming unstable.

The results are presented in a number of formats. In Figures 5.23 and 5.24, the oil and water heights calculated from the numerical method are compared with the measured values and the values obtained from the three-fluid model. It can be seen that the agreement is very good, with a slight underprediction of oil height and slight

overprediction of water height. Because the oil holdup is a function of both the water height and the oil height, it is useful to compare the holdup with the experimental measurements. This is shown in Figure 5.25 where the first of each pair of bars is the experimental result and the second the numerical result. The prediction of both water and oil holdup is very good.

Figure 5.26 shows the pressure gradient. Both the three-fluid model and the numerical model underpredict the pressure gradient with respect to the experimental results, but they agree reasonably well with one another. It should be noted firstly that the error in measurement of such small pressure drops would have been proportionally quite large. Secondly, the best available pressure gradient correlations gave errors of an order of magnitude (or more) in pressure gradient for these points, so the models presented in Chapters 4 and 5 represent a considerable improvement in predictive capabilities.

5.5.3 Nuland

A few measurements of holdup are available in a recent paper by Nuland *et al*[11] who developed a single beam dual-energy gamma densitometer for the measurement of holdup in three-phase flows. The nuclear technique was compared to measurements using quick-closing valves, which in this facility gave very accurate holdup measurements. The single beam was aligned so that it passed vertically through the axis of the pipe and holdup was calculated assuming flat interfaces between the three phases.

Results were presented in the format of holdup measurements against superficial gas velocity. Figure 5.27 shows a comparison of measured values using quick-closing valves and gamma densitometry with the calculated values using the three-fluid model. The value of oil holdup from the gamma densitometry method was generally too low while water holdup was too high; this was believed to be due to interface curvature. The three-fluid model fits the quick-closing valve values very well. Figure 5.28 shows a comparison of the numerical solution with the three-fluid model showing very good agreement between the two methods.

5.6 SUMMARY

In this chapter a numerical method for modelling stratified three-phase flow was derived. Significant features of this modelling were the use of the *bipolar* coordinate system to match the gas and water phases and the use of the mixing length model to calculate effective turbulent viscosity. In the oil phase a rectangular coordinate grid was used.

Calculations using an oil-water model were compared with experimental data from the WASP facility, Russell *et al*, Stapelberg & Mewes and Charles. In the case of Stapelberg & Mewes, the oil-water interface was curved so that a model using a flat interface overpredicted pressure gradient. It was shown how the numerical model could be adapted to take account of this curvature. Very poor agreement was obtained with the results of Charles, who studied flows of water and crude oil. This was believed to be because the flows in these experiments were not stratified, with water covering a much greater fraction of the pipe perimeter than would be the case for stratified flows.

Calculations for oil-water-gas flows were compared to data from Stapelberg & Mewes, Sobocinski and Nuland *et al* showing excellent agreement. In the case of the work of Stapelberg & Mewes, the numerical calculation has been the only method to correctly predict the variation of pressure gradient with gas flowrate for very low flows (laminar in all three phases).

THIS IS A BLANK PAGE

Chapter 6:
FLOW PATTERN TRANSITIONS IN THREE-PHASE FLOW

6.1 INTRODUCTION

In the preceding two chapters, models for stratified three-phase flows in horizontal pipes have been developed, starting with a three-fluid one-dimensional model, and confirming the results of this model using a numerical simulation. However, under the conditions at which many pipelines in the petroleum industry are operated, the slug flow regime often occurs. Although pipelines can be operated in the stratified flow regime, it is more frequently the case that slug flow is observed. This is either due to the liquid and gas velocities which are required in order to transport the required quantities of oil and gas through the pipeline, or due to inclination effects, pipelines rarely being always horizontal. It is important to understand the characteristics of slug flows in the design of sub-sea pipelines and equipment, due to the fluctuations in pressure and in liquid throughput.

Here, the important transition boundary between stratified and slug flow in a purely horizontal pipe is considered, and in particular, the effect of a second liquid phase is examined. Two approaches are considered, starting with steady state ('Kelvin-Helmholtz') theory, as applied by Taitel & Dukler[32], and then proceeding to examine linear stability theory, which considers the time-dependence of wave growth.

From the steady state (Taitel & Dukler) approach, it is quite clear that there can be a large difference in predicting the transition between stratified and slug flows in the two extreme cases; namely, where the oil and water phases flow as separate layers and where the oil and water are well-mixed. This is particularly true when the oil forms the continuous phase of an oil-water dispersion. Thus, the prediction of whether the oil and water form separate phases or are always dispersed is considered, using some simple order-of-magnitude arguments. The presence of a separate water layer, apart from influencing the transition boundary, can also lead to operational problems in industrial pipelines. For example, separated water can accumulate at low points in pipelines, where it then causes excessive corrosion, and possibly the development of leaks. This is known to have occurred in oil pipelines in Bahrain[61], where, at

low velocities, water had been able to settle out and cause significant pitting of the lower part of the pipe walls.

Finally, the smooth-to-wavy transition for an oil-water interface in stratified three-phase flow is considered by adapting the Jeffreys model proposed by Taitel & Dukler for the description of the stratified smooth to stratified wavy transition in gas-liquid flow and comparing the results with the data of Sobocinski[2].

6.2 TRANSITION FROM STRATIFIED TO INTERMITTENT FLOW USING STEADY-STATE (KELVIN-HELMHOLTZ) THEORY

6.2.1 Kelvin-Helmholtz instability in a two-dimensional channel

The Kelvin-Helmholtz instability arises at the interface of two fluid layers of different densities ρ_g and ρ_ℓ flowing horizontally with velocities u_g and u_ℓ. By assuming that the flow is incompressible and inviscid and applying a small perturbation it can be shown (Ishii[74]) that the solution for the wave velocity is given by:

$$C = \frac{\rho_\ell u_\ell + \rho_g u_g}{\rho_\ell + \rho_g} \pm \left[C_\infty^2 - \rho_g \rho_\ell \left(\frac{u_g - u_\ell}{\rho_\ell + \rho_g} \right)^2 \right]^{\frac{1}{2}} \tag{6.1}$$

where

$$C_\infty^2 = \frac{g}{k}\left(\frac{\rho_\ell - \rho_g}{\rho_\ell + \rho_g} \right) + \frac{\sigma k}{(\rho_\ell + \rho_g)} \tag{6.2}$$

The displacement of the interface from the equilibrium configuration is proportional to $\exp[ik(x - Ct)]$ and can therefore grow exponentially if the imaginary part of the wave velocity is non-zero. This will occur when:

$$\left[\frac{g}{k}\left(\frac{\rho_\ell - \rho_g}{\rho_\ell + \rho_g} \right) + \frac{\sigma k}{(\rho_\ell + \rho_g)} \right] < \rho_g \rho_\ell \left(\frac{u_\ell - u_g}{\rho_\ell + \rho_g} \right)^2 \tag{6.3}$$

which rearranges to give:

$$(u_g - u_\ell)^2 \geq \left(\frac{\rho_\ell + \rho_g}{\rho_g \rho_\ell} \right) \left[\sigma k + \frac{g}{k}(\rho_\ell - \rho_g) \right] \tag{6.4}$$

For a system with finite depths h_ℓ and h_g, modified densities of $\rho_g \coth kh_g$ and $\rho_\ell \coth kh_\ell$ should be used, leading to:

$$(u_g - u_\ell)^2 \geq [k^2\sigma + (\rho_\ell - \rho_g)g] \frac{h_g}{\rho_g} \left[\frac{\tanh(kh_g)}{kh_g} + \frac{\rho_g}{\rho_\ell} \frac{\tanh(kh_\ell)}{kh_g} \right] \tag{6.5}$$

For large wavelengths ($k \rightarrow 0$), the gravity term dominates and the stability criterion becomes:

$$(u_g - u_\ell)^2 \geq (\rho_\ell - \rho_g) g \frac{h_g}{\rho_g} \tag{6.6}$$

6.2.2 Taitel & Dukler transition model for flow in a pipe

If it is assumed that $u_g \gg u_\ell$ then equation (6.6) simplifies to give:

$$u_g^2 \geq (\rho_\ell - \rho_g) g \frac{h_g}{\rho_g} \tag{6.7}$$

Taitel & Dukler modified this equation for flow in a pipe for waves of finite amplitude, to give:

$$u_g > C_2 \left[\frac{(\rho_\ell - \rho_g) g \cos\theta A_g}{\rho_g \frac{dA_\ell}{dh}} \right]^{\frac{1}{2}} \tag{6.8}$$

It was suggested that the correction factor, C_2, be estimated by a linear relationship with the liquid height:

$$C_2 - \frac{A'_g}{A_g} \simeq 1 - \frac{h_\ell}{D} \tag{6.9}$$

Equation (6.8) can be expressed in dimensionless form as:

$$Fr^2 \left[\frac{1}{C_2^2} \frac{\hat{u}_g \frac{d\tilde{A}_\ell}{d\tilde{h}_\ell}}{\hat{A}_g} \right] \geq 1 \tag{6.10}$$

where Fr is the Froude number, modified by the density ratio:

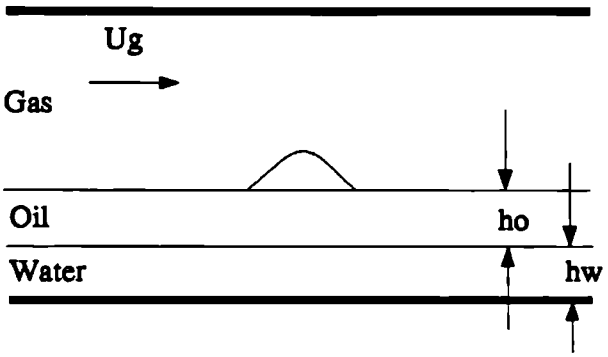
$$Fr = \sqrt{\frac{\rho_g}{(\rho_\ell - \rho_g)}} \frac{U_g}{\sqrt{Dg\cos\theta}} \tag{6.11}$$

This transition boundary is displayed in Figure 2.8 by line A.

6.2.3 Taitel & Dukler transition model applied to oil-water-gas flow: separate oil and water layers

To extend the work in the previous section to the prediction of transition to the slug regime in separated oil-water-gas flow, it is assumed that the instability grows on the gas-oil interface, but using the equilibrium level of oil plus water, calculated using

the three-fluid stratified flow model discussed in Chapter 4, and assuming that the water layer is undisturbed, as shown in the figure below.



In dimensionless form, the criterion becomes:

$$F_T^2 \left[\frac{1}{C_2^2} \frac{\tilde{u}_g \frac{d\tilde{A}_o}{d\tilde{h}_o}}{\tilde{A}_g} \right] \geq 1 \tag{6.12}$$

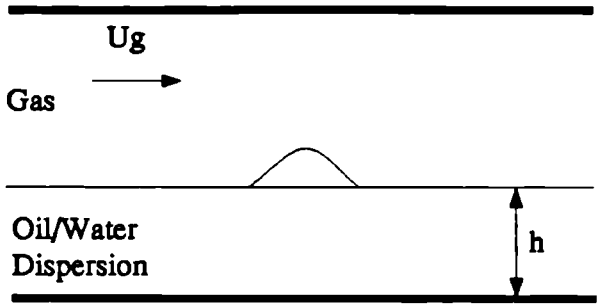
where the Froude number is given by

$$F_T = \sqrt{\frac{\rho_g}{(\rho_o - \rho_g)}} \frac{U_g}{\sqrt{Dg \cos\theta}} \tag{6.13}$$

The oil density is used because the instability is assumed to occur in the oil layer, and thus the stabilising force is the hydrostatic head of an oil wave.

An iterative solution is required to find the transition boundary. For a given gas superficial velocity, an oil velocity is selected and the water velocity calculated to maintain the required water fraction. The oil and water heights are calculated from the three-fluid model and the two values of Froude number are obtained from equations (6.12) and (6.13). The oil superficial velocity (and hence water superficial velocity) is adjusted and the cycle repeated until (6.12) and (6.13) give the same Froude number. Figure 6.1 shows the results of these calculations, for various water fractions, for a flow where the oil/water viscosity ratio was 40, together with the transition lines for two-phase gas-water and gas-oil flows. It will be seen that the different fractions of water have a very small effect, but there is a marked difference between the transition for three-phase flow and the two-phase flows.

6.2.4 Taitel & Dukler transition model applied to oil-water-gas flow: dispersed oil and water layers



In this context, 'dispersed' means that the oil and water phases are mixed and a water layer does not separate out between slugs. If the flow is dispersed, it is necessary to determine which of the two liquids forms the continuous phase. This will depend principally on the surface chemistry and the volumetric ratio of the two liquids; however, it is very difficult to determine a precise inversion point. One method for doing this is from pressure drop measurements, as discussed in Chapter 3. The pressure drop is calculated from one of the available pressure drop correlations, assuming the liquid viscosity to be a volume-average mean of the oil and water viscosities. If the ratio of predicted to measured pressure drop is plotted against the volume fraction of one of the liquids, a sharp transition should be observed at the inversion point. Figure 3.3 shows the results of this analysis applied to Malinowsky's data, which was slug flow where the liquids were dispersed, and it can be seen that inversion occurs at an oil fraction in the liquid phase of about 0.46.

Having established the inversion point, the effective viscosity of the dispersed liquid phases can be estimated from a variety of mixture viscosity equations. One which was found to work well was that of Brinkman[39]:

$$\mu_{\text{eff}} - \frac{\mu_{\text{cont}}}{(1-\phi)^{2.5}} \tag{6.14}$$

It is assumed here that the flow can be treated as a gas-liquid flow with the transition boundary predicted by Taitel & Dukler's method. The above effective viscosity, μ_{eff}, is used in place of the liquid viscosity, while the liquid density, ρ_{eff}, is replaced with a volume average:

$$\rho_{\text{eff}} - \phi\rho_{\text{disp}} + (1-\phi)\rho_{\text{cont}} \tag{6.15}$$

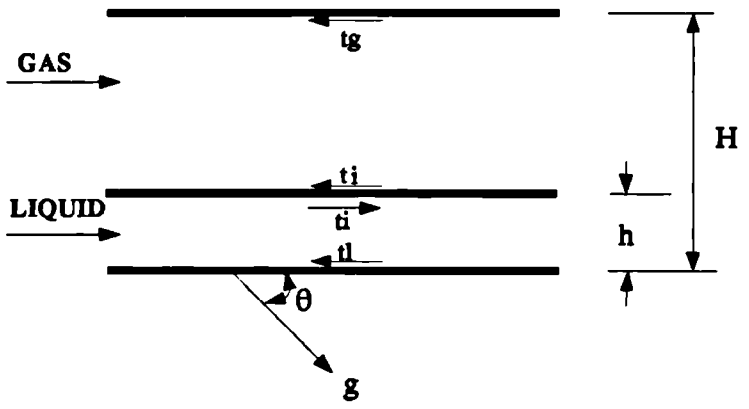
Figure 6.2 shows the resulting transition lines for dispersed liquid phases, for the same oil/water ratio as considered in Figure 6.1 for separated flow. It is assumed here that water fractions less than 50% give rise to dispersions where oil is the continuous phase, and a viscosity in excess of the oil viscosity: transition is therefore predicted at smaller liquid velocity than for gas-oil flow. For water fractions greater than 50%, the flow is assumed to be water-continuous, giving rise to a transition line close to that for gas-water flow, since the effective liquid viscosity is close to that of the water.

Clearly, the prediction of the transition line is very strongly dependent on whether the oil and water form separate phases or flow as a dispersion. This is particularly significant as the inversion point is approached, as demonstrated by the lines for 40% water in Figures 6.1 and 6.2.

6.3 TRANSITION FROM STRATIFIED TO INTERMITTENT FLOW USING LINEAR STABILITY THEORY: TWO-DIMENSIONAL CHANNELS

6.3.1 Conditions for neutral stability for a turbulent-turbulent gas-liquid flow in a two-dimensional channel

This section considers a two-phase flow of gas and liquid in a channel, as depicted in the figure below.



The equations describing neutral instability were obtained by Lin & Hanratty[56] from a linearised form of the liquid momentum balance:

$$\left(\frac{C_R}{u_\ell}\right)^2 - 2\Gamma\left(\frac{C_R}{u_\ell}\right) - h\frac{\hat{\Gamma}_R}{\hat{h}} + \Gamma$$
$$= -\frac{1}{\rho_\ell k u_\ell^2}\left(\frac{\hat{\tau}_{iI}}{\hat{h}} - \frac{\hat{\tau}_{\ell I}}{\hat{h}}\right) + \frac{h}{\rho_\ell u_\ell^2}\left(\frac{\hat{P}_{iR}}{\hat{h}} + \rho_\ell g \sin\theta\right) \tag{6.16}$$

and

$$\left(\frac{\hat{\tau}_{iR}}{\hat{h}} - \frac{\hat{\tau}_{\ell R}}{\hat{h}}\right) - \left(\frac{\tau_i}{h} - \frac{\tau_\ell}{h}\right) + kh\frac{\hat{P}_{iI}}{\hat{h}} + (2\Gamma - 1)\left(\frac{C_R}{u_\ell} - 1\right)\rho_\ell \frac{u_\ell^2}{h}\frac{dh}{dz} - 0 \tag{6.17}$$

The real and complex components of the amplitude of the fluctuation in P_i, the gas pressure at the interface, are derived from a linearized gas phase momentum balance:

$$\frac{\hat{P}_{iR}}{\hat{h}} - \frac{\rho_g}{(II - h)}[C_R^2(\Gamma_g - 1) - \Gamma_g(u_g - C_R)^2$$
$$-u_g^2(II - h)\frac{\hat{\Gamma}_{gR}}{\hat{h}} - (II - h)g\sin\theta - \frac{1}{k\rho_g}\left(\frac{\hat{\tau}_{iI}}{\hat{h}} + \frac{\hat{\tau}_{gI}}{\hat{h}}\right)] \tag{6.18}$$

and

$$\frac{\hat{P}_{iI}}{\hat{h}} - \frac{\rho_g}{(II - h)}[\frac{\tau_g + \tau_i}{\rho_g k(II - h)}$$
$$+\frac{1}{\rho_g k}\left(\frac{\hat{\tau}_{iR}}{\hat{h}} + \frac{\hat{\tau}_{gR}}{\hat{h}}\right) + \frac{(2\Gamma_g - 1)(u_g - C_R)u_g}{(II - h)k}\frac{dh}{dz}] \tag{6.19}$$

The fluctuations in the shear stress terms are derived from the expressions for average shear stresses. All the imaginary components are found to be zero and the real components for the case of turbulent plug flow of both phases are given by:

$$\frac{\hat{\tau}_{iR}}{\hat{h}} - \left[\frac{2}{II - h} + \frac{C_R}{u_\ell}\frac{Re_\ell}{f_i}\left(\frac{\partial f_i}{\partial Re_\ell}\right)\frac{1}{h}\right]\tau_i \tag{6.20}$$

$$\frac{\hat{\tau}_{gR}}{\hat{h}} \simeq \frac{2\tau_g}{(II - h)} \tag{6.21}$$

$$\frac{\hat{\tau}_{\ell R}}{\hat{h}} - \left[1.75\left(\frac{C_R}{u_\ell} - 1\right)\right]\frac{\tau_\ell}{h} \tag{6.22}$$

The velocity profile shape factors for both phases are approximated, for turbulent plug flow of both phases, by using:

$$\bar{\Gamma},\bar{\Gamma}_g = 1 \tag{6.23}$$

and

$$\hat{\Gamma},\hat{\Gamma}_g = 0 \tag{6.24}$$

Making the assumptions that $\bar{u}_g \gg C_R$, that the hydraulic gradient $d\bar{h}/dz$ is negligible and that the interface is smooth so that $\bar{f}_i/\bar{f}_s = 1$, the following condition for initiation of slug flow is derived:

$$\frac{U_g}{\sqrt{gH}}\sqrt{\frac{\rho_g}{\rho_\ell - \rho_g}} \geq K(\varepsilon_g)^{\frac{3}{2}} \tag{6.25}$$

where K is given by:

$$\frac{1}{K^2} = 1 + \left(\frac{\varepsilon_g}{1-\varepsilon_g}\right)^{\frac{5}{7}}\left(\frac{C_R}{\bar{u}_\ell} - 1\right)^2\left[1 + 2\left(\frac{1-\varepsilon_g}{\varepsilon_g}\right)\right]^{\frac{8}{7}}\left(\frac{\rho_g}{\rho_\ell}\right)^{\frac{1}{7}}\left(\frac{\nu_g}{\nu_\ell}\right)^{\frac{2}{7}} \tag{6.26}$$

The wave velocity is derived from equation (6.17) by substitution of equations (6.19), (6.20), (6.21) and (6.22), giving:

$$\frac{C_R}{u_\ell} = \frac{3 + 6\left(\frac{1-\varepsilon_g}{\varepsilon_g}\right)^2\tau_i^+ + \left(2\left(\frac{1-\varepsilon_g}{\varepsilon_g}\right) - 1\right)\tau_i^+}{1.75} \tag{6.27}$$

and the void fraction, α, is obtained by solving the two equations for the dimensionless interfacial shear stress, which are obtained from the friction factor expressions and the steady state liquid phase momentum balance respectively:

$$\bar{\tau}_i^+ = \left(\frac{\rho_g}{\rho_\ell}\right)\left(\frac{U_g}{U_\ell}\right)^{1.75}\left(\frac{1-\varepsilon_g}{\varepsilon_g}\right)^2\left(\frac{\nu_g}{\nu_\ell}\right)^{0.25} \tag{6.28}$$

and

$$\bar{\tau}_i^+ = \frac{1 + \left(\frac{\rho_\ell - \rho_g}{\rho_\ell}\right)\frac{2}{f_\ell}\frac{gH}{U_\ell^2}(1-\varepsilon_g)^3\cos\theta}{\left[1 + 2\left(\frac{1-\varepsilon_g}{\varepsilon_g}\right)\right]} \tag{6.29}$$

For laminar flow of the liquid phase, the equations are slightly different, as given in Section 6.3.2 below.

The transition criterion given by Taitel & Dukler in equation (6.8) may be expressed in a similar format to equation (6.25), but the factor K is given by $K = 1 - h_\ell/II$ which is equivalent to the void fraction, hence giving the modified criterion:

$$\frac{U_g}{\sqrt{gII}}\sqrt{\frac{\rho_g}{\rho_\ell - \rho_g}} \geq (\varepsilon_g)^{\frac{5}{2}} \tag{6.30}$$

It should be noted that the equations presented in this section are obtained from Lin & Hanratty's paper, but have been extensively simplified. For fuller detail, reference should be made to the original paper. Caution is advised, however, as the original paper contains several typographical errors.

6.3.2 Conditions for neutral stability for turbulent-gas laminar-liquid flow in a two-dimensional channel

In the case of a laminar liquid phase, the shape factor can no longer be assumed to be unity. Also, the liquid wall shear stress needs to be modified. Lin & Hanratty showed that in this case:

$$\tau_\ell = \frac{2\mu_\ell u_\ell}{h} = \frac{h\tilde{P}}{3} \tag{6.31}$$

and

$$\Gamma = \frac{4}{3} + \frac{P}{18} + \frac{P^2}{270} \tag{6.32}$$

where

$$\tilde{P} = \frac{dp}{dz} - \rho_\ell g \cos\theta \tag{6.33}$$

and

$$P = \frac{h^2\tilde{P}}{\mu_\ell u_\ell} \tag{6.34}$$

Hence the amplitudes of fluctuating components may be calculated as:

$$\frac{\hat{\tau}_{\ell R}}{\hat{h}} = \frac{3\mu_\ell u_\ell}{h^2}\left(\frac{C_R}{u_\ell} - 2\right) - \frac{1}{2}\frac{\hat{\tau}_{iR}}{\hat{h}} \tag{6.35}$$

$$\frac{\hat{\tau}_{\ell I}}{\hat{h}} = 0, \qquad \frac{\hat{\Gamma}_I}{\hat{h}} = 0 \tag{6.36}$$

$$270\bar{h}\frac{\hat{\Gamma}_R}{\hat{h}} = \left(2 - \frac{C_R}{u_\ell}\right)(2P + 15)(P + 3) + \frac{3}{2}P\frac{\hat{\tau}_{iR}}{\hat{P}\hat{h}}(2P + 15) \qquad (6.37)$$

With the assumption of a smooth interface, substitution of (6.19), (6.20), (6.21) and (6.31) to (6.37) in (6.17) leads to the following expression for the wave velocity:

$$\frac{C_R}{\bar{u}_\ell} = \left(\frac{6 - P}{9}\right)\left[\left(\frac{18}{6 - P} + 1\right) + 6\left(\frac{1 - \varepsilon_g}{\varepsilon_g}\right)^2 \tau_i + \left(3\left(\frac{1 - \varepsilon_g}{\varepsilon_g}\right) - 1\right)\bar{\tau}_i\right] \qquad (6.38)$$

with

$$P = \frac{2}{\frac{1}{3} + (\bar{\tau}_i^+ - 1)^{-1}} \qquad (6.39)$$

For a horizontal flow, from the liquid phase momentum balance and expressions for the friction factors, it may be shown that:

$$U_\ell = \Xi U_g^{1.75} \Pi^{0.75} \frac{\nu_g^{0.25}}{\nu_\ell} \qquad (6.40)$$

where

$$\Xi = \frac{1}{60.15}\left(\frac{1 - \varepsilon_g}{\varepsilon_g}\right)^2\left[1 + \frac{4}{3}\left(\frac{1 - \varepsilon_g}{\varepsilon_g}\right)\right]\left(\frac{\rho_g}{\rho_\ell}\right) \qquad (6.41)$$

Assuming that the amplitude of fluctuation of the liquid phase shape factor is negligible, ie

$$\frac{\hat{\Gamma}_R}{\hat{h}} \simeq 0 \qquad (6.42)$$

then equation (6.16) for a laminar liquid phase gives:

$$\frac{U_\ell^2}{g\Pi}\frac{\Omega}{(1 - \varepsilon_g)^3} + \frac{U_g^2}{g\Pi}\left(\frac{\rho_g}{\rho_\ell}\right)\frac{1}{\varepsilon_g^3} - \left(\frac{\rho_\ell - \rho_g}{\rho_\ell}\right) = 0 \qquad (6.43)$$

$$\Omega = \left(\frac{C_R}{\bar{u}_\ell}\right)^2 - 2\Gamma\left(\frac{C_R}{\bar{u}_\ell}\right) + \bar{\Gamma} \qquad (6.44)$$

And finally, from equations (6.40) and (6.43):

$$\frac{U_g}{\sqrt{g\Pi}}\sqrt{\frac{\rho_g}{\rho_\ell - \rho_g}} - K_\ell(\varepsilon_g)^{\frac{3}{2}} \qquad (6.45)$$

where

$$\frac{1}{K_\ell^2} - 1 + \frac{\rho_\ell}{\rho_g}\left(\frac{\varepsilon_g}{1-\varepsilon_g}\right)^3 \frac{\Xi^2 \Omega (U_g \Pi)^{1.5} \nu_g^{0.5}}{\nu_\ell^2} \tag{6.46}$$

This final equation is given incorrectly by Lin & Hanratty's equation [60] as:

$$K_\ell = \left[1 - \frac{\Omega \Xi^2}{(1-\varepsilon_g)^3}\left(\frac{\nu_g^4}{\nu_\ell^2 g B^3}\right)\left(\frac{\Pi U_g}{\nu_g}\right)^{3.5}\right]^{\frac{1}{2}} \tag{6.47}$$

although the figures in the paper support the use of the correct equation (6.46).

6.3.3 Reduction to the Kelvin-Helmholtz instability

For a system where $u_g \gg u_\ell$ the Kelvin-Helmholtz instability, Sections 6.2.1 and 6.2.2, can be expressed by:

$$u_g^2 \geq (\rho_\ell - \rho_g) g \frac{h_g}{\rho_g} \tag{6.48}$$

which, by substitution of $U_g - u_g/\varepsilon_g$ and $h_g - \varepsilon_g \Pi$, leads to:

$$\frac{U_g}{\sqrt{g\Pi}} \geq \sqrt{\frac{\rho_\ell - \rho_g}{\rho_g}} (\varepsilon_g)^{\frac{3}{2}} \tag{6.49}$$

Examination of equation (6.26) will show that for a flow where inertial terms are negligible, and $(C_R/\bar{u}_\ell - 1) - 0$, the value of K is calculated to be unity, and the Lin & Hanratty instability collapses to the Kelvin-Helmholtz instability. Similarly, for a very viscous liquid phase, equation (6.46) will lead to $K_\ell - 1$.

6.3.4 Application of two-phase linear stability analysis to three-phase flow in a two-dimensional channel

The development of the linear stability analysis from two-phase to three-phase flow is aided by making a number of assumptions. The most important assumption is that at the point of slug initiation the water layer is *undisturbed.* This has been observed in experiments at Hannover University (Stapelberg[67]) and in the WASP facility at Imperial College for three-phase flows in pipes. Thus, the main difference between the two- and three- phase transitions is the treatment of the shear stress at the lower

surface of the liquid in which the instability occurs. In a two-phase flow this stress is at the liquid-wall interface, while in three-phase flow it is at the oil-water interface.

The unusual feature of a two-dimensional three-phase flow is that there is no contact between the oil phase and any solid surface. This means that the oil velocity is higher and the oil holdup lower than in the absence of water and thus a higher superficial velocity of oil can be tolerated before initiation of slug flow. Also, as a result of the lack of oil-wall contact, the velocity profile in the oil phase will be very flat, and the shape factor will be approximately unity, even for laminar flow of the oil phase.

The final assumptions are that there is a negligible hydraulic gradient along the channel and that the gas velocity is much greater than the wave velocity ($u_g \gg C_R$).

Equations (6.16) and (6.18) can therefore be rewritten for three-phase flow as:

$$\left[\left(\frac{C_R}{\bar{u}_o}\right) - 1\right]^2 = \frac{\bar{h}_o}{\rho_o \bar{u}_o^2}\left(\frac{\rho_g}{h_g}\left[-(\bar{u}_g - C_R)^2 - \bar{h}_g g \sin\theta\right] + \rho_o g \sin\theta\right) \qquad (6.50)$$

which may be rearranged to give, for a horizontal flow:

$$\frac{\Omega_3 U_o^2}{gH\varepsilon_o^3} + \frac{U_g^2}{gH\varepsilon_g^3}\left(\frac{\rho_g}{\rho_o}\right) - \left(\frac{\rho_o - \rho_g}{\rho_o}\right) = 0 \qquad (6.51)$$

where

$$\Omega_3 = \left[\left(\frac{C_R}{u_o}\right) - 1\right]^2 \qquad (6.52)$$

The wave velocity, $C_R/\bar{u}_o$ is obtained from equation (6.17), where the main difference in the case of three-phase flow is that the liquid-wall shear stress, τ_ℓ, must be replaced by the oil-water interfacial shear stress, τ_{ow}. For the case of laminar flow of the oil phase,

$$\tau_{ow} = \frac{1}{2}\rho_o f_o (u_o - u_w)^2 \qquad (6.53)$$

with

$$f_o = 16 Re_o^{-1} \qquad (6.54)$$

The amplitude of fluctuation of the oil-water interfacial shear stress is obtained by differentiation of equation (6.53) with respect to the oil layer height,

$$\frac{\hat{\tau}_{ow}}{\hat{h}_o} = \frac{d\tau_{ow}}{dh_o} = \frac{8\mu_o}{D}\left[\frac{2(\bar{u}_o - u_w)}{\bar{u}_o} - \frac{(\bar{u}_o - u_w)^2}{\bar{u}_o^2}\right]\frac{du_o}{dh_o} \qquad (6.55)$$

Lin & Hanratty showed that:

$$\frac{du_o}{dh_o} - \frac{\hat{u}_o}{\hat{h}_o} = \frac{C_R - u_o}{h_o} \tag{6.56}$$

and substituting this, together with equation (6.53), in equation (6.55) it follows that:

$$\frac{\hat{\tau}_{owR}}{\hat{h}_o} - \frac{\tau_{ow}}{h_o}\left[\frac{2u_o}{(u_o - u_w)} - 1\right]\left(\frac{C_R}{h_o} - 1\right) \tag{6.57}$$

and

$$\frac{\hat{\tau}_{owI}}{\hat{h}_o} - 0 \tag{6.58}$$

Substituting equations (6.19), (6.20), (6.21) and (6.57) into a modified version of equation (6.17) gives the following result for the wave velocity:

$$\frac{C_R}{u_o} - \frac{6\left(\frac{\varepsilon_o}{\varepsilon_g}\right)^2 \tau_i^+ + \left(2\left(\frac{\varepsilon_o}{\varepsilon_g}\right) - 1\right)\tau_i^+ + \left(\frac{2\hat{u}_o}{\hat{u}_o - u_w}\right)}{\left(\frac{2\hat{u}_o}{\hat{u}_o - u_w}\right) - 1} \tag{6.59}$$

where

$$\tau_i^+ - \frac{\tau_i}{\tau_{ow}} \tag{6.60}$$

Because of the presence of three phases it is no longer possible to produce a simple relationship between the void fraction and the gas and liquid superficial velocities, as is obtained, for example, from equations (6.28) and (6.29). Instead, by a similar derivation from the steady-state, fully-developed momentum balances for the three phases and friction factor expressions for the shear stresses, it is possible to derive two equations, which together with the relationship

$$\varepsilon_g + \varepsilon_o + \varepsilon_w - 1 \tag{6.61}$$

can be solved simultaneously for the holdup of each phase:

$$\begin{aligned} &\frac{U_g^{1.75}}{\varepsilon_g^2}\left(\frac{II}{\nu_g}\right)^{-0.25} + \left(1 + \frac{\varepsilon_g}{\varepsilon_o}\right)\frac{U_g^{1.75}}{\varepsilon_g^2}\left(\frac{II}{\nu_g}\right)^{-0.25} \\ &-\left(\frac{\varepsilon_g}{\varepsilon_o}\right)\left(\frac{\rho_o}{\rho_g}\right)\left(\frac{C_o}{C_g}\right)\left(\frac{U_o II}{\nu_o}\right)^{-1}\left(\frac{U_o}{\varepsilon_o} - \frac{U_w}{\varepsilon_w}\right)^2 - 0 \end{aligned} \tag{6.62}$$

and

$$\frac{U_g^{1.75}}{\varepsilon_g^2}\left(\frac{\Pi}{\nu_g}\right)^{-0.25} - \left(1+\frac{\varepsilon_o}{\varepsilon_w}\right)\left(\frac{\rho_o}{\rho_g}\right)\left(\frac{C_o}{C_g}\right)\left(\frac{U_o\Pi}{\nu_o}\right)^{-1}\left(\frac{U_o}{\varepsilon_o}-\frac{U_w}{\varepsilon_w}\right)^2 - \left(\frac{\varepsilon_o}{\varepsilon_w}\right)\left(\frac{\rho_w}{\rho_g}\right)\left(\frac{\Pi}{\nu_w}\right)^{-0.25}\frac{U_w^{1.75}}{\varepsilon_w^2} = 0 \tag{6.63}$$

The solution of this pair of equations can be quite difficult as they are highly coupled. A procedure for solution of equations of this type was discussed in Section 4.2.4.

6.3.5 Comparison of two-dimensional models

In Sections 6.3.1 and 6.3.4, equations were given which allow the calculation of the conditions under which transition from stratified to slug flow will occur. Additionally, equations were presented in Section 6.3.2 for the transition in a two-phase flow with a laminar liquid phase.

Firstly, a comparison should be made with the results presented in Lin & Hanratty's paper. Figure 6.3 shows the transitions calculated in the present work for three cases:

(a) Inviscid Kelvin-Helmholtz transition for turbulent gas and turbulent liquid. (Equation (6.25) with K = 1).

(b) Transition for turbulent gas and turbulent liquid as given by equations (6.25) and (6.26).

(c) Transition for turbulent gas and laminar liquid as given by equations (6.45) and (6.46).

In these examples, a viscosity of 1 mPas was used for a turbulent liquid phase and 100 mPas for a laminar liquid phase. Other properties are shown in Figure 6.4, taken from Lin & Hanratty's paper. There is excellent agreement between the present calculations and those carried out by Lin & Hanratty.

The next comparison is between the inviscid Kelvin-Helmholtz prediction and the modification suggested by Taitel & Dukler. Essentially these correspond to $K = 1$ and $K = \varepsilon_g$ respectively in equation (6.25). This comparison is shown in Figure 6.5 for both water (1 mPas) and oil (100 mPas) liquid phases, together with the calculations using the Lin & Hanratty analysis. It will be seen that the Taitel &

Dukler modification is almost sufficient to convert from the simple Kelvin-Helmholtz transition to the more complex model of Lin & Hanratty which includes liquid inertial effects. Thus the correction of

$$K - \varepsilon_g \tag{6.64}$$

can be interpreted as a correction for the destabilising effects of liquid inertia in a 2D-channel flow as well as a pipe flow, as discussed by Lin & Hanratty.

Calculations using the model derived for three-phase flow were carried out and proved difficult in the two-dimensional geometry; more difficult in fact than was subsequently found for flow in pipes. This may well be because the system itself is not stable. Since it occurs rarely, if at all, in practice, the results are summarised only briefly here. Figure 6.6 shows a comparison for the following flows in a channel of height 75 mm:

(a) Inviscid Kelvin-Helmholtz transition for water

(b) Lin & Hanratty transition line for water (1 mPas)

(c) Lin & Hanratty transition line for oil (10 mPas)

(d) Three-phase transition line with water forming 45% of the total liquid flow

The transition line for the three-phase calculation lies above both the oil and water transition lines predicted by the Lin & Hanratty equations. The total liquid holdup would be expected to be similar to that obtained for a water only flow for the same liquid velocity because the more viscous oil phase has no contact with the channel walls. It should be noted that the oil is travelling at a higher velocity than would be the case in the absence of water, giving a lower relative velocity between the gas and oil layers. Thus a higher liquid velocity can be tolerated before a transition will occur.

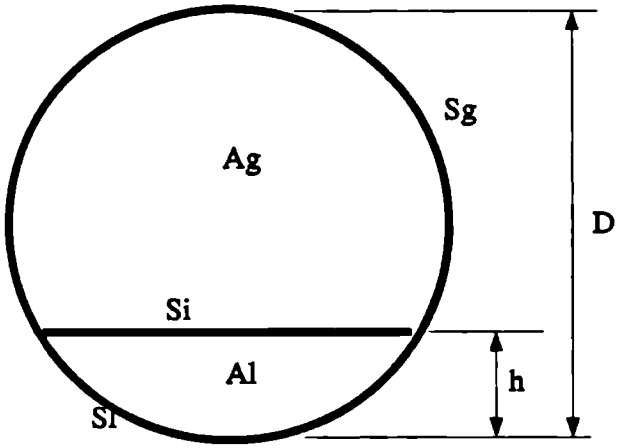
The effect of varying the water fraction is shown by a few points in Figure 6.7. As the fraction of water increases, the transition approaches the inviscid (Kelvin-Helmholtz) line for water. From a simplistic viewpoint, the more viscous oil may be viewed as making the growth of a wave more difficult, while the holdup (liquid level) is largely determined by the properties of the water phase; however, the assumption in the model that the instability occurs at the gas-oil interface becomes increasingly invalid as the oil layer becomes sufficiently thin.

As the water fraction reduces, the oil viscosity has an increasing effect on the holdup. In this case, the transition line moves towards the viscous (Lin & Hanratty) line for oil.

6.4 TRANSITION FROM STRATIFIED TO INTERMITTENT FLOW USING LINEAR STABILITY THEORY: FLOWS IN PIPES

6.4.1 Conditions for neutral stability for a turbulent-turbulent gas-liquid flow in a pipe (Lin & Hanratty)

The instability analysis developed for flow in a channel can be extended to flow in a pipe by the use of appropriate geometric parameters, shown in the figure below, which are related to the dimensionless liquid height, $\tilde{h}$:



$$\tilde{h} = \frac{h}{D} \tag{6.65}$$

$$\tilde{S}_i = 2\sqrt{\tilde{h} - \left(\tilde{h}\right)^2} \tag{6.66}$$

$$\tilde{S}_\ell = \cos^{-1}\left(1 - 2\tilde{h}\right) \tag{6.67}$$

$$\tilde{S}_g - \pi - \tilde{S}_\ell \tag{6.68}$$

$$\tilde{A}_\ell = \frac{1}{4}\left[\tilde{S}_\ell - \tilde{S}_i\left(1 - 2\tilde{h}\right)\right] \tag{6.69}$$

$$\tilde{A}_g - \frac{\pi}{4} - \tilde{A}_\ell \tag{6.70}$$

The amplitudes of the fluctuations of these parameters may be obtained by differentiating the above expressions with respect to $\tilde{h}$, giving:

$$\frac{\hat{\tilde{S}}_i}{\hat{\tilde{h}}} = \frac{d\tilde{S}_i}{d\tilde{h}} = \frac{2\left(1 - 2\hat{h}\right)}{\tilde{S}_i} \tag{6.71}$$

$$\frac{\hat{\tilde{S}}_\ell}{\hat{\tilde{h}}} - \frac{2}{\tilde{S}_i} \tag{6.72}$$

$$\frac{\hat{\tilde{S}}_g}{\hat{\tilde{h}}} - - \frac{\hat{\tilde{S}}_\ell}{\hat{\tilde{h}}} \tag{6.73}$$

$$\frac{\hat{\tilde{A}}_\ell}{\hat{\tilde{h}}} - \frac{1}{4}\left[\left(\frac{\hat{\tilde{S}}_\ell}{\hat{\tilde{h}}}\right) + 2\tilde{S}_i - \left(1 - 2\hat{h}\right)\left(\frac{\hat{\tilde{S}}_i}{\hat{\tilde{h}}}\right)\right] \tag{6.74}$$

By using similar arguments to those for a 2D-channel flow, it may be shown that the neutral stability equations for a two-phase flow in a pipe, assuming turbulent plug flow in each phase, are:

$$\left[\left(\frac{C_R}{u_\ell}\right)^2 - 2\left(\frac{C_R}{u_\ell}\right) + 1\right]\frac{\hat{A}_\ell}{\hat{h}}$$
$$- -\frac{1}{\rho_\ell k u_\ell^2}\left(\bar{S}_i\frac{\hat{\tau}_{iI}}{\hat{h}} - S_\ell\frac{\hat{\tau}_{\ell I}}{\hat{h}}\right) + \frac{A_\ell}{\rho_\ell u_\ell^2}\left(\frac{\hat{P}_{iR}}{\hat{h}} + \rho_\ell g \sin\theta\right) \tag{6.75}$$

and

$$\left(S_i\frac{\hat{\tau}_{iR}}{\hat{h}} - S_\ell\frac{\hat{\tau}_{\ell R}}{\hat{h}}\right) + \left[\left(\tau_i\frac{\hat{S}_i}{\hat{h}} - \tau_\ell\frac{\hat{S}_\ell}{\hat{h}}\right) + \frac{\hat{A}_\ell}{\hat{h}}\left(\frac{\tau_\ell S_\ell - \tau_i S_i}{A_\ell}\right)\right]$$
$$+ kA_\ell\frac{\hat{P}_{iI}}{\hat{h}} + \left(\frac{C_R}{u_\ell} - 1\right)\frac{dA_\ell}{dz} = 0 \tag{6.76}$$

It will be seen that the main difference from the two-dimensional equations is the inclusion of the geometrical parameters. Since these parameters fluctuate with change in liquid height, the number of terms in the equations is increased.

The pressure variation in the gas phase is obtained once again from the gas phase momentum and mass balances:

$$\frac{\hat{P}_{iR}}{\hat{h}} = \frac{\rho_g}{(A-\bar{A}_\ell)}\left[-\frac{\hat{A}_\ell}{\hat{h}}(\bar{u}_g - C_R)^2 \right.$$
$$\left. -(A-\bar{A}_\ell)g\sin\theta - \frac{1}{k\rho_g}\left(\bar{S}_i\frac{\hat{\tau}_{iI}}{\hat{h}} + \bar{S}_g\frac{\hat{\tau}_{gI}}{\hat{h}}\right)\right] \tag{6.77}$$

and

$$\frac{\hat{P}_{iI}}{\hat{h}} = \frac{\rho_g}{(A-A_\ell)}\left[\frac{\hat{A}_\ell}{\hat{h}}\frac{\bar{u}_g(\bar{u}_g - C_R)}{(A-A_\ell)}\frac{d\bar{A}_\ell}{dz} + \frac{\bar{S}_i\bar{\tau}_i + \bar{S}_g\bar{\tau}_g}{\rho_g k(A-\bar{A}_\ell)}\frac{\hat{A}_\ell}{\hat{h}}\right.$$
$$\left. +\frac{1}{\rho_g k}\left(\bar{S}_i\frac{\hat{\tau}_{iR}}{\hat{h}} + \bar{S}_g\frac{\hat{\tau}_{gR}}{\hat{h}} + \bar{\tau}_i\frac{\hat{S}_i}{\hat{h}} + \bar{\tau}_g\frac{\hat{S}_g}{\hat{h}}\right)\right] \tag{6.78}$$

The fluctuations in the shear stress terms are derived from the expressions for average shear stresses. These are now more complicated than in the two-dimensional case, because the fluctuation in the hydraulic diameter (and hence Reynolds number) has a complicated dependence on the liquid height:

$$\frac{\hat{D}_\ell}{D_\ell} = \frac{\hat{A}_\ell}{\bar{A}_\ell} - \frac{\hat{S}_\ell + \hat{S}_i}{\bar{S}_\ell + \bar{S}_i} \tag{6.79}$$

Hence the real parts of the amplitudes of the wave-induced variation of the three shear stresses are given by:

$$\frac{\hat{\tau}_{\ell R}}{\hat{h}} = \left[1.75\left(\frac{C_R}{u_\ell}\right)\frac{\hat{A}_\ell}{\hat{h}}\frac{1}{A_\ell} - 2\frac{\hat{A}_\ell}{\hat{h}}\frac{1}{\bar{A}_\ell} + \frac{1}{4}\frac{\hat{S}_\ell}{\hat{h}}\frac{1}{\bar{S}_\ell}\right]\tau_\ell \tag{6.80}$$

$$\frac{\hat{\tau}_{iR}}{\hat{h}} = \left[2\frac{\hat{A}_\ell}{\hat{h}}\frac{1}{(A-\bar{A}_\ell)} + \frac{\partial f_i}{\partial Re_\ell}\frac{\bar{Re}_\ell}{\bar{f}_i}\left(\frac{C_R}{u_\ell}\frac{\hat{A}_\ell}{\hat{h}}\frac{1}{A_\ell} - \frac{\hat{S}_\ell}{\hat{h}}\frac{1}{\bar{S}_\ell}\right)\right]\bar{\tau}_i \tag{6.81}$$

$$\frac{\hat{\tau}_{gR}}{\hat{h}} = \left[2\frac{\hat{A}_\ell}{\hat{h}}\frac{1}{(A-\bar{A}_\ell)} + \frac{1}{4}\left(\frac{\hat{S}_g}{\hat{h}} + \frac{\hat{S}_i}{\hat{h}}\right)\left(\frac{1}{S_g + S_i}\right)\right]\bar{\tau}_g \tag{6.82}$$

The dimensionless wave velocity may be obtained by substitution of these quantities into equation (6.76). Here the interface is assumed smooth:

$$f_i/f_s \simeq 1 \tag{6.83}$$

and the hydraulic gradient is assumed negligible:

$$\frac{dA_\ell}{dz} \simeq 0 \tag{6.84}$$

Distances are made dimensionless with respect to the pipe diameter, areas by D^2 and shear stresses by the liquid wall shear stress, so that

$$\tau_i^+ - \frac{\tau_i}{\tau_\ell} \tag{6.85}$$

Hence

$$\frac{C_R}{u_\ell} - \frac{Num}{Den} \tag{6.86}$$

where

$$\begin{aligned} Num - {} & 2\frac{\tilde{S}_\ell}{\tilde{A}_\ell}\frac{\hat{\tilde{A}}_\ell}{\hat{\tilde{h}}} + \psi_\ell\frac{\hat{\tilde{S}}_\ell}{\hat{\tilde{h}}} + 2\left(1+\frac{\tilde{\tilde{A}}_\ell}{\tilde{A}_g}\right)\frac{\tilde{S}_i}{\tilde{A}_g}\frac{\hat{\tilde{A}}_\ell}{\hat{\tilde{h}}}\tau_i^+ \\ & + \tilde{S}_g\frac{\tilde{A}_\ell}{\tilde{A}_g}\tau_i^+\left(2\frac{\hat{\tilde{A}}_\ell}{\hat{\tilde{h}}}\frac{1}{\tilde{A}_g} + \frac{1}{4\left(\tilde{S}_g+\tilde{S}_i\right)}\left(\frac{\hat{\tilde{S}}_g}{\hat{\tilde{h}}}+\frac{\hat{\tilde{S}}_i}{\hat{\tilde{h}}}\right)\right) + \left(1+\frac{\tilde{A}_\ell}{\tilde{A}_g}\right)\tau_i^+\frac{\hat{\tilde{S}}_i}{\hat{\tilde{h}}} \\ & - \frac{\hat{\tilde{S}}_\ell}{\hat{\tilde{h}}} + \frac{\tilde{A}_\ell}{\tilde{A}_g}\frac{\hat{\tilde{S}}_g}{\hat{\tilde{h}}}\tau_i^+ + \left(\frac{\tilde{S}_\ell - \tau_i^+\hat{S}_i}{\tilde{A}_\ell}\right)\frac{\hat{\tilde{A}}_\ell}{\hat{\tilde{h}}} + \left(\frac{\tilde{A}_\ell}{\tilde{A}_g}\right)\left(\frac{\hat{S}_g+\tilde{S}_i}{\tilde{A}_g}\right)\frac{\hat{\tilde{A}}_\ell}{\hat{\tilde{h}}}\tau_i^+ \end{aligned} \tag{6.87}$$

and

$$Den - (2+\psi_\ell)\frac{\tilde{S}_\ell}{\tilde{A}_\ell}\frac{\hat{\tilde{A}}_\ell}{\hat{\tilde{h}}} \tag{6.88}$$

where

$$\psi_\ell - \frac{df_\ell}{dRe_\ell}\frac{Re_\ell}{f_\ell} \tag{6.89}$$

Clearly, $\psi_\ell = -1$ for laminar flow of the liquid phase while for turbulent flow, the friction factor relation:

$$f - 0.079Re^{-0.25} \tag{6.90}$$

would lead to $\psi_\ell - -0.25$.

All quantities in this equation depend on the liquid height, $\tilde{h}$ which may be obtained by solution of the momentum balance for the liquid at *steady-state*, together with the friction factor relationships for shear stresses. A convenient way to do this is to derive the two expressions for dimensionless interfacial shear stress by these two routes and equate them:

$$\tau_i^+ - \left(\frac{\rho_g}{\rho_\ell}\right)\left(\frac{U_g}{U_\ell}\right)^{1.75}\left(\frac{\nu_g}{\nu_\ell}\right)^{0.25}\left(\frac{D_\ell}{D_g}\right)^{0.25}\left(\frac{A_\ell}{A_g}\right)^{1.75} \tag{6.91}$$

and

$$\bar{\tau}_i^+ = \frac{\left[\frac{\bar{\tilde{S}}_\ell}{\bar{\tilde{A}}_\ell} - \frac{2\cos\theta}{0.0791}\left(\frac{D_\ell U_\ell}{\nu_\ell}\right)^{0.25}\left(\frac{U_\ell^2}{gD}\right)^{-1}\left(\frac{\bar{\tilde{A}}_\ell}{\tilde{A}}\right)^2\right]}{\left(\frac{\bar{\tilde{S}}_g}{\bar{\tilde{A}}_g} + \frac{\bar{\tilde{S}}_i}{\bar{\tilde{A}}_g} + \frac{\bar{\tilde{S}}_i}{\bar{\tilde{A}}_\ell}\right)} \tag{6.92}$$

Note that for *horizontal* flow, $\cos\theta = 0$.

Finally, the condition for neutral stability is obtained from equation (6.75) which yields the following equation in terms of geometric parameters defined earlier, the gas and liquid superficial velocities and the gas and liquid densities:

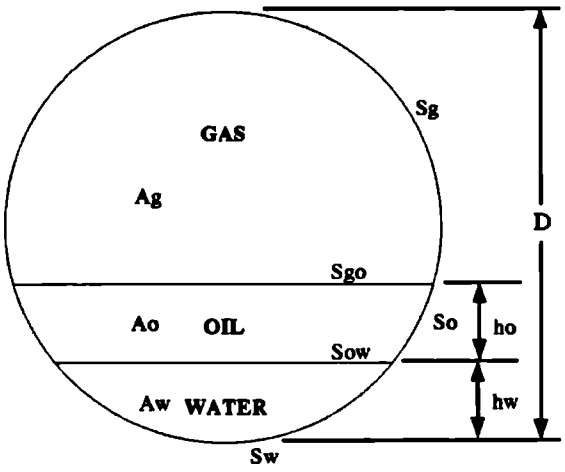
$$\frac{U_\ell^2 \Omega_p}{gD}\left(\frac{\tilde{A}^2}{\bar{\tilde{A}}_\ell^3}\right)\left(\frac{\hat{\tilde{A}}_\ell}{\hat{h}}\right) + \frac{U_g^2}{gD}\left(\frac{\rho_g}{\rho_\ell}\right)\left(\frac{\tilde{A}^2}{\bar{\tilde{A}}_g^3}\right)\left(\frac{\hat{\tilde{A}}_\ell}{\hat{h}}\right) - 1 = 0 \tag{6.93}$$

where

$$\Omega_p = \left(\frac{C_R}{\bar{u}_\ell} - 1\right)^2 \tag{6.94}$$

6.4.2 Application of Lin & Hanratty two-phase analysis to three-phase flow in a pipe

The development of the instability analysis for a three-phase flow in a pipe is a combination of the preceding sections. The assumptions made in deriving the analysis for three-phase flow in a 2D-channel are also made here, together with a geometrical treatment extended from Section 6.4.1. In a circular geometry, there is also a contact between the oil and the wall; however, the velocity profile in the oil phase is still assumed to be very flat, so that the shape factor is unity. The geometrical parameters for this flow configuration are shown in the figure below.



The geometrical parameters are related to the dimensionless water and oil heights, $\tilde{h}_w$ and $\tilde{h}_o$, as follows:

$$\tilde{S}_g = \cos^{-1}\left(2\left(\tilde{h}_w + \tilde{h}_o\right) - 1\right) \tag{6.95}$$

$$\tilde{S}_w = \cos^{-1}\left(1 - 2\tilde{h}_w\right) \tag{6.96}$$

$$\tilde{S}_o - \pi - \tilde{S}_g - \tilde{S}_w \tag{6.97}$$

$$\tilde{S}_{go} - \sqrt{1 - \left(2\left(\tilde{h}_w + \tilde{h}_o\right) - 1\right)^2} \tag{6.98}$$

$$\tilde{S}_{ow} = \sqrt{1 - \left(1 - 2\tilde{h}_w\right)^2} \tag{6.99}$$

$$\tilde{A}_g - \frac{1}{4}\left[\tilde{S}_g - \left(2\left(\tilde{h}_w + \tilde{h}_o\right) - 1\right)\tilde{S}_{go}\right] \tag{6.100}$$

$$\tilde{A}_w = \frac{1}{4}\left[\tilde{S}_w - \left(1 - 2\tilde{h}_w\right)\tilde{S}_{ow}\right] \tag{6.101}$$

$$\tilde{A}_o = \frac{\pi}{4} - \tilde{A}_g - \tilde{A}_w \tag{6.102}$$

Because of the assumption that the water layer is undisturbed at the point of slug initiation, the water height, $\tilde{h}_w$, is constant and hence the only fluctuating terms are those that depend on the oil height, $\tilde{h}_o$. The dependence of the amplitude of fluctuating components on the amplitude of fluctuation in $\tilde{h}_o$ is determined by differentiation with respect to $\tilde{h}_o$ as was performed in Section 6.4.1:

$$\frac{\hat{\tilde{S}}_g}{\hat{\tilde{h}}_o} - \frac{d\tilde{S}_g}{d\tilde{h}_o} - -\frac{2}{\tilde{S}_{go}} \tag{6.103}$$

$$\frac{\hat{\tilde{S}}_{go}}{\hat{\tilde{h}}_o} = -2\left(\frac{2\left(\tilde{h}_w + \tilde{h}_o\right) - 1}{\tilde{S}_{go}}\right) \tag{6.104}$$

$$\frac{\hat{\tilde{S}}_o}{\hat{\tilde{h}}_o} - -\frac{\hat{\tilde{S}}_g}{\hat{\tilde{h}}_o} \tag{6.105}$$

$$\frac{\hat{\bar{S}}_{ow}}{\hat{h}_o} = \frac{\hat{\bar{S}}_w}{\hat{h}_o} - 0 \tag{6.106}$$

$$\frac{\hat{\bar{A}}_g}{\hat{h}_o} = \frac{1}{4}\left[\frac{\hat{\bar{S}}_g}{\hat{h}_o} - \left(2\left(\bar{\tilde{h}}_w + \bar{\tilde{h}}_o\right) - 1\right)\frac{\hat{\bar{S}}_{go}}{\hat{h}_o} - 2\tilde{S}_{go}\right] \tag{6.107}$$

and

$$\frac{\hat{\bar{A}}_o}{\hat{h}_o} = -\frac{\hat{\bar{A}}_g}{\hat{h}_o} \tag{6.108}$$

The neutral stability equations (6.75) and (6.76) must be adapted for three-phase flow. In particular, extra shear stress terms are introduced: this is because the 'lower' side of the oil now has contact with both the pipe wall and the water phase, rather than just the pipe wall in the case of a two-phase pipe flow, or just the water phase in the case of a three-phase channel flow.

$$\left[\left(\frac{C_R}{u_o}\right)^2 - 2\left(\frac{C_R}{u_o}\right) + 1\right]\frac{\hat{A}_o}{\hat{h}_o}$$
$$= -\frac{1}{\rho_o k \bar{u}_o^2}\left(\bar{S}_{go}\frac{\hat{\tau}_{goI}}{\hat{h}_o} - S_o\frac{\hat{\tau}_{oI}}{\hat{h}_o} - S_{ow}\frac{\hat{\tau}_{owI}}{\hat{h}_o}\right) + \frac{A_o}{\rho_o \bar{u}_o^2}\left(\frac{\hat{P}_{iR}}{\hat{h}_o} + \rho_o g \sin\theta\right) \tag{6.109}$$

and

$$\left[\left(\tau_{go}\frac{\hat{S}_{go}}{\hat{h}_o} - \bar{\tau}_o\frac{\hat{S}_o}{\hat{h}_o} - \bar{\tau}_{ow}\frac{\hat{S}_{ow}}{\hat{h}_o}\right) + \frac{\hat{A}_o}{\hat{h}_o}\left(\frac{\tau_{ow}\bar{S}_{ow} + \tau_o S_o - \bar{\tau}_{go}S_{go}}{A_o}\right)\right]$$
$$+\left(\bar{S}_{go}\frac{\hat{\tau}_{goR}}{\hat{h}_o} - \bar{S}_o\frac{\hat{\tau}_{oR}}{\hat{h}_o} - \bar{S}_{ow}\frac{\hat{\tau}_{owR}}{\hat{h}_o}\right) + kA_o\frac{\hat{P}_{iI}}{\hat{h}_o} + \left(\frac{C_R}{u_o} - 1\right)\frac{dA_o}{dz} = 0 \tag{6.110}$$

The variation of gas phase pressure is obtained from the gas phase momentum and mass balances, giving similar equations to (6.77) and (6.78):

$$\frac{\hat{P}_{iR}}{\hat{h}_o} = \frac{\rho_g}{\bar{A}_g}\left[-\frac{\hat{A}_o}{\hat{h}_o}(u_g - C_R)^2 - \bar{A}_g g \sin\theta - \frac{1}{k\rho_g}\left(S_{go}\frac{\hat{\tau}_{goI}}{\hat{h}_o} + S_g\frac{\hat{\tau}_{gI}}{\hat{h}_o}\right)\right] \tag{6.111}$$

and

$$\frac{\hat{P}_{iI}}{\hat{h}} = \frac{\rho_g}{\bar{A}_g}\left[\frac{\hat{A}_o}{\hat{h}_o}\frac{\bar{u}_g(\bar{u}_g - C_R)}{\bar{A}_g}\frac{dA_o}{dz} + \frac{\bar{S}_{go}\bar{\tau}_{go} + \bar{S}_g\bar{\tau}_g}{\rho_g k \bar{A}_g}\frac{\hat{A}_o}{\hat{h}_o}\right.$$
$$\left.+\frac{1}{\rho_g k}\left(\bar{S}_{go}\frac{\hat{\tau}_{goR}}{\hat{h}_o} + S_g\frac{\hat{\tau}_{gR}}{\hat{h}_o} + \bar{\tau}_{go}\frac{\hat{S}_{go}}{\hat{h}_o} + \bar{\tau}_g\frac{\hat{S}_g}{\hat{h}_o}\right)\right] \tag{6.112}$$

The gas-wall shear stress and the gas-oil interfacial shear stress can be evaluated as in the two-dimensional case, in equations (6.81) and (6.82). The oil-wall shear stress, τ_o, may be calculated as follows:

$$\tau_o = \frac{1}{2} f_o \rho_o u_o^2 \tag{6.113}$$

where

$$f_o = C_o Re_o^{-\ell} \tag{6.114}$$

Hence the amplitude of the fluctuation in oil-wall shear stress is given by:

$$\frac{\hat{\tau}_{oR}}{\hat{h}_o} = \left[\frac{C_R}{u_o} \left(\frac{2+\psi_o}{A_o} \right) \frac{\hat{A}_o}{\hat{h}_o} - \frac{2}{A_o} \frac{\hat{A}_o}{\hat{h}_o} - \frac{\psi_o}{S_o} \frac{\hat{\tilde{S}}_o}{\hat{h}_o} \right] \tau_o \tag{6.115}$$

where

$$\psi_o - \frac{df_o}{dRe_o} \frac{Re_o}{f_o} \tag{6.116}$$

and is -1 for laminar flow and -0.25 for turbulent flow of the oil phase. The oil-water interfacial shear stress, τ_{ow}, is obtained by multiplying the oil-wall shear stress by a factor, γ, obtained by the steady-state stratified flow model described by in Chapter 4. Hence:

$$\frac{\hat{\tau}_{ow}}{\hat{h}_o} - \gamma \frac{\hat{\tau}_o}{\hat{h}_o} \tag{6.117}$$

where the proportionality factor, γ, is assumed to be unaffected by the perturbation to the system.

The wave velocity is obtained by substitution of equations (6.81), (6.82), (6.112), (6.115) and (6.117) into equation (6.110), again making the assumptions that the gas-oil interface is smooth and the hydraulic gradient is negligible. This leads to an expression for the wave velocity of the form:

$$\frac{C_R}{u_o} - \frac{Num}{Den} \tag{6.118}$$

where

$$\begin{aligned} Num = {} & 2\tilde{S}_{go} \frac{\bar{\tau}_{go}^{+}}{\tilde{A}_g} \frac{\hat{\tilde{A}}_o}{\hat{\tilde{h}}_o} + \left(\tilde{S}_o + \gamma \tilde{S}_{ow} \right) \left[\frac{\psi_o}{\tilde{S}_o} \frac{\hat{\tilde{S}}_o}{\hat{\tilde{h}}_o} + \frac{2}{\tilde{A}_o} \frac{\hat{\tilde{A}}_o}{\hat{\tilde{h}}_o} \right] + \left(\tau_{go}^{+} \frac{\hat{\tilde{S}}_{go}}{\hat{\tilde{h}}_o} - \frac{\hat{\tilde{S}}_o}{\hat{\tilde{h}}_o} \right) \\ & + \frac{\hat{\tilde{A}}_o}{\hat{\tilde{h}}_o} \left(\frac{\gamma \tilde{S}_{ow} + \tilde{S}_o - \tau_{go}^{+} \tilde{S}_{go}}{\tilde{A}_o} \right) + \frac{\tilde{A}_o}{\tilde{A}_g} \left[\left(\frac{\tau_{go}^{+} \tilde{S}_{go} + \bar{\tau}_{go}^{+} \tilde{S}_g}{\tilde{A}_g} \right) \frac{\hat{\tilde{A}}_o}{\hat{\tilde{h}}_o} + 2\tilde{S}_{go} \frac{\tau_{go}^{+}}{\tilde{A}_g} \frac{\hat{\tilde{A}}_o}{\hat{\tilde{h}}_o} \right. \\ & \left. + \bar{\tilde{S}}_g \left[2 \frac{\tau_{go}^{+}}{\tilde{A}_g} \frac{\hat{\tilde{A}}_o}{\hat{\tilde{h}}_o} + \frac{\tau_{go}^{+}}{4\left(\tilde{S}_g + \tilde{S}_{go} \right)} \left(\frac{\hat{\tilde{S}}_g}{\hat{\tilde{h}}_o} + \frac{\hat{\tilde{S}}_{go}}{\hat{\tilde{h}}_o} \right) \right] + \tau_{go}^{+} \frac{\hat{\tilde{S}}_{go}}{\hat{\tilde{h}}_o} + \tau_{go}^{+} \frac{\hat{\tilde{S}}_g}{\hat{\tilde{h}}_o} \right] \end{aligned} \tag{6.119}$$

and

$$\text{Den} = (2+\psi_o)\frac{\hat{\tilde{A}}_o}{\hat{\tilde{h}}_o}\frac{\left(\tilde{S}_o + \gamma\bar{\tilde{S}}_{ow}\right)}{\tilde{A}_o} \tag{6.120}$$

where

$$\bar{\tau}_{go}^{+} = \frac{\tau_{go}}{\tau_o} \tag{6.121}$$

and

$$\bar{\tau}_{go} \simeq \tau_g \tag{6.122}$$

The equation for neutral stability is developed from equation (6.109) by substitution of equation (6.111) and replacing the mean velocities with the superficial velocities, noting that:

$$\bar{u}_o = \frac{U_o\hat{A}}{\hat{A}_o} \tag{6.123}$$

and

$$(\bar{u}_g - C_R) \simeq u_g - \frac{U_g\hat{A}}{\tilde{A}_g} \tag{6.124}$$

giving

$$\frac{U_o^2\Omega_p}{gD}\left(\frac{\tilde{A}^2}{\tilde{A}_o^3}\right)\left(\frac{\hat{\tilde{A}}_o}{\hat{\tilde{h}}_o}\right)+\frac{U_g^2}{gD}\left(\frac{\rho_g}{\rho_o}\right)\left(\frac{\tilde{A}^2}{\tilde{A}_g^3}\right)\left(\frac{\hat{\tilde{A}}_o}{\hat{\tilde{h}}_o}\right) - 1 = 0 \tag{6.125}$$

where

$$\Omega_p = \left(\frac{C_R}{u_o} - 1\right)^2 \tag{6.126}$$

The water and oil heights, $\tilde{h}_w$ and $\tilde{h}_o$ must be calculated from the steady-state oil-water-gas stratified flow model, from Chapter 4.

6.4.3 Reduction of three-phase flow equations to two-phase flow equations for zero water flow

In the case where there is zero water flow, terms involving $\hat{S}_{ow}$ become zero from equation (6.99). Hence (6.119) can be simplified and rearranged to give

$$\begin{aligned}\text{Num} = {} & \frac{2\bar{\tilde{S}}_o}{\tilde{A}_o}\frac{\hat{\tilde{A}}_o}{\hat{\tilde{h}}_o} + \varphi_o\frac{\hat{\tilde{S}}_o}{\hat{\tilde{h}}_o} + 2\tilde{S}_{go}\frac{\tau_{go}^+}{\tilde{A}_g}\left(1+\frac{\tilde{A}_o}{\tilde{A}_g}\right)\frac{\hat{\tilde{A}}_o}{\hat{\tilde{h}}_o} \\ & + \bar{\tilde{S}}_g\frac{\tilde{A}_o}{\bar{\tilde{A}}_g}\tau_{go}^+\left[\frac{2}{\tilde{A}_g}\frac{\hat{\tilde{A}}_o}{\hat{\tilde{h}}_o} + \frac{1}{4\left(\tilde{S}_g+\hat{S}_{go}\right)}\left(\frac{\hat{\tilde{S}}_g}{\hat{\tilde{h}}_o}+\frac{\hat{\tilde{S}}_{go}}{\hat{\tilde{h}}_o}\right)\right] + \left(1+\frac{\tilde{A}_o}{\tilde{A}_g}\right)\tau_{go}^+\frac{\hat{\tilde{S}}_{go}}{\hat{\tilde{h}}_o} \\ & - \frac{\hat{\tilde{S}}_o}{\hat{\tilde{h}}_o} + \frac{\bar{\tilde{A}}_o}{\bar{\tilde{A}}_g}\frac{\hat{\tilde{S}}_g}{\hat{\tilde{h}}_o}\tau_{go}^+ + \frac{\hat{\tilde{A}}_o}{\hat{\tilde{h}}_o}\left(\frac{\tilde{S}_o-\tau_{go}^+\tilde{S}_{go}}{\tilde{A}_o}\right) + \left(\frac{\tilde{S}_{go}+\tilde{S}_g}{\tilde{A}_g}\right)\frac{\tilde{A}_o}{\tilde{A}_g}\frac{\hat{\tilde{A}}_o}{\hat{\tilde{h}}_o}\tau_{go}^+\end{aligned} \tag{6.127}$$

and (6.120) to give:

$$\text{Den} - (2+\varphi_o)\frac{\hat{\tilde{A}}_o}{\hat{\tilde{h}}_o}\frac{\tilde{S}_o}{\tilde{A}_o} \tag{6.128}$$

which agree with equations (6.87) and (6.88). The equation for neutral stability (6.125) also reduces to that for the two-phase case, since all the geometric parameters become equal to those for two-phase flow when the water height becomes zero.

6.4.4 Comparison of models

The two-phase and three-phase equations described above are compared in Figures 6.8 and 6.9 for a simple test case of the following parameters:

Oil Viscosity	10 mPas
Water Viscosity	1 mPas
Gas Viscosity	0.0222 mPas
Oil Density	850 kg/m^3
Water Density	998 kg/m^3
Gas Density	1.224 kg/m^3
Pipe Diameter	0.0779 m

For oil-gas and water-gas flow, the transition line between stratified and intermittent flow was calculated using both the Taitel & Dukler method, and the Lin & Hanratty method (described in Section 6.4.1). It can be readily seen that the Lin & Hanratty

method predicts a smaller liquid velocity for transition at the same gas velocity than the Taitel & Dukler method. This is consistent with the observations for two-dimensional flow, as shown in Figure 6.5.

For three-phase flow, the predicted transition line lies between the lines for two-phase flows predicted by the two methods above. This again is consistent with earlier observations of flows in channels. Higher liquid velocities are required for transition at higher water fractions, as shown by comparison between Figures 6.8 and 6.9 which show the transition lines for 30%/50% water and 30%/70% water respectively. At a higher water fraction, the holdup is smaller for the same total liquid superficial velocity, and thus a greater liquid velocity can be tolerated before transition occurs; this velocity is greater than that for the case of gas-water flow due to the effect of the more viscous oil layer moving fast on the water surface. At water fractions approaching unity, the transition would be expected to approach that predicted by inviscid Kelvin-Helmholtz theory, which gives higher liquid flowrates even than Taitel & Dukler. Note that under these circumstances the *oil-water* interface would probably no longer be stable, and this would influence the transition.

6.4.5 Comparisons with experimental data

The method described in the previous section for calculation of the transition between stratified and slug flow is tested here against experimental data points from two sources, namely Sobocinski[2] and Stapelberg[67]. The method of comparison was the same in each case: the liquid velocity required for transition was calculated while fixing the gas superficial velocity and water fraction. The data points and calculated transition velocities are tabulated in Appendix C, together with the transition velocity predicted by the modified Taitel & Dukler method described in Section 6.2.3.

a) Sobocinski

This study was for a three-phase flow of air, water and kerosene; the oil phase therefore had a low viscosity, around 3.8 mPas. None of the data points included slug flows, the flows being in the stratified and stratified-annular regimes. Flows in the stratified region only are compared here, since at higher flowrates there was

significant mixing between the oil and water phases, contrary to the assumptions of the transition model.

Figure 6.10 shows the results for these data points: the *bars* represent the actual measured (oil + water) superficial velocity and the calculated total liquid superficial velocity for transition, while the *points* show the percentage difference in these two quantities. A negative percentage difference indicates that a stratified flow would be expected, while a positive difference would indicate a slug flow. Sobocinski's stratified flow points clearly lie decisively in the stratified flow region.

b) Stapelberg

This study involved the use of a mineral oil with a viscosity in the region of 30 mPas in a pipe of diameter 23.8 cm. The data points spanned the stratified and slug regions, and this data is therefore a good test of the transition prediction. Additionally, the flow was observed to be consistent with the assumptions of the transition model in that the water layer was often undisturbed by the formation of slug flow between the oil and air phases.

Figure 6.11 shows the comparison of these data points with the calculations, in the same format as discussed above for Sobocinski's data. The slug flow points are well within the predicted slug flow region, while the stratified flow points are extremely close to the transition line.

6.5 SEPARATION OF WATER PHASE IN THREE-PHASE PIPE FLOWS

In three-phase flows where the water is the continuous phase, separate layers of oil and water are often seen to appear in the film region between liquid slugs. The appearance of a separate layer depends on the time for layer formation compared with the time between slugs, which are assumed to fully disperse the oil and water phases.

A dynamic criterion is required to determine the timescale on which separation takes place, in flows where a water layer would be expected in the film region, but not in the liquid slug. The *minimum* time for separate layers to appear will be the time for the largest oil drops to rise in quiescent water, since the interest is in the time for separate layers to start appearing. Turbulent motion of the fluids would increase this

time, and the presence of smaller drops means that a complete separation would take longer. The average rising distance to consider is assumed to be half the combined height of the oil and water layers as the concern is the arrival of oil drops at the gas-liquid interface.

The largest drop size is given by a critical Weber number, as discussed by Hinze[75]:

$$We_c = \frac{\rho_{cont}\overline{v^2}D_{max}}{\sigma} \tag{6.129}$$

where $\overline{v^2}$ is the average value of the squares of velocity differences over a length scale of D_{max}. This is determined from the rate of energy input per unit mass, $\dot{E}$:

$$\overline{v^2} \simeq 2.0\left(\dot{E}D_{max}\right)^{\frac{2}{3}} \tag{6.130}$$

From experimental observations of maximum drop size as a function of energy input, Hinze showed that:

$$We_c \simeq 1.2 \tag{6.131}$$

and hence from equations (6.129), (6.130) and (6.131):

$$D_{max} \simeq 0.74\left(\frac{\sigma}{\rho_{cont}}\right)^{\frac{3}{5}}\dot{E}^{-\frac{2}{5}} \tag{6.132}$$

It is now assumed that the rate of energy input per unit mass can be estimated from the pressure gradient for the slug. By a dimensional analysis, it can be shown that:

$$\dot{E} = \frac{u_s}{\rho_s}\left(\frac{dp}{dz}\right)_{slug} \tag{6.133}$$

where ρ_s is the slug density, assumed to be a volume average of the oil and water densities and u_s is the slug velocity, which is given by Gregory & Scott[33] as:

$$u_s = 1.35(U_g + U_o + U_w) \tag{6.134}$$

The slug pressure gradient is given by:

$$\left(\frac{dp}{dz}\right)_{slug} = \frac{2f\rho_s u_s^2}{D} \tag{6.135}$$

where

$$f - 0.079Re_s^{-0.25} \tag{6.136}$$

and

$$Re_s - \frac{\rho_s u_s D}{\mu_{eff}} \tag{6.137}$$

The effective viscosity, μ_{eff}, appropriate in this case will be that for a suspension of oil drops in water, given by the Brinkman[39] equation:

$$\mu_{eff} = \frac{\mu_w}{(1-\phi)^{2.5}} \tag{6.138}$$

The time taken for an oil drop to rise in water is obtained from the equation of motion of a drop and the settling distance. The equation of motion for a drop of diameter D and density ρ_o rising at a velocity U in a fluid of density ρ_w and viscosity μ is:

$$\rho_o \frac{\pi}{6} D^3 \frac{dU}{dt} - (\rho_w - \rho_o)\frac{\pi}{6} D^3 g - 3\pi\mu DU - \frac{1}{2}\rho_w \frac{\pi}{6} D^3 \frac{dU}{dt}$$
$$-\frac{3}{2} D^2 \sqrt{\tau \rho_w \mu} \int_{-\infty}^{t} \frac{dU}{dt'} \frac{dt'}{\sqrt{t-t'}} \tag{6.139}$$

where the terms are inertia, buoyancy, Stokes law drag, inertial added mass and viscous added mass respectively. At terminal velocity, the dU/dt terms become zero and by assuming that the drop is moving at its terminal velocity for a significant time, the viscous added mass term tends to zero. Making the above assumptions, equation (6.139) gives:

$$U_t - \frac{(\rho_w - \rho_o) D^2 g}{18\mu} \tag{6.140}$$

and to take account of the increased viscosity of the continuous phase due to the presence of many drops, the effective viscosity given by equation (6.138) is used in (6.140). In the real situation under consideration, the motion of the continuous phase and the viscous added mass term will decrease the average settling velocity. For simplicity, however, the average settling velocity is taken to be half the terminal velocity.

The settling distance is obtained from the equilibrium oil and water heights given by the stratified flow model in Section 4.5. Thus the settling time is:

$$t_{setg} - \frac{0.5\left(\tilde{h}_w + \tilde{h}_o\right) D}{0.5 U_t} \tag{6.141}$$

The interval between slugs is determined from the slug frequency. There are few published equations for the calculation of slug frequency, the earliest being that of Gregory & Scott[33], whose method was derived from data for carbon dioxide-water flow. This method, however, does not take into account the fluid physical properties. A more recent paper by Tronconi[34] has a more mechanistic basis, and assumes that the slug frequency is one half of the frequency of the unstable wave precursors to slugs, giving the following equation for slug frequency:

$$\omega = 0.61 \frac{\rho_g}{\rho_\ell} \frac{u_g}{h_g} \tag{6.142}$$

Stapelberg *et al*[10] found that better correlation of slug frequency for air-oil and oil-water-air flow was obtained by making the slug frequency one quarter the unstable wave frequency which would give:

$$\omega = 0.305 \frac{\rho_g}{\rho_\ell} \frac{u_g}{h_g} \tag{6.143}$$

The interval between slugs is the reciprocal of the frequency, thus giving:

$$t_{slug} = 3.3 \frac{\rho_\ell}{\rho_g} \frac{h_g}{u_g} \tag{6.144}$$

The boundary between flows with a separate water layer and flows which have continuously dispersed liquids is therefore given by the values of gas and liquid velocities which give equal settling time from equation (6.141) and slug interval from equation (6.144). This boundary is plotted in Figure 6.12 for various oil fractions. As the oil fraction is increased, the greater effective viscosity of the water means that oil drops take longer to reach the interface and thus the region of separated flow is diminished. Further comparison of this method is made with experimental observations from the WASP facility in Section 9.2.3.

6.6 OIL-WATER INTERFACE MIXING (TRANSITION FROM STRATIFIED TO WAVY FLOW)

The transition from stratified to wavy flow is considered at both interfaces (ie gas-oil and oil-water) by a similar analysis to that given by Taitel & Dukler, adapted

from Jeffreys[76]. The phenomenon of wave generation is quite complicated and not well understood, but it is known that waves are formed when there is a sufficient relative velocity between two layers of fluids (but not sufficient to cause transition to intermittent or annular flow regimes). Jeffreys suggested the following condition for wave generation:

$$(u_g - C)^2 C > \frac{4\nu_\ell g(\rho_\ell - \rho_g)}{s\rho_g} \tag{6.145}$$

where s is a 'sheltering coefficient' which Jeffreys suggested should take a value of about 0.3. However, Taitel & Dukler argued that it should be much lower, and used a value of 0.01. The velocity of propagation of the waves, C is approximately 1.0 to 1.5 times the mean film velocity, u_ℓ. At the gas-liquid interface, the gas velocity u_g is much greater than the wave velocity, and so the criterion for transition from stratified-smooth to stratified-wavy is given by:

$$u_g \geq \left[\frac{4\nu_\ell g(\rho_\ell - \rho_g)}{s\rho_g u_\ell}\right]^{\frac{1}{2}} \tag{6.146}$$

At the oil-water interface, the velocities of the two phases are similar and so the approximation that $u_g \gg C$ no longer applies; hence the criterion for transition from a smooth to a wavy interface is given by:

$$(u_o - u_w) \geq \left[\frac{4\nu_w g(\rho_w - \rho_o)}{s\rho_o u_w}\right]^{\frac{1}{2}} \tag{6.147}$$

Comparison with Sobocinski's data shows that the oil-gas smooth to wavy transition criterion works well with s = 0.01 as shown in Figure 6.13. The oil-water interface mixing criterion works best if s is taken to be 0.007, as shown in Figure 6.14. Note that one of the stratified points is very much inside the wavy region of both graphs. This suggests that the original observation may be in error. The pressure drop for this particular point was 17.5 Pa/m which is much higher than other stratified points and is more consistent with a stratified-wavy/interface-mixing point (Illustrating the difficulties of visual flow characterisation).

6.7 SUMMARY

The most important flow pattern transition covered in this chapter was that from stratified to intermittent flow. This was considered first by using steady-state (Kelvin-Helmholtz) theory as applied by Taitel & Dukler in their semi-theoretical two-phase flow pattern map. Following this, linear stability theory was considered, firstly for two-phase flows in two-dimensional channels and extending it to three-phase flows in circular pipes. Use was made in the work of the analysis of Lin & Hanratty, but the consideration of a second liquid phase was entirely new. Comparisons were made between the methods described and data from Sobocinski and Stapelberg, with good predictions being obtained from the linear stability theory approach.

Two further issues concerned with flow patterns in three-phase flows were then considered. These were firstly the separation of a water phase in three-phase slug flow which is important in pipelines where a separate water phase can cause corrosion. the separation was considered by a simple criterion balancing the time taken for drops to settle in the film region with the time interval between slugs. This will be compared to experimental observations from the WASP facility in Chapter 9. The second issue was mixing at the interfaces in stratified flows. This was considered using the Jeffreys model adapted by Taitel & Dukler and compared to the experimental data of Sobocinski.

Chapter 7:
SIMPLE MODELS FOR THREE-PHASE SLUG FLOWS

7.1 INTRODUCTION

In Chapters 4 and 5 stratified three-phase flows were considered, firstly by simple one-dimensional models and then more fully using numerical solutions. In Chapter 6 the transition between stratified and slug flows was considered, along with other flow pattern issues concerned with three-phase flows. In this chapter, attention is turned to the calculation of pressure gradient and holdup in three-phase slug flows.

Slug flows exist over a wide range of flowrates in horizontal pipelines and therefore commonly occur in industrial applications; this is particularly true in offshore subsea pipelines in the petroleum industry. Due to the large fluctuations in pressure and mass flowrate in slug flows, it is important to be able to make calculations of the pressure gradient and liquid holdup when designing pipelines and processing equipment.

A simple model for gas-liquid slug flow was presented by Dukler & Hubbard[77]. The slug was considered to progress by scooping up liquid from the film in its front and shedding the liquid at its tail. The principal contributions to the pressure drop are the acceleration of liquid picked up at the slug front and the frictional resistance of the back section of the slug.

In this chapter, after discussion of the Dukler & Hubbard model, modifications to include the effect of a second liquid phase are proposed. In addition to calculation of mean pressure gradient, a method of calculation of average holdup (of oil and of water) is described for the case of a flow where oil and water form separate layers in the film region.

7.2 DUKLER & HUBBARD MODEL FOR TWO-PHASE SLUG FLOWS

The physical model for slug flow proposed by Dukler & Hubbard is shown schematically in Figure 7.1. The pressure drop across a slug unit is considered to be composed of the pressure drop resulting from acceleration of the slow-moving film to the slug velocity, Δp_a and the pressure drop required to overcome wall shear

in the back section of the slug, Δp_f. The pressure drop in the film region is assumed to be negligible.

The accelerational pressure drop for a slug of stable length is given from the force required to accelerate the slow-moving film to the slug velocity. If x is the rate at which mass is picked up by the slug:

$$\Delta p_a = \frac{x}{A}(u_s - u_{fe}) \tag{7.1}$$

where u_s is the mean velocity of the fluid in the slug and u_{fe} is the velocity of the film just in front of the slug. The frictional pressure drop is given by assuming that the gas and liquid phases are homogeneously mixed. The two-phase frictional pressure drop method of Dukler *et al*[64] was suggested. The frictional pressure drop is given by:

$$\Delta p_f = \frac{2f_s[\rho_\ell R_s + \rho_g(1 - R_s)]u_s^2(\ell_s - \ell_m)}{D} \tag{7.2}$$

where ℓ_s is the length of the slug and ℓ_m the length of the mixing eddy, or acceleration zone, at the front of the slug. The friction factor for homogeneously mixed phases is given by:

$$f_s = 0.00140 + \frac{0.125}{Re_s^{0.32}} \tag{7.3}$$

where the Reynolds number is defined by:

$$Re_s = Du_s\frac{\rho_\ell R_s + \rho_g(1 - R_s)}{\mu_\ell R_s + \mu_g(1 - R_s)} \tag{7.4}$$

The pick-up and shedding model requires two characteristic slug velocities. These are the mean velocity of the fluid in the slug relative to the pipe wall, u_s and the observed rate of advance of the slug, u_t. Dukler & Hubbard showed that the mean velocity of fluid in the slug is given by:

$$u_s = U_g + U_\ell \tag{7.5}$$

and that the rate of advance of the slug is given by:

$$u_t = u_s + \frac{x}{\rho_\ell A R_s} \tag{7.6}$$

since picking up mass at the front of the slug at a rate x gives an apparent increase in velocity. Equation (7.6) may be conveniently written as:

$$u_t - (1 + C)u_s \tag{7.7}$$

where

$$C - \frac{x}{\rho_\ell A R_s u_s} \tag{7.8}$$

and may be related to the Reynolds number by:

$$C - 0.021 \ln (Re_s) + 0.022 \tag{7.9}$$

Next, the length of the slug and the film region must be calculated. This is achieved by considering the deceleration of the film behind the slug and the relationship between the film velocity, u_f and the holdup in the film, R_f. This is a complex calculation, discussed at length by Dukler & Hubbard. The length of a slug unit is given by:

$$\ell_u - \frac{u_t}{\omega} - \frac{(1 + C)u_s}{\omega} \tag{7.10}$$

and the length of the film region is:

$$\ell_f - \ell_u - \ell_s \tag{7.11}$$

where the length of the slug, ℓ_s is calculated from a material balance on the liquid, giving:

$$\ell_s - \frac{u_s}{\omega(R_s - R_{fe})}\left[\frac{U_\ell}{u_s} - R_{fe} + C(R_s - R_{fe})\right] \tag{7.12}$$

The holdup in the film just before the front of the slug, R_{fe} is calculated from the hydrodynamics of the film. The solution is given by an integral:

$$\int_{R_{fe}}^{R_s} \Omega(R_f) dR_f - \frac{\ell_f}{D} \tag{7.13}$$

where

$$\Omega(R_f) - \frac{\frac{C^2 R_f^2}{R_f^2} - \frac{1}{Fr}\left[\frac{\pi R_f \sin(\theta/2) + 2\sin^2(\theta/2)}{2(1-\cos\theta)} - \frac{1}{2}\cos(\theta/2)\right]}{f_f B^2 \theta/\pi} \tag{7.14}$$

The calculation of ℓ_f is iterative. From a guess of ℓ_s, the film length is calculated from (7.11) and then the integral in equation (7.13) is evaluated by adding steps of

dR_f until the estimate of ℓ_f is reached. The value of R_{fe} thus obtained is used to give a new value of ℓ_s from equation (7.12).

The following definitions are required for the evaluation of $\Omega(R_f)$ in equation (7.14). The Froude number is given by:

$$Fr = \frac{u_s^2}{gD} \tag{7.15}$$

The angle subtended by the interface at the centre of the pipe, θ is related to the holdup by:

$$R_f = \frac{\theta - \sin\theta}{2\pi} \tag{7.16}$$

and the ratio of the film velocity to the slug velocity is:

$$B = \frac{u_f}{u_s} = 1 - C\left(\frac{R_s - R_f}{R_f}\right) \tag{7.17}$$

Having completed this iterative calculation, the only outstanding issue is to calculate the length of the mixing eddy at the slug front. The suggestion by Dukler & Hubbard was to relate this distance to the 'velocity head' by:

$$\ell_m = \frac{0.3(u_s - u_{fe})^2}{2g} \tag{7.18}$$

7.3 MODIFICATIONS FOR THREE-PHASE FLOWS

7.3.1 Acceleration zone

The accelerational pressure drop at the slug front is related to the liquid density as shown in equation (7.8). In three-phase flows the liquid density is assumed to be a volume-average of the oil and water densities:

$$\rho_{mix} = \phi\rho_o + (1 - \phi)\rho_w \tag{7.19}$$

This assumption may not be true in a case where the film is composed of separate oil and water layers immediately ahead of the slug front. For example, in the experiments

of Stapelberg *et al*[10] a separate water layer existed throughout the slug, and thus the appropriate density to use would be that of the oil phase, giving a 10–15% difference in the accelerational contribution. This may partially explain the overprediction of mean pressure gradient in those particular experiments.

A second issue to address in three-phase slug flow is the breaking up of two separate liquids at the slug front into droplets. The energy required to create the extra surface associated with the droplets is provided by an irreversible pressure drop. Similar arguments to those used in Section 6.5 may be used to make an estimate of this pressure loss. The two liquids are assumed to be separate at the front of the slug and completely dispersed by the end of the eddy mixing region. In a time interval ℓ_m/u_t a volume of oil equal to

$$\frac{\pi D^2 \ell_m \phi}{4} \tag{7.20}$$

is dispersed into drops of diameter d_p, which have a surface area per unit volume of $6/d_p$. Thus the rate of creation of surface area is given by:

$$\frac{dA_d}{dt} = \frac{3\pi D^2 \phi u_t}{2d_p} \tag{7.21}$$

The energy required per unit surface area is given by the surface tension, σ and dividing by the mass of material in the slug, $\pi D^2 \ell_m \rho_\ell / 4$ gives the rate of input of surface energy per unit mass:

$$\dot{E} - \frac{6\phi u_t \sigma}{\rho_\ell d_p \ell_m} \tag{7.22}$$

From the work of Hinze[75] it was shown (Section 6.5) that the maximum drop size was related to the energy input by:

$$d_p - 0.74\left(\frac{\sigma}{\rho}\right)^{\frac{3}{5}} \dot{E}^{-\frac{2}{5}} \tag{7.23}$$

By combination of equations (7.22) and (7.23) the droplet diameter may be eliminated, leading to:

$$\dot{E} \simeq 33.0\left(\frac{\sigma}{\rho_\ell}\right)^{\frac{2}{3}} \left(\frac{u_t \phi}{\ell_m}\right)^{\frac{5}{3}} \tag{7.24}$$

The irreversible pressure loss associated with this energy requirement is given by:

$$\left(\frac{dp}{dz}\right) = 33.0\left[\frac{\rho u_t^2 \sigma^2 \phi^5}{\ell_m^5}\right]^{\frac{1}{3}} \tag{7.25}$$

and hence the additional pressure drop contribution from drop dispersion is given by:

$$\Delta p_{drops} = 33.0\left[\frac{\rho u_t^2 \sigma^2 \phi^5}{\ell_m^2}\right]^{\frac{1}{3}} \tag{7.26}$$

Substituting order-of-magnitude values for the various quantities in (7.26) it can be seen that the pressure drop contribution from this mechanism is perhaps 1% of the acceleration pressure drop, and may therefore be neglected. ($\Delta p_a \sim C\rho u^2 = O(10^3)$ while $\Delta p_{drops} = O(10^1)$)

7.3.2 Slug body

The calculation of the frictional contribution to the pressure gradient is affected by the viscosity of the liquid. This can vary considerably depending on the distribution of the oil and water phases, as was demonstrated in Chapter 3. It is assumed that normally the oil and water will be fully dispersed by the end of the mixing eddy region and that the effective liquid viscosity would be given by the Brinkman equation (3.9):

$$\mu_{mix} = \frac{\mu_{cont}}{(1-\phi)^k} \tag{7.27}$$

using the appropriate continuous phase viscosity. In the rare cases where the water remains as a separate phase through the slug, for example in the experiments reported by Stapelberg *et al*, this would not be the most appropriate viscosity to use. Probably the most realistic frictional pressure drop calculation under these circumstances would be to treat the slug as a stratified liquid-liquid flow with an oil superficial velocity given by:

$$U_o - \phi u_s \tag{7.28}$$

and water superficial velocity of:

$$U_w = (1-\phi)u_s \tag{7.29}$$

Stapelberg *et al* used an effective liquid viscosity given by a volume average of the oil and water viscosities in their calculations. This would overestimate the frictional pressure gradient and may explain the overprediction of their results using the Dukler & Hubbard method, particularly in respect of the increasing error at increasing mixture velocity.

7.3.3 Film region

The contribution to the total pressure drop of the film region is negligible. This is evident both from experimental measurements of pressure gradient as a function of time, and by observing that the film region is essentially a stratified flow with a low liquid holdup. The pressure gradient in such a flow is of the same order as in a gas flow in a pipe, where the pressure gradient would be proportional to ρu^2. This would amount to only a small fraction of the frictional pressure contribution of the slug, as given by equation (7.2).

However, the holdup of liquid in the film is not insignificant, and it is useful to be able to calculate the mean oil holdup and mean water holdup over the whole slug unit. If the two liquids were fully dispersed over the whole unit then the oil/water holdup ratio would be equal to the input oil/water ratio. However, it is often the case that the oil and water separate in the film region, as discussed in Section 6.5. Thus a simple model might assume that the oil and water were homogeneously mixed in the slug, but were separate in the film, the average holdup over the length of the film being given by the stratified flow model described in Section 4.5. For this model the superficial velocities of the three phases in the film region are required. The gas superficial velocity may be assumed to be the mean gas superficial velocity, but the oil and water superficial velocities must be calculated by subtracting the flowrate in the slug from the mean flowrate. The total time for a complete slug unit to pass is given by $1/\omega$ with the time occupied by a slug being ℓ_s/u_t. A mass balance on the oil phase therefore gives:

$$U_o A\frac{1}{\omega} - u_s A R_s \phi \frac{\ell_s}{u_t} + U_{of} A\left(\frac{1}{\omega} - \frac{\ell_s}{u_t}\right) \tag{7.30}$$

where U_{of} is the oil superficial velocity in the film. By rearrangement:

$$U_{of} = \frac{U_o - u_s R_s \phi \left(\frac{\omega \ell_s}{u_t}\right)}{1 - \frac{\omega \ell_s}{u_t}} \tag{7.31}$$

and similarly the water superficial velocity in the film is given by:

$$U_{wf} = \frac{U_w - u_s R_s (1-\phi) \left(\frac{\omega \ell_s}{u_t}\right)}{1 - \frac{\omega \ell_s}{u_t}} \tag{7.32}$$

Having obtained the oil and water holdup in the film, R_{of} and R_{wf} by solution of the three-fluid stratified flow model, the mean holdup over the slug unit is calculated as follows. The length of the slug is ℓ_s and the length of the film region is ℓ_f. Hence the mean oil holdup, $\bar{R}_o$, is given by:

$$\bar{R}_o = \frac{R_s \phi \ell_s + R_{of} \ell_f}{\ell_s + \ell_f} \tag{7.33}$$

and the mean water holdup by:

$$R_w = \frac{R_s (1-\phi) \ell_s + R_{wf} \ell_f}{\ell_s + \ell_f} \tag{7.34}$$

7.4 SUMMARY

In this chapter it has been demonstrated how the Dukler & Hubbard model for gas-liquid slug flow can been extended to allow calculations for three-phase flows. It appears that using a volume-average density and a Brinkman viscosity for the combined effect of the oil and water phases is a sufficient modification, as was suggested for the extension of pressure gradient correlations to three-phase flows in Chapter 3. The pressure drop contribution from dispersion of one phase into droplets in the other phase at the front of the slug was demonstrated to be negligible. The calculation of mean holdup in flows of the type found in the WASP experiments was described.

The models contained in this chapter are compared with experimental results obtained by the present author using the WASP facility in Chapter 9.

Chapter 8:
HIGH PRESSURE MULTIPHASE FLOW FACILITY

8.1 DESCRIPTION OF WASP FACILITY

8.1.1 History

The WASP (Water, Air, Sand, Petroleum) project was started in 1987 as a collaborative project supported by the Science and Engineering Research Council and the Thermal Hydraulics Division at Harwell. The aim of the project was to study flows of importance in the Petroleum Industry by constructing a new high pressure multiphase flow facility in the Department of Chemical Engineering at Imperial College. This facility was designed with the following features:

(a) Operation with up to *four* phases, namely air, water, oil and sand (suspended in the water phase).

(b) High pressure operation (up to 50 bar), the air supply being supplied from the hypersonic wind tunnel air reservoirs in the adjacent Aeronautics Department.

(c) Industrial-scale dimensions, with a test section diameter of 3″ (78 mm) and length of 40 m, which may be inclined by $\pm 5^{\circ}$ to the horizontal.

(d) Flow visualisation.

(e) Computer control and data acquisition systems.

The first experiments were concerned with air-water flows at pressures up to 25 bar. Due to increasing interest from industry, however, the programme quickly moved to the study of oil-water-air flows. Following the reorganisation of the UKAEA in 1990, support for the project was provided by AEA Petroleum Services, and after the expiry of the original SERC grants, a Consortium was formed of companies in the oil and gas sectors (Figure 8.1). This Consortium is now providing support for a number of projects making use of a wide range of the features of the facility.

The need for a new facility such as this is demonstrated in Figure 8.2 where the pipe diameters and operating pressure of various experimental facilities are compared with

pipelines taken from the UK National Multiphase Flow Database*. It will be seen that facilities used in published studies of three-phase flows are generally low pressure loops with small diameter test sections, while industrial pipelines are of much larger diameter and have higher operating pressures. The WASP facility therefore bridges this gap, and it should be noted that due to the greater density of air compared to natural gas, the effective pressure is greater than that shown. The diameter of the test section is a compromise between a large diameter to approach industrial sizes and a small diameter to minimise the costs of the pipeline and liquid flowrates, and because the length available for the facility was limited, a smaller diameter gives a greater length/diameter ratio.

8.1.2 Layout and design

A schematic diagram of the facility is given in Figure 8.3 and an overall photograph in Figure 8.4. The air supply is drawn from either the hypersonic wind tunnel high pressure air reservoirs in the Aeronautics Department (for high pressure experiments) or from the site compressed air main (for low pressure experiments — up to approximately 5 bar). The liquids are taken separately from two pressurised tanks (Figure 8.5), one for oil, the other for water (or water/sand slurry), flowing either under the action of the applied air pressure, or centrifugal pumps.

After metering, the three streams are combined in the mixer section which can be seen in Figure8.5. The internal design of this section was intended to introduce the three phases as closely as possible to stratified layers, as this was believed to lead to the most reliable results for slug flows.

From the mixer section, the main test section of the rig continues as a straight, horizontal tube for approximately 40 m. The test section was built of seamless stainless steel tube in sections of length 7 m with tongue-and-groove flanged joints to ensure continuity and concentricity of the bore. An additional feature is the capability to incline the test section by up to 5° by means of adjustable supports and flexible connecting pipes at the inlet. (The maximum angle of inclination is constrained by the height of the test section above the ground). Pipelines laid in subsea conditions in

* See Section 3.5.2

the oil industry follow the topology of the sea bed, and small upward and downward inclinations usually occur. Even a small angle of inclination (particularly uphill) can have a large influence on the stratified to slug flow transition. A photograph of the test section is shown in Figure 8.6.

Towards the end of the test section is the visualisation section. This was constructed of a polycarbonate tube of length 0.8 m with a wall thickness of 31 mm, mounted in a steel jacket (with window slots) which was designed to take the stresses. Although this tube was capable of withstanding the full rig pressure, brittle fractures are possible in this plastic material, and for this reason a containment box was built around the whole section in case of failure. This can be seen on the right hand side of Figure 8.7.

At the end of the test section is the slug catcher vessel, shown on the left hand side of Figure 8.7. The main function of this vessel is to separate the air and the liquids at full rig pressure. The size of the slug catcher is therefore sufficient to contain several times the volume of the test section and the vessel is fitted with baffles and plates inside to dissipate the momentum of the liquid phases. The liquids (oil + water) drain from the bottom of the slug catcher to a 'dump tank' where the oil and water separate under gravity. Water and oil can be pumped back serially through a return line to their respective tanks after a suitable settling time.

The air stream was originally taken from the top of the slug catcher, through a silencer, to atmosphere, but it was found that during transient phases of operation, particularly during shut-down, there could be significant carry-over of liquid through the air line. Hence the air exit was modified using plastic 500 mm ducting (as used in ventilation systems) to route the air and any carried-over liquid back to the dump tank, with negligible back pressure.

The test section is shown schematically in Figure 8.8, together with the lengths of the component sections and the location of the instrumentation points.

8.2 CONTROL & INSTRUMENTATION

8.2.1 Control system

The rig was intended for operation in a semi-transient manner, the air from the high

pressure air supply being blown down through the rig in a series of pressure steps. At high air flowrates, this process may take only a few minutes and so a computer control system was required. The main component of the control system was an ANALOGIC ANDS4400 monitor and control unit, which operated the control loops and binary controls (on/off valves and motors). This was interfaced to a PC to allow setting of control parameters (gain, offset, etc) and the set points of the control loops and to supervise the settings of the binary controls. All the information was displayed on a graphical schematic of the rig. Five control loops were available, to control:

(a) Air superficial velocity → Inlet air control valve V1

(b) Oil superficial velocity → Oil control valve V13

(c) Water superficial velocity → Water control valve V12

(d) Rig outlet pressure → Slug catcher air control valve V3

(e) Slug catcher liquid level → Slug catcher liquid outflow valve V2

It was found that some of the control parameters (particularly the gain of the air velocity control loop) were significantly affected by the rig pressure and therefore had to be tuned carefully to particular operating conditions to avoid the development of unstable oscillations.

Data collection from the rig was also under computer operation. Signals from the flow meters and pressure transducers were connected, via an analogue to digital convertor, into another PC. These signals were converted to flowrates and pressures and superimposed onto the video signal from the video camera, and fed into a video recorder[†]. Thus flow visualisation and the relevant numerical data were all stored on video tape. The numerical data was also recorded in files on the computer system at an adjustable time interval (usually set to 2 seconds).

8.2.2 Flow metering

The water flowrate was measured using a Danfoss magnetic flow meter covering the whole range of flowrates from 0 to 1.5 m/s. The smallest flow rate which could be accurately measured was 0.075 m/s, since fluctuations dominated at smaller flowrates.

---

† This superimposition was achieved using an EGA Genlock Adaptor, supplied by Vine Micros

The oil flowrate was measured using a BS1042 orifice plate. Orifices of 15 mm and 25 mm diameter were used for these tests, giving ranges of superficial velocity of 0 to 0.30 m/s and 0 to 1.0 m/s respectively. The smallest superficial velocity which could be accurately measured was 0.06 m/s using the 15 mm orifice and 0.16 m/s using the 25 mm orifice.

The air flowrate was also measured using an orifice of 15 mm diameter, which at the pressures used in these experiments gave a flowrate range up to about 3 m/s.

The flowrates are measured over a period of several minutes, and the average thus obtained can be relied upon to ±0.001 m/s for each phase in the ranges indicated.

8.2.3 Pressure drop measurement

Pressure gradient was measured by using two Druck PDCR820 general purpose transducers of range 3.5 bar to obtain the pressure drop over a length of 11.10 m (before the quick-closing valves were installed) and 14.58 m (after the quick-closing valves were installed). Two individual transducers, mounted flush to the test section, were used in order to avoid the problems of trapped liquid in long lines to the transducers. The accuracy of these transducers was stated to be ±0.1% of full range, thus giving an error of ±7 mbar in the difference. However, by pressurising the test section, the difference in the response of the two transducers could be determined accurately, and the error in pressure drop was estimated to be ±2 mbar. This procedure also allowed a correction to be made for the temperature difference between the two transducers, one being located outside and one inside the control room.

8.2.4 Liquid tank levels

When operating the rig it is essential to know the volume of oil and water in their respective tanks, to know when to terminate an experiment, or to change the flowrates to make best use of the available reserves. The levels in these tanks were measured by differential pressure gauges between the top and the bottom of the two tanks.

The level in the slug catcher was also an important parameter in the control of the rig. If the level was too low, gas passed with the liquid through the lower exit into the dump tank. This led to excessive noise and vibration. If the level was too high, there

was the risk of flooding the slug catcher and carrying liquid over into the gas vent. The level was measured by means of a stainless steel float connected to displacement transducer. The design of the float itself was constrained by the size of the hole in the slug catcher through which it had to be passed, the weight of the float and its supporting rods and the maximum pressure it was required to stand. Fortunately a suitable float was available off the shelf, which satisfied the requirements.

8.2.5 Flow visualisation

For low pressure operation, the flow could be observed by eye, and a simple description of the flow made. All the flows observed were in the slug flow regime, but important characteristics such as whether water and oil separated or not and the nature of the continuous phase could be determined. The flow pattern was recorded continuously using a Panasonic MV-10 VHS Camcorder, and occasionally using a Hadland Photonics High Speed Videoscope which had a framing rate synchronised to powerful stroboscopic Xenon lights of strobe duration 20 μsec. However, flow visualisation using video was found to be disappointingly poor; this was because of poor light transmission through the fluids (particularly the oil phase) and the perspex shielding, and also due to the difficulty of focussing the cameras when the pipe walls were covered with oily films.

8.2.6 Holdup measurement

Apart from the pressure gradient and flow pattern, one of the most important parameters in multiphase flow is the *holdup*, or mean fraction of the pipe cross-section which is occupied by each of the phases. For all flow patterns apart from smooth stratified flow, the prediction of holdup by analytical or numerical solutions is difficult, if not impossible at present. There is therefore a need for experimental measurements of holdup in order to develop, validate and improve prediction methods.

There are several methods for the measurement of holdup in two-phase (gas-liquid) flow which can be extended to three-phase (oil-water-gas) flow. The most readily applicable methods are volume averaging by trapping the fluids in a section of pipe, and nuclear techniques. While the former method gives a direct measure of

the fractions of the phases, nuclear techniques give more localised and continuous measurement. In the present work, holdup measurements were carried out using the quick-closing valve method. Current work on the WASP facility is aimed at using a dual-energy gamma absorption method to obtain local oil and water fractions, for which the quick-closing valve technique provides important calibration data.

The design of quick-closing valve unit chosen was to replace one of the 7 m sections of the main test line of the rig with a new section equipped with a full-bore ball valve at either end. These valves were operated by air actuators which were supplied with compressed air from a gas cylinder via a single large-bore manifold to ensure simultaneous operation. The air actuators were modified to enable rapid operation and typically the closing time was around 0.5 sec. It is believed that simultaneous operation of the valves is more important than fast operation, and experiments by Hashizume[78] showed no effect on measured void fraction of shut-off time ranging from 0.05 sec to 2 sec. When the valves were closed, the control system was arranged to simultaneously cut power to the liquid pumps, to prevent a surge in pressure. Even so, a significant pressure rise was noticed, for example as shown in Figure 8.9.

The holdup section was equipped with a liquid drain and air inlet, to allow the trapped liquids to be blown out into 25-litre plastic drums. These were left to settle (since the process of blowing the liquid out tended to mix the oil and water) and then transferred to glass measuring cylinders which were specially manufactured from 4″ bore glass tubing. This was found to be a more satisfactory way of operating than to drain the liquids directly into the cylinders, which were 5 feet in length and heavy when full. The volumes of liquid lost on the transfers were negligible compared to the total volume collected.

8.3 OIL SELECTION

The selection of an oil for the experiments was influenced by many factors which are summarised in Table 8.1. Some of these factors were concerned with safety and

some with practical and operational issues. Each area is considered below.

Table 8.1: Factors influencing choice of oil

Flammability Properties	Flashpoint Autoignition Temperature Formation of Vapour and Sprays
Health and Environment	Toxicity (Additives) Disposal Spillages
Physical Properties	Viscosity Density
Practical Features	Miscibility with water Separation from water Foaming and air release Micro-organisms

8.3.1 Flammability properties

The flashpoint of an oil is determined under standard laboratory conditions, which do not necessarily represent the practical situation well, but can be used as a guide to oil selection.

Clearly, there is a wide spectrum of flashpoints for liquid petroleum products, ranging from petrol (10°C) to heavy oils (above 300°C). There is a broad correlation between flashpoint and viscosity and the heavier oils can be ruled out on the grounds of excessive viscosity. Two types of oil considered were light lubricating oils, eg Shell Tellus Oil (which have flashpoints in the region of 200–220°C) and synthetic phosphate ester fluids (230–240°C).

The autoignition temperature is also determined under standard conditions, and may be considerably affected by the properties of the surfaces and by the pressure. A study into the possibility of autoignition effects in the WASP facility was performed by Hall[79], and many of the issues concerned with autoignition are discussed by Richardson *et al*[80].

The formation of vapour at ambient temperature will be negligible for an oil whose flashpoint exceeds 200°C since there is no significant source of heating in the rig. Formation of sprays is not an important issue at low pressure, due to the small driving force which could cause a spray to form.

8.3.2 Health and environment

Most oils must be handled with minimum skin contact and must be disposed of correctly; there is little that can be improved by oil selection. Thus this area was accommodated by careful operating procedures, particularly in the case of oil spillages.

8.3.3 Physical properties

The most important properties of the fluid in the present context are the density and viscosity. The density of most oils is in the region of 850–880 kg/m^3. The density of phosphate ester fluids is around 1100 kg/m^3, which is greater than that of water and would therefore sink to the bottom of the pipe in a horizontal pipe. This type of oil was therefore ruled out for use in these experiments.

The viscosity of oil in a subsea pipeline is likely to be several times that of water. Thus, a light lubricating oil (viscosity ratio about 50) was considered more suitable than for example kerosene (viscosity ratio less than 5).

8.3.4 Practical features

Most oils are immiscible with water, but may disperse due to turbulent effects during flow. It is most important that the dispersion settles out quickly on standing. Ideally the oil should have a low viscosity so that water droplets can readily settle from the oil phase. This contradicts the earlier requirements of high flashpoint and relatively high viscosity.

Many specialised oils contain anti-foaming additives, which would clearly help in this experimental programme due to the mixing of the fluids with air. Finally, growth of micro-organisms could present a problem, particularly if by-products of their growth

led to stabilisation of an emulsion of water drops in the oil. This is still a topic which is being investigated by the WASP project team

8.3.5 Summary

The most suitable oil from the safety and physical properties point of view was considered to be a Shell Tellus Oil. The lightest oil in this range was chosen, as this had a viscosity of about 40 times that of water. However, a number of disadvantages of this oil became apparent, as discussed in the next section.

8.4 OIL PROPERTIES

8.4.1 Separation from water

Once the oil had been circulated in the rig a few times it was noticed that a stable suspension of water in the oil phase had formed. Thus, the two fluid phases became water and 'water-in-oil suspension' rather than water and oil. This oil is thus referred to as 'used' oil and determination of its density showed that the water content in the used oil was about 7%. These two phases were found to mix and separate very quickly and to behave as water-continuous or oil-continuous flows, according to the oil/water ratio, and were therefore assumed to behave as two immiscible phases.

Some tests were carried out on the separation times of combinations of clean and used oil and water by shaking samples in small phials 25 mm in diameter and 100 mm long and observing the rise of the interface with time. Settling out took less than 5 minutes in all cases. It was not found possible to produce a water-in-oil phase on this small scale similar to the 'used' oil from the rig. A possibility was that bacterial activity in the rig fluids, over a period of weeks, was helping to stabilise the dispersion of water in oil.

8.4.2 Viscosity

Viscosity measurements were carried out for both clean unused oil and for a representative sample from the test facility. A Bohlin rheometer was used and a range of strain rates applied to see if the behaviour of the oil was Newtonian. The results are given in Figure 8.10. The viscosities at the lowest strain rates should

be ignored, as the readings were unstable, but it is clear that at higher strain rates that both clean and used oils were Newtonian, with a difference of 11% between the clean oil and the used oil viscosities. (This corresponds to a water content in the oil phase of about 4% using Brinkman[39]). The value of the clean oil viscosity corresponded to that from the Shell Oils data sheet at the same temperature, and thus the viscosity of the used oil was assumed to be given by the clean oil viscosity plus 11%, as shown in Figure 8.11.

8.4.3 Density

The density was measured at 24.7°C for the clean oil and for a representative sample from the rig, giving 860.5 kg/m^3 and 870.2 kg/m^3 respectively. These figures correspond to a fraction of 7% water in the oil phase, which was accepted as more accurate than the value obtained by viscosity measurements.‡ The Shell data sheet gave a value of 865.0 kg/m^3 at 15°C, and the (almost negligible) temperature dependence was assumed to be linear, giving

$$\rho_{oil} - 860.5 + 4.5\left(\frac{24.7 - T}{9.7}\right) \tag{8.1}$$

for the pure oil, which must be further corrected for the effect of the suspended water:

$$\rho_{ow} - (1 - \phi_w)\rho_{oil} + \phi_w\rho_{water} \tag{8.2}$$

where ϕ_w is the water fraction in the mixture.

8.4.4 Growth of micro-organisms

Samples were taken from the oil-water interface and cultures grown to establish the presence of bacteria. One population of a *pseudomonas* was found to be thriving. It would appear that this bacteria lives off the oil, but requires nitrate, present in small quantities in the water. The activity is therefore at its maximum at the interface and both the presence of the bacteria and their by-products may help to stabilise water-in-oil dispersions. This problem is currently under review for future projects.

‡ The mixture density is a simple volume average of the two pure liquid densities, whereas the mixture viscosity is related to the dispersed phase volume fraction by an empirical equation.

THIS IS A BLANK PAGE

Chapter 9:
EXPERIMENTAL INVESTIGATION OF THREE-PHASE OIL-WATER-GAS FLOWS

9.1 EXPERIMENTAL PROGRAMME

The three-phase oil-water-air flow experimental programme was conducted in two parts. Pressure gradients and flow visualisations were taken in August and September 1991, and then following the installation of the holdup measurement section, a further series of experiments were performed in the period March-June 1992 to measure holdup, together with pressure gradient and flow visualisation. The main difference between the two sets of experiments was the generally higher temperature (and hence lower oil viscosity) in the earlier experiments. The ranges of experimental parameters are shown in Table 9.1.

Table 9.1: Ranges of parameters in WASP three-phase experiments

Air Superficial Velocity	0.98 - 4.1 m/s
Oil Superficial Velocity	0 - 0.54 m/s
Water Superficial Velocity	0 - 0.83 m/s
Temperature	13 - 24°C
Slug Catcher Pressure	1.10 - 3.36 bar abs
Oil/Water Viscosity Ratio	40 - 60
Oil/Water Density Ratio	0.878

The experimental data points and calculations from them are tabulated in Appendix D:

Table D.1	Measured quantities
Table D.2	Physical properties
Table D.3	Holdup measurements
Table D.4	Equilibrium stratified flow holdup and slug frequencies
Table D.5	Stratified-slug transition calculations
Table D.6	Pressure gradient correlations (linear liquid viscosity)
Table D.7	Pressure gradient correlations (Brinkman liquid viscosity)

9.2 RESULTS

9.2.1 Pressure gradient

a) Comparisons with pressure gradient correlations (Chapter 3)

Pressure gradient measurements from the experiments were compared with correlations, following the work described in Chapter 3. There, it was found that where the oil and water phases were well-mixed, the best agreement with the data was given by the Beggs & Brill[5] correlation with a suitable adjustment for the liquid viscosity. Previous workers had taken the effective viscosity as a mean of the oil and water viscosities weighted by volume fraction. This tended to produce curves of the ratio of measured to calculated pressure gradient against water fraction with a characteristic 'hump'. A more accurate approach is to use one of the equations for the viscosity of a dispersion of one liquid in another, for example that due to Brinkman[39]:

$$\mu_{\text{mix}} = \frac{\mu_{\text{cont}}}{(1-\phi)^{2.5}} \tag{9.1}$$

Since the largest part of the pressure drop is due to the motion of the liquid slugs, where the oil and water are well-mixed, it would be expected that this approach would apply to the WASP results. Thus, measured pressure gradient was compared to calculated pressure gradient using various correlations and using both the liquid viscosity calculated from equation (9.1) and the volume average method. Table 9.2 shows a comparison of the percentage errors in these calculations. The root mean square average is the best indication to the reliability of a correlation, together with the standard deviation. However, a simple average is also a useful quantity, since it shows whether a correlation consistently over- or under-predicts. Hence it is clear that the Beggs & Brill correlation is the best of those compared to this data and that most correlations over-predict pressure gradient. Table 9.3 shows the performance of the Beggs & Brill correlation when compared to the two-phase data points, and also using the linear liquid viscosity calculation.

Table 9.2: Errors in pressure gradient calculations from correlations using Brinkman viscosity

Correlation	RMS Error %	Standard Deviation	Average Error %
McAdams	31	29	-12
Schlichting	38	37	7
Beggs & Brill	27	21	18
Dukler	89	36	81
Friedel	83	59	59
Lockhart & Martinelli	38	31	22

Table 9.3: Errors in pressure gradient calculations using the Beggs & Brill correlation

Method	RMS Error %	Standard Deviation
Air-oil flow	14	10
Air-water flow	17	12
Three-phase flow (linear viscosity)	87	52
Three-phase flow (Brinkman viscosity)	27	21

A number of figures are presented to demonstrate the behaviour of the pressure gradient in three-phase flow. Figure 9.1 shows a comparison of calculated with measured pressure gradient, using the Beggs & Brill correlation and both the linear and Brinkman liquid viscosities; the superior behaviour of the Brinkman viscosity is clear. Figure 9.2 shows a comparison of pressure gradient calculated from the Beggs & Brill correlation with measured values for both two-phase (air-oil and air-water) and three-phase flows. In Figure 9.1 it is clear that the linear viscosity over-predicts pressure gradient in the water-continuous region ($\phi \lesssim 0.6$) while underpredicting in the oil-continuous region. This is further demonstrated by Figure 9.3 which shows the error in calculation as a function of oil fraction and Figure 9.4 which shows the ratio of calculated to measured pressure gradient against oil fraction. Both these

graphs show results using the linear and the Brinkman viscosities. The reason for the behaviour described becomes clear by looking at Figure 9.5 which shows the effective liquid viscosity as a function of oil fraction, as calculated by the two different viscosity methods. The linear viscosity is clearly too high in the water-continuous region and far too low in the oil-continuous region.

The inversion point at which the flow changed from water-continuous to oil-continuous was found to be at an oil fraction of about 0.6. Some points with smaller oil fractions were also found to have been oil-continuous: this was determined from both the visual observations and from the large pressure gradients. In some cases, the prediction of pressure gradient in the inversion region was not as good as was found at lower oil fractions: this was thought to be due to the formation of a transient dispersion of one phase in the other, whose properties could neither be described by assuming a water- or an oil-continuous flow.

Figures 9.6 and 9.7 show the variation with oil fraction of the ratio of calculated to measured pressure gradient, for all the correlations compared; the behaviour is summarised by the average errors listed in Table 9.2.

Finally, it should be observed that there was no difference detected in the agreement between measured and calculated pressure gradients from the two different phases of the experimental programme. The average error between measurements and calculations (using the Brinkman viscosity equation) is well within the margins expected when applying the Beggs & Brill correlation to *two-phase* flows, and the Brinkman viscosity correction may therefore be satisfactorily used to explain the effect of a second liquid phase in this system.

b) Comparison with slug flow models (Chapter 7)

As well as comparisons with correlations above, the experimental pressure gradient measurements were compared with the three-phase slug model adapted from Dukler & Hubbard[77] which was presented in Chapter 3. Comparisons were also made between pressure gradients measured for two-phase air-oil and air-water slug flows and the Dukler & Hubbard model. Table 9.4 shows the errors in the pressure gradient calculations compared to the measurements for the various types of flows.

Table 9.4: Errors in pressure gradient calculations using the adapted Dukler & Hubbard slug flow model

Method	RMS Error %	Standard Deviation	Average Error %
WC air-oil-water flow	19	17	+9
OC air-oil-water flow	29	11	-27
Air-water flow	16	15	+5
Air-oil flow	16	9	-14

The most important results are those for water-continuous three-phase flows (the majority of the data points) where it will be seen that there is a considerable improvement of the modified Dukler & Hubbard model over the Beggs & Brill correlation. It is to be expected that a model for a particular type of flow would give more accurate predictions than a general correlation. Figure 9.8 shows a comparison of calculated against measured pressure gradient for the water-continuous three-phase flows using the slug flow model and Figure 9.9 includes the calculations using the Beggs & Brill correlation with the Brinkman viscosity correction.

9.2.2 Holdup

The measurement of holdup presented particular problems due to the intermittent nature of the flow. The ratio of the length of the trapped section (6.78 m) to the length and frequency of slugs was such that a particular trapped volume could vary enormously, depending on whether or not a liquid slug was trapped. Time delay between activating the control and the valves actually closing, together with the slightly unpredictable behaviour of these flows meant that it was not possible to ensure that consistent samples were trapped.

However, the experimental technique is important for future work and there is no published work on holdup in three-phase slug flow. Previous workers (eg Malinowsky[3]) have not published their data, claiming it to be too unreliable.

Very generally, the average holdup in slug flow seems to be similar across the range of flow conditions covered in this study. The important feature, therefore, is how the

holdup of oil and water vary separately, as a function of the input oil/water ratio. The oil/water ratio is related to the oil fraction by:

$$\mathrm{OWR} = \frac{u_{os}}{u_{ws}} = \frac{\phi}{1-\phi} \tag{9.2}$$

and hence the inversion point of $\phi = 0.6$ corresponds to an oil/water ratio of 1.5.

Figures 9.10 and 9.11 show the measurements of holdup of oil and water respectively, plotted against the oil/water ratio, showing the expected tendency for water holdup to decrease and oil holdup to increase with increasing oil/water ratio. Also shown on these figures are the values of holdup calculated from the equilibrium stratified flow model described in Chapter 4. The measured water holdup follows the trend of the stratified flow model calculations well, although the values are always smaller than those from the stratified model. The measured oil holdup agrees less well with the stratified flow model, but still shows the same general trend. There are a number of possible reasons for this discrepancy:

1. Not all the liquid trapped in the holdup section may have been collected, this being a particular problem in experiments in horizontal pipes. However, considerable care was taken to ensure that all the liquid was blown out of the pipe and comparison with other experiments (eg Russell *et al*[13]) suggests that 95% of the liquid should be recovered. The 5% loss does not explain the larger differences shown in Figures 9.10 and 9.11.
2. The equilibrium stratified flow model is not a good guide to the expected holdup in slug flow. A large proportion of the liquid is conveyed as fast-moving liquid slugs, so that the holdup in the intervening 'stratified' portions must be considerably smaller than the equilibrium stratified flow holdup.
3. The measured oil holdup tended to be particularly small in cases where the total holdup itself was small (corresponding to regions between slugs) for water-continuous flows, where the oil/water ratio was less than 1.5. Observations of the flows indicated that for water-continuous flows where a separate oil layer formed, the height of this layer was much smaller than the stratified flow model calculations would suggest (Table D.4). It would therefore appear that the majority of the oil phase is conveyed by the liquid

slugs, with a much smaller proportion in the region between slugs. This was not observed to be the case for oil-continuous flows, where the oil holdup values were much larger.

These measurements of holdup therefore show two important features. Firstly, that the experimental technique itself appears to be reliable, while confirming the view that 'holdup' in slug flow is a difficult quantity to characterise due to the intermittent nature of the flow. This technique could be used to measure holdup in stratified flows satisfactorily. Secondly, there are indications that the transport of the liquid phases is complicated. In water-continuous flows, oil was preferentially transported in the liquid slugs, while in oil-continuous flows there appears to be good distribution of the phases. The large viscosity of the oil phase is likely to play an important role in this process.

It is useful to compare the measurements of holdup with the calculations from the slug flow model presented in Section 7.3.3. The slug body was considered to be well-mixed, while the film region was assumed to be separate. The average holdup over the slug unit (which is the measured quantity in the experiments) is obtained by a volumetric average over the film and slug regions. The results of these calculations for all the water-continuous flows are shown in Figures 9.12 and 9.13 in the same format as used in Figures 9.10 and 9.11. In the case of the water holdup, agreement between the slug flow model and the measured values is very good, and a considerable improvement on the stratified flow model. For the oil holdup, however, there is only a slight improvement from the stratified flow model to the slug flow model. This almost certainly arises from an over-estimation of the oil holdup in the film region, which in practice is much smaller than the value obtained from the stratified flow model. This is because for part (or all) of the length of the film, a large proportion of the oil is carried as droplets within the water phase, which leads to a greater oil velocity and smaller oil holdup than would be the case with a separate oil layer. Indeed, it is doubtful whether a smooth oil layer (as assumed in the stratified flow model) is ever formed in the film regions in these experiments. In comparison, smooth oil layers were observed to be formed in the experiments reported by Stapelberg *et al.*

9.2.3 Flow visualisation

As discussed in the previous chapter, the WASP facility was fitted with a visualisation section at the outlet end of the test section. This was monitored with a video camera, but the transmission of light and focussing was difficult in three-phase flows due to scattering of light by the oil phase. Good pictures could therefore not be obtained, but observation was made of the flows by eye for each experimental point. A brief flow pattern description is given for each point listed in Table D.1 and these may be explained more fully as follows:

WATER SLUG	Two-phase air-water slug flow.
OIL SLUG	Two-phase air-oil slug flow.
WC SLUG SEP	Three-phase slug flow with water as the continuous phase. Separation of oil and water layers in the film region was observed.
WC SLUG SEP (Oily film)	WC SLUG SEP flow where drainage of the film after a slug was observed to be slower than for water. These points were very close to the inversion point to oil-continuous flows.
WC SLUG SEP (Borderline)	WC SLUG SEP flow where separation of oil and water layers in the film region was observed intermittently depending on the interval between slugs.
WC SLUG DISP	Three-phase slug flow with water as the continuous phase. The oil and water were dispersed throughout (no separate layers in the film region).
WC SLUG DISP (Oily film)	WC SLUG DISP flow where drainage of the film after a slug was observed to be slower than for water. These points were very close to the inversion point to oil-continuous flows.
OC SLUG DISP	Three-phase slug flow with oil as the continuous phase. All oil-continuous flows were dispersed throughout (no separate layers in the film region).

An additional observation was that in WC SLUG SEP flows, the water layer was undisturbed at the slug front and only became mixed with the oil phase approximately 2 to 4 pipe diameters further downstream. This is important in modelling the stratified

to slug flow transition, as discussed in Section 6.4. The particular features of the flow pattern observations, namely slug frequency, separated (WC SLUG SEP) to dispersed (WC SLUG DISP) transition and stratified to slug flow transition are discussed separately below.

a) Slug frequency

The slug frequency was calculated by counting the number of slugs in a fixed time interval. Figure 9.14 shows a plot of slug frequency against the total liquid superficial velocity. Two trends are apparent from this graph: firstly, for water-continuous flows, there is a roughly linear increase in slug frequency with the liquid velocity up to about 0.6 m/s and a roughly constant frequency above 0.6 m/s. Secondly, for oil-continuous flows, the frequency is higher than for water-continuous flows. (It was also observed in the experiments that the slugs in oil-continuous flows moved much faster than slugs in water-continuous flows.)

In Section 2.4.3, the correlation of Tronconi[34] was discussed, the slug frequency being given by:

$$\omega - \frac{1}{2}\left(1.22\frac{\rho_\ell}{\rho_g}\frac{u_g}{h_g}\right) \tag{9.3}$$

Stapelberg *et al*[10] suggested that for three-phase flow this should be modified by changing the $\frac{1}{2}$ to $\frac{1}{4}$. This equation does not explicitly consider the liquid velocity and in the light of the observations above, it appears that this is an important parameter. Nevertheless, the frequencies were calculated using both Tronconi's equation and Stapelberg's modification; these results are plotted in Figure 9.15. There is much greater scatter in these calculations than the data in Figure 9.14 would suggest. The mean errors are given in Table 9.5 with very little difference between using Stapelberg's factor of $\frac{1}{4}$ and using $\frac{1}{3.33}$, based on minimising the errors in calculated frequency.

Table 9.5: Errors in slug frequency calculations

Method	Factor in Equation 9.3	RMS Error %	Standard Deviation
Tronconi	$\frac{1}{2}$	77	49
Stapleberg	$\frac{1}{4}$	32	24
'Best fit'	$\frac{1}{3.33}$	30	29

The gas velocity and liquid height for these calculations were calculated using the equilibrium stratified flow model discussed in Chapter 4. This may itself introduce some error, as was seen when measured holdup was compared to the stratified flow model in Section 9.2.2.

b) Separated-dispersed transition

The transition between slug flows where the oil and water can form separate layers and flows where they are always dispersed was discussed in Section 6.5. A comparison of the WASP data with this transition is shown in Figure 9.16 where the measured gas velocity is plotted against the gas velocity calculated for transition (using the liquid velocity and oil fraction from the data points). Where the measured velocity is greater than the calculated transition velocity, the flow would be expected to be dispersed, while a smaller measured velocity would imply a flow where separation is expected. It should be remembered that the estimate of transition was based on some fairly crude arguments, but appears to work reasonably.

c) Stratified-slug transition

The transition between stratified and slug flows was considered in Chapter 6. A transition criterion based on steady-state (Kelvin-Helmholtz) theory was discussed in Section 6.2 and a criterion based on linear stability theory in Sections 6.3 and 6.4. The data from the WASP experiments can be compared to these transition criteria in a similar way to the data of Sobocinski and of Stapelberg in Section 6.4.5.

The transition criterion derived from linear stability theory was derived for three-phase flows with separate oil and water layers at the point of slug initiation and with the assumption that the water layer is undisturbed by the development of the slug.

This was observed to be the case in the WASP experiments where an undisturbed water layer persisted for 3 or 4 pipe diameters downstream of the slug front. The comparison of experimental data with the linear stability theory is shown in Figure 9.17 where the calculated superficial liquid velocity for transition is compared to the measured superficial liquid velocity at fixed superficial gas velocity and water fraction. The greater the difference between the measured velocity and the calculated transition velocity, the more likely the flow to be in the slug flow regime. In fact, in the experiments, all flows were observed to be in the slug flow regime, and Figure 9.17 shows that this is to be expected. A number of points will be seen to be very close to the transition boundary; it was found that the slug frequency in these cases was much smaller, compared to the other points.

It is interesting to compare the slug frequency with the difference between the measured liquid velocity and the calculated liquid velocity for transition. This is shown in Figure 9.18 where it will be seen that there is a good correlation between the two quantities. However, this agreement is probably only true over a relatively limited range of flowrates and should not be extrapolated to other situations without further experimental observations.

The calculations using modified Kelvin-Helmholtz theory are shown in Table D.5. This method predicts transition velocities significantly higher than by the linear stability theory and often inconsistent with the experimental observations (i.e. more flows expected to be stratified). This is probably because the steady-state transition depends principally on the *total* liquid holdup, which is relatively insensitive to variation in water fraction for example, while the linear stability theory considers both the oil and water holdup separately.

9.3 SUMMARY

For three-phase oil-water-air flow, new experimental data has been presented, covering pressure gradients, slug frequency, flow patterns observation and holdup measurement. Comparisons have been made with methods described in earlier chapters, showing very favourable agreement in most cases.

THIS IS A BLANK PAGE

Chapter 10:
CONCLUSIONS

10.1 CONCLUSIONS

10.1.1 Pressure gradient correlations

The most consistently reliable correlation for frictional pressure gradient in three-phase slug flow was the Beggs & Brill[5] correlation with an effective liquid viscosity given by the Brinkman[39] equation. Agreement with a number of data sources was found to be within the range expected for correlation of gas-liquid pressure gradient, but this still resulted in mean errors of the order of ±20%. It was found that the effective liquid viscosity approach could still be applied in flows where oil-water separation occurred, since the major contribution to the pressure gradient was from the motion of the slugs, where the liquids are usually well-mixed. None of the published correlations tested were found to be applicable to three-phase stratified flow data.

10.1.2 Multi-fluid stratified flow models

The two-fluid model derived by Taitel & Dukler[32] was extended to oil-water flows and oil-water-gas flows. In the former case, by comparison with numerical solutions, it was found that the ratio of the viscosities of the two phases could be an important parameter. As the viscosities become closer, the two-fluid model becomes less accurate. This is not a problem in gas-liquid flow where the gas viscosity is usually only a small fraction of the liquid viscosity, but can become significant in oil-water flows.

The three-fluid model for stratified oil-water-gas flows is an important advance, since besides allowing the calculation of holdup of oil and water in three-phase stratified flow, it can also be used as a basis for modelling flow pattern transitions. Excellent agreement was observed between the three-fluid model and experimental holdup data from the literature. Pressure gradient could also be calculated, with reasonable agreement.

10.1.3 Numerical stratified flow models

Use of bipolar coordinate grids and the mixing length turbulence model was successfully applied to numerical solutions for stratified oil-water and oil-water-gas flows. Comparisons were made with a range of experimental data for both systems.

The numerical techniques were particularly useful in the analysis of data from Stapelberg & Mewes[73]. Firstly, for oil-water flow it was possible to confirm the reduction in pressure gradient as a result of curvature of the interface (so that more of the pipe wall was wetted by water). Secondly, the numerical model was the only method which predicted the correct dependence of pressure gradient on gas flowrate for laminar three-phase flows.

10.1.4 Flow pattern transitions in three-phase flows

One of the most significant advances in this thesis is the ability to predict the transition from stratified to slug flow in three-phase systems. Firstly, the steady-state analysis of Taitel & Dukler was modified for three-phase flows where the oil and water were dispersed (using the Brinkman liquid viscosity) or separated (using the three-fluid model to calculate equilibrium liquid holdup). This highlighted the large difference in transition boundaries which could exist between the two extreme assumptions. The second approach was to apply linear stability theory, adapted from the work of Lin & Hanratty[56], to three-phase flows with separate oil and water layers. In common with experimental observations, the water layer was assumed to be undisturbed at the point of slug initiation. The results of this work were found to agree well with experimental data from Stapelberg[66] and the WASP facility (Section 9.2.3).

A second important area of three-phase flow pattern modelling to consider was the boundary of the region in which a separate water layer can occur in the regions between liquid slugs. This was calculated by considering the balance between the time required for drops to settle in the film region and the time interval between slugs. Although simple (and crude) this boundary was found to work well for observations from the WASP facility (Section 9.2.3).

10.1.5 Simple models for three-phase slug flows

The model proposed by Dukler & Hubbard[77] for gas-liquid slug flow was analysed and some simple modifications to account for the effect of a second liquid phase were suggested. In particular a volume-average density and a Brinkman viscosity were used for the combined oil and water phases. By averaging the holdup in the slug body and the film region, estimates were made of the average holdup of oil and water over the whole slug unit, and these were compared with experimental measurements from the WASP facility.

10.1.6 Experimental studies of three-phase flows

The experimental investigation of three-phase oil-water-air flow has provided new information on pressure gradients, flow patterns, slug frequency and holdup, complementing and extending the data available from the literature. Comparisons were made in Section 9.2 between this data and the methods described in Chapters 3 to 6 with good agreement being shown.

10.2 RECOMMENDATIONS FOR FURTHER WORK

Both the experimental data and the analysis presented would no doubt benefit from further work. In an area with as little published work as this, the scope for further development in enormous. Some suggestions are given below.

10.2.1 Further analysis

One of the areas which could be examined is to extend the stratified flow modelling to inclined flows. It is known that inclinations of just a few degrees (particularly uphill flow) can have a significant effect upon the holdup and pressure gradient. This would also affect the transition to slug flow and would be of considerable benefit in offshore pipeline design.

10.2.2 Further experimental data

The experiments described with the WASP facility should be extended to cover stratified flow and possibly annular flow. Holdup measurements for stratified flow

where the oil/water viscosity ratio is large (eg the Shell Tellus oil used in this study) would be particularly useful. The ranges of operating parameters (gas and liquid flowrates and the pressure) should be extended.

It is possible with the WASP facility to incline the test section by a few degrees; experiments with inclined flows would provide data for comparison with an extended stratified flow model.

It would also be useful to have operational pipeline data for comparison with the methods described for pressure gradients, water separation and holdup, with complete information concerning physical properties, pipeline topology, etc. Such data is hard to obtain.

REFERENCES

[1] **D.P.Sobocinski and R.L.Huntington**, "Concurrent flow of air, gas-oil and water in a horizontal pipe," *Transactions of the ASME*, pp. 252-256, 1958.

[2] **D.P.Sobocinski**, "Horizontal co-current flow of water, gas-oil and air," Master's thesis, University of Oklahoma, 1955.

[3] **M.S.Malinowsky**, "An experimental study of oil-water and air-oil-water flowing mixtures in horizontal pipes," Master's thesis, University of Tulsa, 1975.

[4] **G.C.Laflin and K.D.Oglesby**, "An experimental study on the effects of flow rate, water fraction and gas-liquid ratio on air-oil-water flow in horizontal pipes," Master's thesis, University of Tulsa, 1976.

[5] **H.D.Beggs and J.P.Brill**, "A study of two-phase flow in inclined pipes," *Journal of Petroleum Technology, Transactions*, vol. 255, pp. 607-617, 1973.

[6] **F.H.Poettmann and P.G.Carpenter**, "The multiphase flow of gas, oil and water through vertical flow strings with application to the design of gas-lift installations," *Drilling and Production Practice*, pp. 257-317, 1952.

[7] **M.R.Tek**, "Multiphase flow of water, oil and natural gas through vertical flow strings," *Journal of Petroleum Technology*, pp. 1029-1036, Oct. 1961.

[8] **A.I.Guzhov V.F.Medvedev and V.A.Savelev**, "Movement of gas/water/oil mixtures through pipelines," *International Chemical Engineering*, vol. 14, no. 4, pp. 713-714, 1974.

[9] **R.Sh.Shakirov**, "Pressure of hydraulic resistances during the motion of gas-oil-water mixtures in pipes," *Gazovoe Delo*, vol. 11, pp. 17-20, 1969. (In Russian).

[10] **H.H.Stapelberg F.Dorstewitz M.Nädler and D.Mewes**, "The slug flow of oil, water and gas in horizontal pipelines," in *5th International Conference on Multiphase Production*, (Cannes, France), pp. 527-552, June 1991.

[11] **S.Nuland K.Skarsvag G.Sæther and P.Fuchs**, "Phase fractions in three-phase gas-oil-water flow," in *5th International Conference on Multiphase Production*, (Cannes, France), pp. 3-30, June 1991.

[12] **M.Açikgöz F.França and R.T.Lahey**, "An experimental study of three-phase flow regimes," *International Journal of Multiphase Flow*, vol. 18, no. 3, pp. 327-336, 1992.

[13] **T.W.F.Russell G.W.Hodgson and G.W.Govier**, "Horizontal pipeline flow of mixtures of oil and water," *Canadian Journal of Chemical Engineering*, vol. 37, pp. 9-17, 1959.

[14] **M.E.Charles G.W.Govier and G.W.Hodgson**, "The horizontal pipeline flow of equal density oil-water mixtures," *Canadian Journal of Chemical Engineering*, vol. 39, pp. 27-36, 1961.

[15] **A.I.Guzhov A.P.Grishin and V.F.Medvedev**, "Emulsification during pipe flow of two liquids," *Neftyanoe Khozeistvo*, vol. 8, pp. 58-61, 1973. (In Russian).

[16] **H.H.Stapelberg and D.Mewes**, "The flow of two immiscible liquids and gas in horizontal pipes: Pressure drop and flow regimes," in *European Two-Phase Flow Group Meeting*, no. H3, (Varese, Italy), May 1990.

[17] **S.Arirachakaran K.D.Oglesby M.S.Malinowsky et al**, "An analysis of oil/water flow phenomena in horizontal pipes," *SPE Paper 18836*, pp. 155–167, 1989.

[18] **K.D.Oglesby**, "An experimental study on the effects of oil viscosity, mixture velocity and water fraction on horizontal oil-water flow," Master's thesis, University of Tulsa, 1979.

[19] **S.Arirachakaran**, "An experimental study of two-phase oil-water flow in horizontal pipes," Master's thesis, University of Tulsa, 1983.

[20] **R.V.A.Oliemans G.Ooms H.L.Wu and A.Duijvestijn**, "Core-annular oil/water flow: The turbulent-lubricating-film model and measurements in a 5cm pipe loop," *International Journal of Multiphase Flow*, vol. 13, no. 1, pp. 23–31, 1987.

[21] **T.Fujii J.Ohta N.Takenaka et al**, "The flow characteristics of a horizontal immiscible equal-density liquid-liquid two-phase flow," in *International Conference on Multiphase Flows '91*, (Tsukuba, Japan), pp. 195–198, Sept. 1991.

[22] **R.W.Lockhart and R.C.Martinelli**, "Proposed correlation of data for isothermal two-phase, two-component flow in pipes," *Chemical Engineering Progress*, vol. 45, no. 1, pp. 39–48, 1949.

[23] **D.Chisholm**, "A theoretical basis for the Lockhart-Martinelli correlation for two-phase flow," *International Journal of Heat and Mass Transfer*, vol. 10, pp. 1767–1778, 1967.

[24] **P.Schlichting**, "The transport of oil-water-gas mixtures in oil field gathering systems," *Erdöl-Erdgas-Zeitschrift*, vol. 86, pp. 235–249, 1971. (In German).

[25] **M.E.Charles and L.U.Lilleleht**, "Correlation of pressure gradients for the stratified laminar-turbulent pipeline flow of two immiscible liquids," *Canadian Journal of Chemical Engineering*, vol. 44, pp. 47–49, 1966.

[26] **P.Theissing**, "A generally valid method for calculating frictional pressure drop in multiphase flow," *Chemie Ingenieur Technik*, vol. 52, no. 4, pp. 344–345, 1980. (In German).

[27] **L.Friedel**, "Improved friction pressure drop correlations for horizontal and vertical two-phase pipe flow," in *European Two Phase Flow Group Meeting*, no. E2, (Ispra, Italy), June 1979.

[28] **D.Chisholm**, "Pressure gradients due to friction during the flow of evaporating two-phase mixtures in smooth tubes and channels," *International Journal of Heat and Mass Transfer*, vol. 16, pp. 347–348, 1973.

[29] **F.N.Schneider P.D.White and R.L.Huntington**, "Horizontal two-phase oil and gas flow," *Pipeline Industry*, pp. 47–51, 1954.

[30] **O.Baker**, "Simultaneous flow of oil and gas," *Oil and Gas Journal, July 26th*, pp. 185–195, 1954.

[31] **J.M.Mandhane G.A.Gregory and K.Aziz**, "A flow pattern map for gas-liquid flow in horizontal pipes," *International Journal of Multiphase Flow*, vol. 1, pp. 537–553, 1974.

[32] **Y.Taitel and A.E.Dukler**, "A model for predicting flow regime transitions in horizontal and near-horizontal gas-liquid flow," *AIChE Journal*, vol. 22, no. 1, pp. 47–55, 1976.

[33] **G.A.Gregory and D.S.Scott**, "Correlation of liquid slug frequency and velocity in horizontal co-current gas-liquid slug flow," *AIChE Journal*, vol. 15, no. 6, pp. 933–935, 1969.

[34] **E.Tronconi**, "Prediction of slug frequency in horizontal two-phase slug flow," *AIChE Journal*, vol. 36, no. 5, pp. 701–708, 1990.

[35] **E.C.Bingham**, "Viscosity and fluidity," *American Chemical Journal*, vol. 35, no. 3, pp. 195–217, 1906.

[36] **S.Arrhenius**, "On the internal friction of solutions in water," *Zeitschrift für Physikalische Chemie (Leipzig)*, vol. 1, pp. 285–298, 1887. (In German).

[37] **A.Einstein**, "A new definition of molecular dimensions," *Annalen der Physik (4)*, vol. 19, pp. 289–306, 1906. (In German).

[38] **G.I.Taylor**, "The viscosity of a fluid containing small drops of another fluid," *Proceedings of the Royal Society of London*, vol. 138A, pp. 41–48, 1932.

[39] **H.C.Brinkman**, "The viscosity of concentrated suspensions and solutions," *Journal of Chemical Physics*, vol. 20, no. 4, p. 571, 1952.

[40] **P.E.Rycroft**, "Transmission section: Chairman's address," *Journal of the Institution of Electrical Engineers*, vol. 90, no. 25, pp. 39–42, 1943.

[41] **E.G.Richardson**, "On the viscosity of emulsions," *Kolloid Zeitschrift*, vol. 65, no. 1, pp. 32–37, 1933. (In German).

[42] **E.Hatschek**, *The Viscosity of Liquids*. London: Bell & Sons Ltd, 1928.

[43] **L.T.Monson**, "Viscosity of petroleum emulsions," *Industrial and Engineering Chemistry*, vol. 30, no. 11, pp. 1287–1291, 1938.

[44] **W.Woelflin**, "The viscosity of crude oil emulsions," *API Drilling and Production Practice*, pp. 148–153, 1942.

[45] **T.W.F.Russell and M.E.Charles**, "The effect of the less viscous liquid in the laminar flow of two immiscible liquids," *Canadian Journal of Chemical Engineering*, vol. 37, pp. 18–34, 1959.

[46] **R.B.Bird W.E.Stewart and E.N.Lightfoot**, *Transport Phenomena*, ch. 2.5 (Adjacent Flow of Two Immiscible Liquids), pp. 54–56. New York: Wiley, 1973.

[47] **M.M.Denn**, *Process Fluid Mechanics*, ch. 18.3 (Laminar-Laminar Stratified Flow), pp. 344–351. New Jersey: Prentice-Hall Inc, 1st ed., 1980.

[48] **H.Bateman**, *Partial Differential Equations of Mathematical Physics*, ch. 3.81 (Bipolar co-ordinates), pp. 260–263. Cambridge University Press, 1952.

[49] **K.B.Ranger and A.M.J.Davis**, "Steady pressure-driven two-phase stratified laminar flow through a pipe," *Canadian Journal of Chemical Engineering*, vol. 57, pp. 688–691, 1979.

[50] **M.Bentwich**, "Two-phase viscous axial flow in a pipe," *Transactions of the ASME, Journal of Basic Engineering*, vol. 86, pp. 669–672, Dec. 1964.

[51] **A.R.Gemmell and N.Epstein**, "Numerical analysis of stratified laminar flow of two immiscible Newtonian liquids in a circular pipe," *Canadian Journal of Chemical Engineering*, vol. 40, pp. 215–224, 1962.

[52] **M.E.Charles and P.J.Redberger**, "The reduction of pressure gradients in oil pipelines by the addition of water: Numerical analysis of stratified flow," *Canadian Journal of Chemical Engineering*, vol. 40, pp. 70–75, 1962.

[53] **M.E.Charles**, "Water layer speeds heavy-crude flow," *Oil and Gas Journal, August 28th*, pp. 68–72, 1961.

[54] **O.Shoham and Y.Taitel**, "Stratified turbulent-turbulent gas-liquid flow in horizontal and inclined pipes," *AIChE Journal*, vol. 30, no. 3, pp. 377–385, 1984.

[55] **R.I.Issa**, "Prediction of turbulent, stratified, two-phase flow in inclined pipes and channels," *International Journal of Multiphase Flow*, vol. 14, no. 2, pp. 141–154, 1988.

[56] **P.Y.Lin and T.J.Hanratty**, "Prediction of the initiation of slugs with linear stability theory," *International Journal of Multiphase Flow*, vol. 12, no. 1, pp. 79–98, 1986.

[57] **S.G.Brand**, "Thistle: The engineering challenge of a field in decline," in *Chemical Engineering in Mature Oil and Gas Fields*, (Aberdeen, Scotland), Institution of Chemical Engineers, Apr. 1992.

[58] **C.M.Laing**, "Gas-lift design and performance analysis in the North West Hutton field," *Journal of Petroleum Technology*, pp. 96–102, Jan. 1991.

[59] **R.W.Leach**, "Pipeline designed for viscous crude," *The Pipeline Engineer*, pp. D25–D27, Nov. 1957.

[60] **M.Wicks and J.P.Fraser**, "Entrainment of water by flowing oil," *Materials Performance*, vol. 14, no. 5, pp. 9–12, 1975.

[61] **R.N.Duncan**, "Gathering lines corrosion in the Bahrain crude field," *Materials Performance*, vol. 22, no. 12, pp. 13–14, 1983.

[62] **G.F.Hewitt**, *Handbook of Multiphase Systems*, ch. 2.2.3 (Empirical Relationships for Frictional Pressure Gradient). New York: Hemisphere, 1982.

[63] **W.H.McAdams W.K.Woods and L.C.Heroman**, "Vaporization inside horizontal tubes — II Benzene-oil mixtures," *Transactions of the ASME*, vol. 64, pp. 193–200, 1942.

[64] **A.E.Dukler M.Wicks and R.G.Cleveland**, "Pressure drop and hold-up in two-phase flow," *AIChE Journal*, vol. 10, no. 1, pp. 38–51, 1964.

[65] **G.C.Yeh F.H.Haynie and R.A.Moses**, "Phase-volume relationship at the point of phase inversion in liquid dispersions," *AIChE Journal*, vol. 10, no. 2, pp. 260–265, 1964.

[66] **H.H.Stapelberg**, "Three-phase flow of oil, water and air." Private Communication, 1991.

[67] **H.H.Stapelberg**, *The Slug Flow of Oil, Water and Air in Horizontal Tubes*. PhD thesis, University of Hannover, 1991. (In German).

[68] **A.S.Fayed and L.Otten.**, "Comparing measured with calculated multiphase flow pressure drop," *Oil and Gas Journal, August 22nd*, pp. 136–144, 1983.

[69] **S.M.Richardson**, *Fluid Mechanics*. New York: Hemisphere, 1989.

[70] **G.L.Shires M.A.Mendes-Tatsis S.A.Fisher A.R.W.Hall and G.F.Hewitt**, "An experimental study of oil/water flow regimes and pressure drop in a horizontal pipe," Tech. Rep. MPS/14, Department of Chemical Engineering, Imperial College, Apr. 1992. (Commercial-in-Confidence).

[71] **H.H.Stapelberg and D.Mewes**, "The flow of two immiscible liquids and air in a horizontal pipe," in *Advances in Gas-Liquid Flows 1990*, (Dallas, USA), pp. 89–96, Nov. 1990.

[72] **M.Bentwich**, "Two-phase axial laminar flow in a pipe with naturally curved interface," *Chemical Engineering Science*, vol. 31, pp. 71–76, 1976.

[73] **H.H.Stapelberg and D.Mewes**, "Experimental studies of the stratified flow of two immiscible liquids and air in a horizontal pipe," in *European Two-Phase Flow Group Meeting*, no. G2, (Paris, France), 1989.

[74] **M.Ishii**, *Handbook of Multiphase Systems*, ch. 2.4.1 (Interfacial Waves and Instabilities). New York: Hemisphere, 1982.

[75] **J.O.Hinze**, "Fundamentals of the hydrodynamic mechanism of splitting in dispersion processes," *AIChE Journal*, vol. 1, no. 3, pp. 289–295, 1955.

[76] **H.Jeffreys**, "On the formation of water waves by wind," *Proceedings of the Royal Society*, vol. A107, p. 189, 1925.

[77] **A.E.Dukler and M.G.Hubbard**, "A model for gas-liquid slug flow in horizontal and near horizontal tubes," *Industrial and Engineering Chemistry Fundamentals*, vol. 14, no. 4, pp. 337–347, 1975.

[78] **K.Hashizume**, "Flow pattern, void fraction and pressure drop of refrigerant two-phase flow in a horizontal pipe — I. Experimental data," *International Journal of Multiphase Flow*, vol. 9, no. 4, pp. 399–410, 1983.

[79] **A.R.W.Hall**, "Cavity pressurisation ignition in the WASP rig at Imperial College, London," Tech. Rep. AEA-APS-0057, AEA Petroleum Services, Jan. 1991.

[80] **S.M.Richardson G.Saville and J.F.Griffiths**, "Autoignition - occurrence and effects," *Transactions of the IChemE (Part B)*, vol. 68, pp. 239–244, Nov. 1990.

THIS IS A BLANK PAGE

NOMENCLATURE

Symbol	Description	Units	Dimensions
A	Cross-sectional area	m^2	L^2
C	Wave velocity	ms^{-1}	LT^{-1}
c	Half interfacial length	m	L
D	Pipe diameter or hydraulic diameter	m	L
dp_F/dz	Frictional pressure gradient	Pa/m	$ML^{-2}T^{-2}$
$\dot{E}$	Rate of energy dissipation per unit mass	W/kg	L^2T^{-3}
f	Friction factor		
g	Acceleration due to gravity	ms^{-2}	LT^{-2}
H	Separation of parallel flat plates	m	L
h	Height of liquid layer	m	L
i	$\sqrt{-1}$		
k	Einstein factor (2.5)		
k	Wave number (2τ/wavelength)	m^{-1}	L^{-1}
L	Characteristic length	m	L
ℓ_m	Mixing length	m	L
$\dot{m}$	Mass flux	$kgm^{-2}s^{-1}$	$ML^{-2}T^{-1}$
P_i	Interfacial gas pressure	Pa	$ML^{-1}T^{-2}$
p	Pressure	Pa	$ML^{-1}T^{-2}$
Q	Volumetric flowrate	m^3s^{-1}	L^3T^{-1}
R	Pipe radius	m	L
S	Perimeter	m	L
s	Sheltering coefficient		
T	Temperature	°C	θ
t	Time	s	T
U	Characteristic velocity	ms^{-1}	LT^{-1}
U	Superficial velocity	ms^{-1}	LT^{-1}
u	Velocity	ms^{-1}	LT^{-1}
V	Volumetric flowrate factor		
x	Quality (gas mass fraction)		
Y	Inclination parameter		

Greek Letters

α	Half angle subtended by interface at centre of pipe		rad
Γ	Velocity profile shape factor $\left(\frac{1}{hU^2}\int_0^h u^2 dy\right)$		
γ	Ratio of oil-water to oil-wall shear stresses		
γ	Contact angle between interface and pipe wall		rad
ϵ_g	Void fraction		
ϵ	Surface energy per unit surface	Jm^{-2}	MT^{-2}
θ	Angle of inclination of pipe to horizontal	rad	rad
λ	Baker physical property parameter		
λ	Viscosity parameter		
μ	Dynamic viscosity	Pas	$ML^{-1}T^{-1}$
ν	Kinematic viscosity	m^2s^{-1}	L^2T^{-1}
ρ	Density	kgm^{-3}	ML^{-3}
σ	Surface tension	Nm^{-1}	MT^{-2}
τ	Shear stress	Nm^{-2}	$ML^{-1}T^{-2}$
ϕ	Oil fraction in liquid phase		
ψ	Baker physical property parameter		
ω	Slug frequency	IIz	T^{-1}

Dimensionless Groups

Fr	Froude number U^2/gL
Re	Reynolds number $\rho UL/\mu$
We	Weber number $\rho U^2 L/\sigma$
$\tilde{P}$	Dimensionless pressure gradient $L^2\left(\frac{dp}{dz}\right)/\mu U$
X^2	Martinelli parameter $(dp/dz)_\ell/(dp/dz)_g$

Marks above symbols

~	Dimensionless quantity
-	Mean value
^	Fluctuating quantity

Superscripts

/	Perturbed quantity
o	Property of pure component

Subscripts

a	Air
cont	Continuous phase

disp	Dispersed phase
g	Gas
go	Gas-oil interface
H	Homogeneous property
I	Imaginary part
i	Interfacial property
inv	Value at the inversion point
ℓ	Liquid
ℓo	Liquid with *total* mass flux
m	Mean value
mix	Property of a mixture
o	Oil
ow	Oil-water interface
R	Real part
tp	Two-phase quantity
w	Water

THIS IS A BLANK PAGE

FIGURES

THIS IS A BLANK PAGE

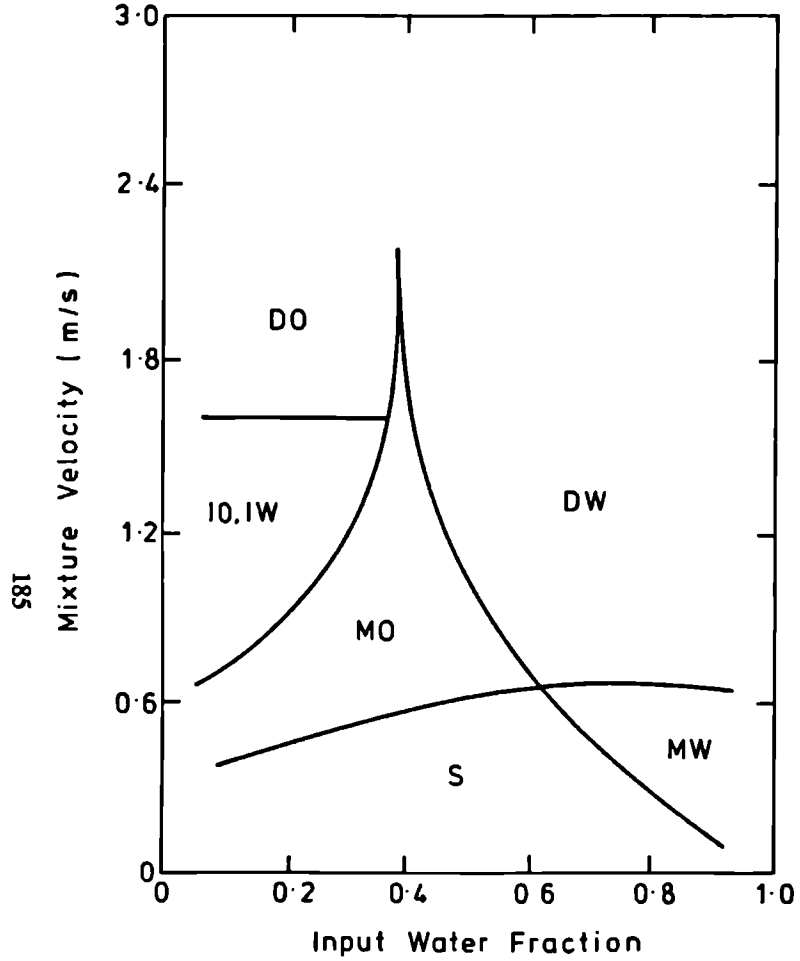


FIGURE 2·1. LIQUID-LIQUID FLOW PATTERN MAP (ADAPTED FROM GUZHOV)

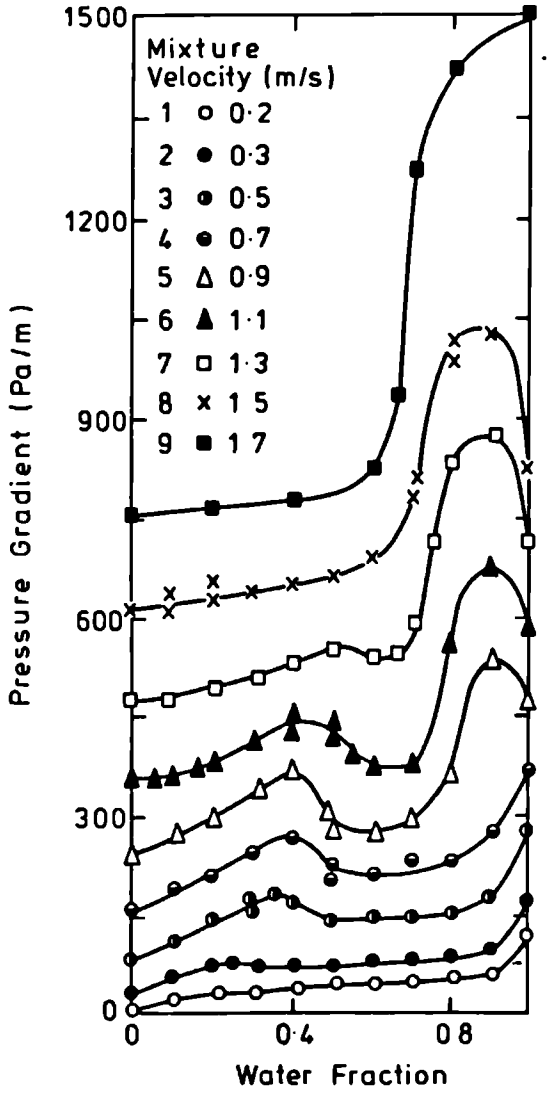


FIGURE 2·2. PRESSURE GRADIENT IN LIQUID-LIQUID FLOW (GUZHOV)

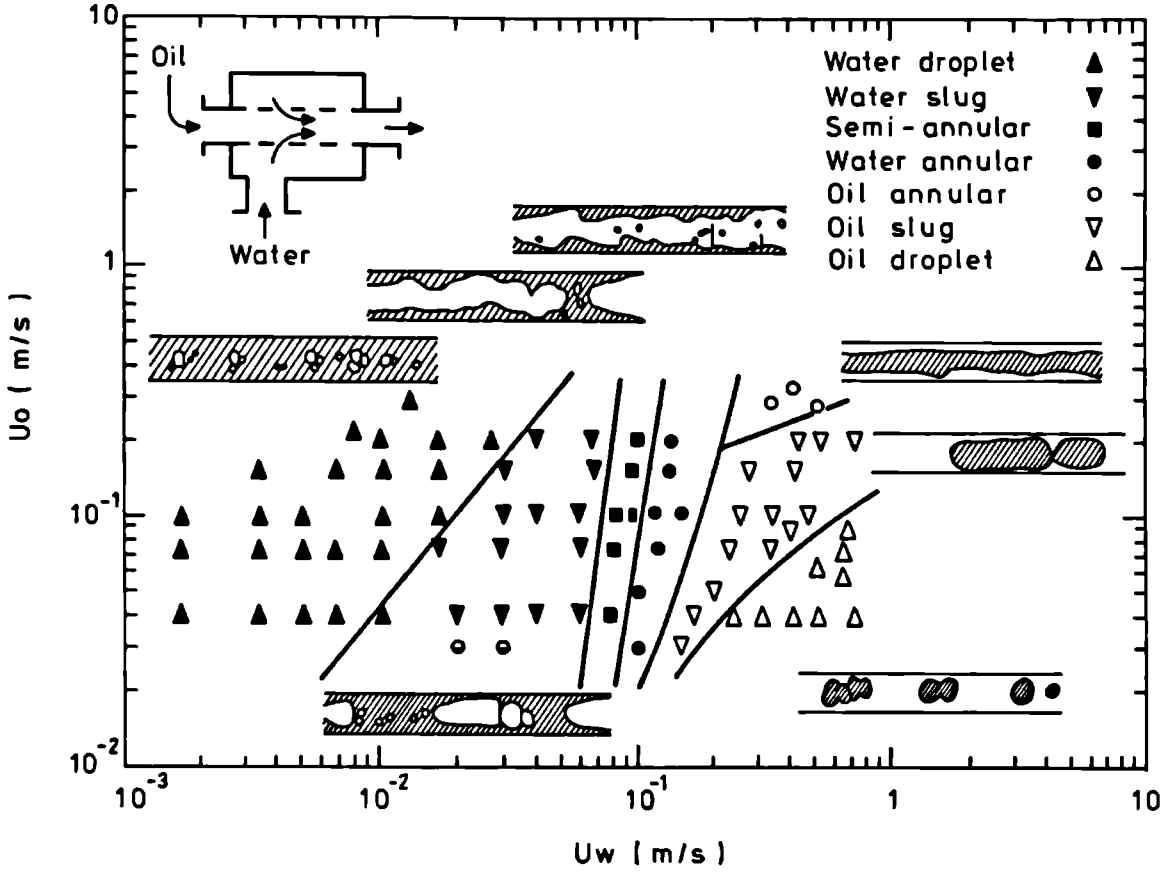


FIGURE 2 3. FLOW PATTERN MAP FOR LIQUID - LIQUID EQUAL DENSITY FLOW (FUJII)

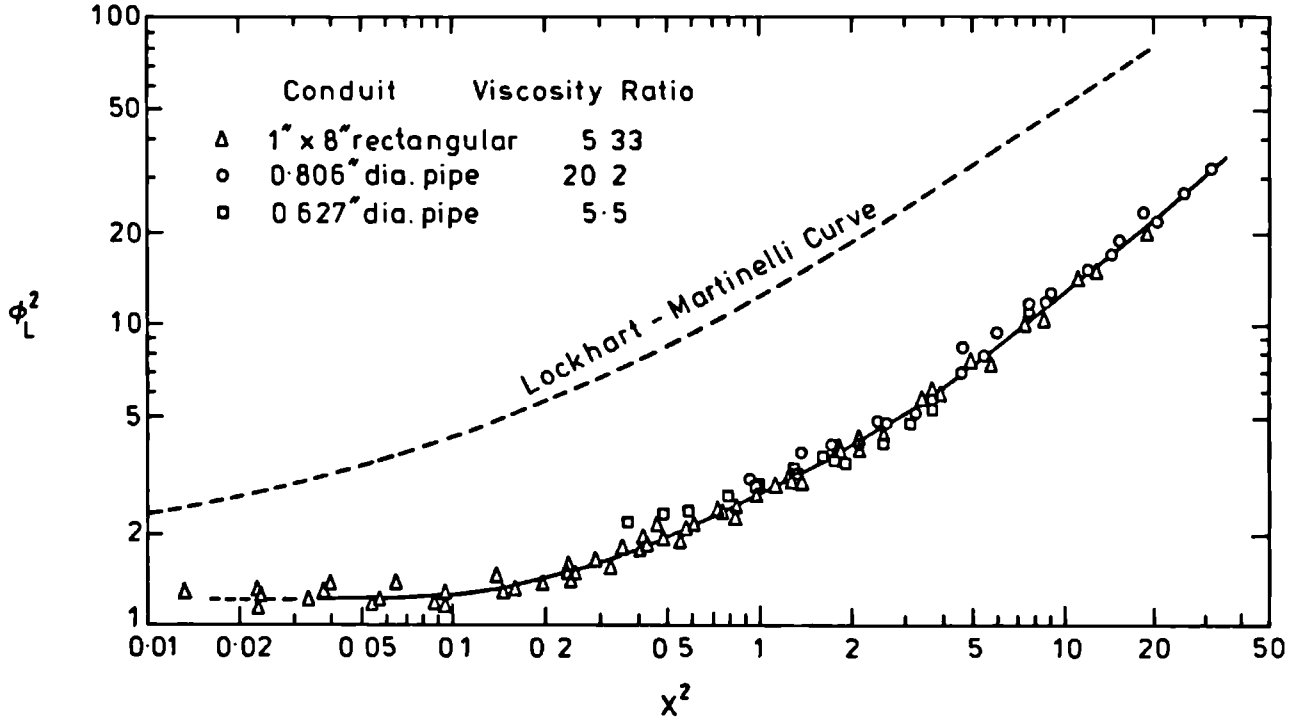


FIGURE 2·4. PRESSURE GRADIENT CORRELATION FOR LIQUID - LIQUID FLOW (CHARLES & LILLELEHT 1966)

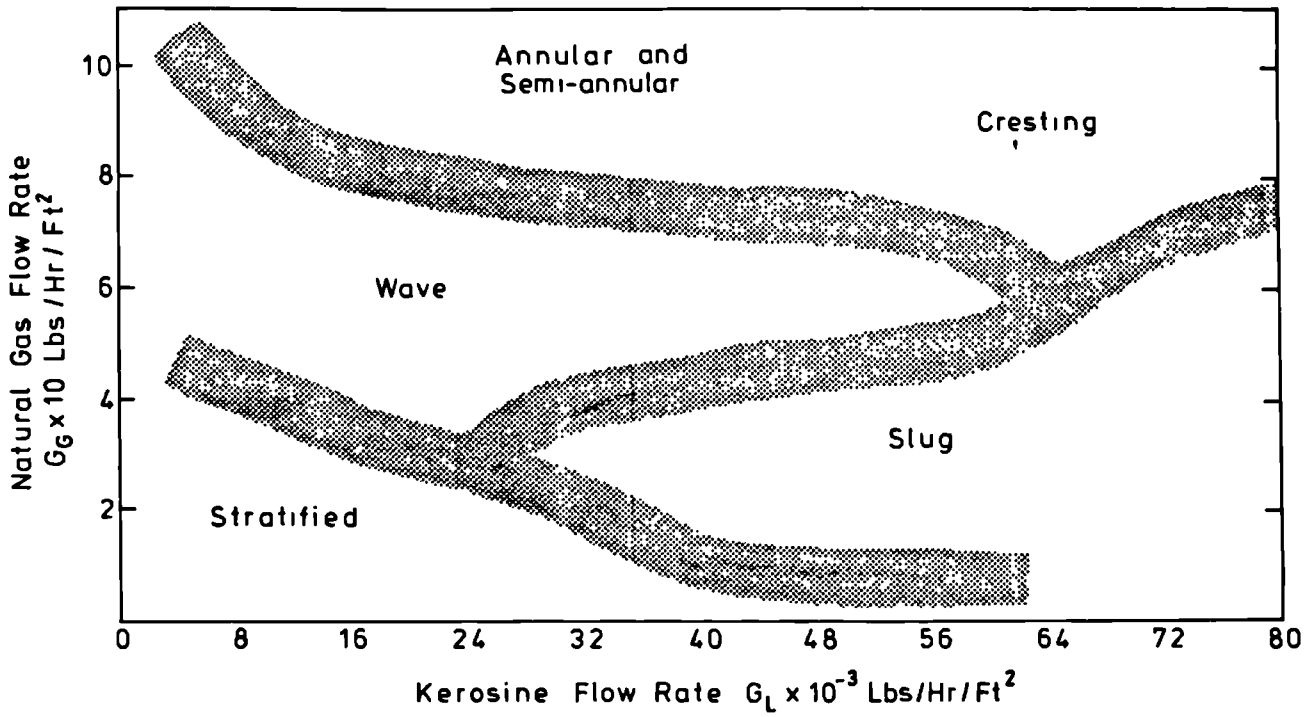


FIGURE 25. GAS-LIQUID FLOW PATTERN MAP (SCNE DER)

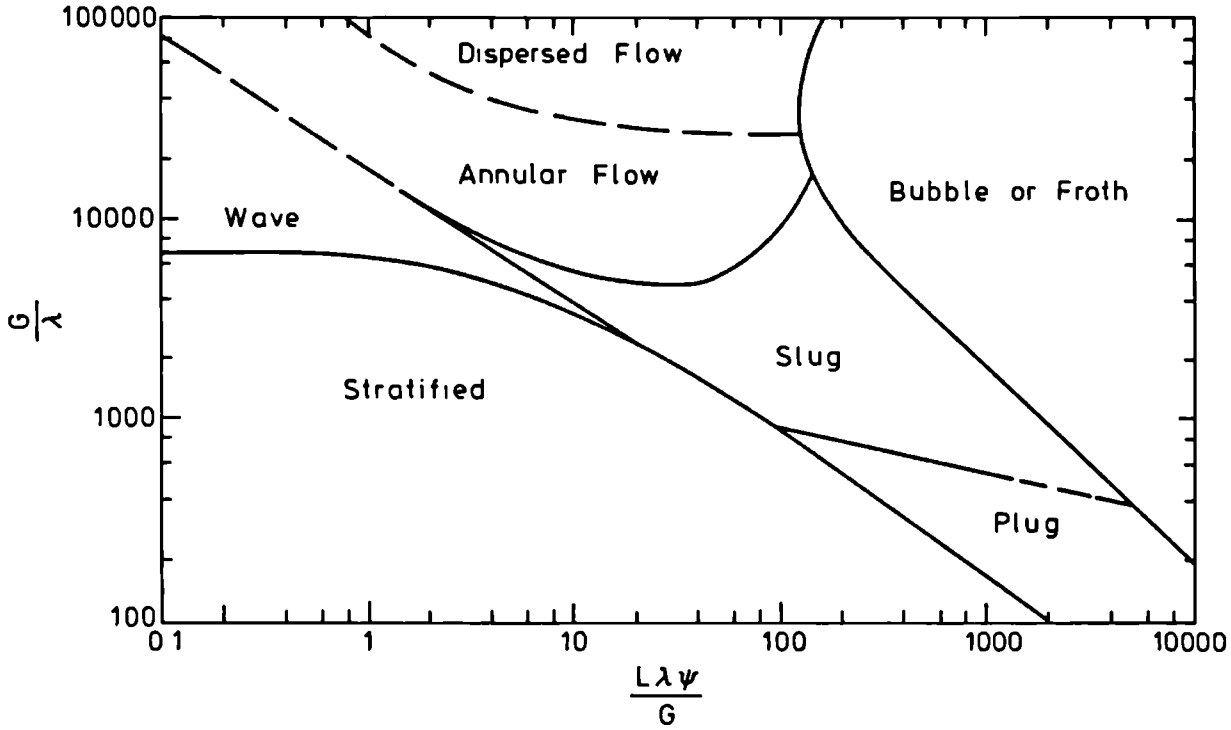
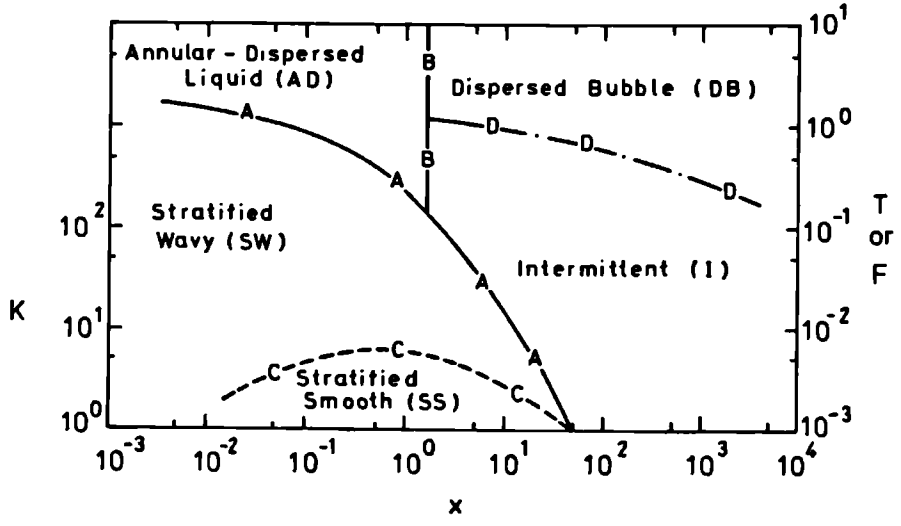


FIGURE 26 GAS-LIQUID FLOW PATTERN MAP (BAKER)



188

Curve : A & B C D
Coordinate : F vs X K vs X T vs X

$$X = \left[\frac{(dP/dx)_L^S}{(dP/dx)_G^S}\right]^{1/2} \qquad F = \sqrt{\frac{\rho_G}{(\rho_L-\rho_G)}}\frac{U_G^S}{\sqrt{Dg\cos\alpha}}$$

$$T = \left[\frac{|(dP/dx)_L^S|}{(\rho_L-\rho_G)g\cos\alpha}\right]^{1/2} \qquad K = \left[\frac{\rho_G U_G^{S^2} U_L^S}{(\rho_L-\rho_G)g\nu_L\cos\alpha}\right]^{1/2}$$

FIGURE 2·8. GENERALISED GAS-LIQUID FLOW PATTERN MAP (TAITEL & DUKLER)

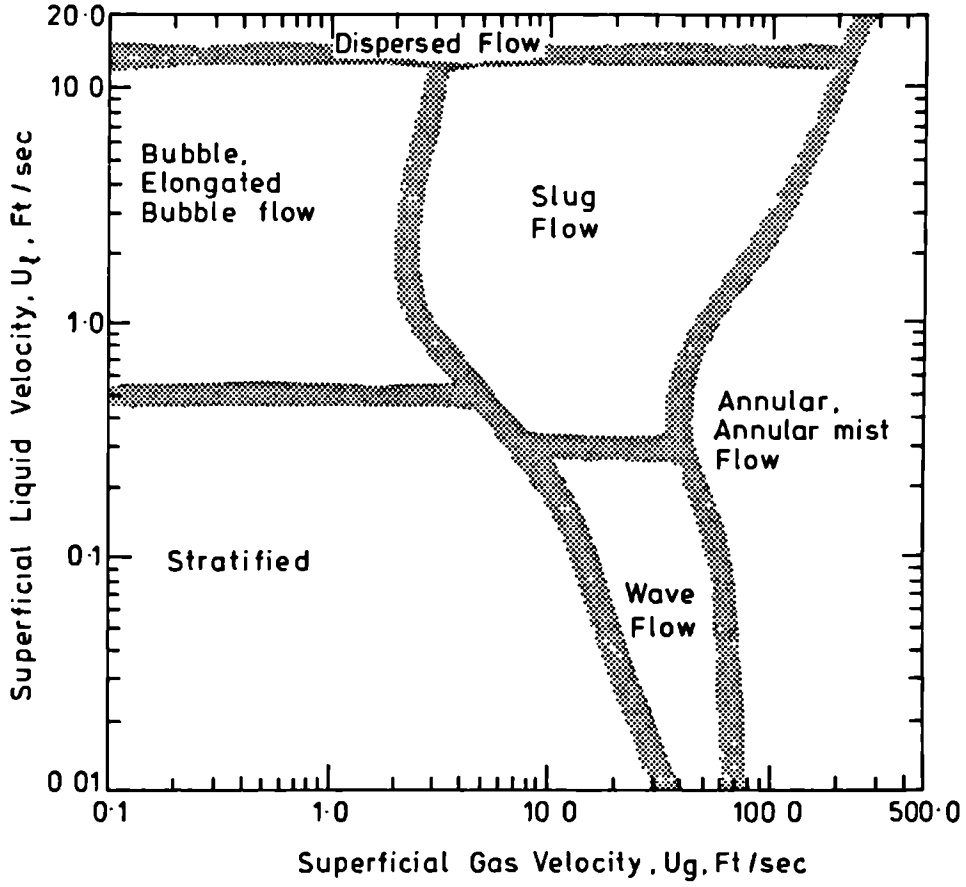
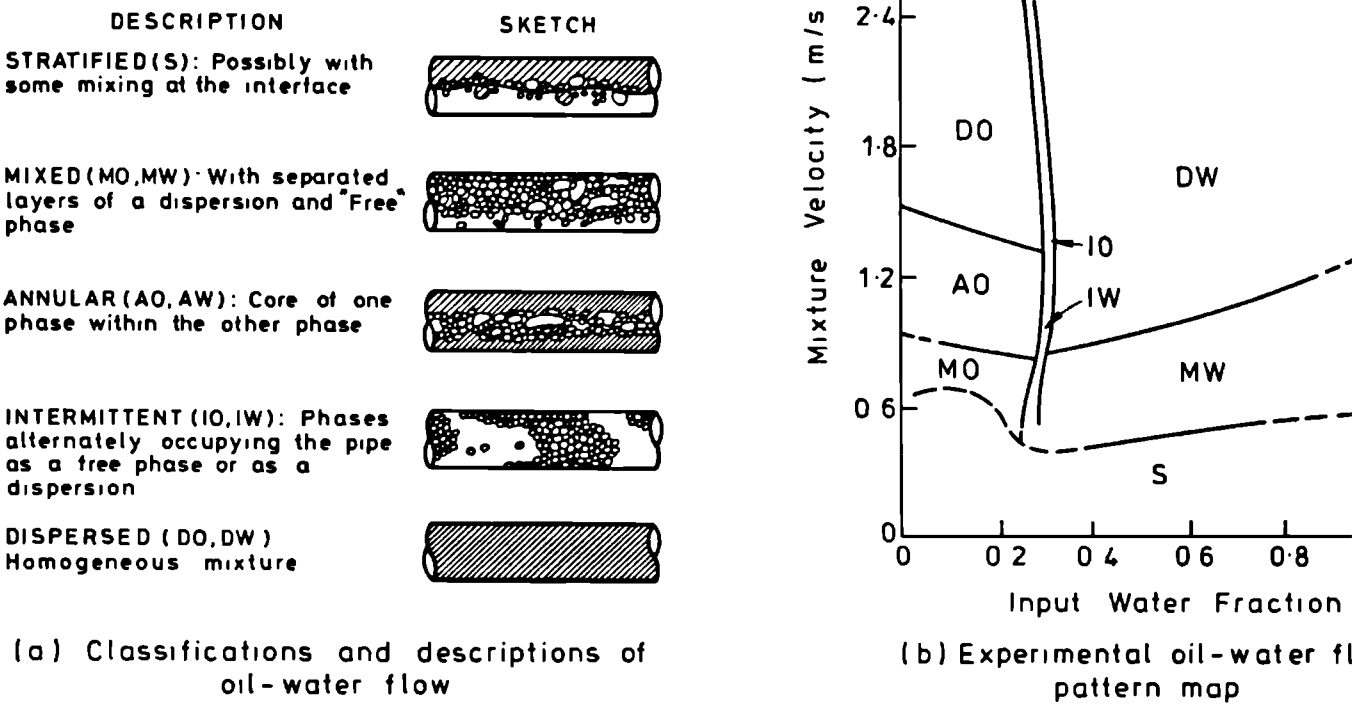


FIGURE 2·7. GAS-LIQUID FLOW PATTERN MAP (MANDHANE)



(a) Classifications and descriptions of oil-water flow

(b) Experimental oil-water fl pattern map

FIGURE 2 9 LIQUID-LIQUID FLOW PATTERN MAP (ARIRACHAKARAN)

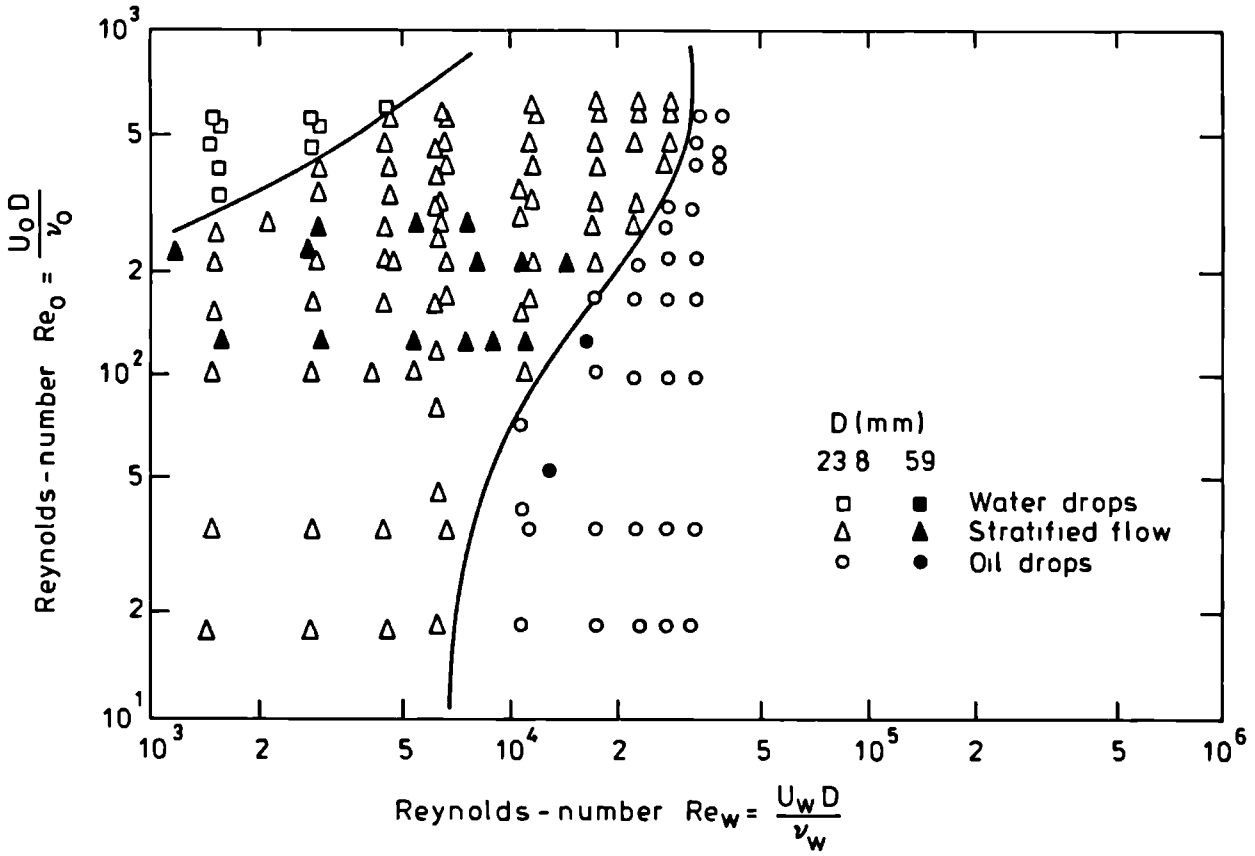
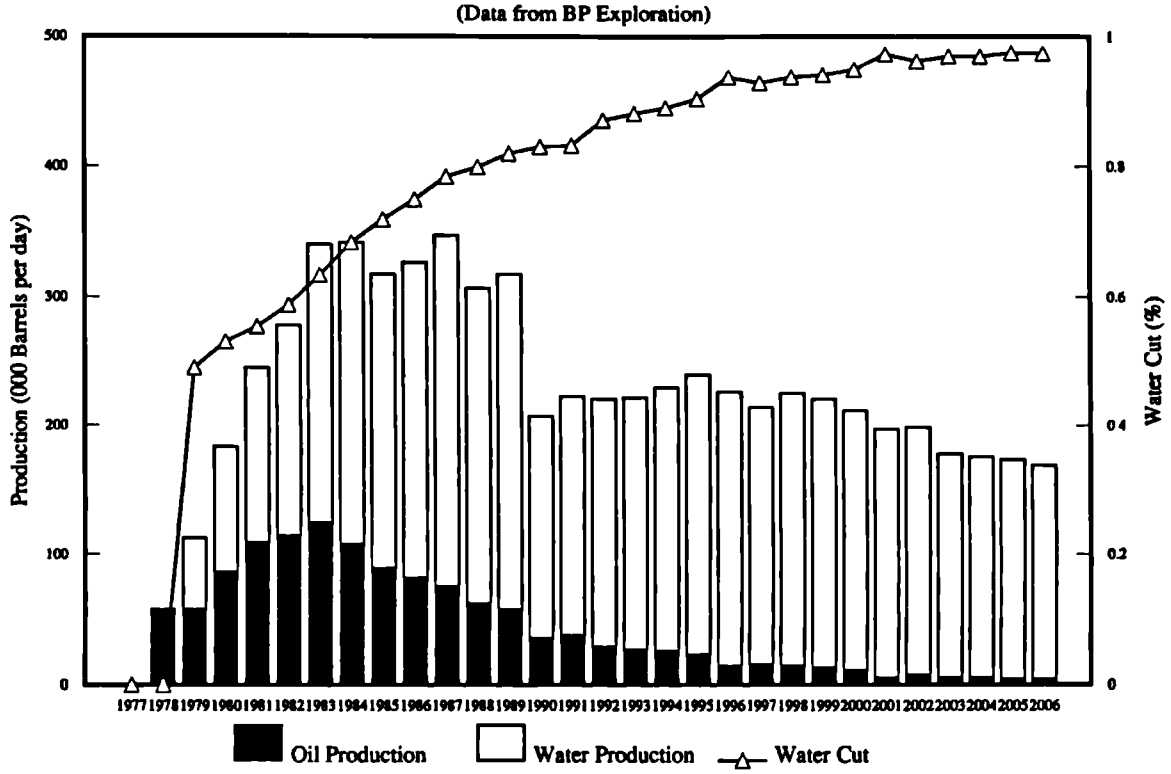


FIGURE 2 10 LIQUID-LIQUID FLOW PATTERN MAP (STAPELBERG & MEWES)

FIGURE 2.11: THISTLE PLATFORM PRODUCTION PROFILE

(Data from BP Exploration)



AEA PETROLEUM SERVICES
ARW HALL 22/6/92

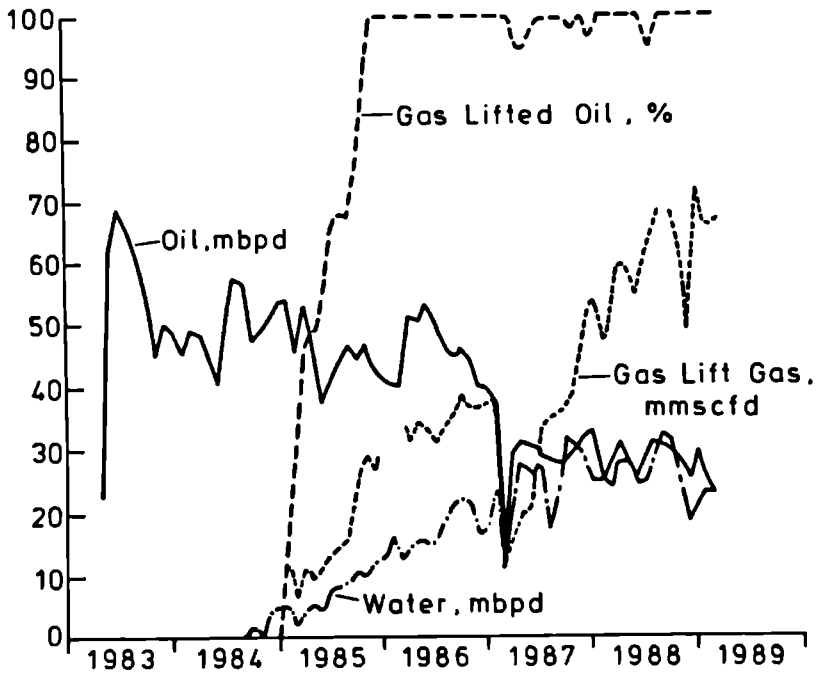


FIGURE. 2 12. NORTH WEST HUTTON PRODUCTION (LAING)

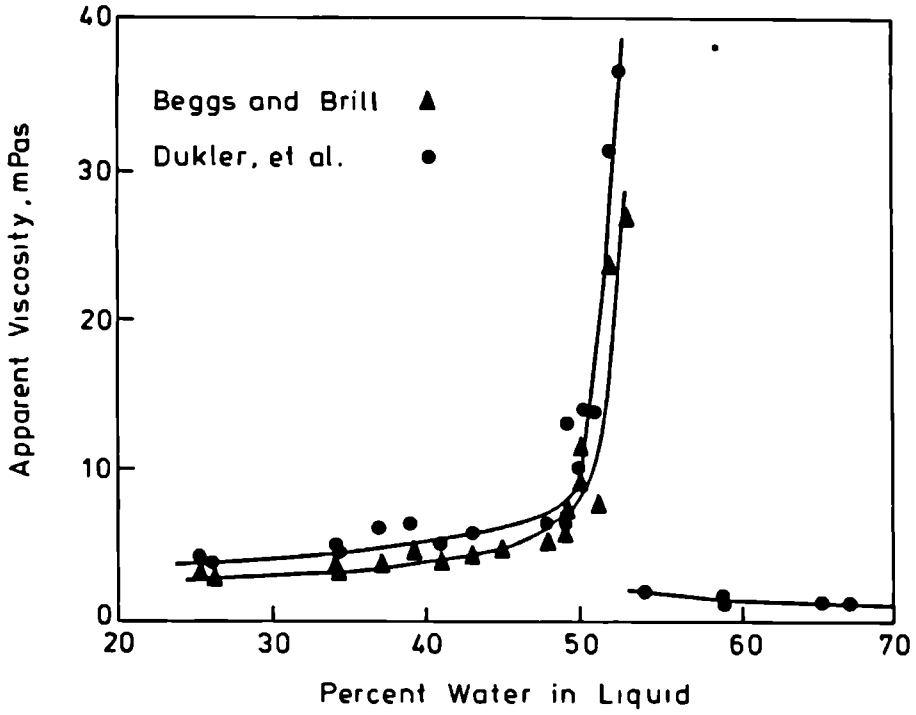
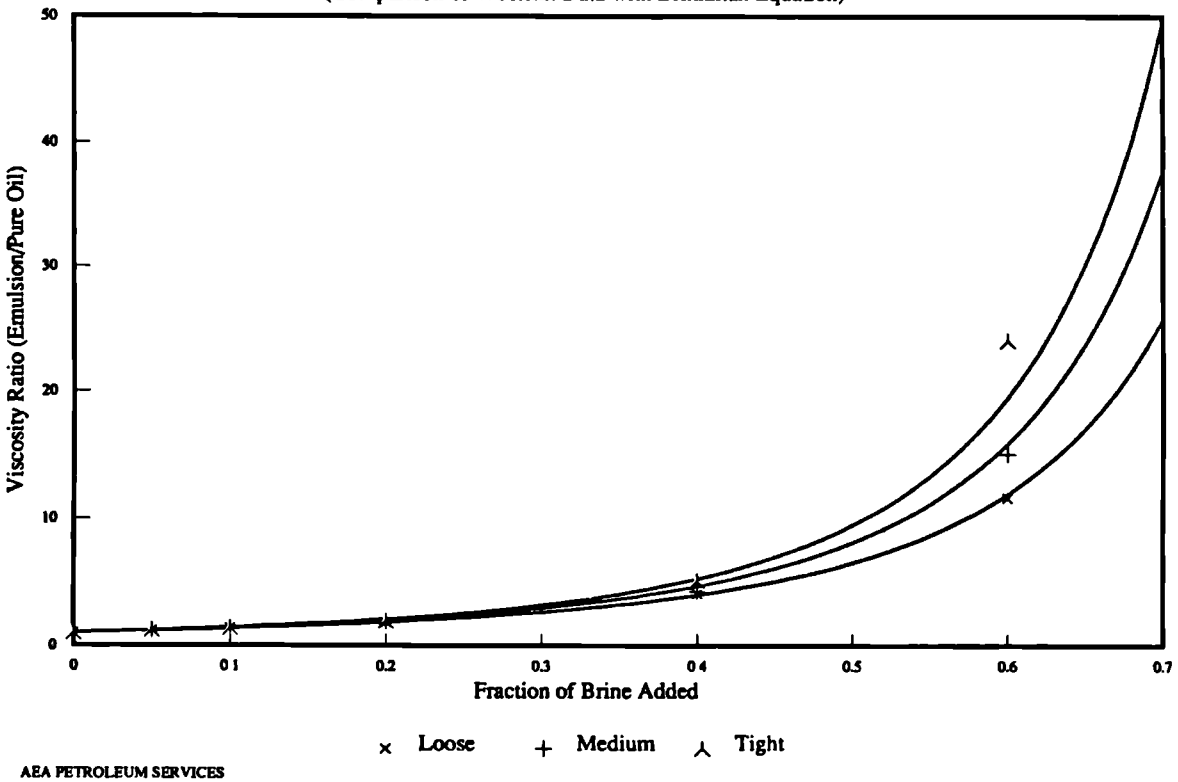


FIGURE 31. APPARENT LIQUID VISCOSITY FROM PRESSURE GRADIENT CALCULATIONS (MALINOWSKY)

FIGURE 3.2: EMULSION VISCOSITY

(Comparison of Woelflin Data with Brinkman Equation)



AEA PETROLEUM SERVICES
ARW HALL 13/7/92

FIGURE 3.3: COMPARISON OF MALINOWSKY DATA WITH BEGGS & BRILL CORRELATION

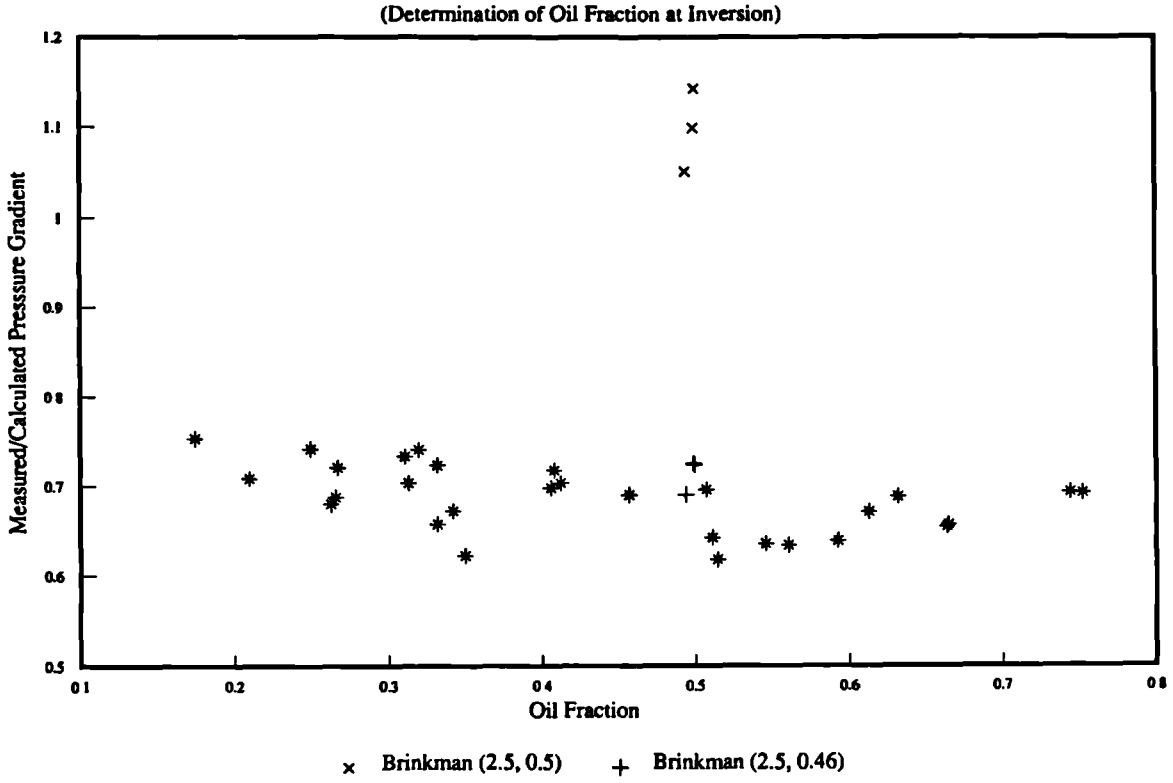


FIGURE 3.4: COMPARISON OF MALINOWSKY DATA WITH BEGGS & BRILL CORRELATION

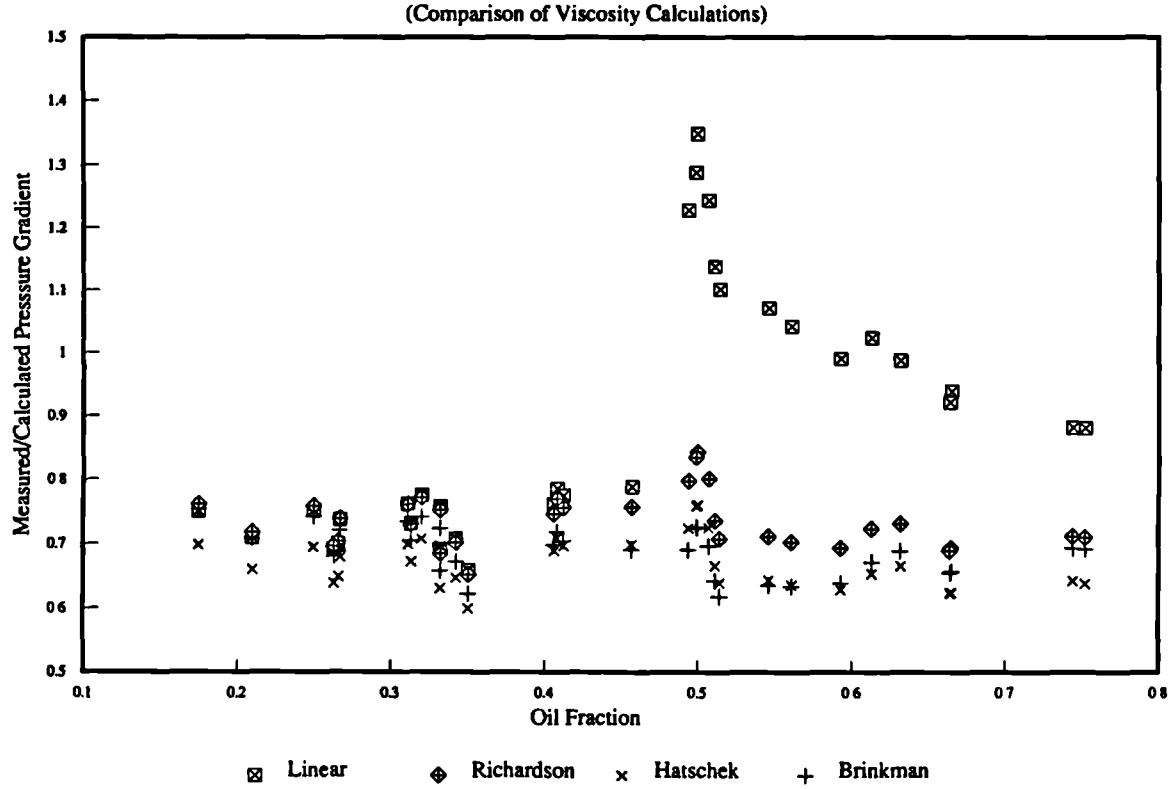


FIGURE 3.5: COMPARISON OF MALINOWSKY DATA WITH BEGGS & BRILL CORRELATION

(Comparison of Brinkman Coefficient, k)

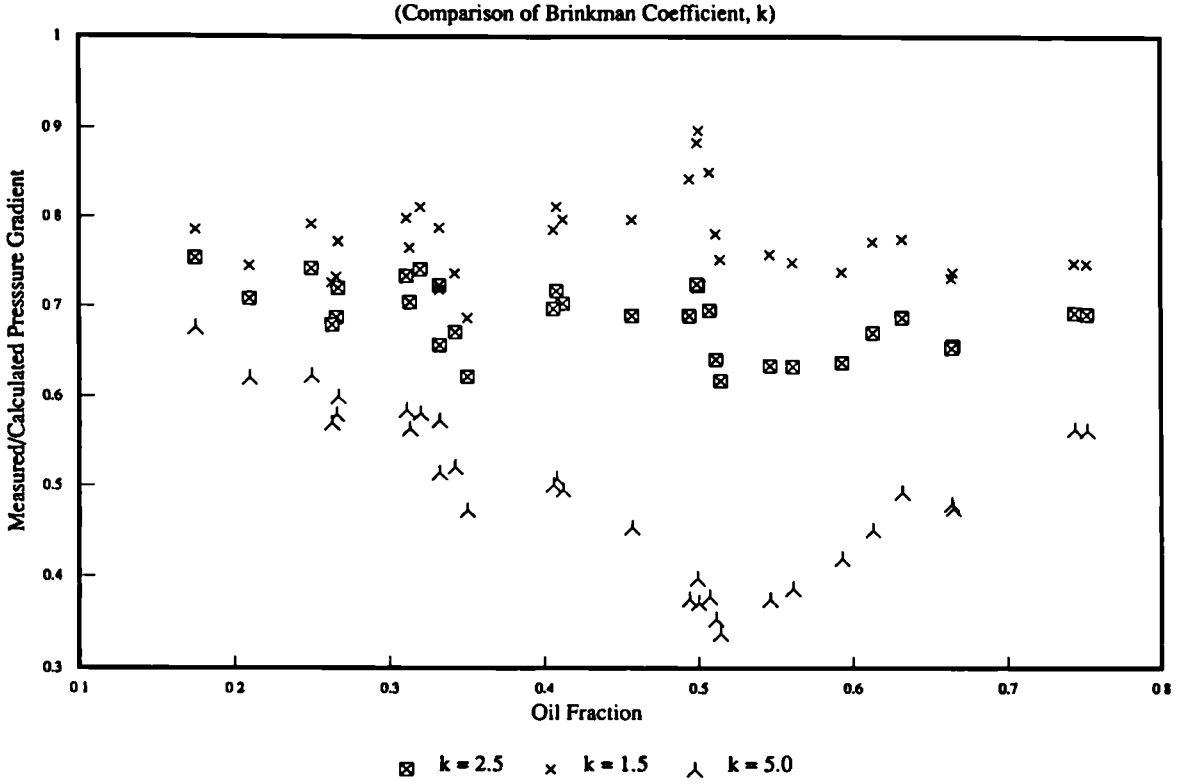


FIGURE 3.6: COMPARISON OF MALINOWSKY DATA WITH CORRELATIONS

(Using Brinkman Equation)

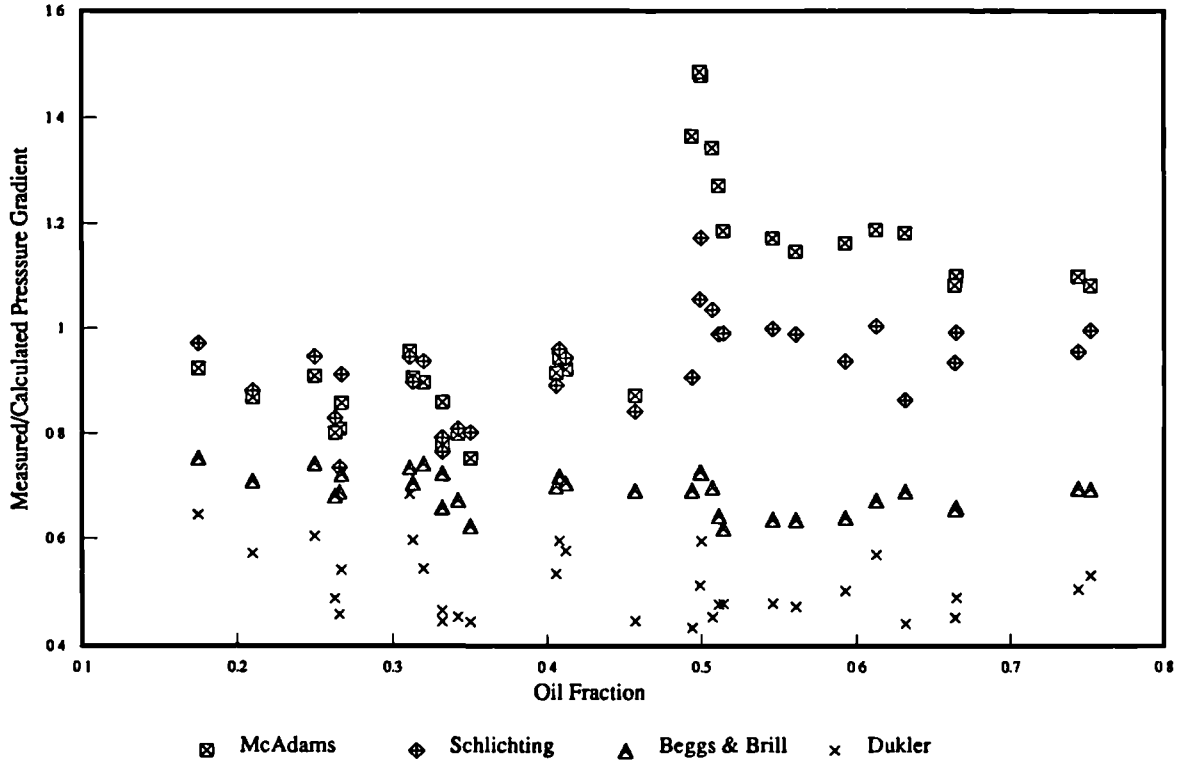


FIGURE 3.7: COMPARISON OF MALINOWSKY DATA WITH CORRELATIONS
(Using Brinkman Equation)

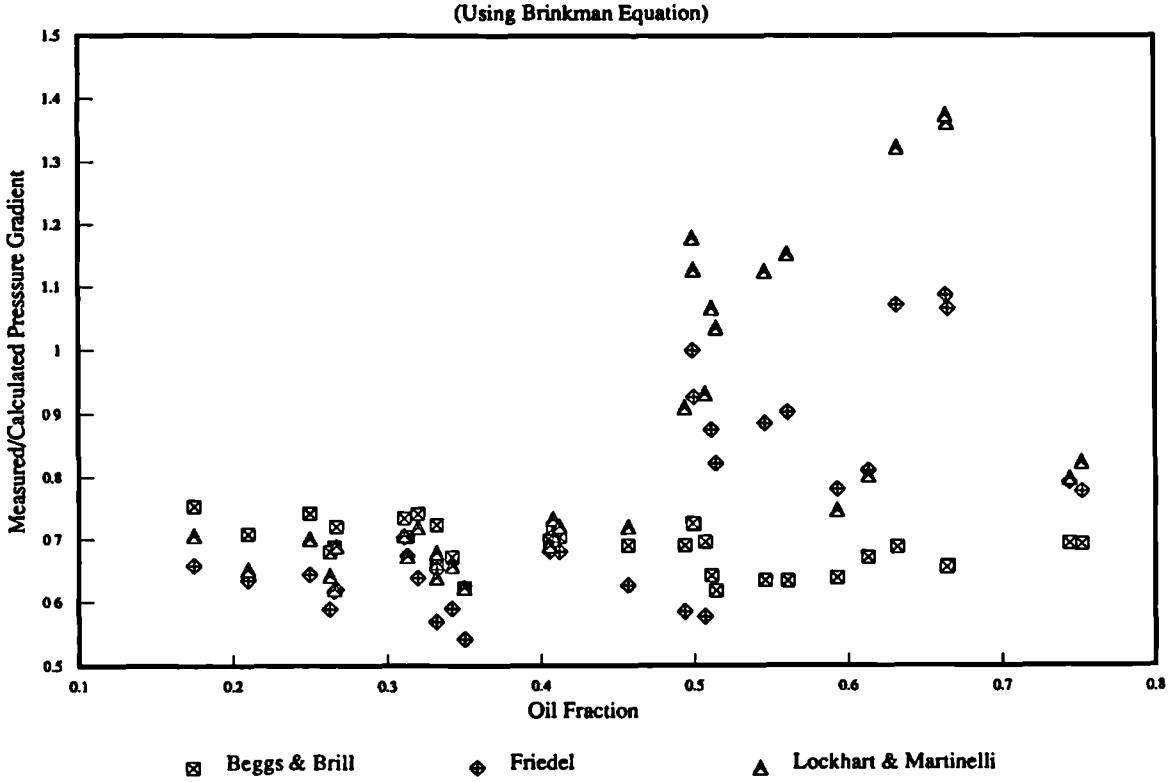


FIGURE 3.8: COMPARISON OF LAFLIN & OGLESBY DATA WITH BEGGS & BRILL CORRELATION
(Determination of Oil Fraction at Inversion)

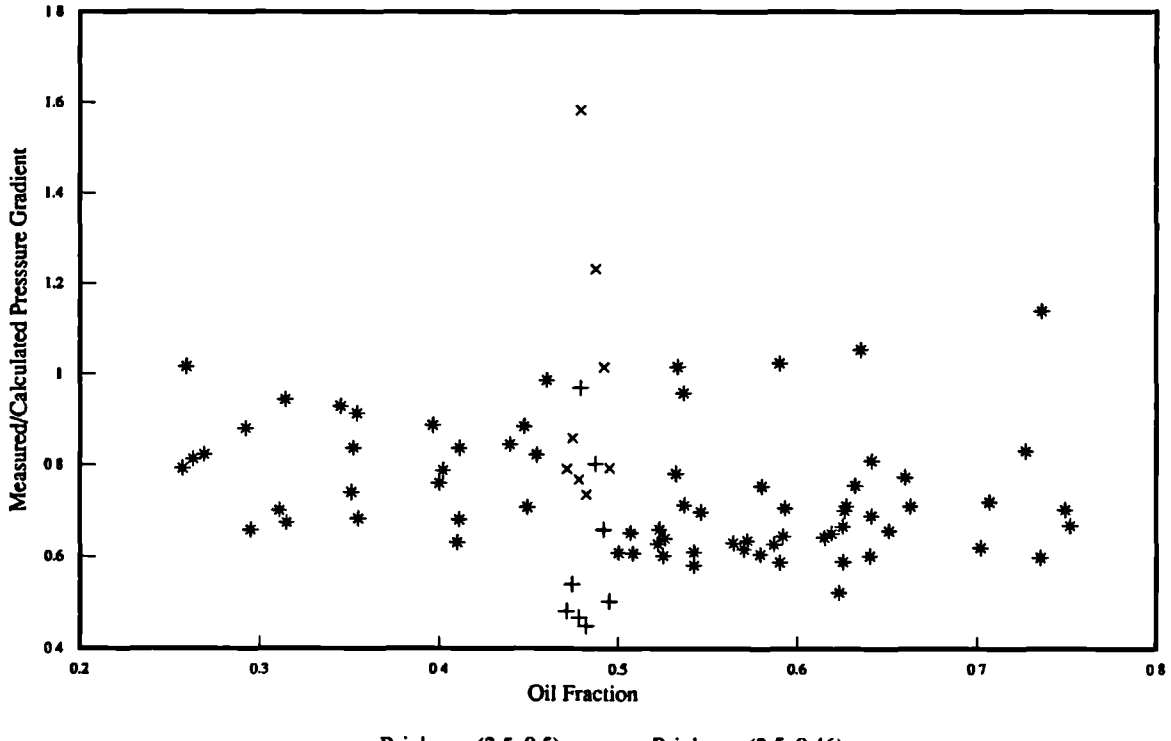


FIGURE 3.9: COMPARISON OF LAFLIN & OGLESBY DATA WITH BEGGS & BRILL CORRELATION
(Comparison of Viscosity Calculations)

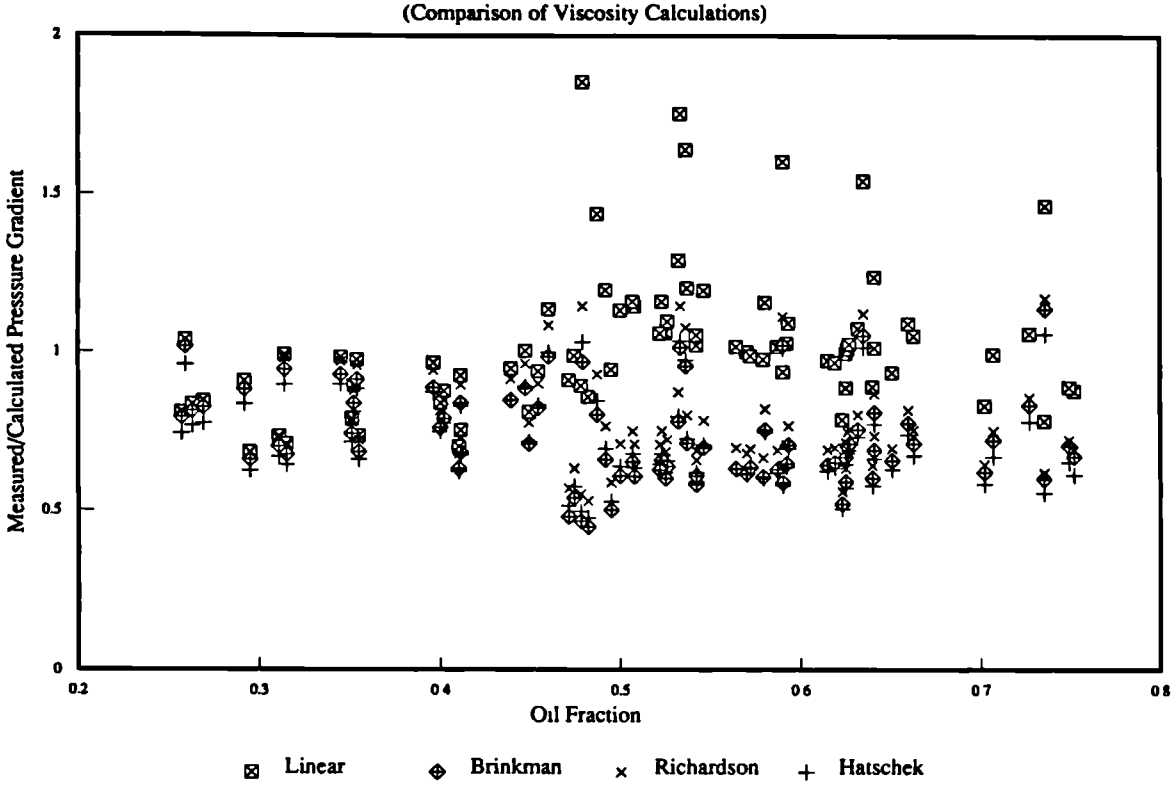


FIGURE 3.10: COMPARISON OF LAFLIN & OGLESBY DATA WITH BEGGS & BRILL CORRELATION
(Comparison of Brinkman Coefficient, k)

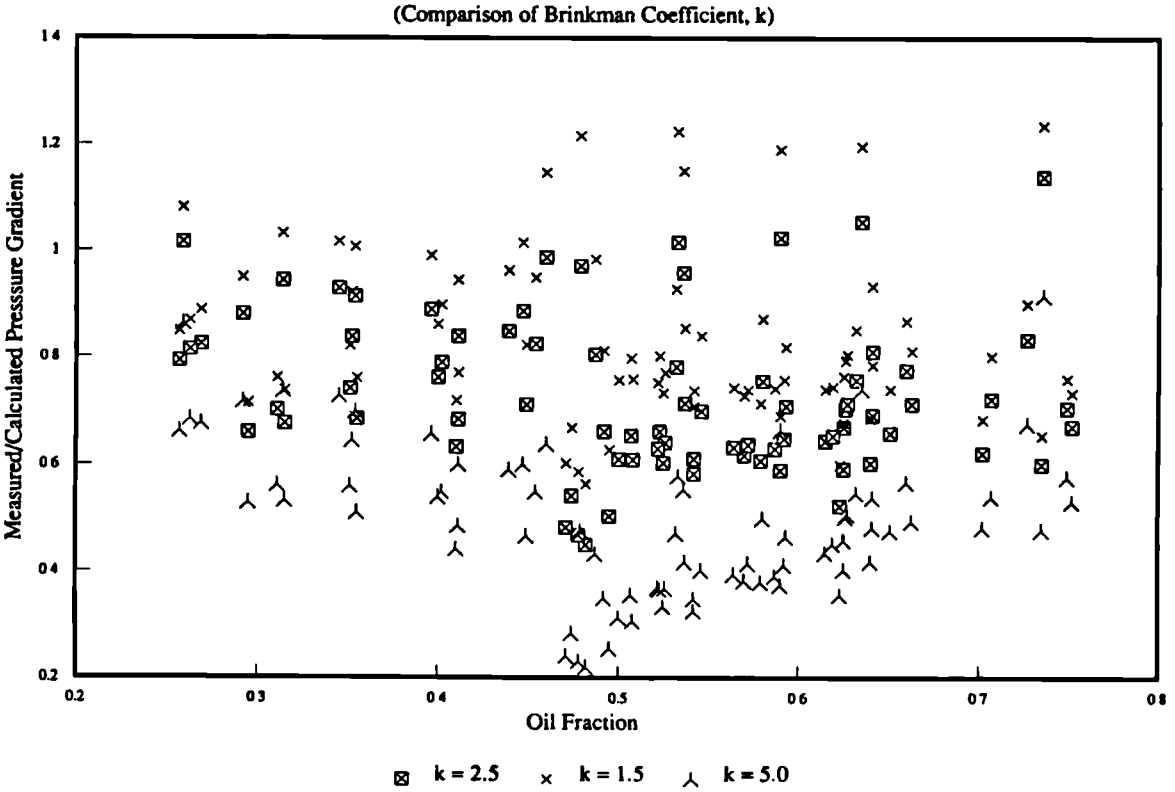


FIGURE 3.11: COMPARISON OF LAFLIN & OGLESBY DATA WITH CORRELATIONS
(Using Brinkman Equation)

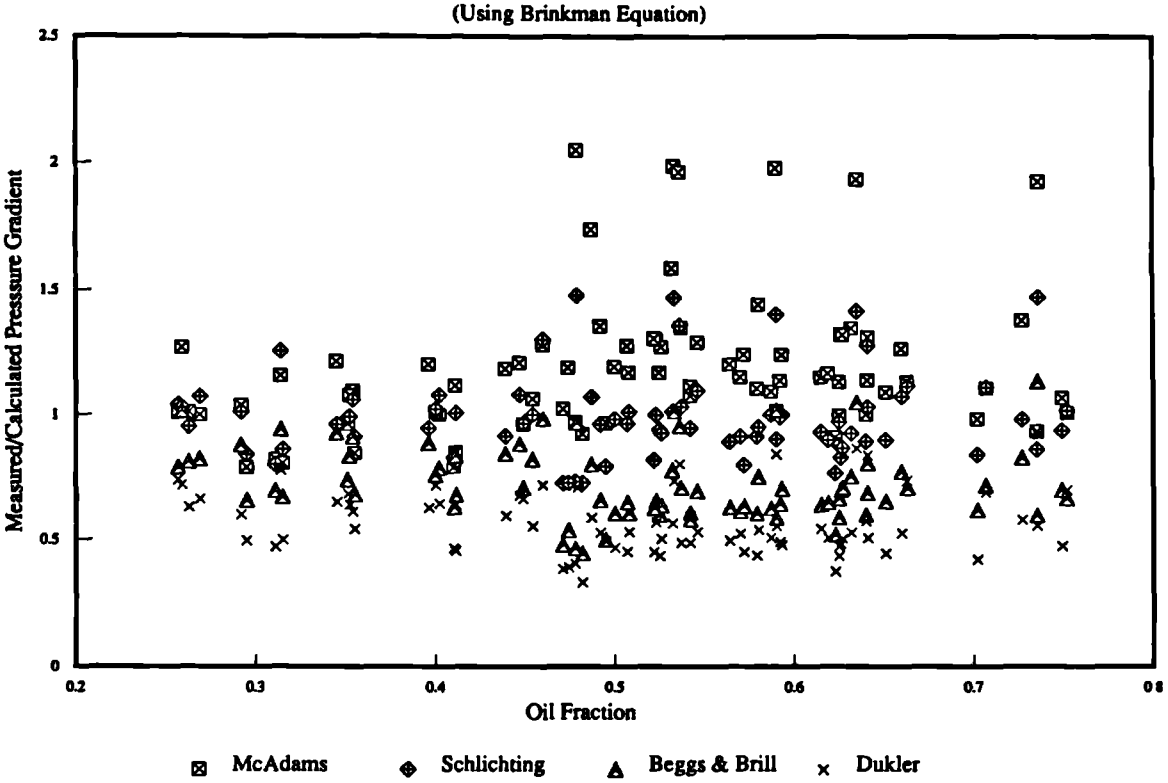


FIGURE 3.12: COMPARISON OF LAFLIN & OGLESBY DATA WITH CORRELATIONS
(Using Brinkman Equation)

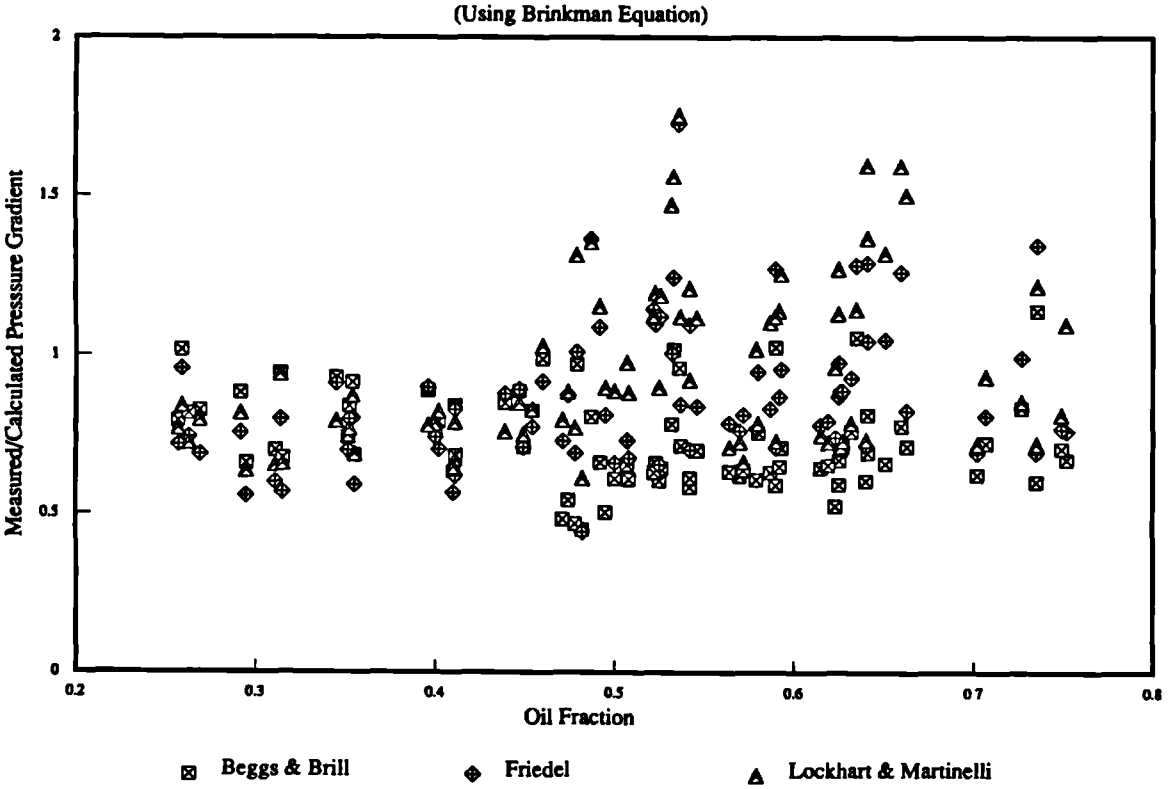


FIGURE 3.13: COMPARISON OF SOBOCINSKI DATA WITH BEGGS & BRILL CORRELATION
(Linear Viscosity Equation)

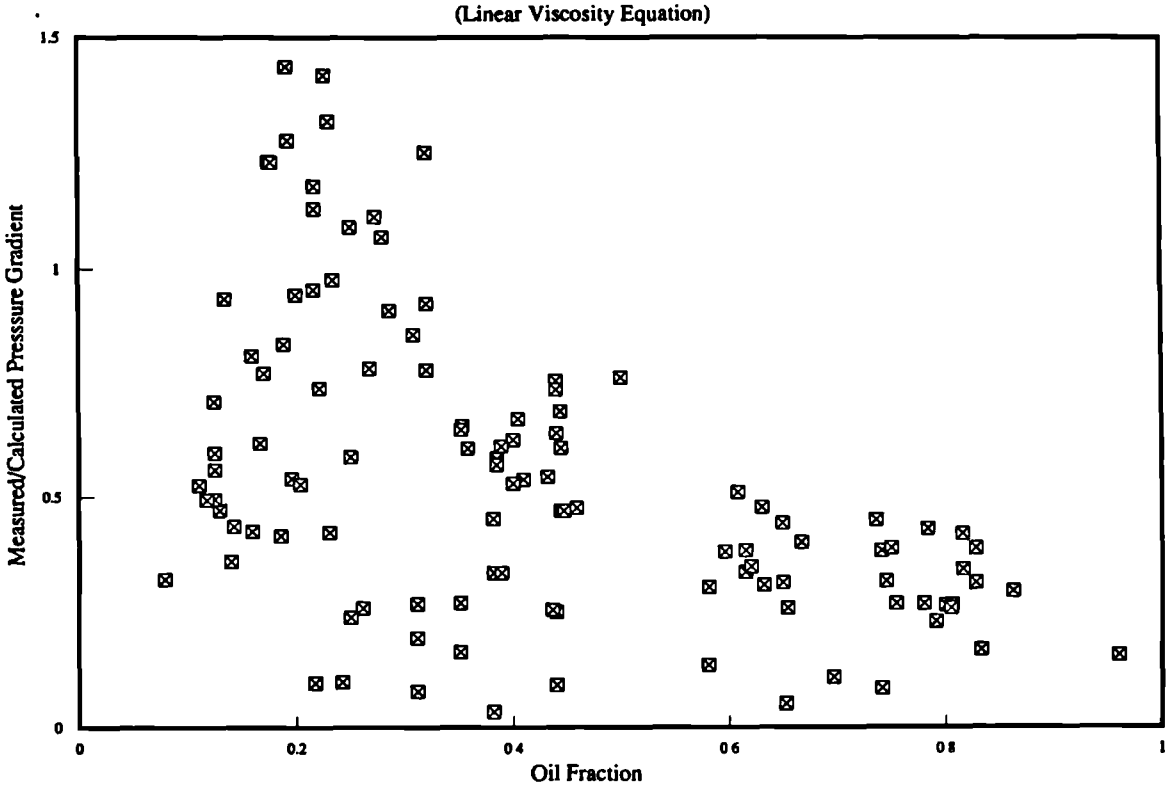


FIGURE 3.14: COMPARISON OF SOBOCINSKI DATA WITH BEGGS & BRILL CORRELATION
(Location of Inversion Point)

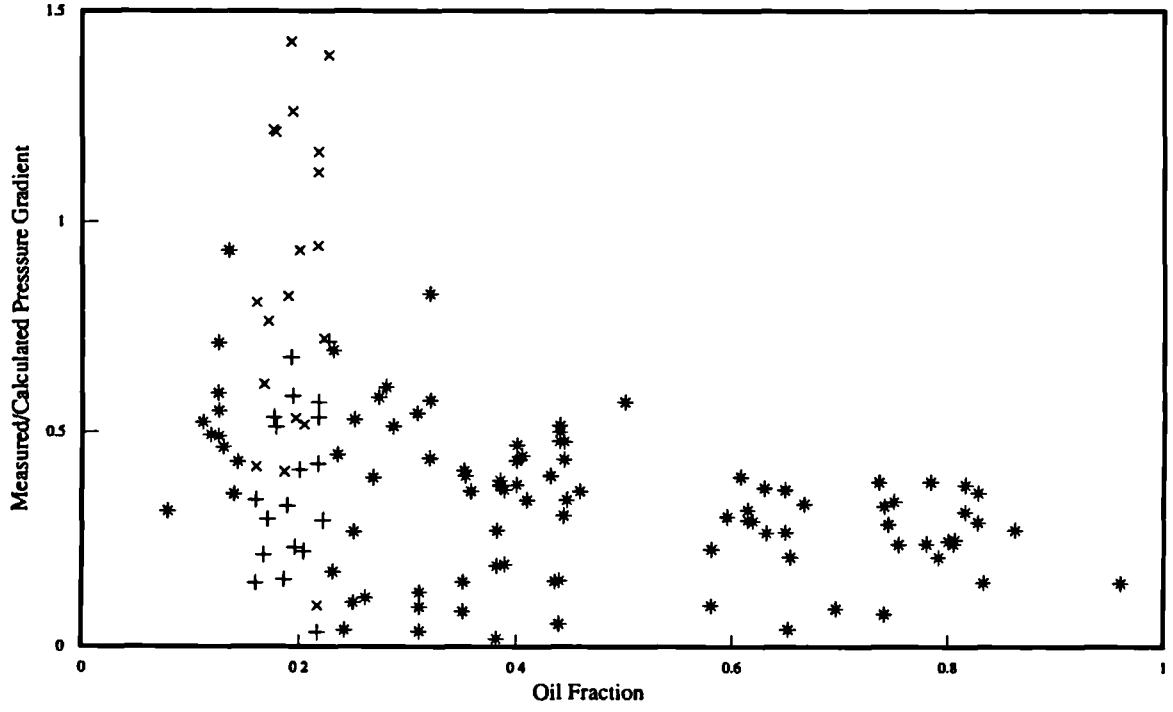


FIGURE 3.15: STAPELBERG PRESSURE GRADIENT DATA

(Comparison with Beggs & Brill Correlation)

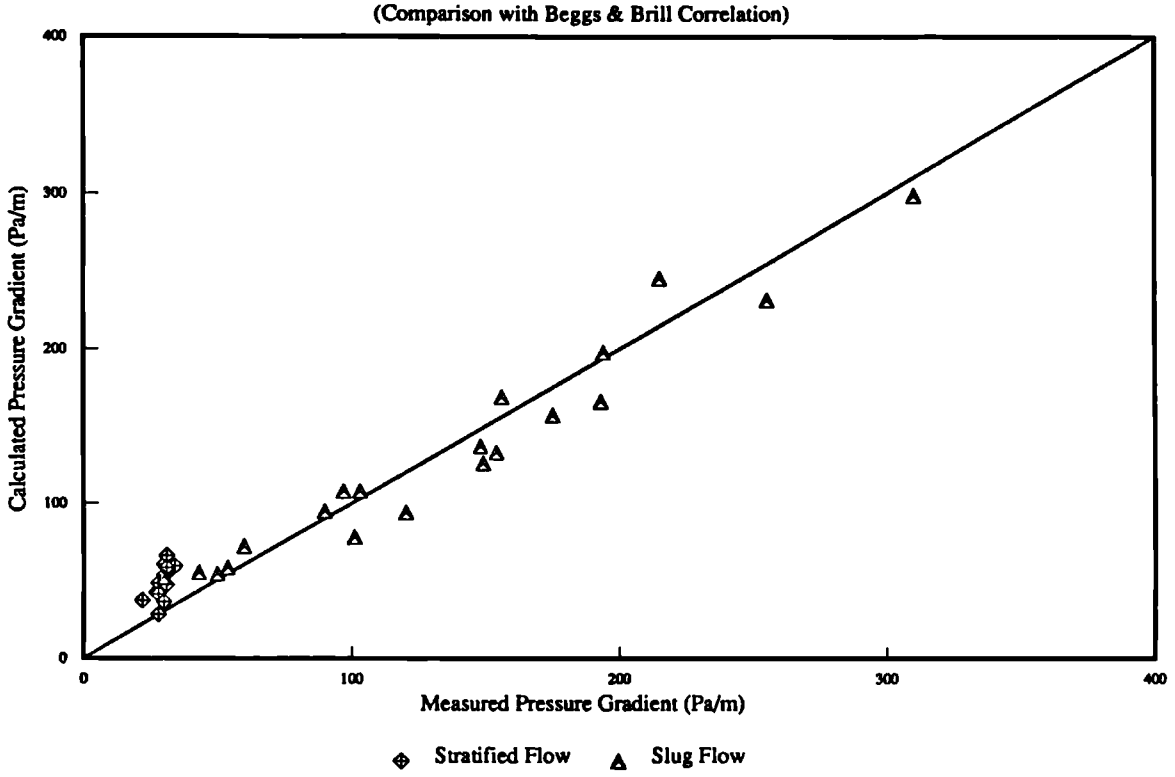


FIGURE 3.16: COMPARISON OF MEASURED WITH CALCULATED PRESSURE GRADIENTS

(Fayed & Otten, 12 and 16 inch data)

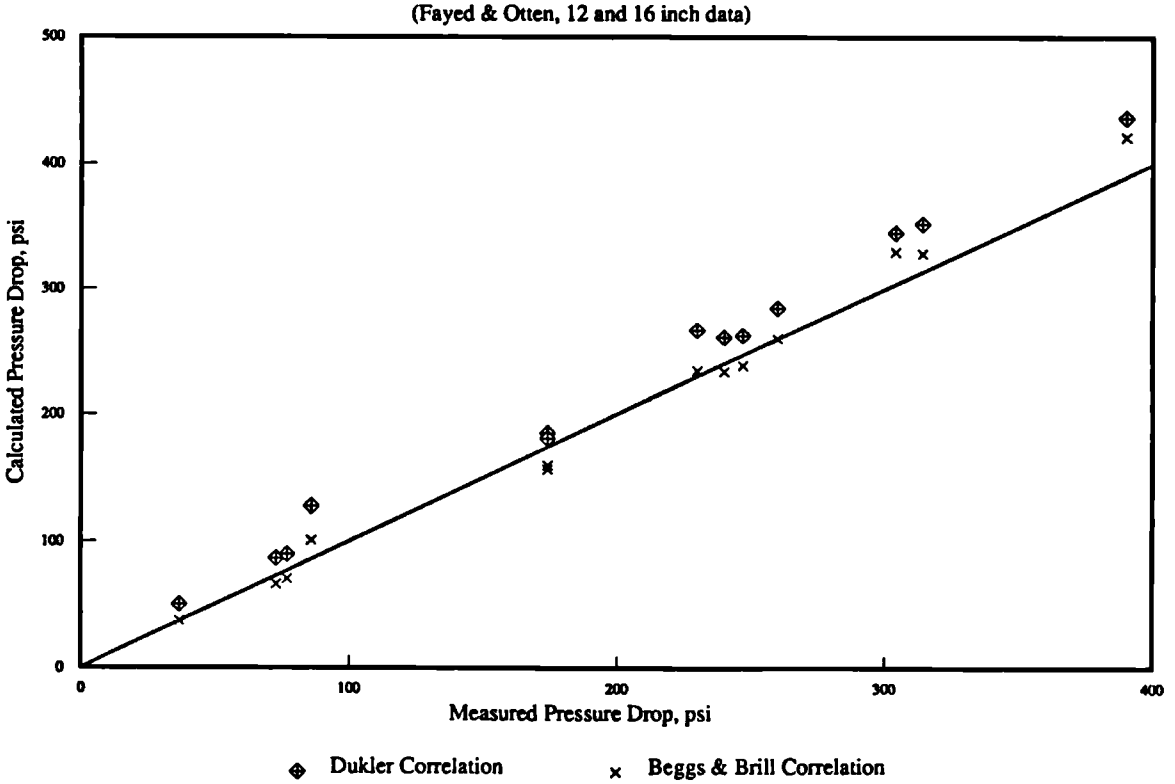


FIGURE 3.17: PRESSURE GRADIENT FOR 6-INCH PIPELINES

(Fayed & Otten Data)

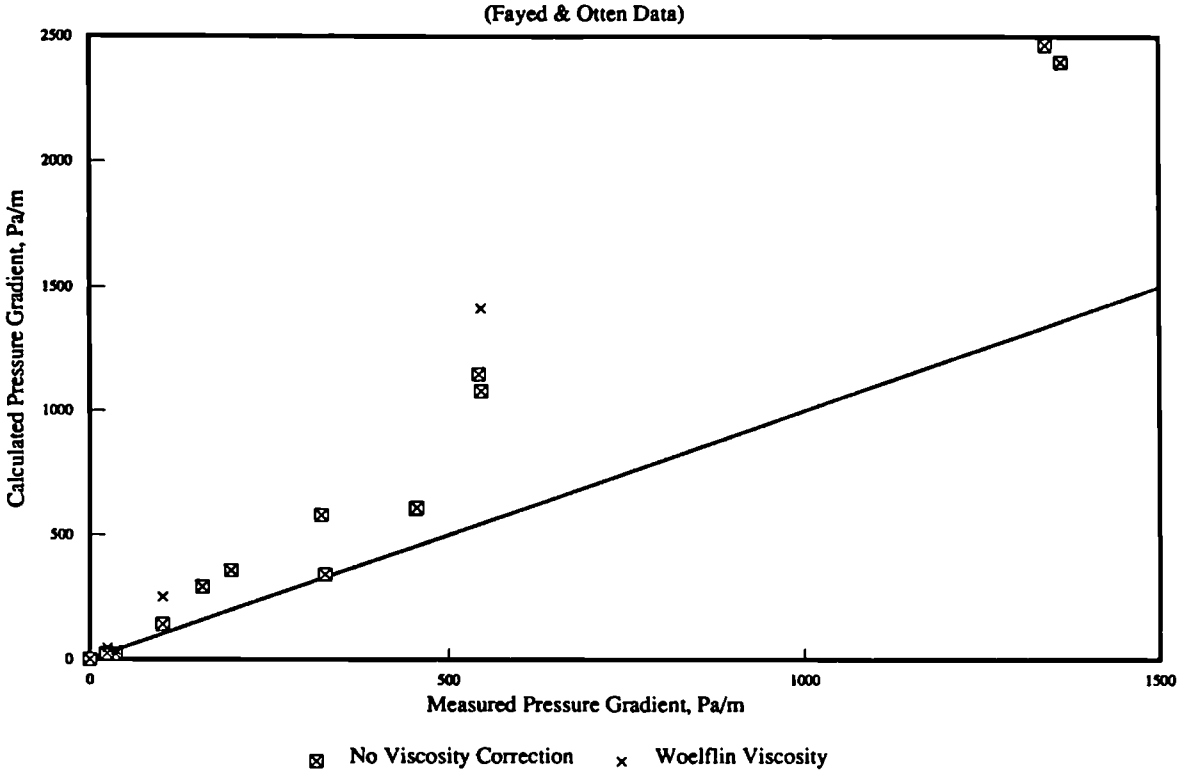


FIGURE 4.1: LOWER PHASE HEIGHT IN LAMINAR-LAMINAR TWO-PHASE FLOW

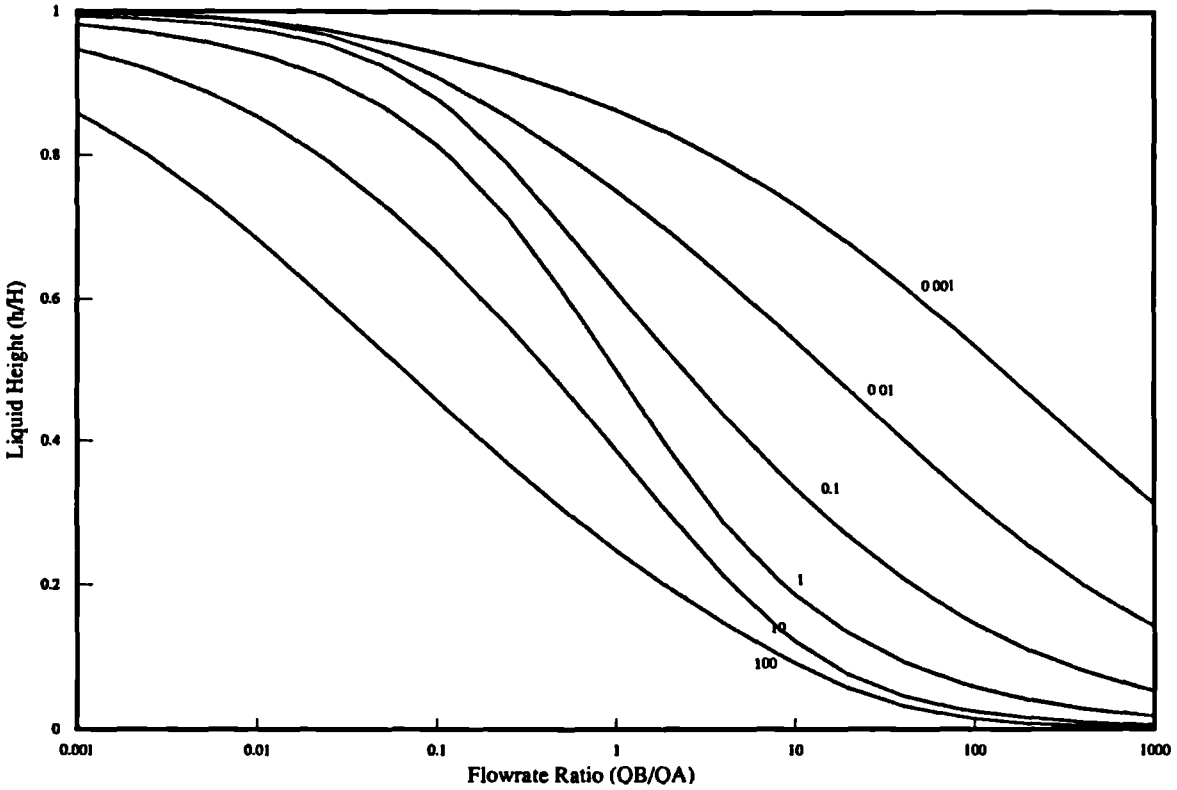


FIGURE 4.2: LIQUID HEIGHT FOR HORIZONTAL STRATIFIED TWO-PHASE FLOW
(Turbulent Gas - Turbulent Liquid)

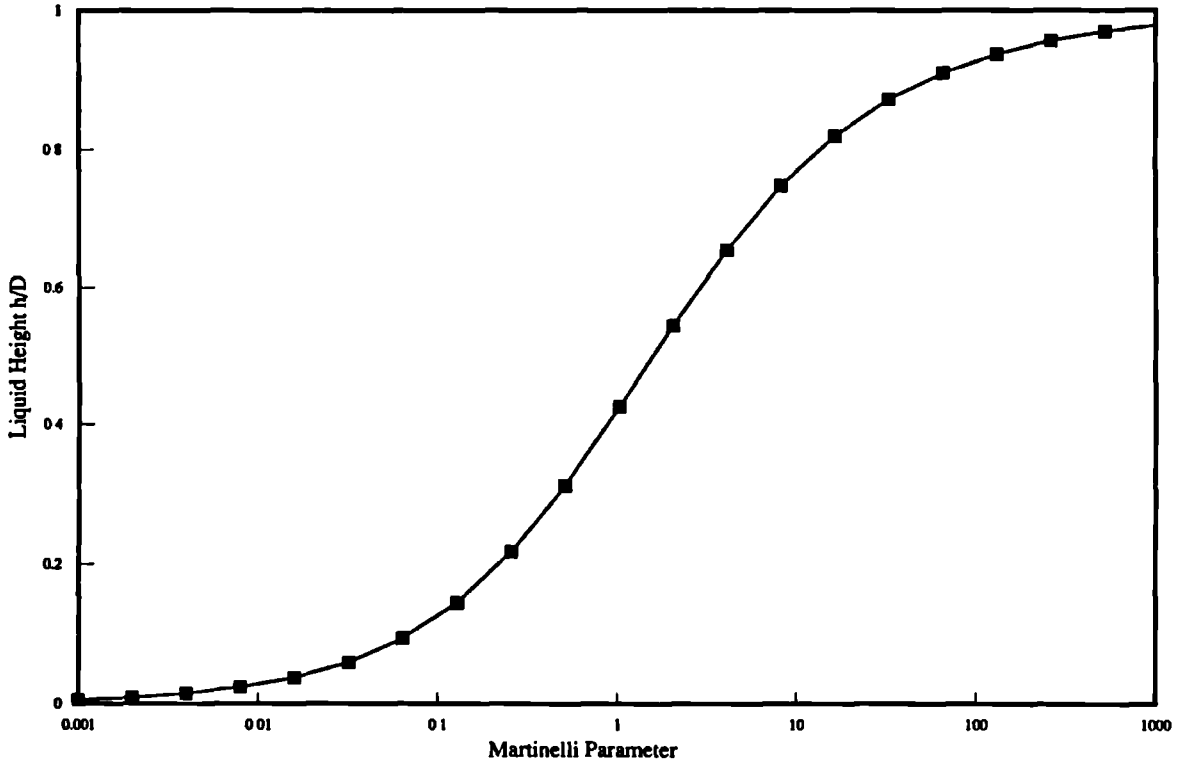
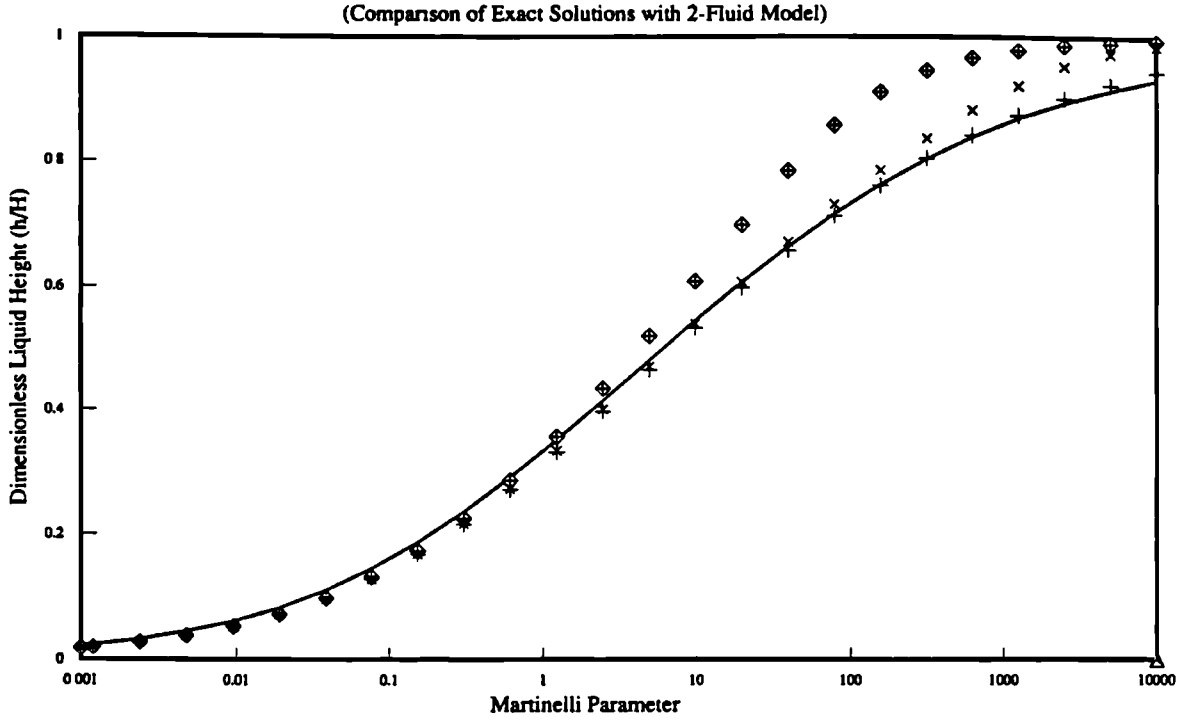


FIGURE 4.3: GAS/LIQUID FLOW BETWEEN FLAT PLATES

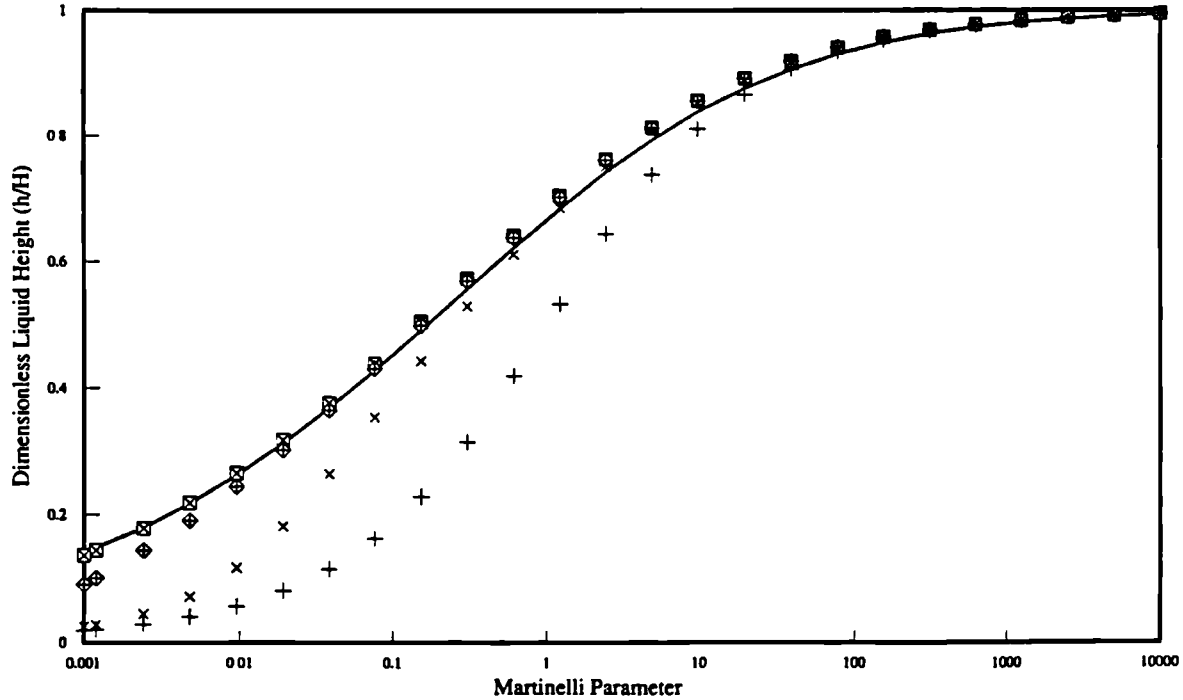
(Comparison of Exact Solutions with 2-Fluid Model)



◈ $\tilde{\mu} = 0.1$ × $\tilde{\mu} = 0.01$ + $\tilde{\mu} = 0.001$ —— Approx

FIGURE 4.4: LIQUID/LIQUID FLOW BETWEEN FLAT PLATES

(Comparison of Exact Solutions with 2-Fluid Model)



⊠ $\tilde{\mu} = 1000$ ◈ $\tilde{\mu} = 100$ × $\tilde{\mu} = 10$ + $\tilde{\mu} = 1$ —— Approx

FIGURE 4.5: GAS/LIQUID FLOW IN A CIRCULAR PIPE

(Comparison of Numerical Calculations with 2-Fluid Model)

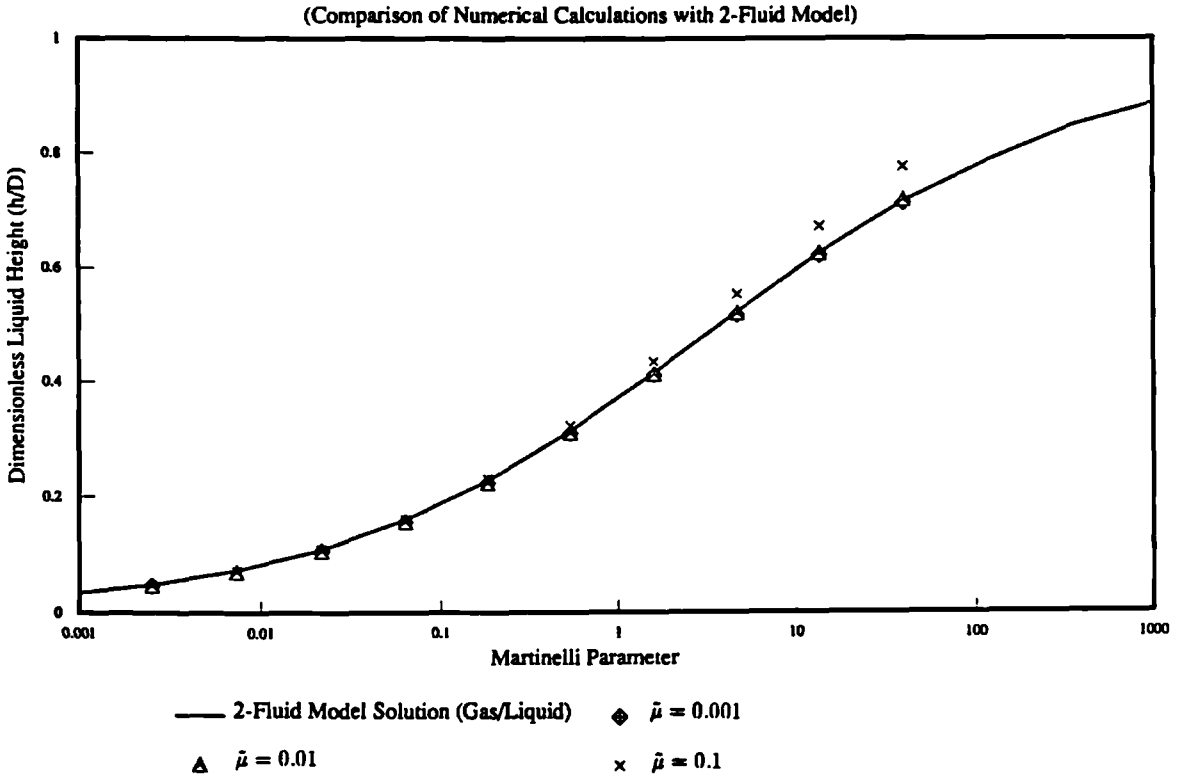


FIGURE 4.6: LIQUID/LIQUID FLOW IN A CIRCULAR PIPE

(Comparison of Numerical Calculations with 2-Fluid Model)

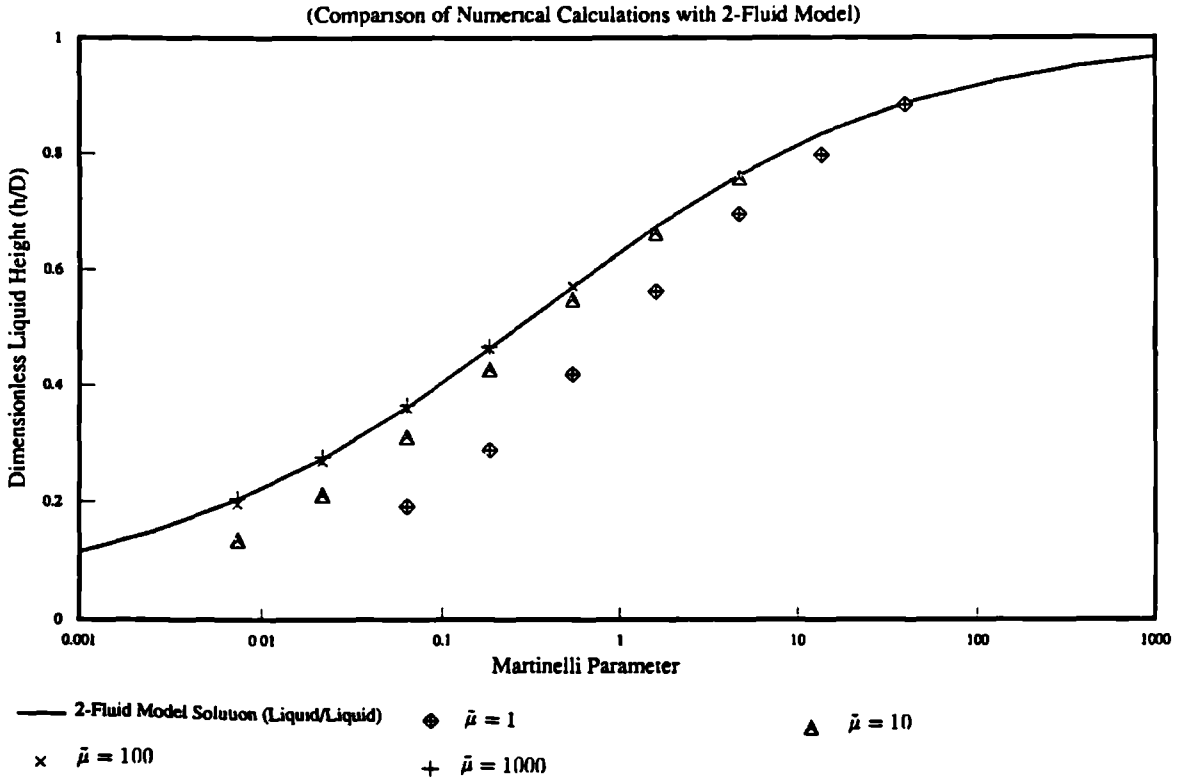


FIGURE 4.7: HEIGHT OF WATER LAYER IN OIL/WATER/GAS FLOW

(Comparison of 3-Fluid Model with Sobocinski data)

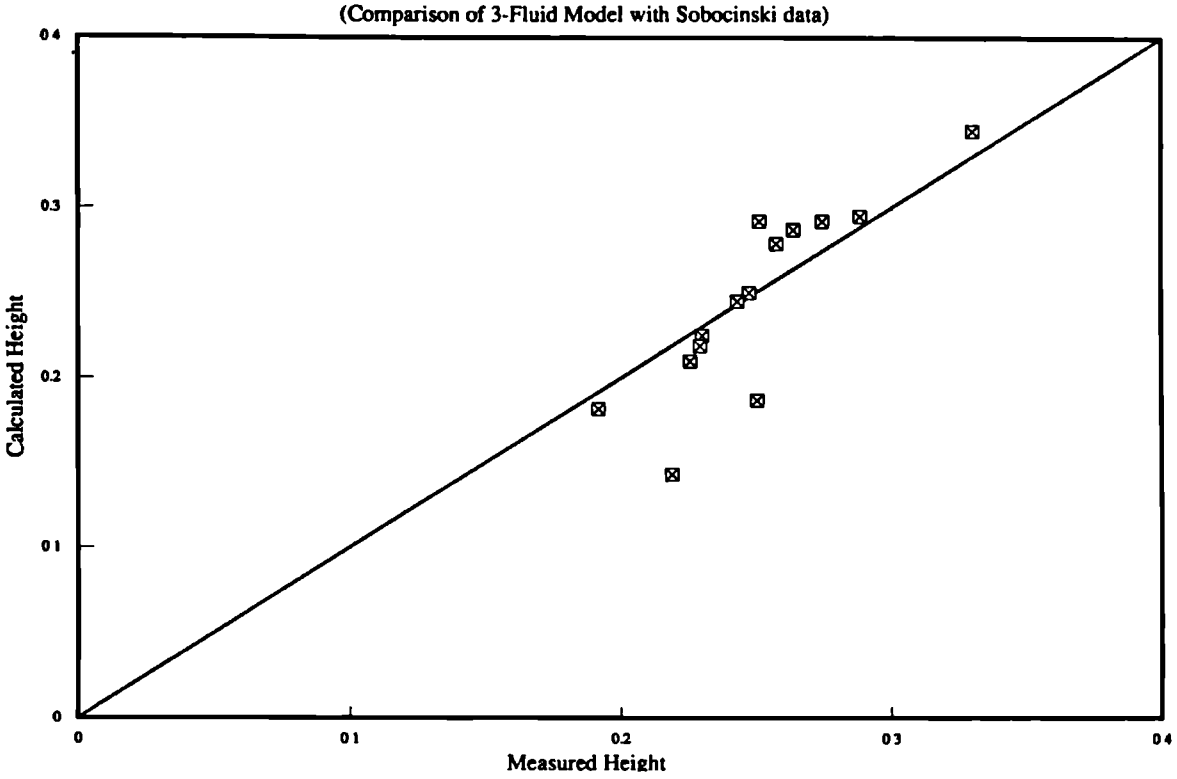


FIGURE 4.8: HEIGHT OF OIL LAYER IN OIL/WATER/GAS FLOW

(Comparison of 3-Fluid Model with Sobocinski data)

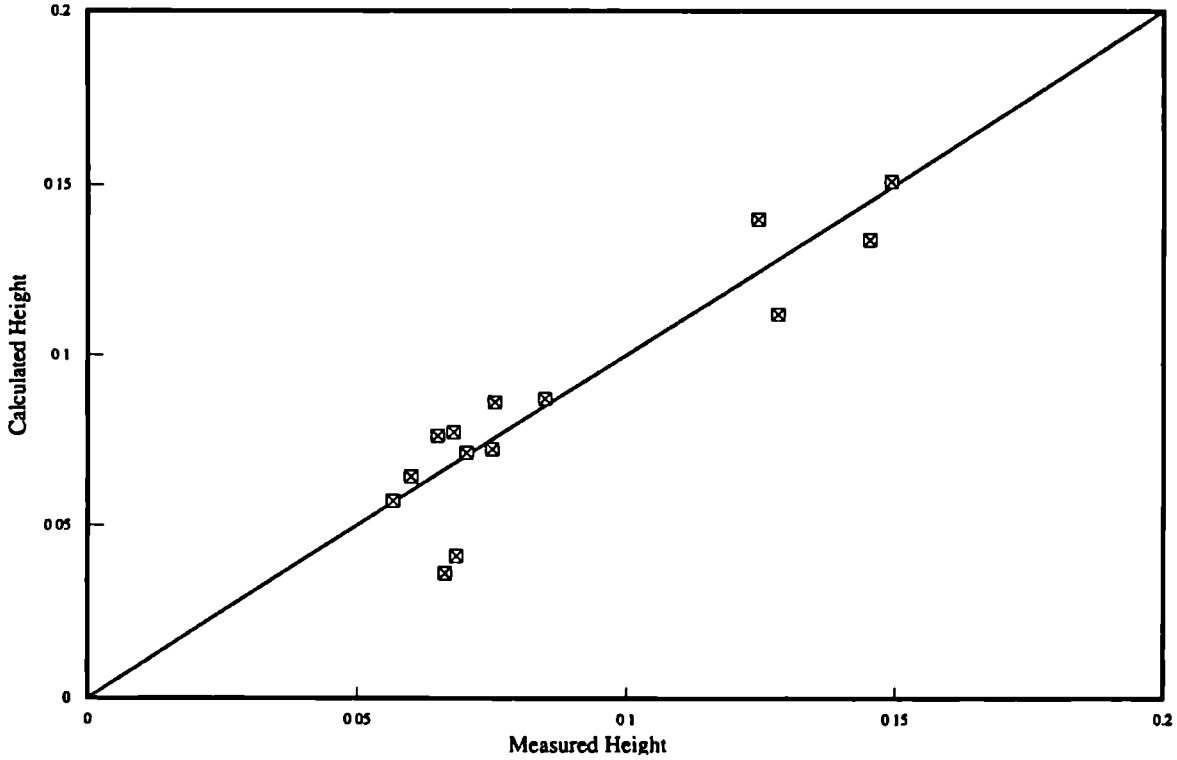


FIGURE 4.9: LIQUID LAYER HEIGHTS IN OIL/WATER/GAS FLOW

(Comparison of 3-Fluid Model with Stapelberg Data)

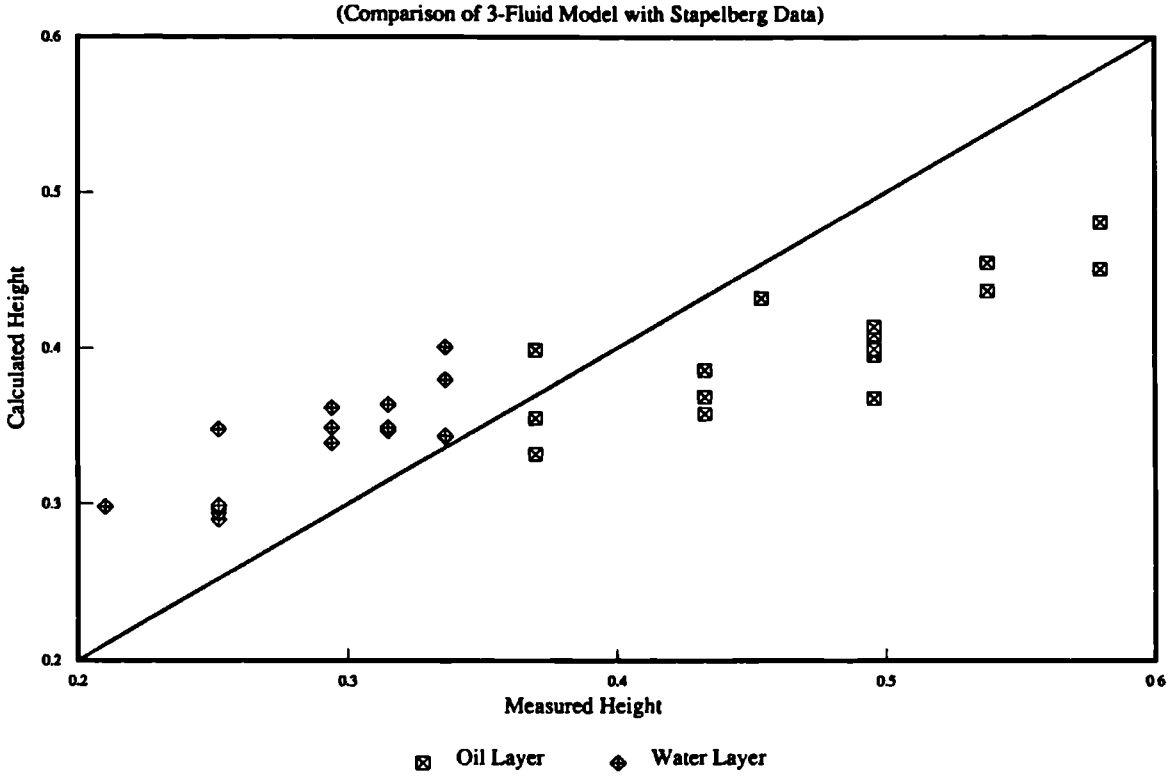


FIGURE 5.1: PRESSURE GRADIENT CALCULATION

(Numerical Simulation of WASP Experiment)

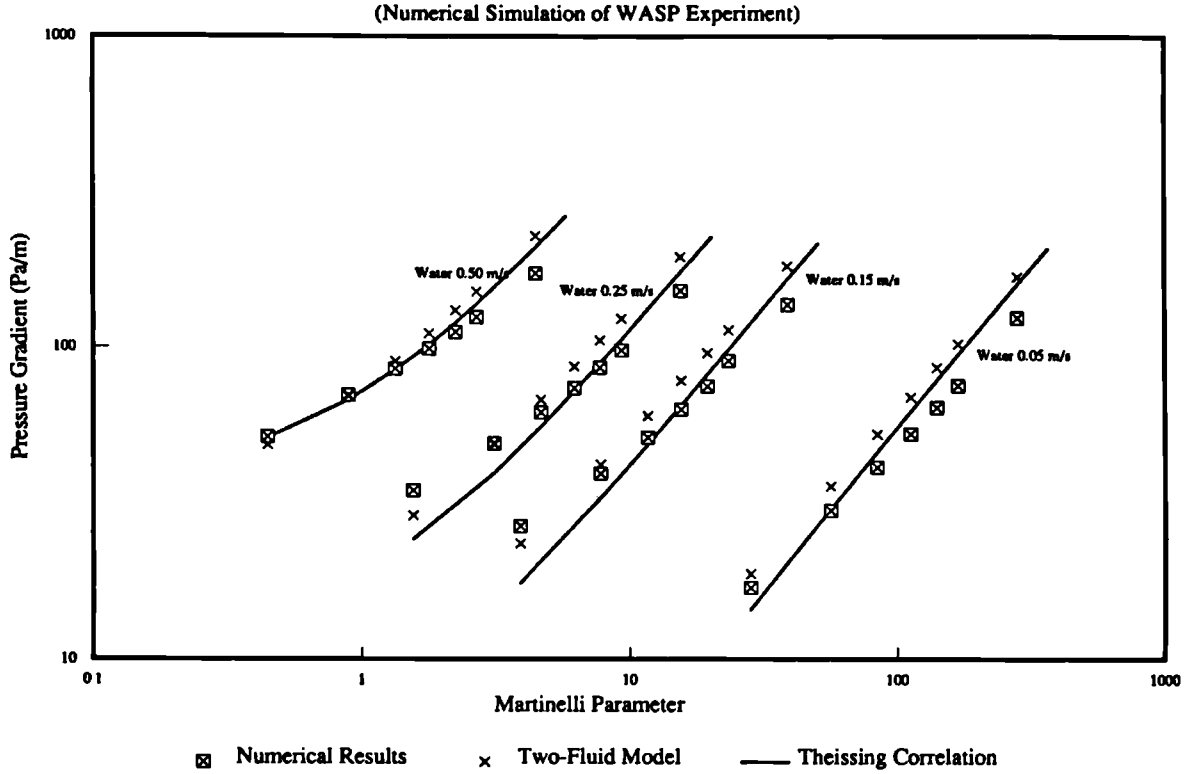


FIGURE 5.2: HOLDUP CALCULATION

(Numerical Simulation of WASP Experiment)

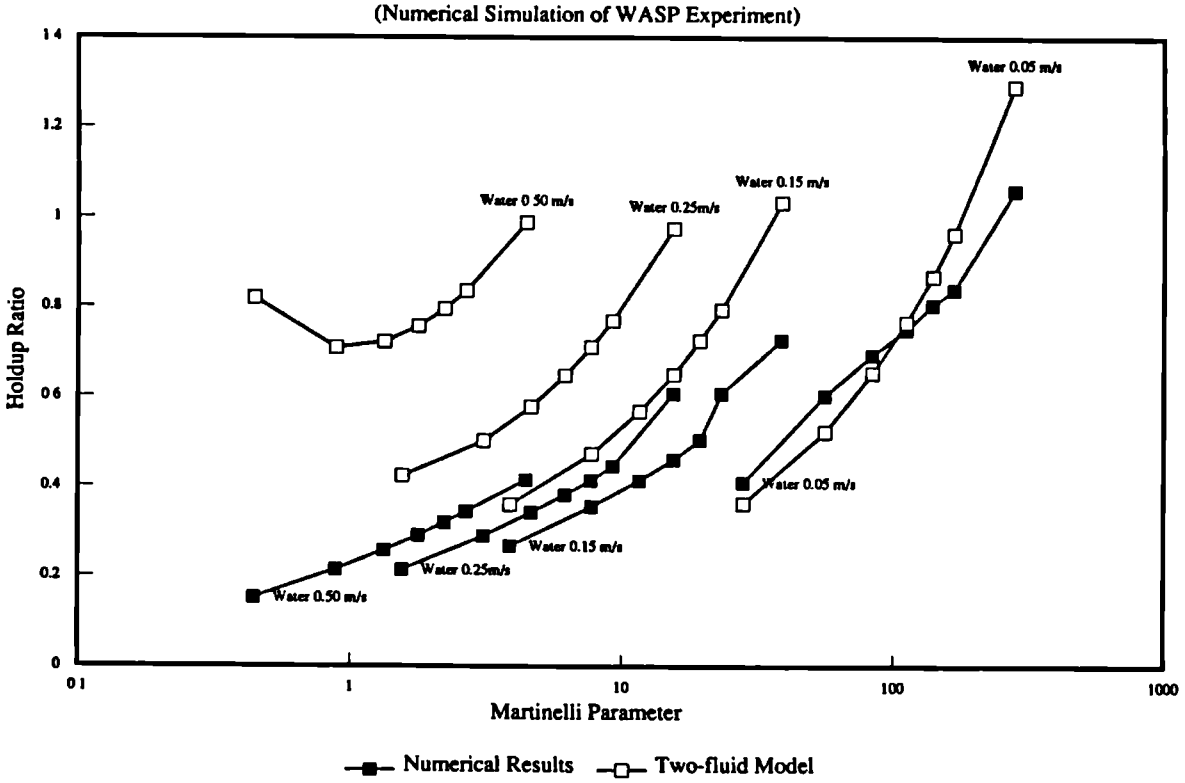


FIGURE 5.3: OIL SHEAR STRESS CALCULATION

(Numerical Simulation of WASP Experiment)

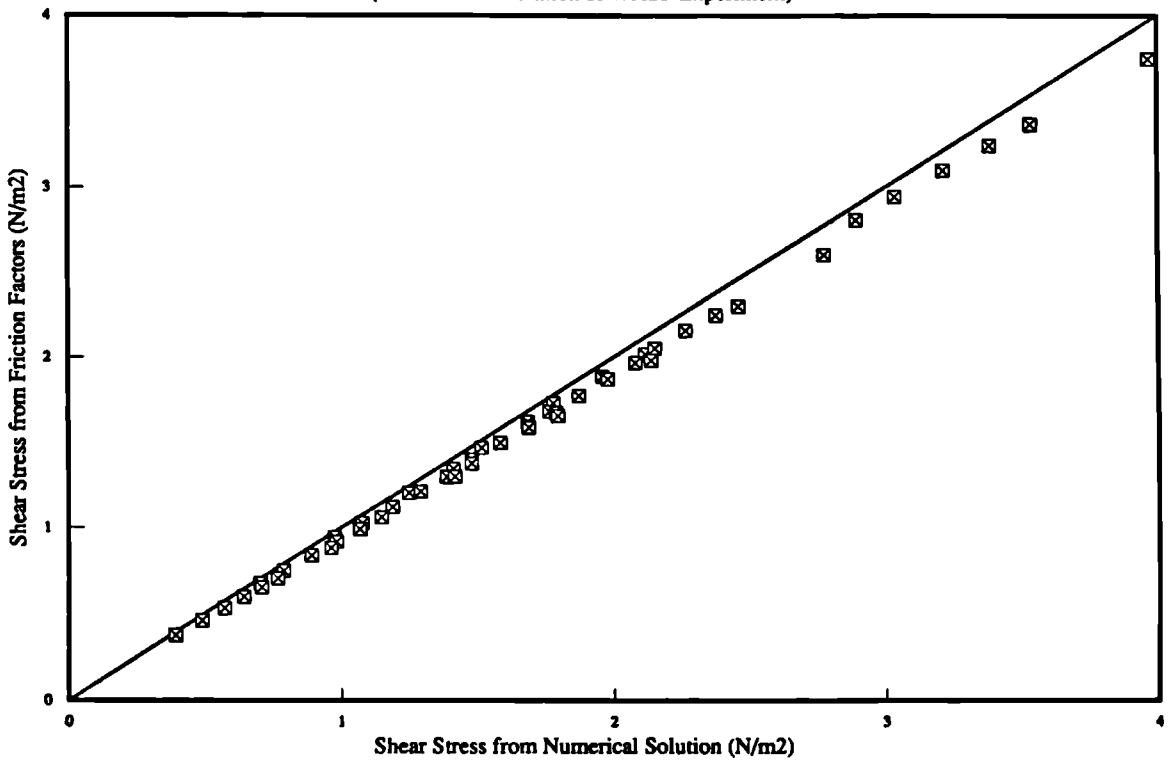


FIGURE 5.4: WATER SHEAR STRESS CALCULATION

(Numerical Simulation of WASP Experiment)

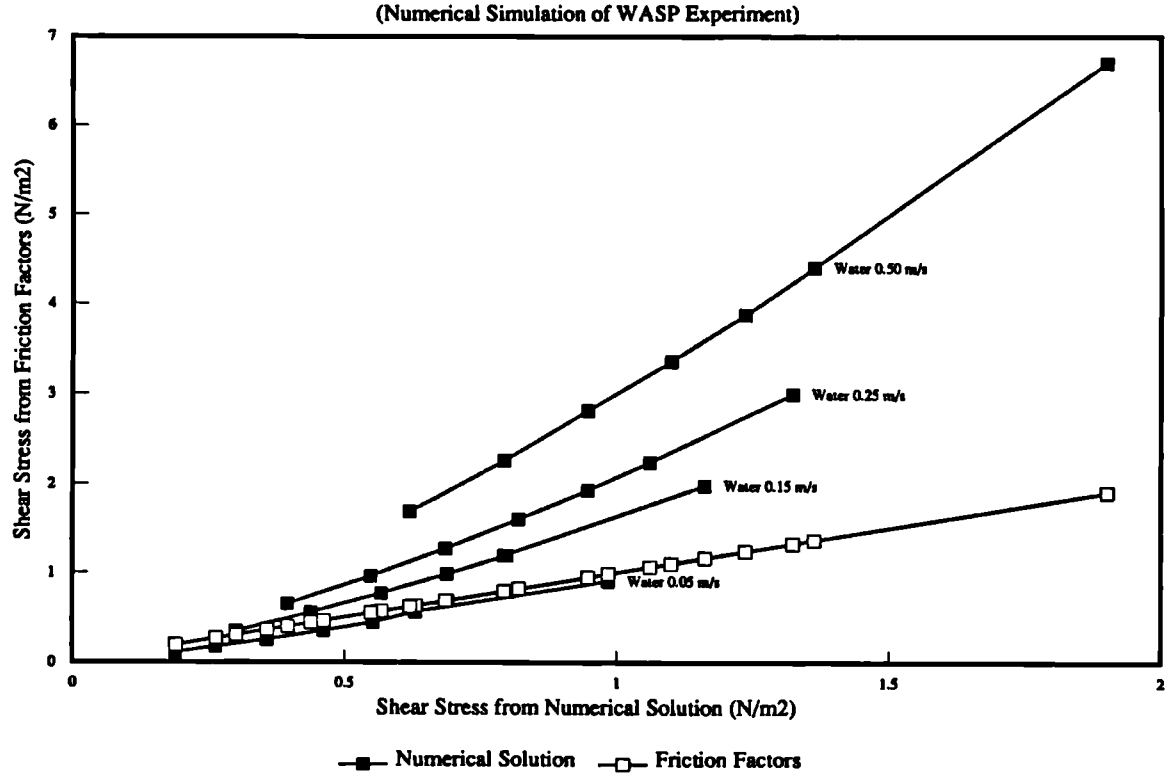


FIGURE 5.5: INTERFACIAL SHEAR STRESS CALCULATION

(Numerical Simulation of WASP Experiment)

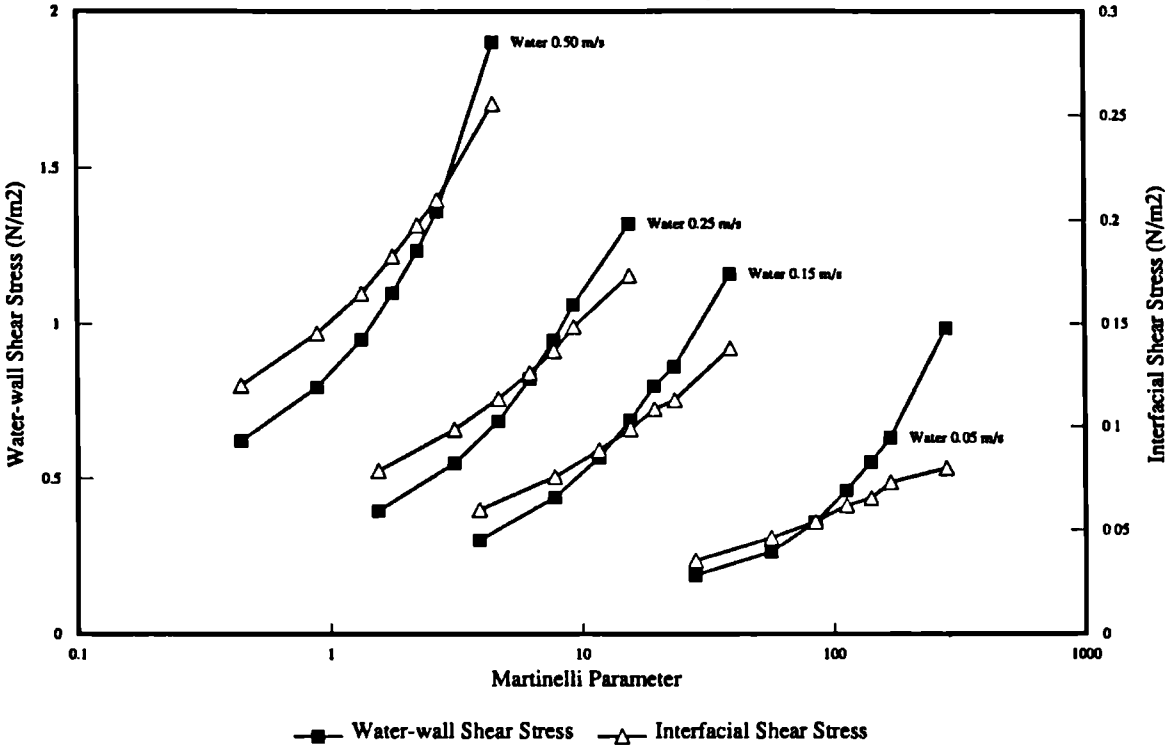


FIGURE 5.6: COMPARISON OF PRESSURE GRADIENT WITH MODELS

(Oil Superficial Velocity 0.15 m/s)

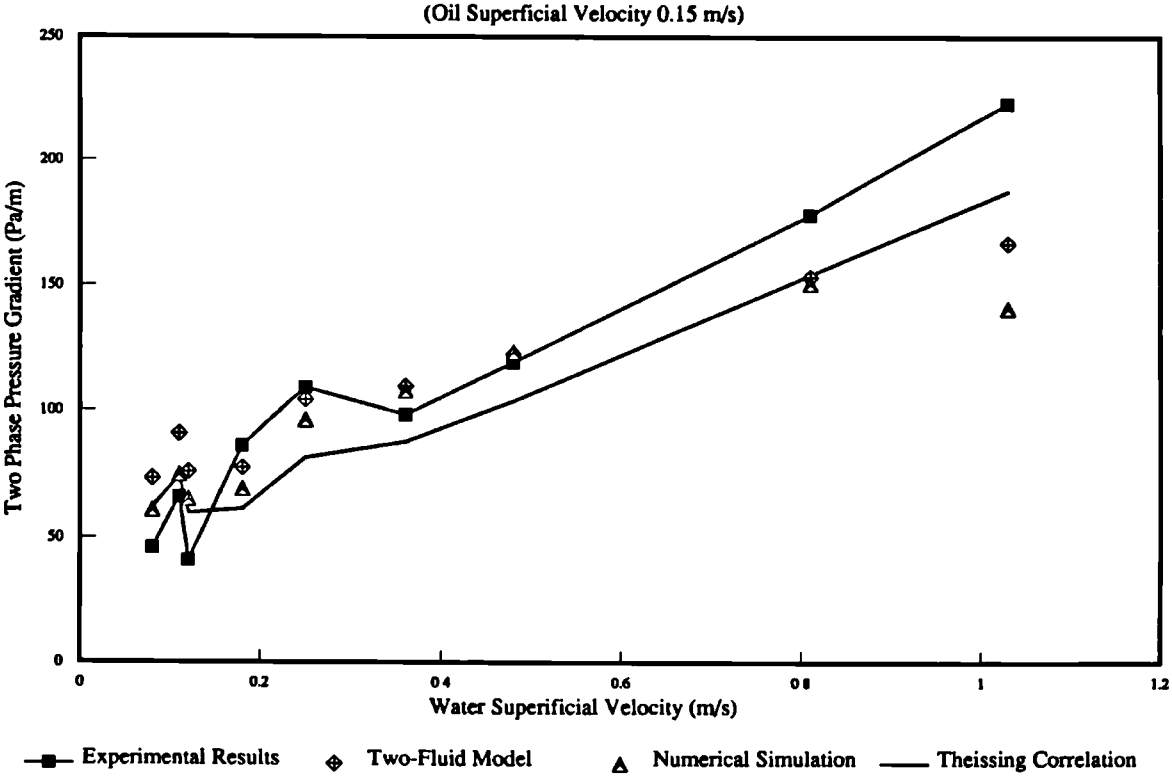


FIGURE 5.7: COMPARISON OF PRESSURE GRADIENT WITH MODELS

(Oil Superficial Velocity 0.26m/s)

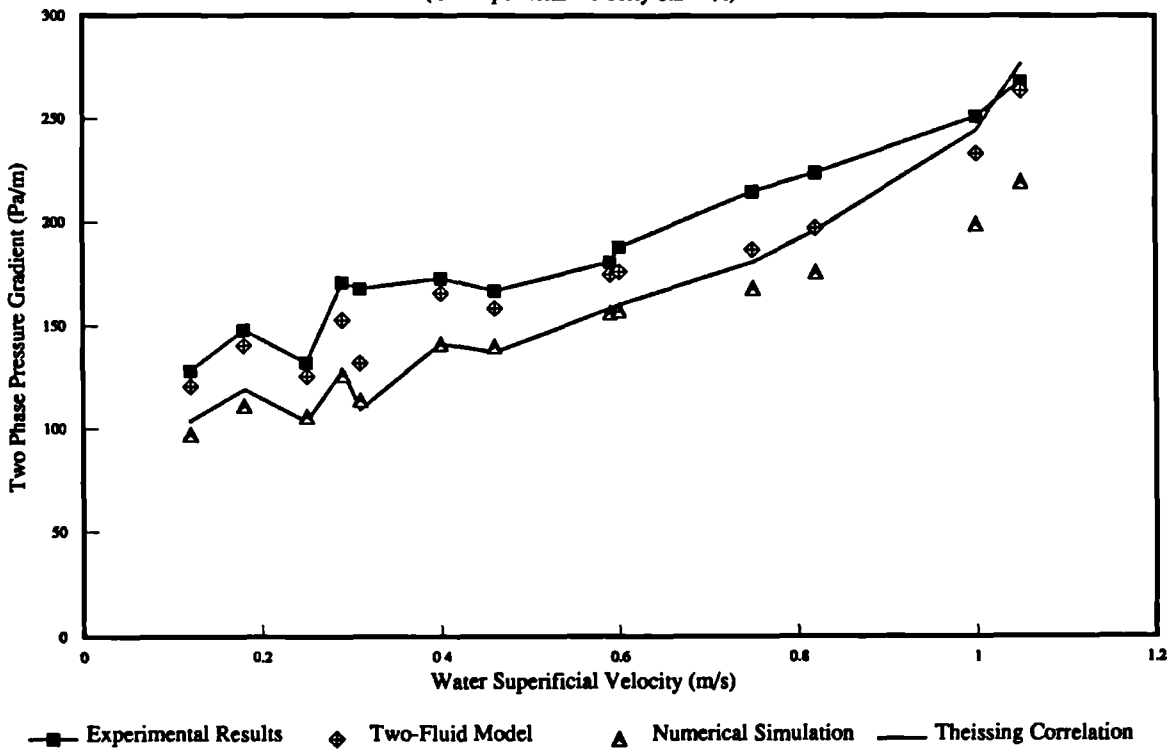


FIGURE 5.8: COMPARISON OF PRESSURE GRADIENT WITH MODELS

(Oil Superficial Velocity 0.55m/s)

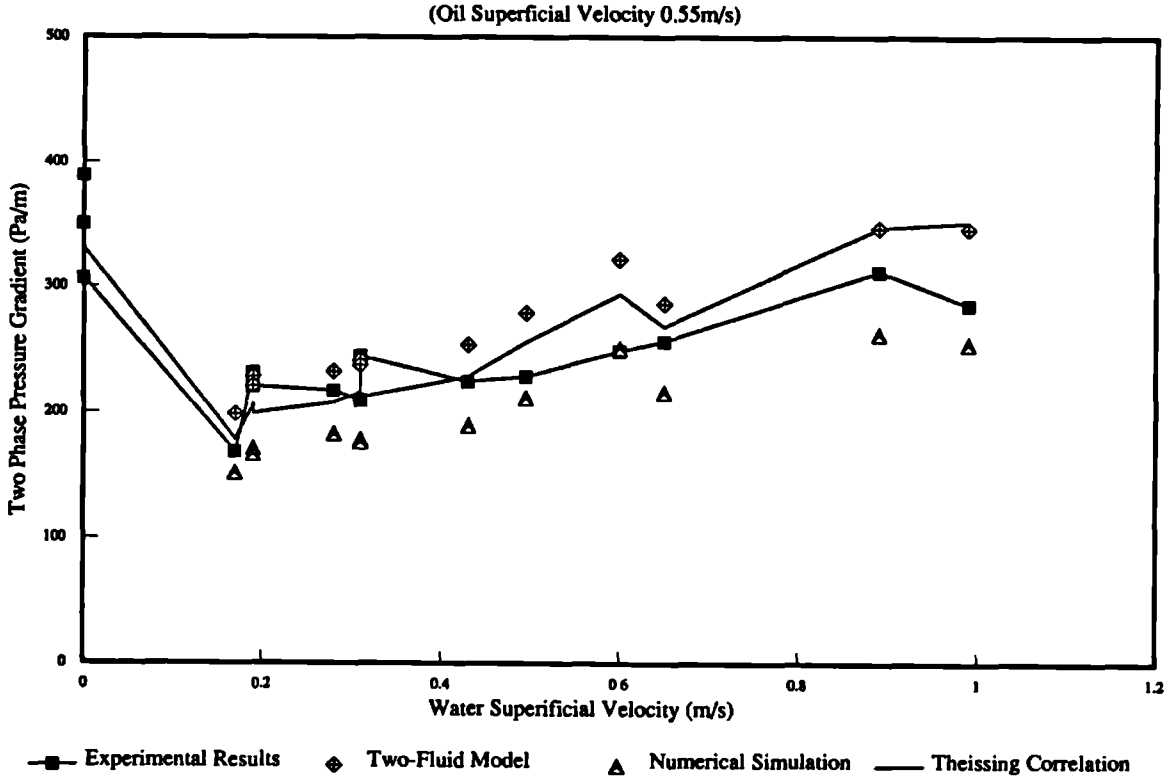


FIGURE 5.9: COMPARISON OF PRESSURE GRADIENT WITH MODELS

(Oil Superficial Velocity 0.87m/s)

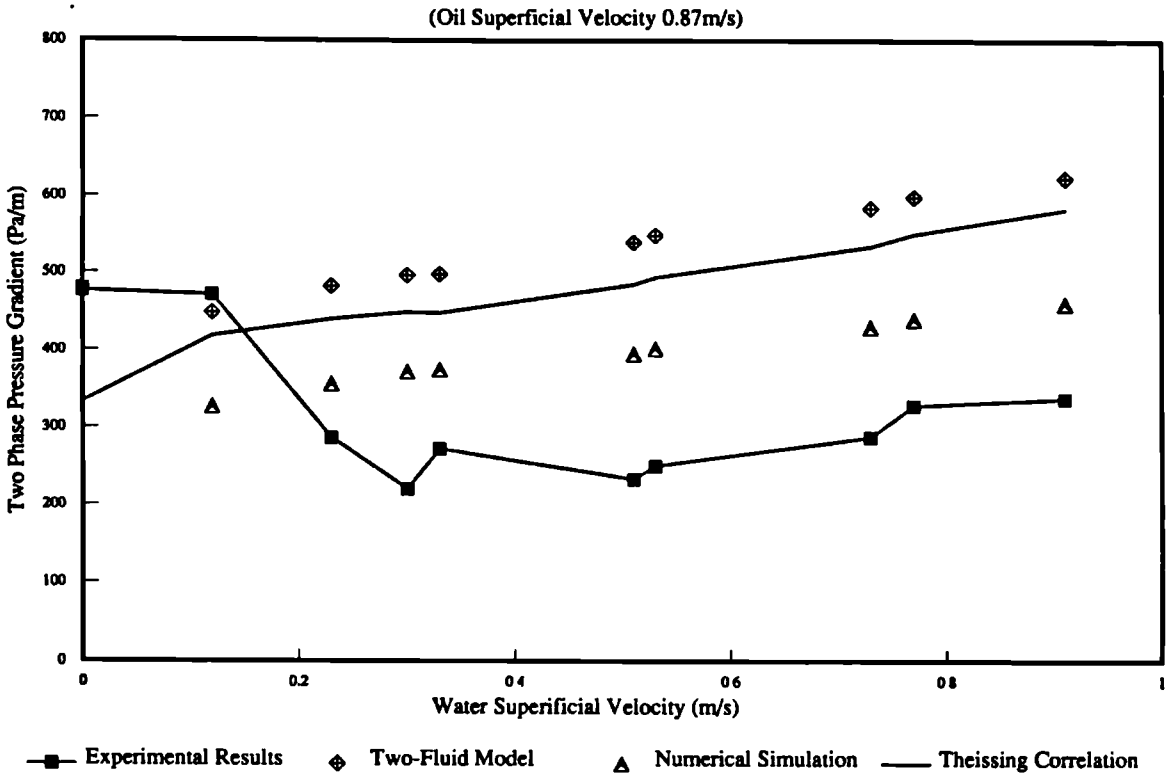


FIGURE 5.10: COMPARISON OF HOLDUP RATIO WITH MODELS

(Oil Superficial Velocity 0.15m/s)

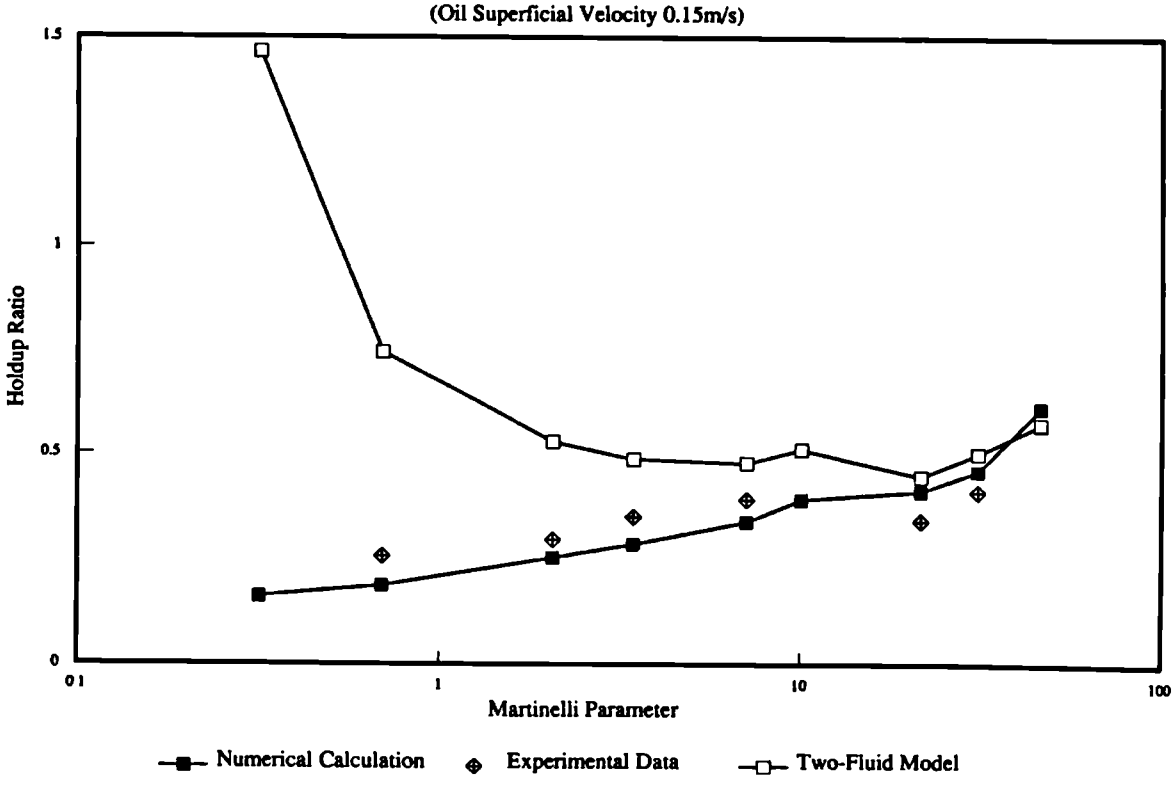


FIGURE 5.11: COMPARISON OF HOLDUP RATIO WITH MODELS

(Oil Superficial Velocity 0.26m/s)

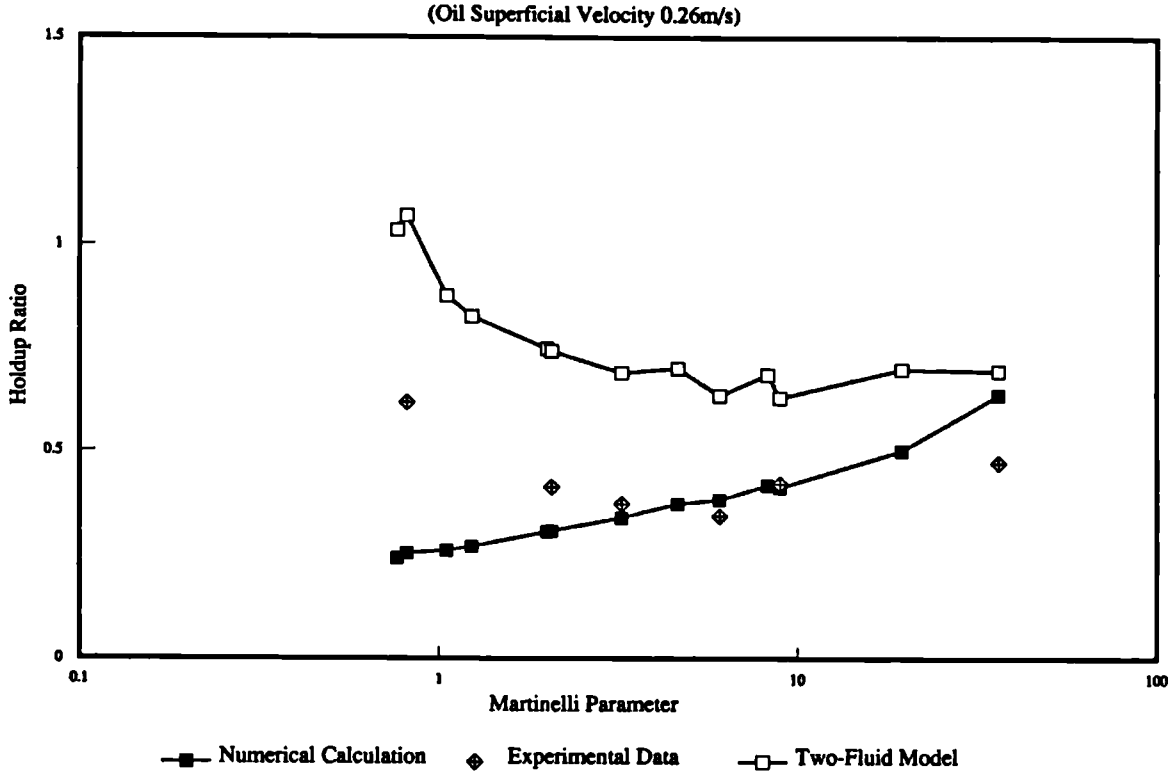


FIGURE 5.12: COMPARISON OF HOLDUP RATIO WITH MODELS

(Oil Superficial Velocity 0.55m/s)

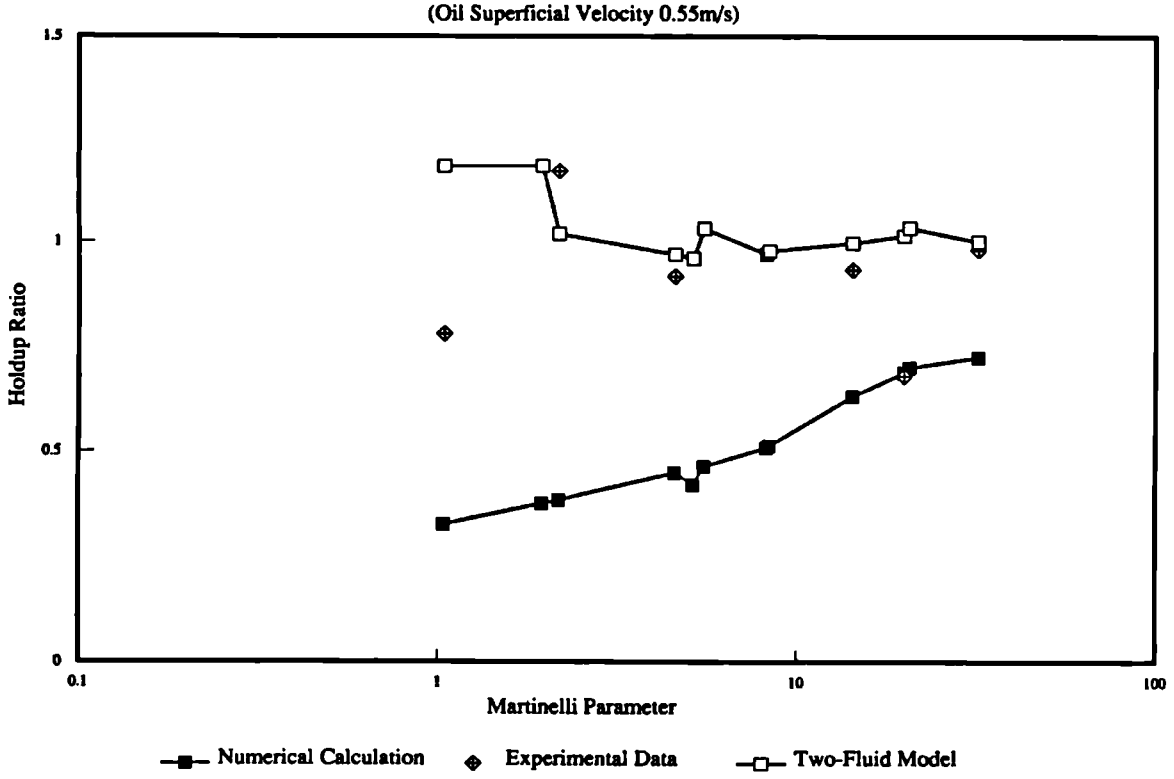


FIGURE 5.13: PRESSURE GRADIENT CALCULATION

(Numerical Simulation of Russell 1959)

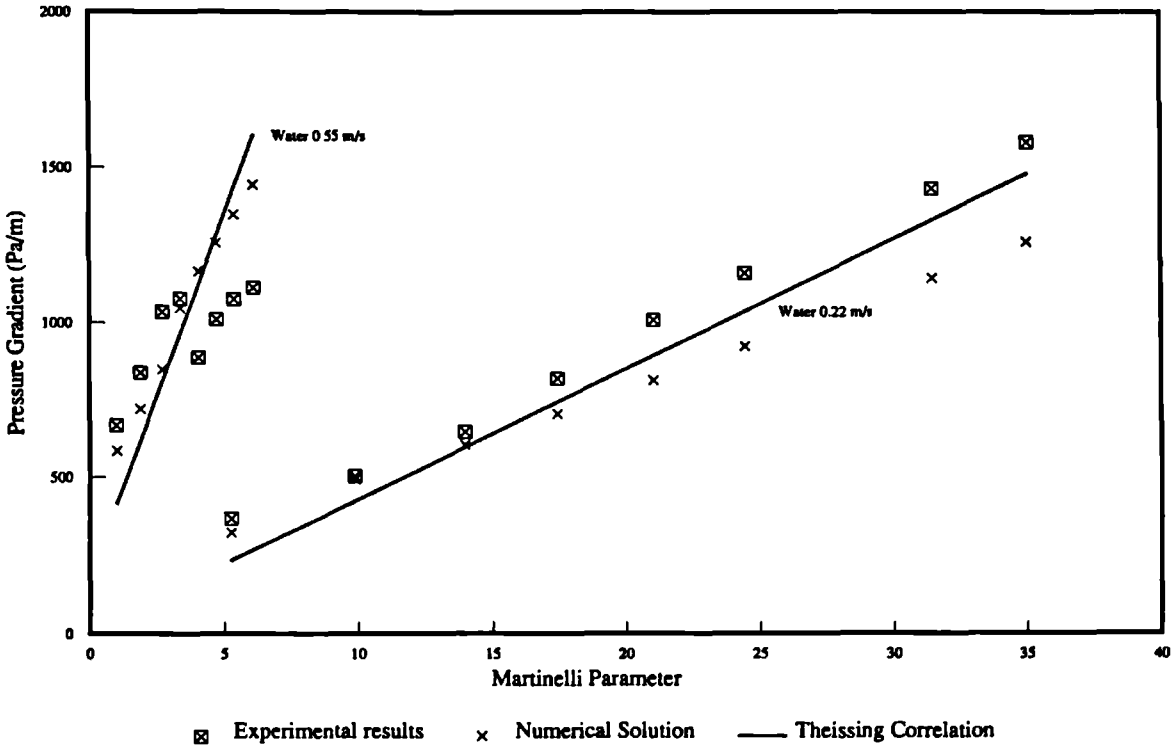


FIGURE 5.14: HOLDUP CALCULATION

(Numerical Simulation of Russell 1959)

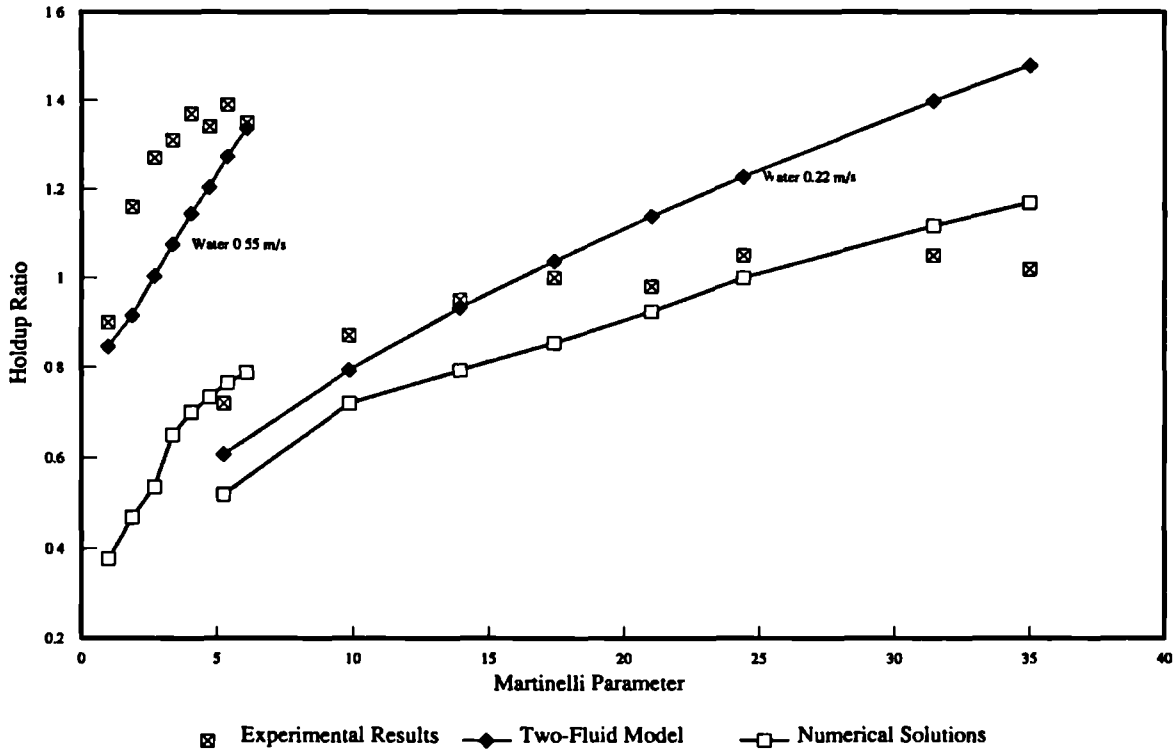


FIGURE 5.15: WATER SHEAR STRESS CALCULATION

(Numerical Simulation of Russell 1959)

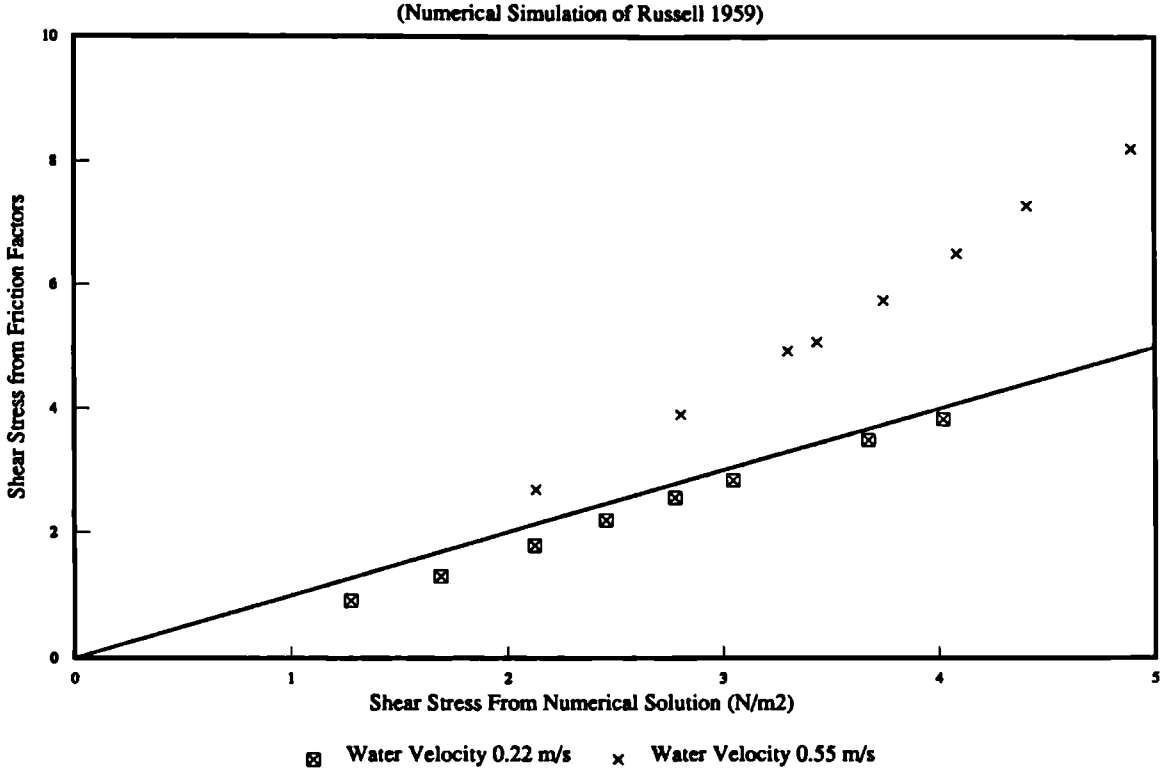


FIGURE 5.16: OIL SHEAR STRESS CALCULATION

(Numerical Simulation of Russell 1959)

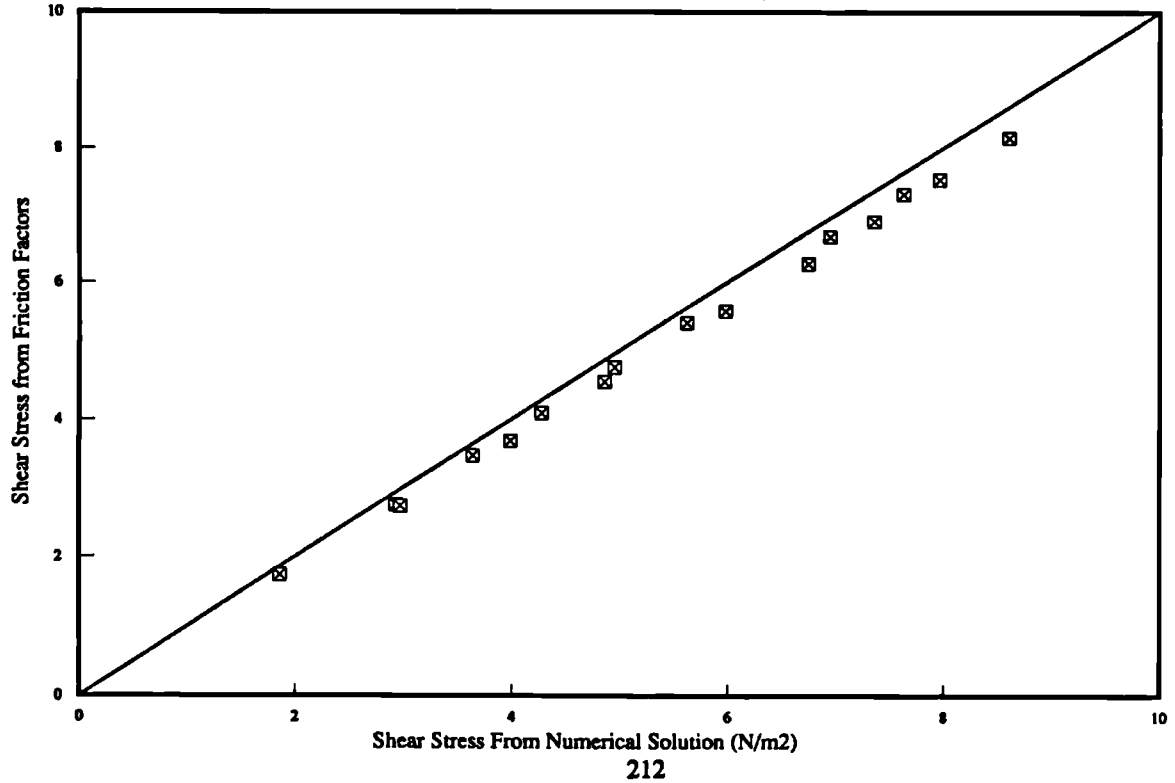


FIGURE 5.17: INTERFACIAL SHEAR STRESS CALCULATION

(Numerical Simulation of Russell 1959)

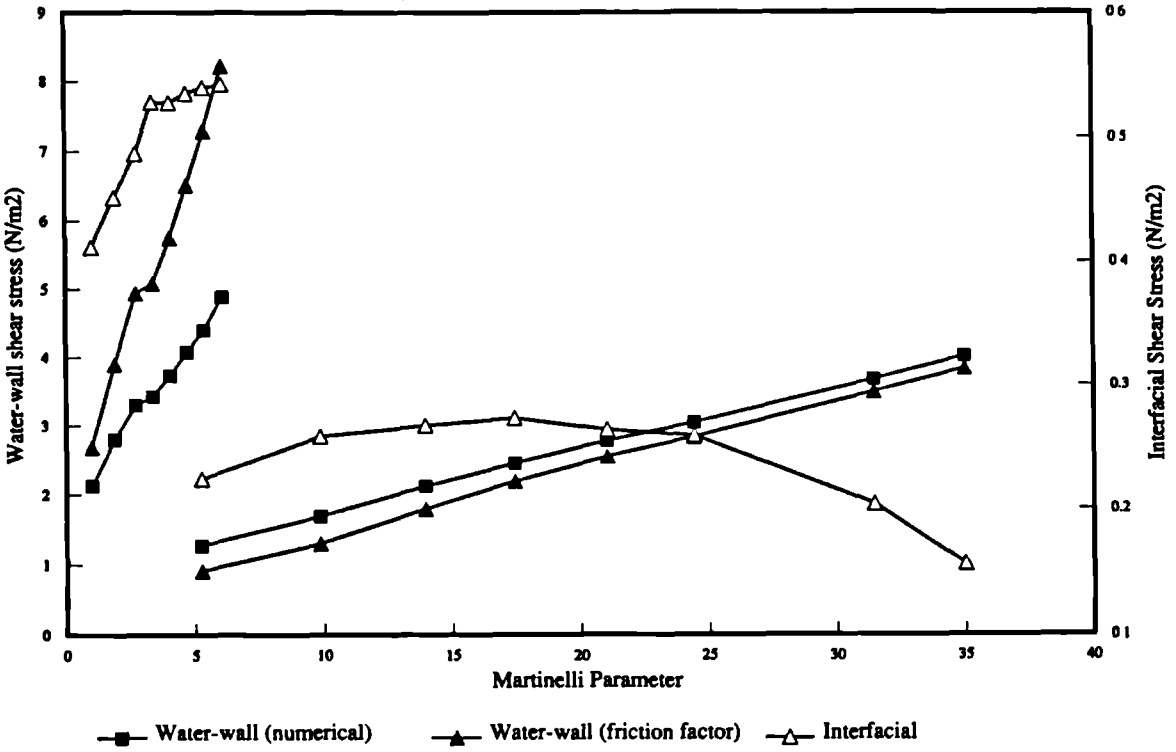


FIGURE 5.18: PRESSURE GRADIENT CALCULATION

(Numerical Simulation of Stapelberg Data)

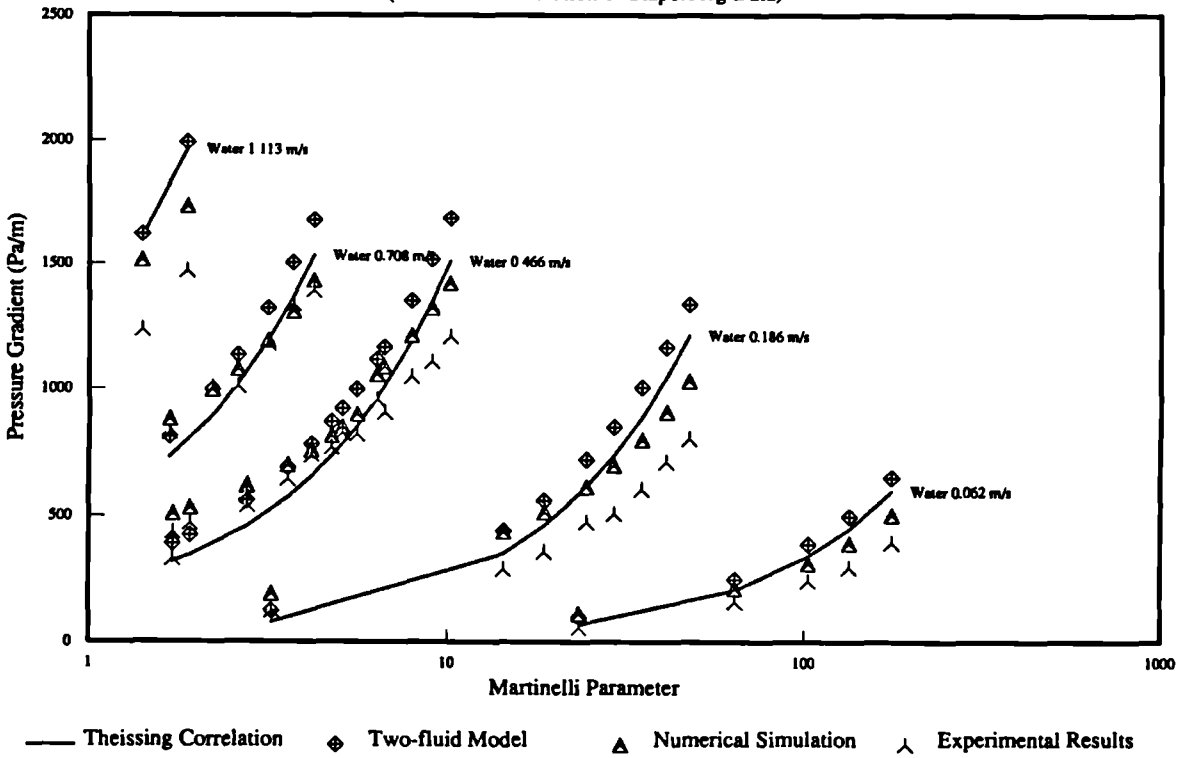
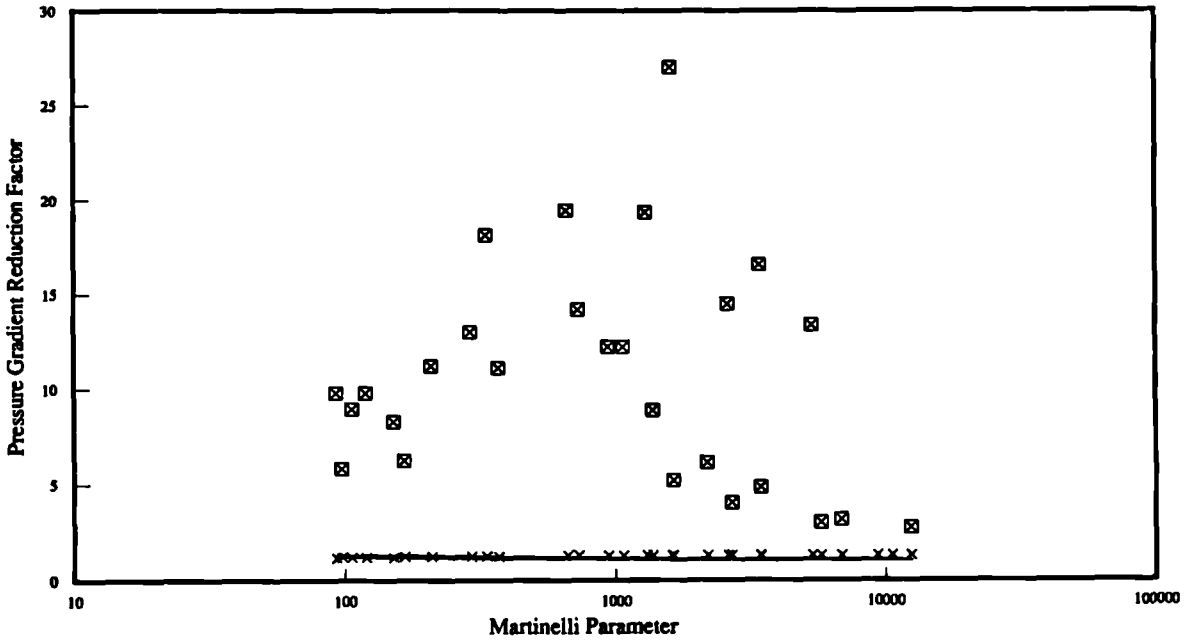


FIGURE 5.19: PRESSURE GRADIENT CALCULATION

(Numerical Simulation of Charles 1961)

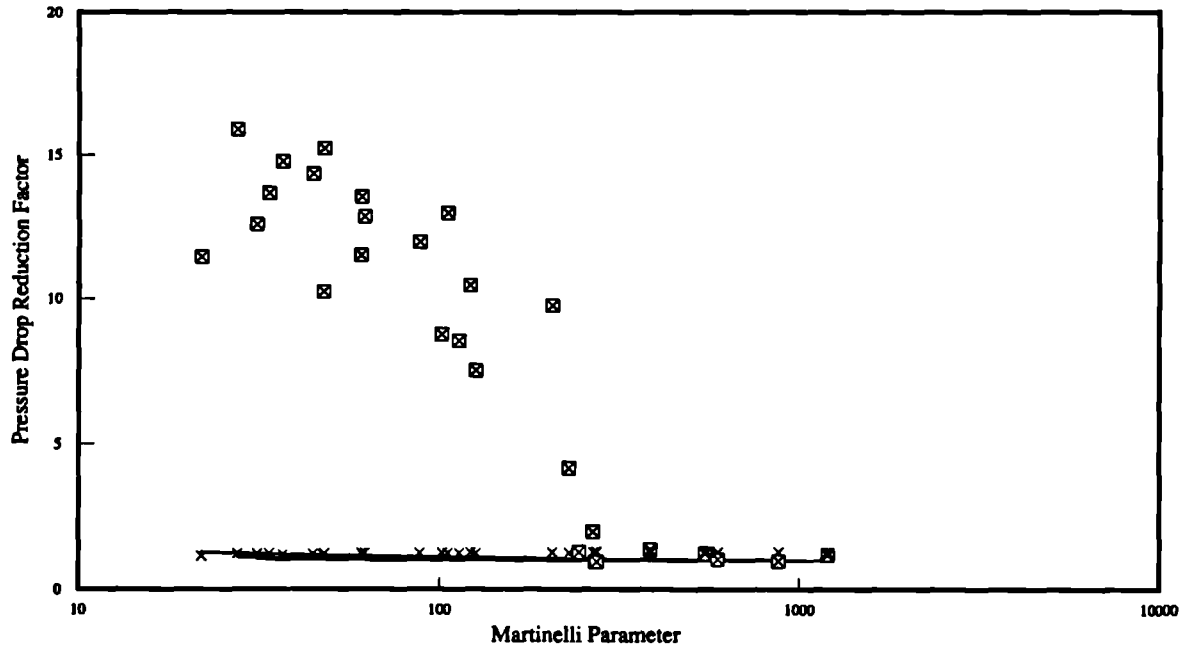


⊠ Experimental Results for 1.04" Pipe × Numerical Solution

—— Theissing Correlation

FIGURE 5.20: PRESSURE GRADIENT CALCULATION

(Numerical Simulation of Charles Data)



⊠ Experimental Results for 2.45" Pipe × Numerical Solution

—— Theissing Correlation

FIGURE 5.21: COORDINATE GRIDS FOR THREE-PHASE FLOW

(Bipolar/Rectangular/Bipolar)

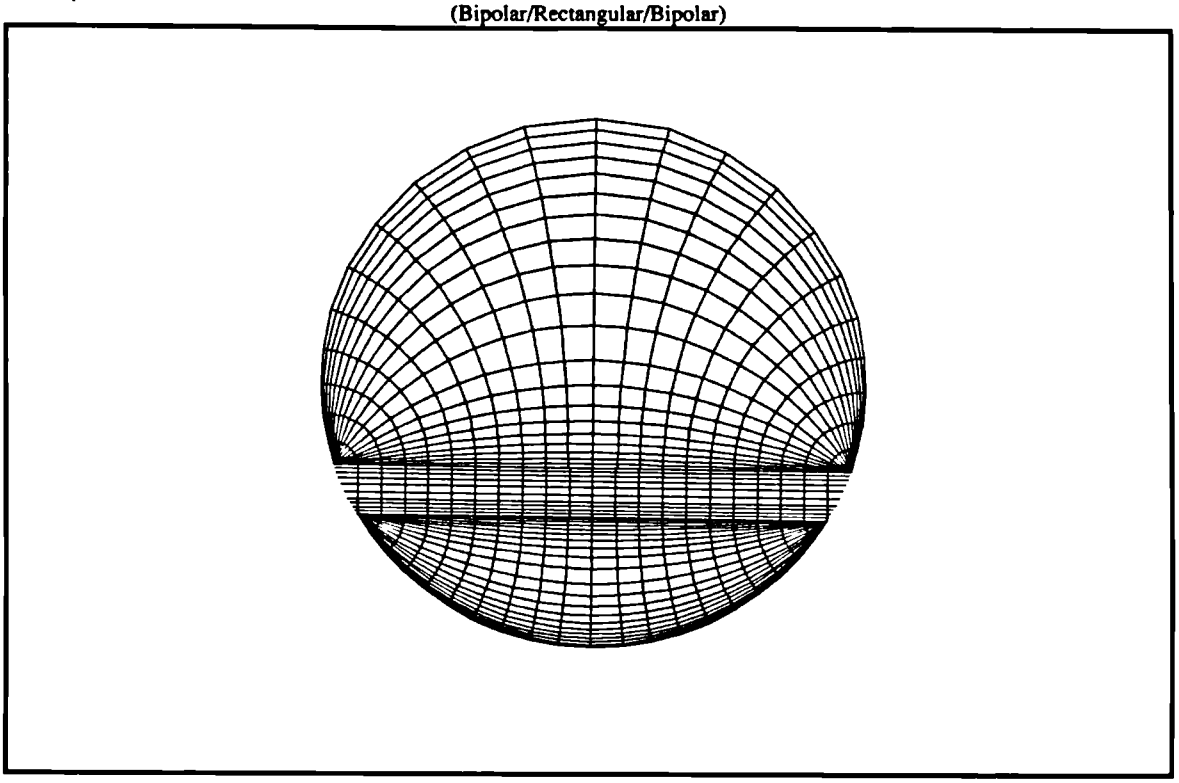


FIGURE 5.22: STAPELBERG & MEWES LAMINAR 3-PHASE FLOW

(Numerical Simulation: Re,oil = 28)

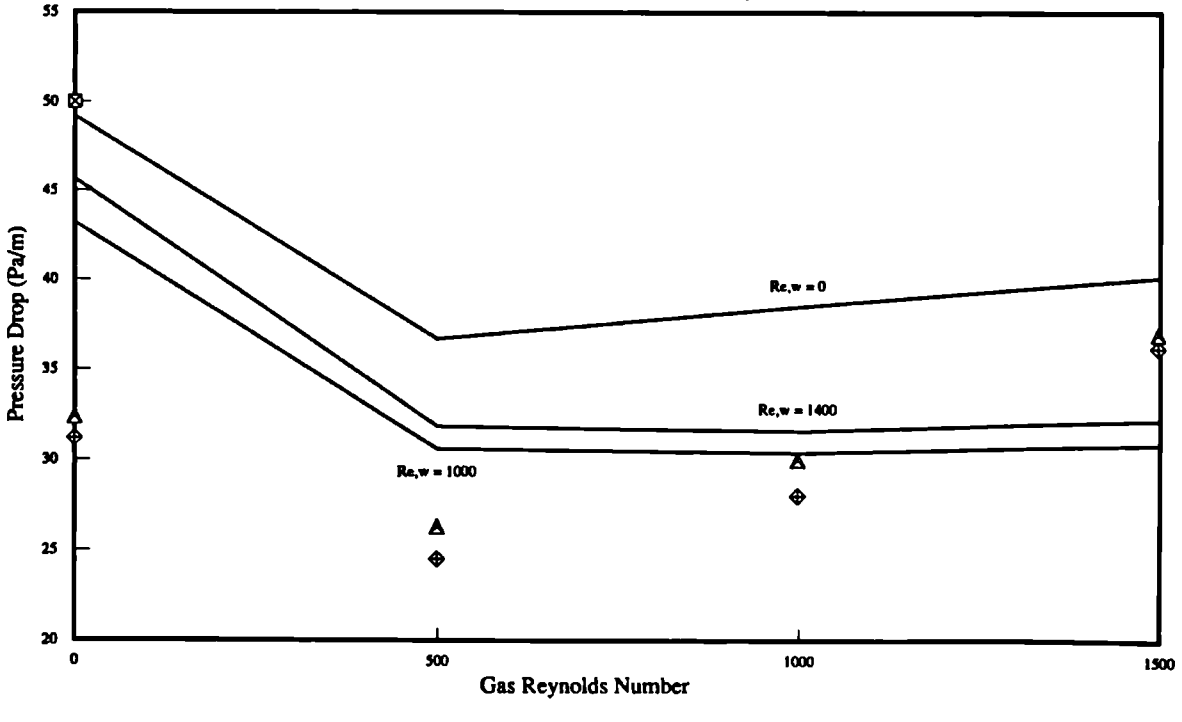


FIGURE 5.23: CALCULATION OF OIL HEIGHT

(Sobocinski Data vs Numerical Solution)

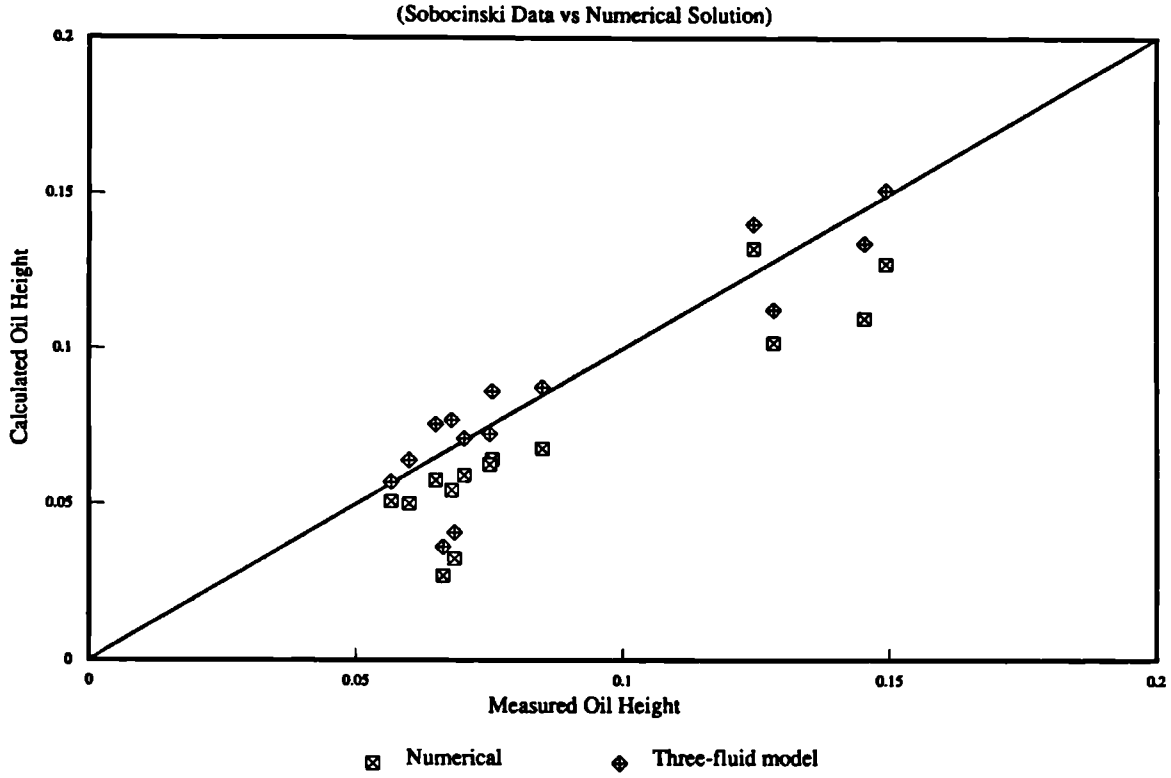


FIGURE 5.24: CALCULATION OF WATER HEIGHT

(Sobocinski Data vs Numerical Solution)

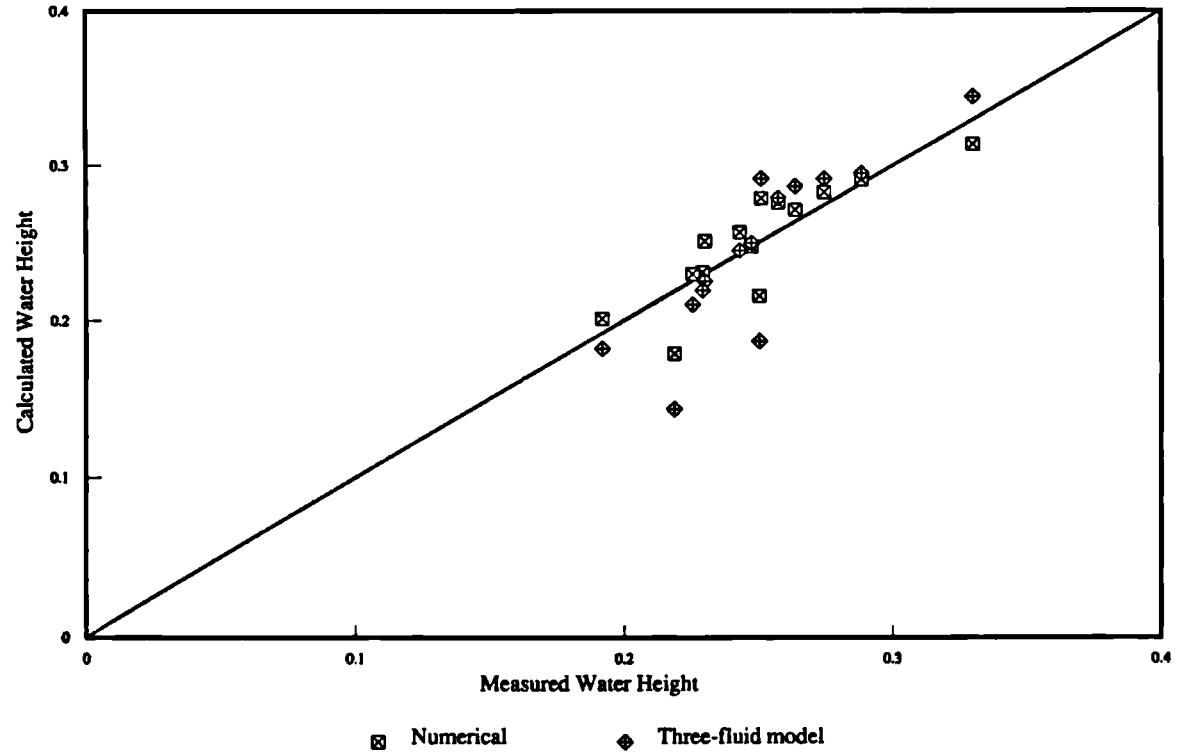


FIGURE 5.25: THREE-PHASE HOLDUP

Sobocinski Data (left bar) vs Numerical Solution (right bar)

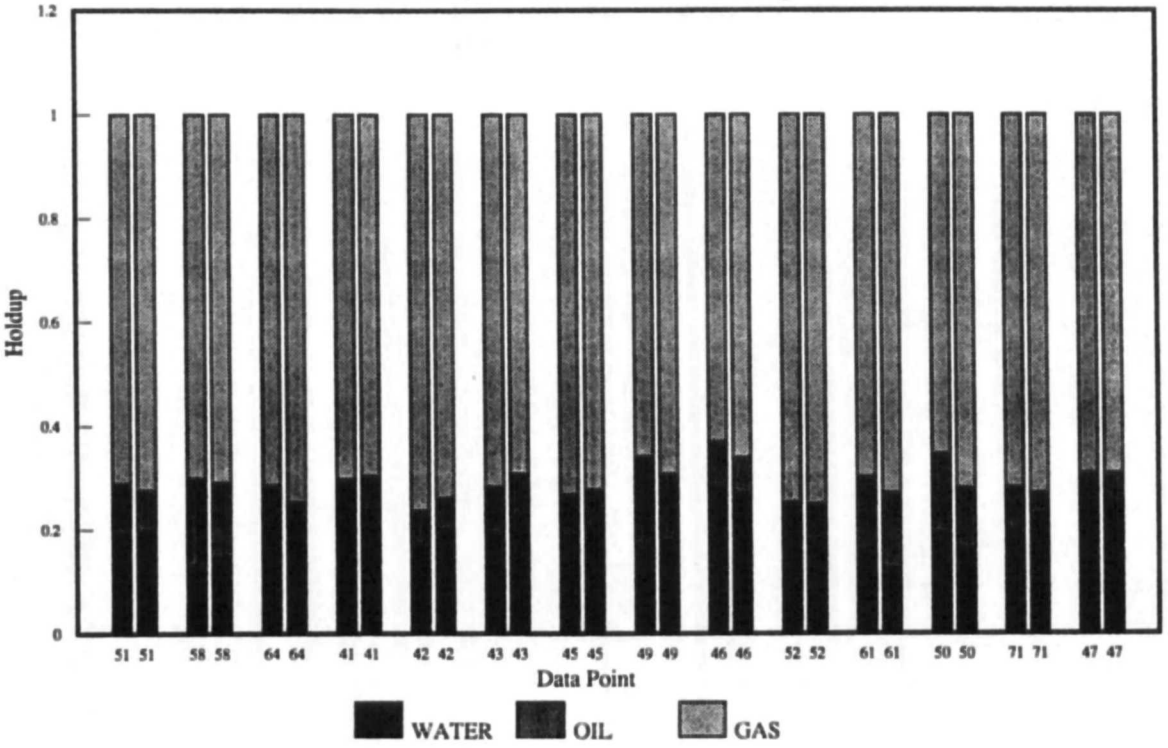


FIGURE 5.26: CALCULATION OF PRESSURE GRADIENT

(Sobocinski Data vs Numerical Solution)

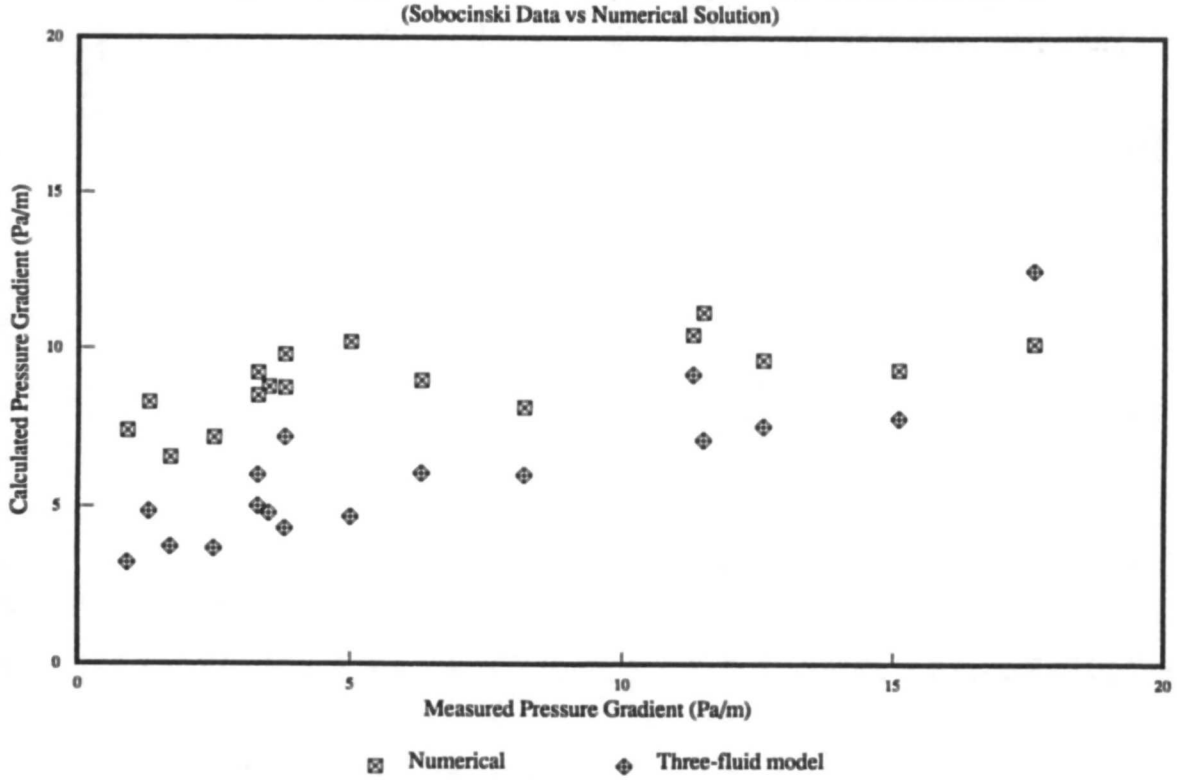


FIGURE 5.27: THREE-PHASE HOLDUP PREDICTION

(Nuland et al)

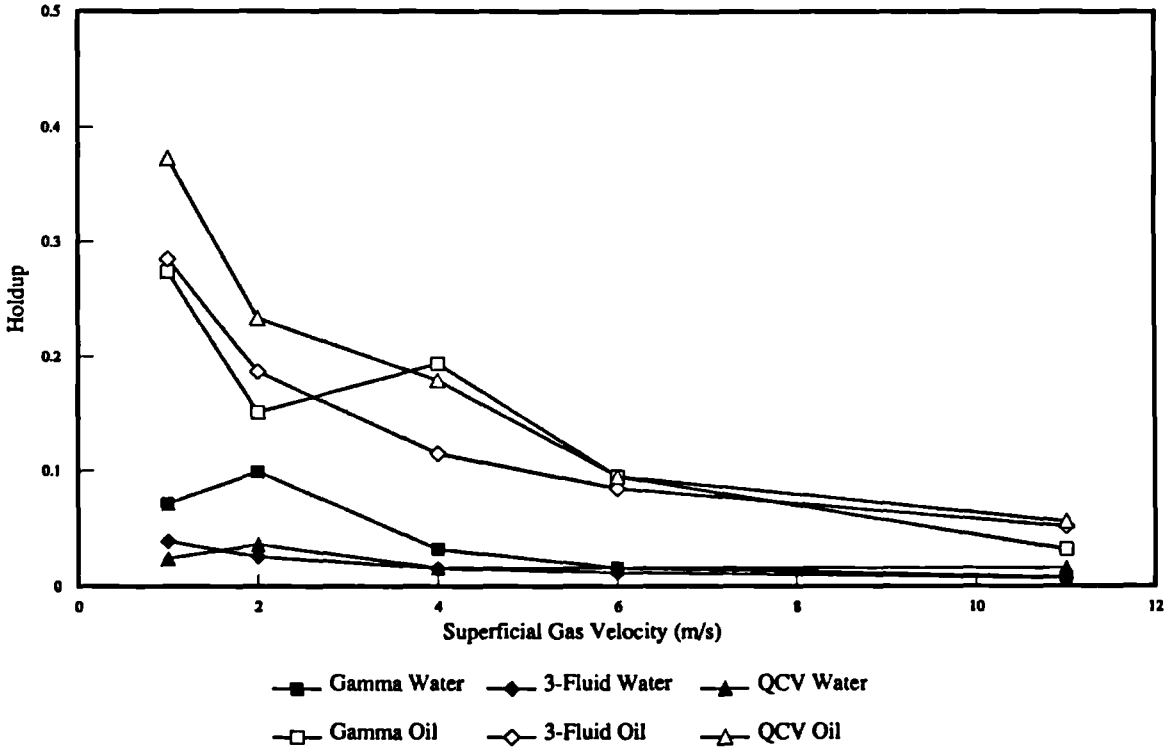


FIGURE 5.28: THREE-PHASE HOLDUP PREDICTION

(Nuland et al)

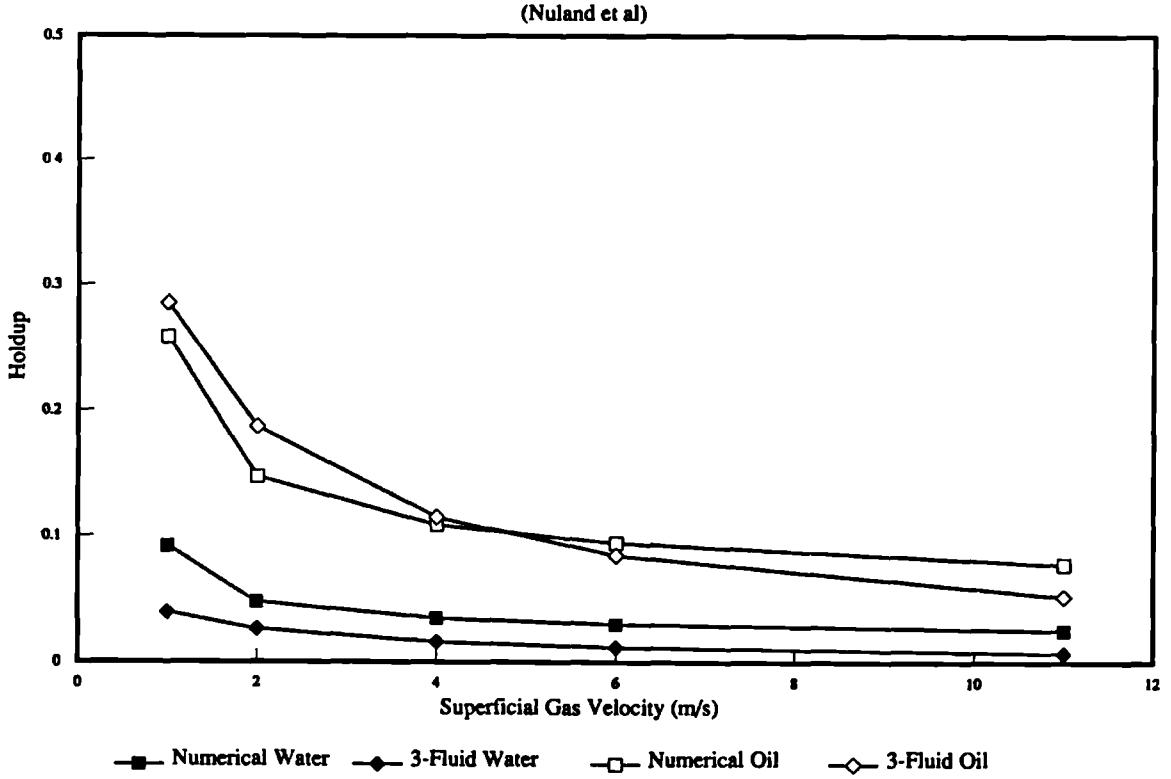


FIGURE 6.1: STRATIFIED-INTERMITTENT TRANSITION

(Separated Oil and Water Layers)

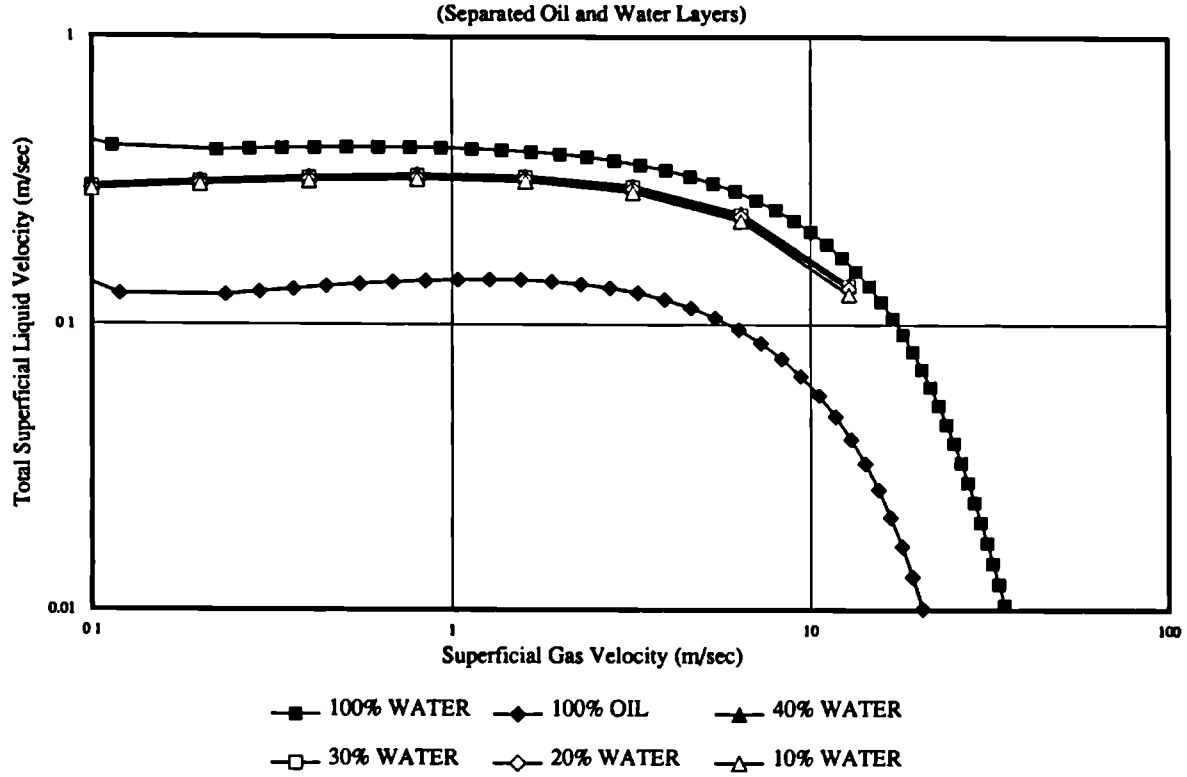


FIGURE 6.2: STRATIFIED-SLUG TRANSITION IN OIL/WATER/GAS FLOW

(Dispersed Liquid Phases)

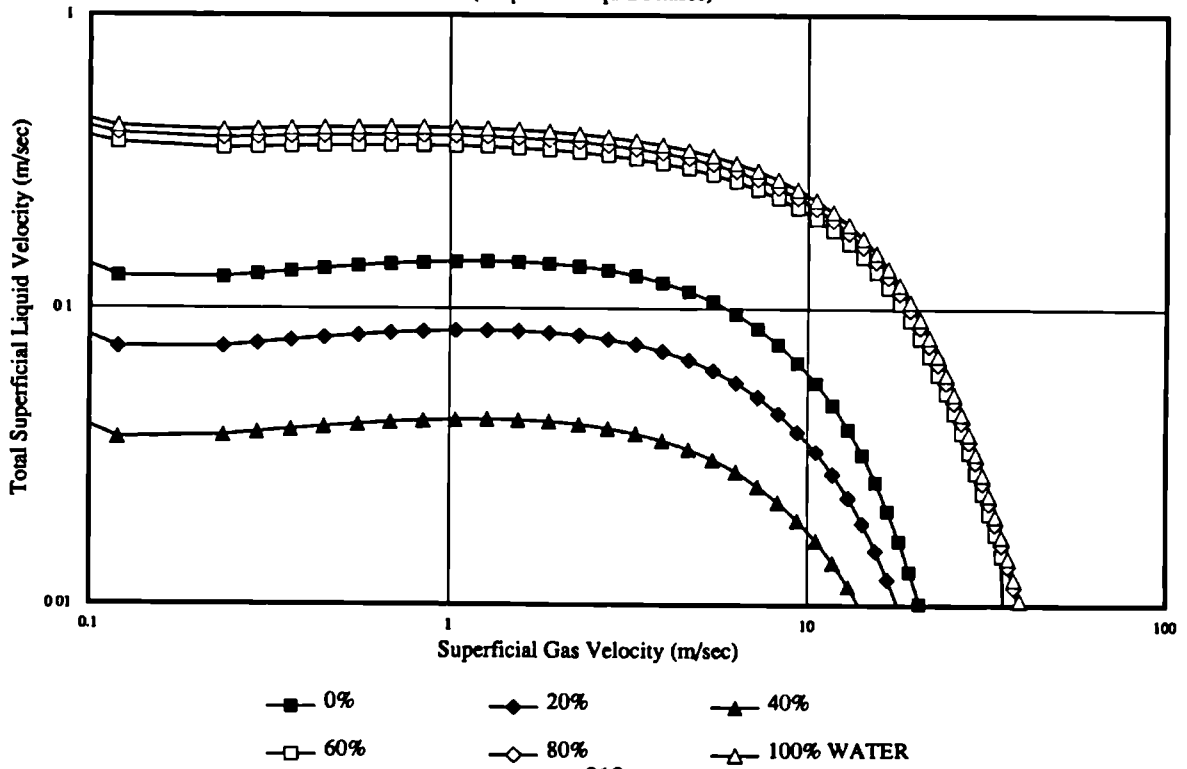
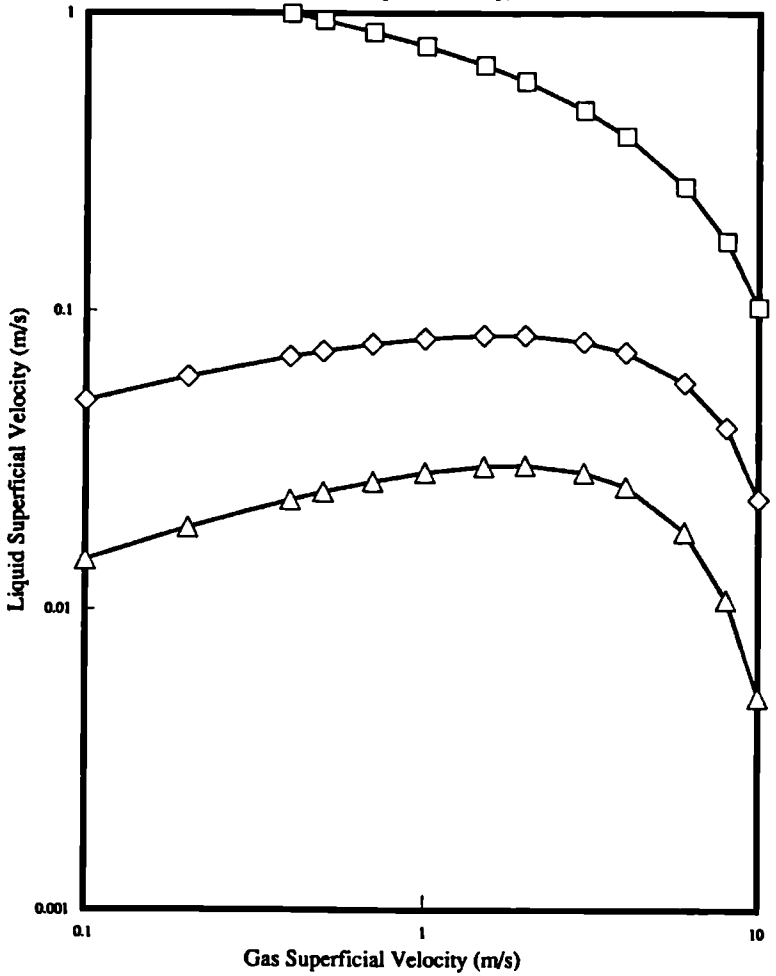


FIGURE 6.3: NEUTRAL STABILITY CALCULATIONS (FLOW IN A CHANNEL)
(Effect of Liquid Viscosity)



Inviscid Kelvin-Helmholtz (1mPas Liquid)
Lin & Hanratty (1mPas Liquid)
Lin & Hanratty (100mPas Liquid)

AEA PETROLEUM SERVICES
ARW HALL 25/6/92

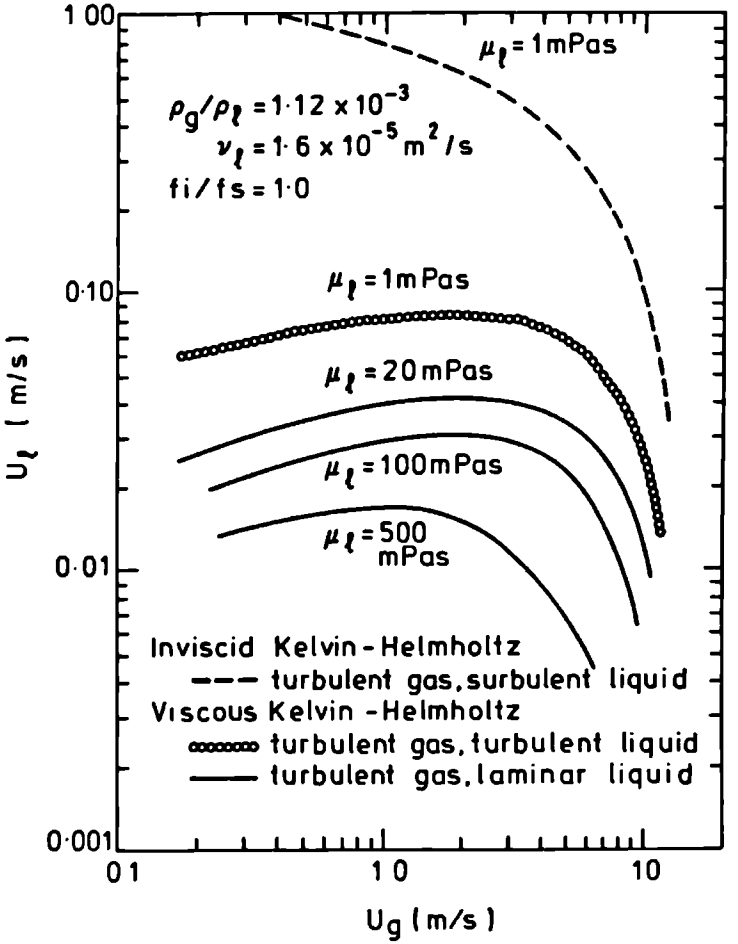


FIGURE 6·4. NEUTRAL STABILITY CALCULATIONS
(Two-phase flow in a channel - Lin & Hanratty)

FIGURE 6.5: NEUTRAL STABILITY CALCULATIONS

(2-Phase Flow in a 2-D Channel: Comparison of Oil and Water)

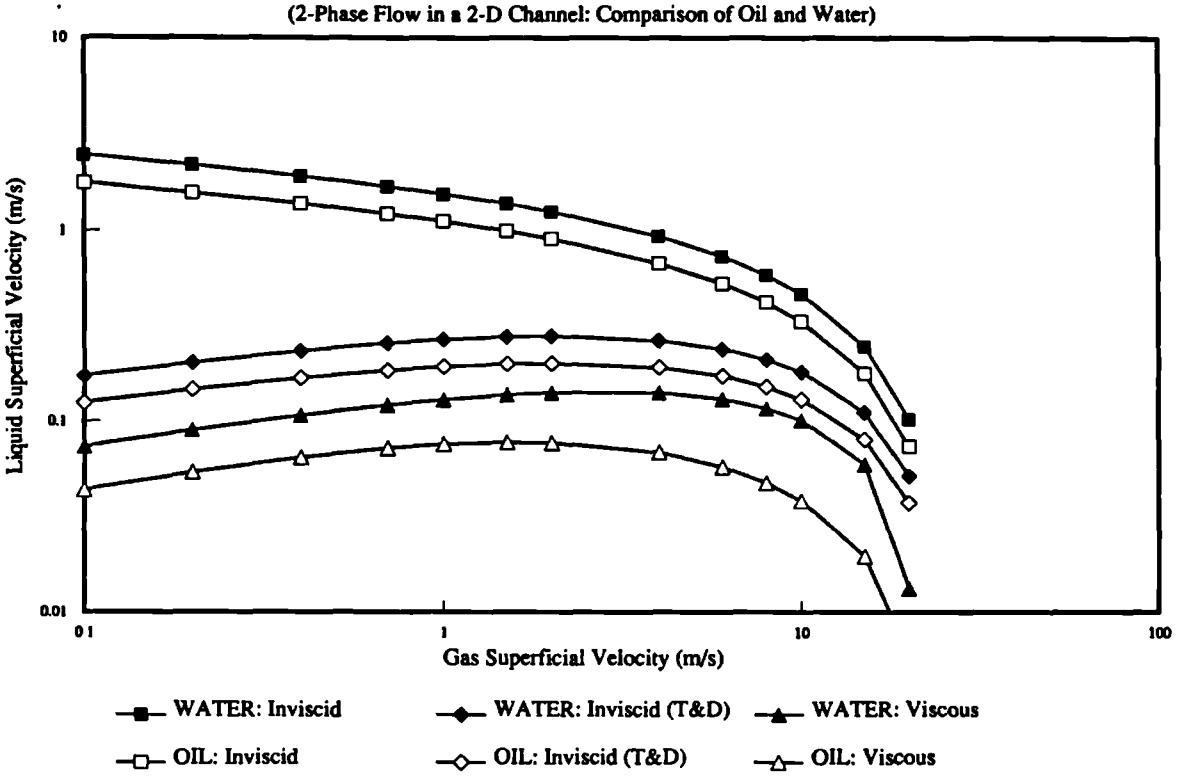


FIGURE 6.6: NEUTRAL STABILITY CALCULATIONS

(3-Phase Flow in a 2-D Channel: Effect of second liquid phase)

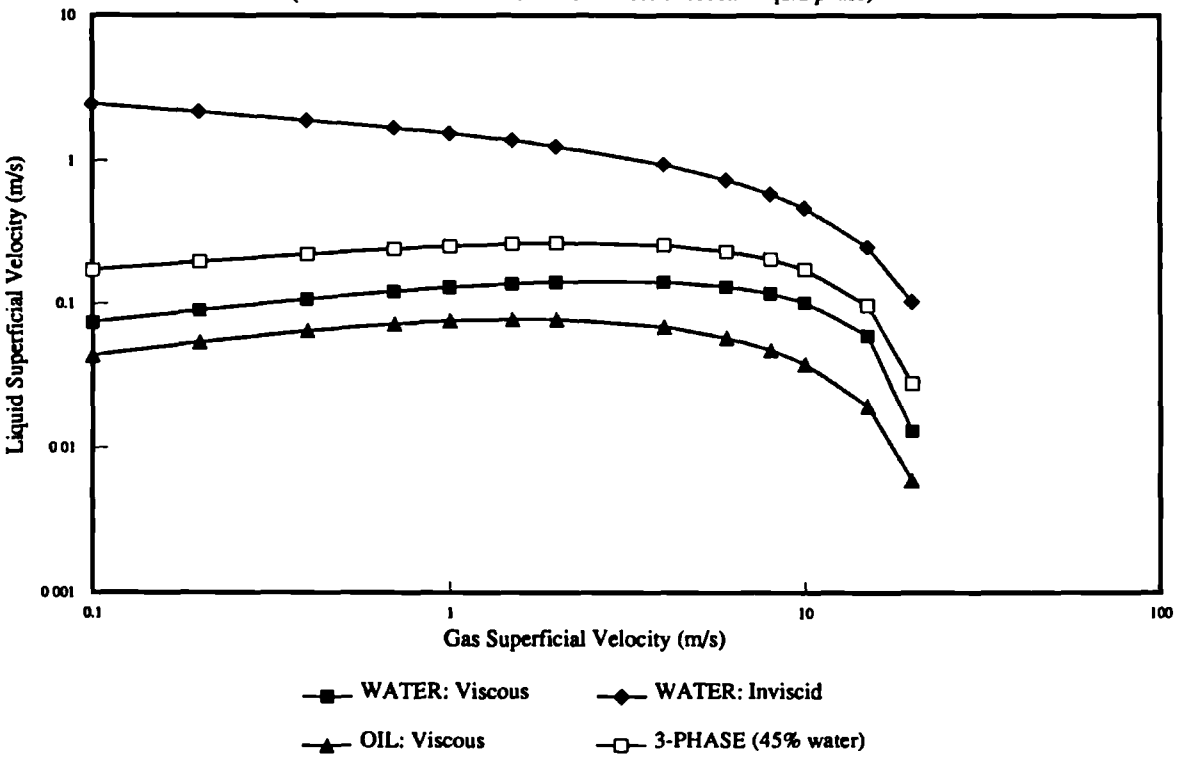


FIGURE 6.7: NEUTRAL STABILITY CALCULATIONS

(3-Phase Flow in a 2-D Channel: Effect of Water Fraction)

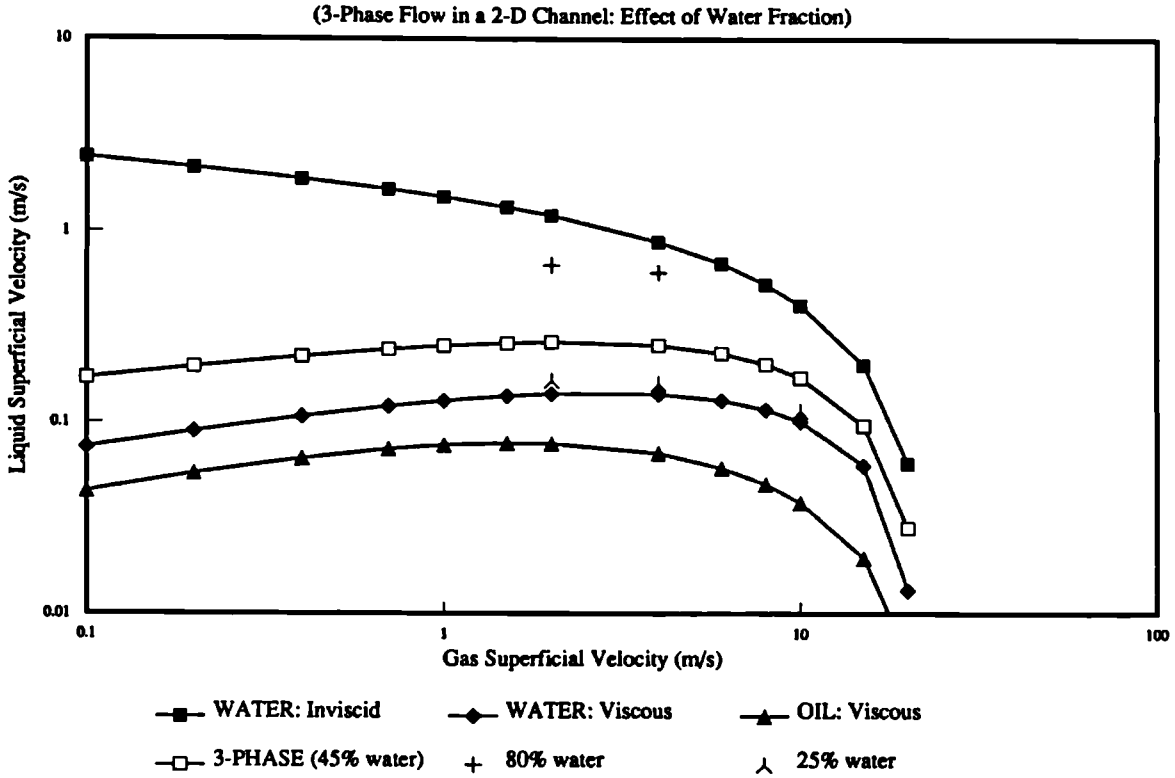


FIGURE 6.8: THREE-PHASE STRATIFIED-SLUG FLOW TRANSITION

(Flow in a Pipe: 30% and 50% Water)

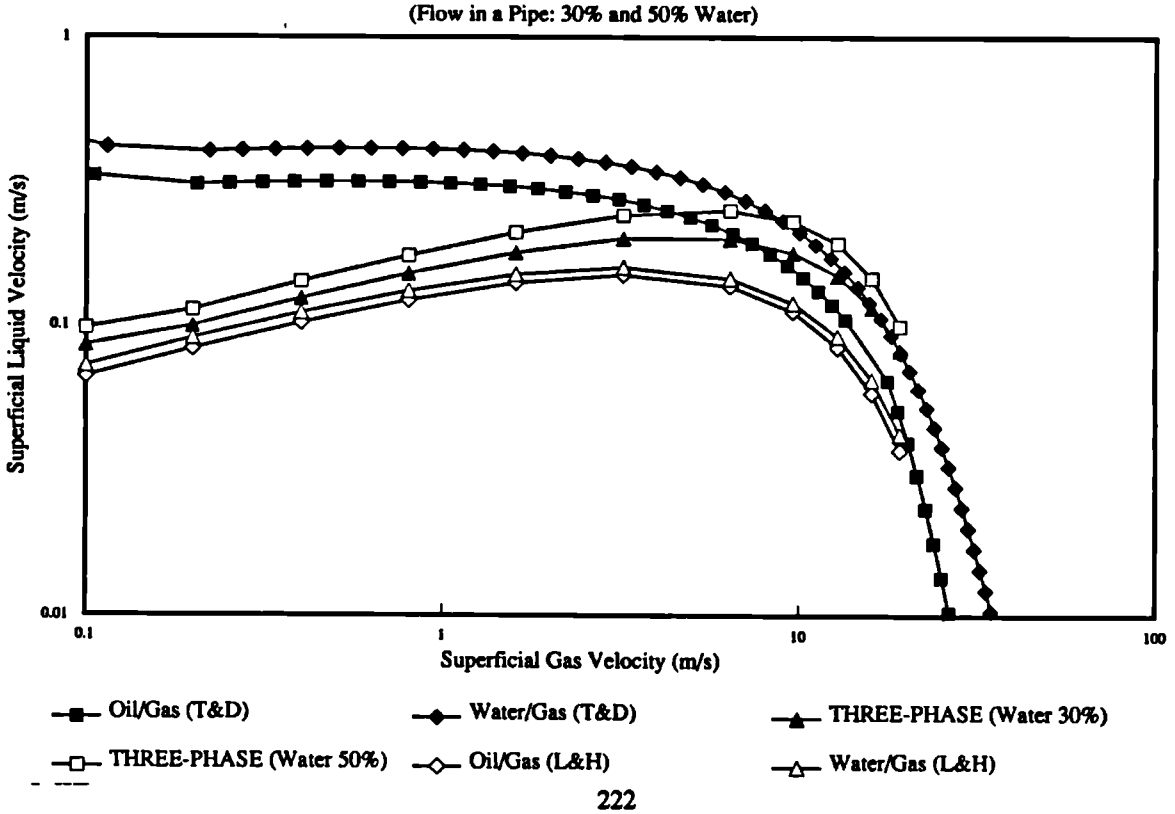


FIGURE 6.9: THREE-PHASE STRATIFIED-SLUG FLOW TRANSITION

(Flow in a Pipe: 30% and 70% Water)

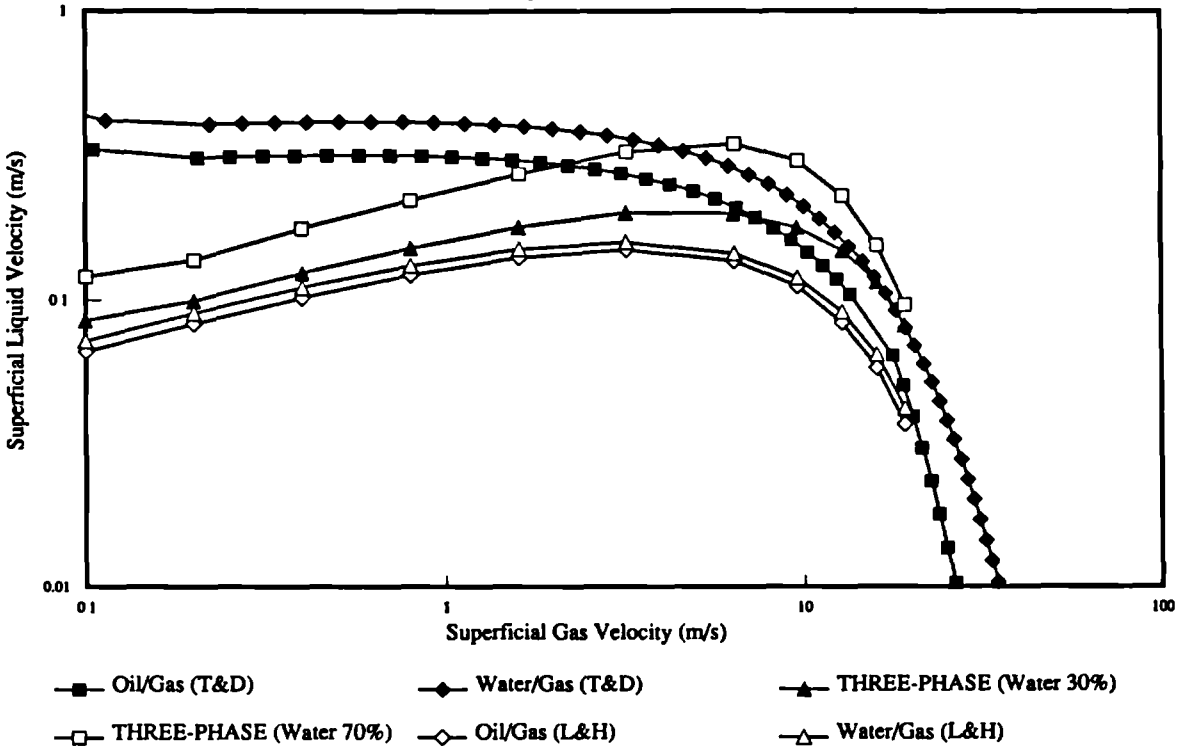


FIGURE 6.10: COMPARISON OF SOBOCINSKI DATA WITH TRANSITION PREDICTION

(Three phase Stratified Flows)

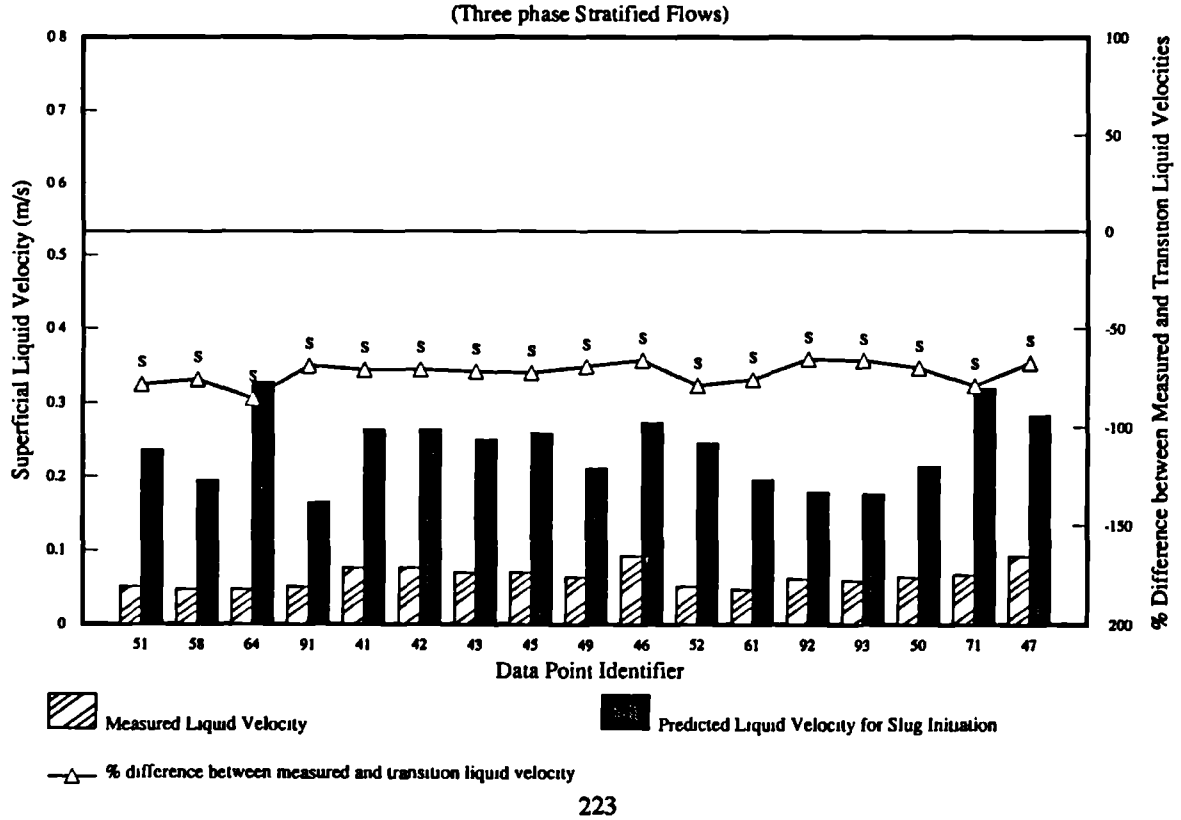


FIGURE 6.11: COMPARISON OF STAPELBERG DATA WITH TRANSITION PREDICTION

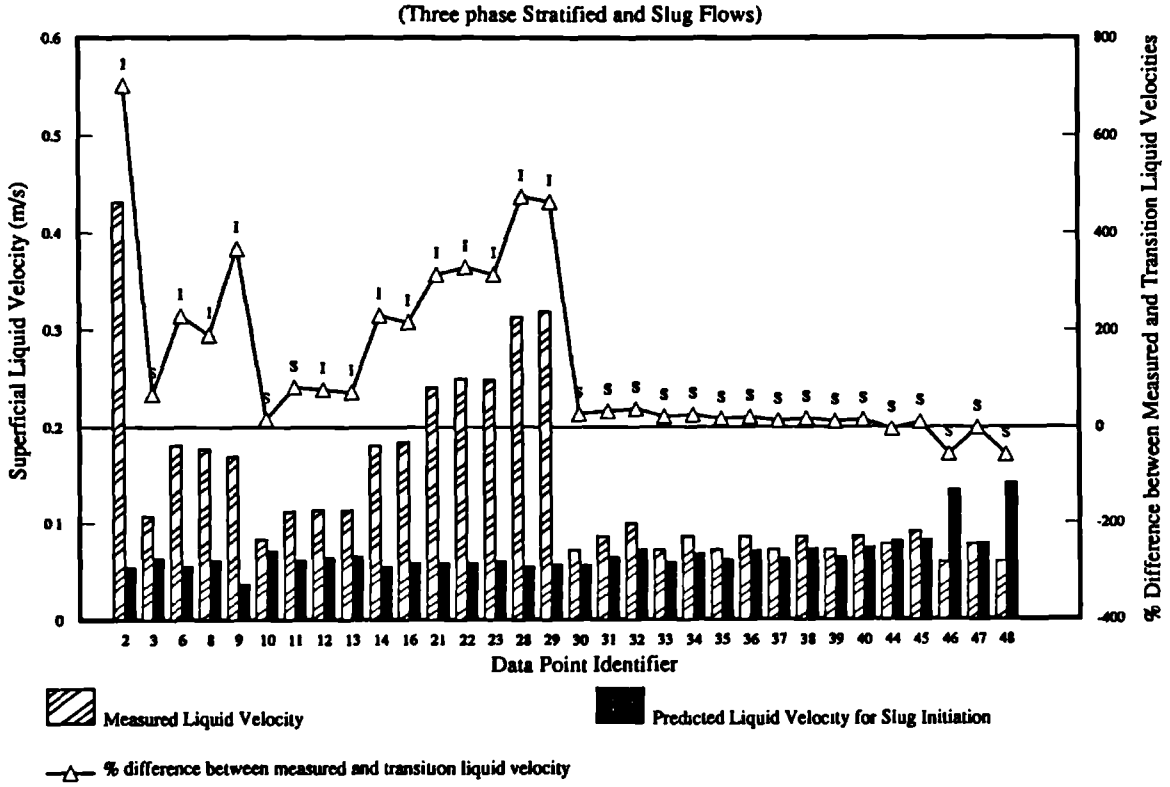


FIGURE 6.12: PREDICTION OF WATER SEPARATION

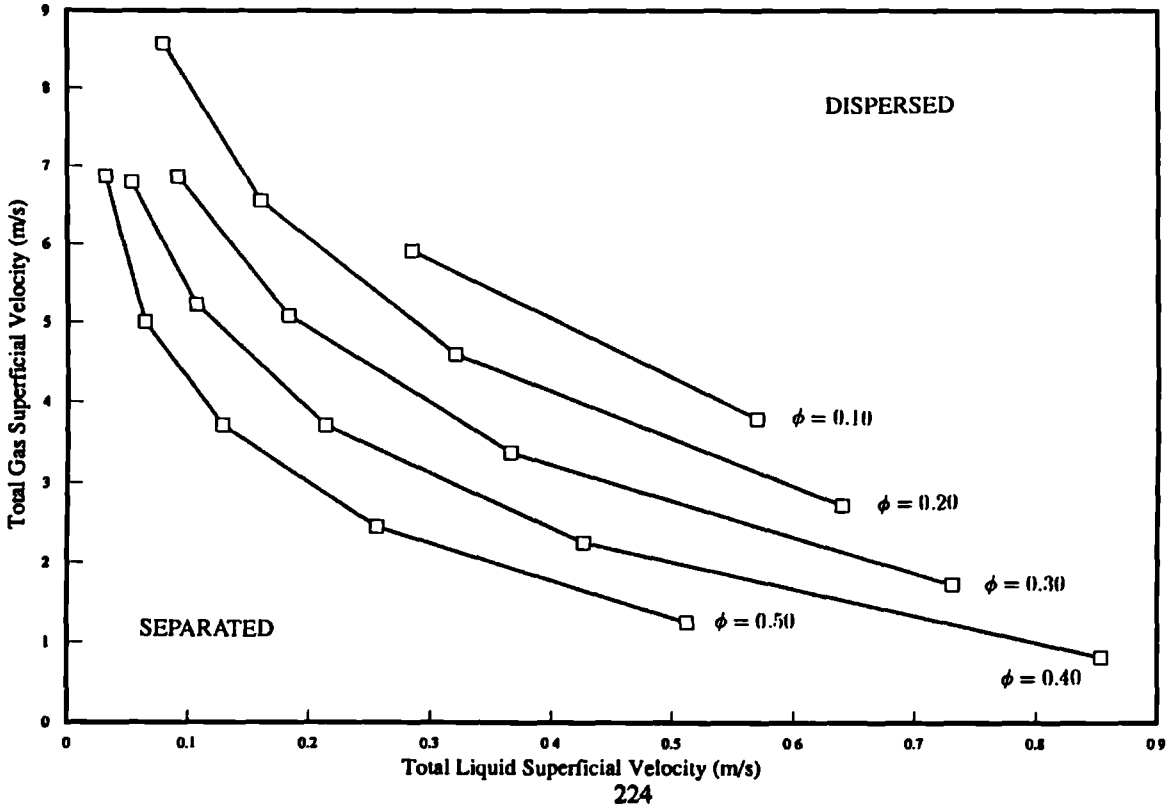


FIGURE 6.13: OIL-WATER-GAS INTERFACIAL STABILITY

(Sobocinski Data - Gas/Oil Interface)

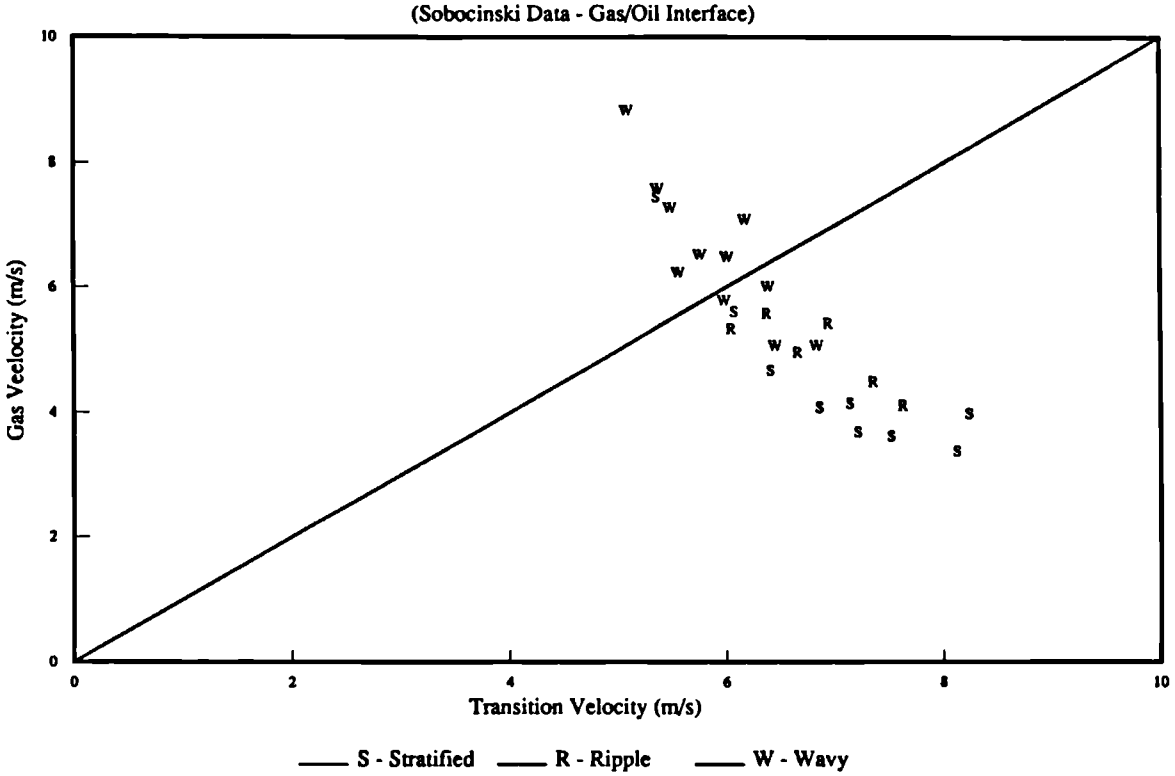
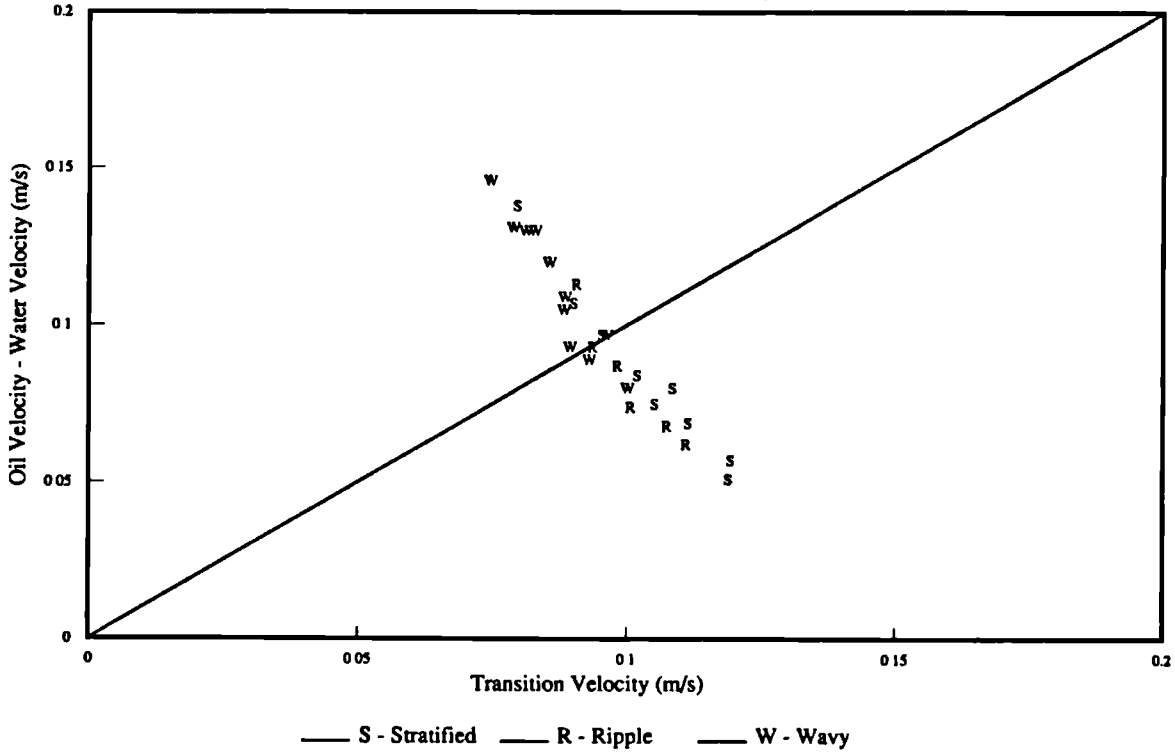


FIGURE 6.14: OIL-WATER-GAS INTERFACIAL STABILITY

(Sobocinski Data - Oil/Water Interface)



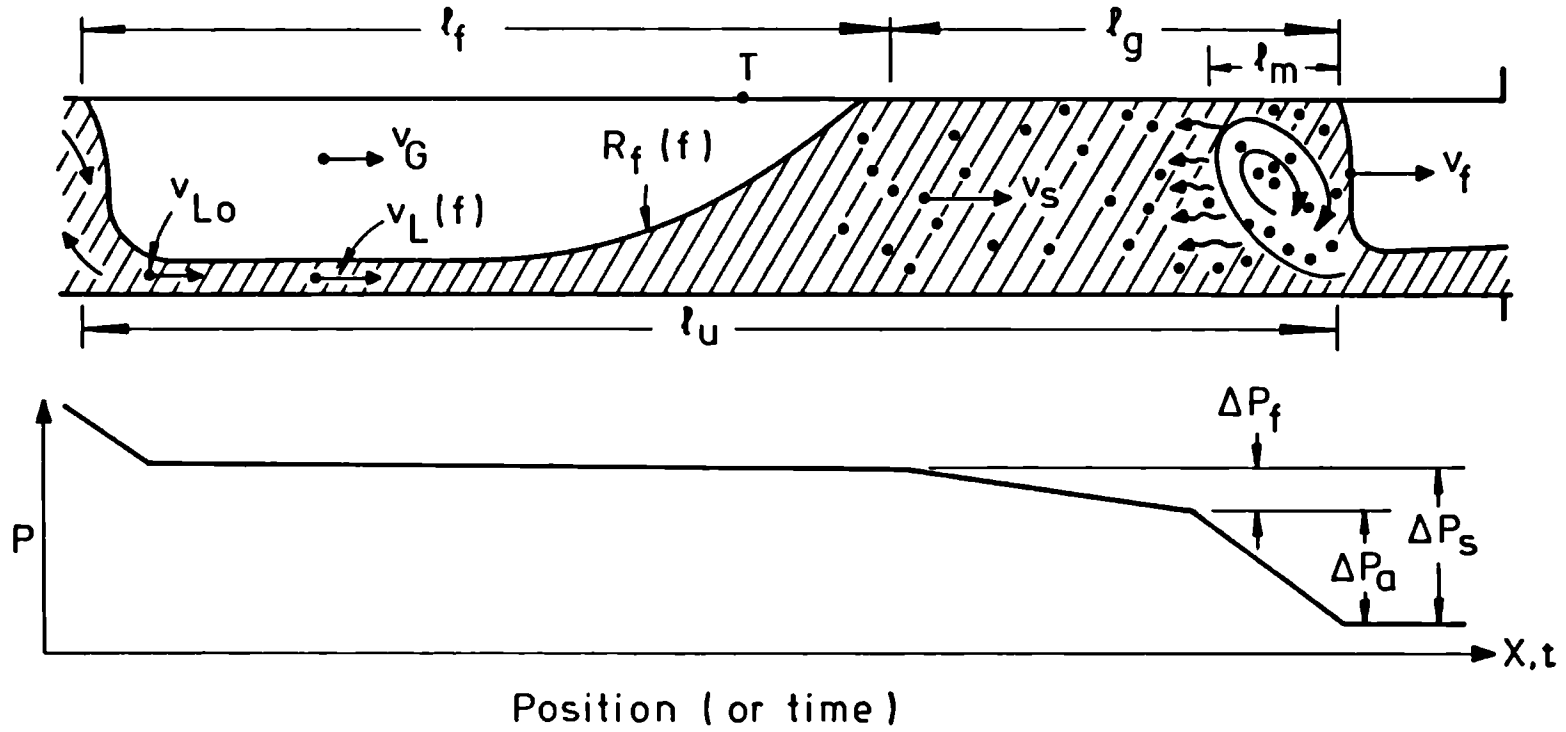
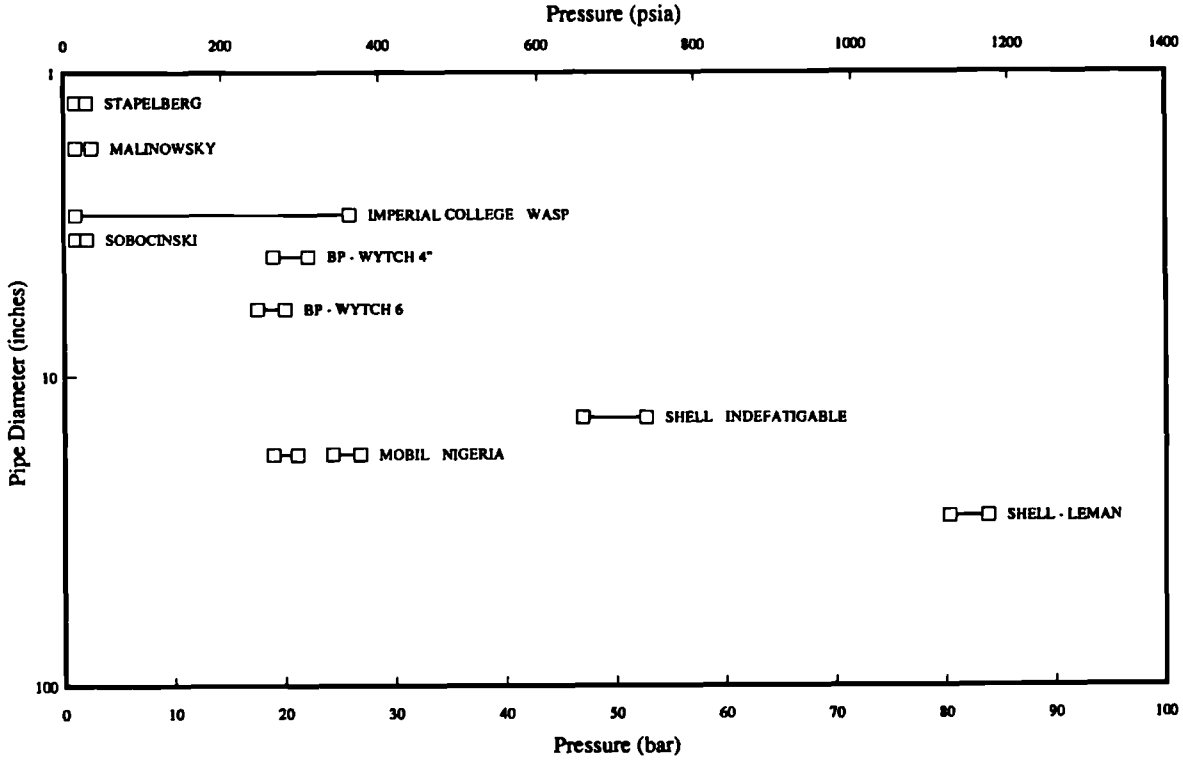


FIGURE 7·1. PHYSICAL MODEL FOR SLUG FLOW (DUKLER & HUBBARD)

FIGURE 8.1: DEVELOPMENT OF THE WASP CONSORTIUM

Year	Phase	Support
1987-1990	Construction and commissioning Operation with air and water at high pressure	SERC UKAEA Harwell Laboratory
1990-1991	Operation with air-oil-water at ambient pressure	AEA Petroleum Services SERC
Autumn 1991	Formation of WASP Consortium	AEA Petroleum Services British Gas Esso Institut Français du Petrole Instituto Mexicano del Petroleo Norsk Hydro OSO (Department of Energy) Texaco
1992-	Air-oil-water at ambient pressure Inclined slug flows Stratified flows Air-oil-water at high pressure Development of nuclear instrumentation	WASP Consortium SERC

FIGURE 8.2: OIL-WATER-GAS FLOW CONDITIONS



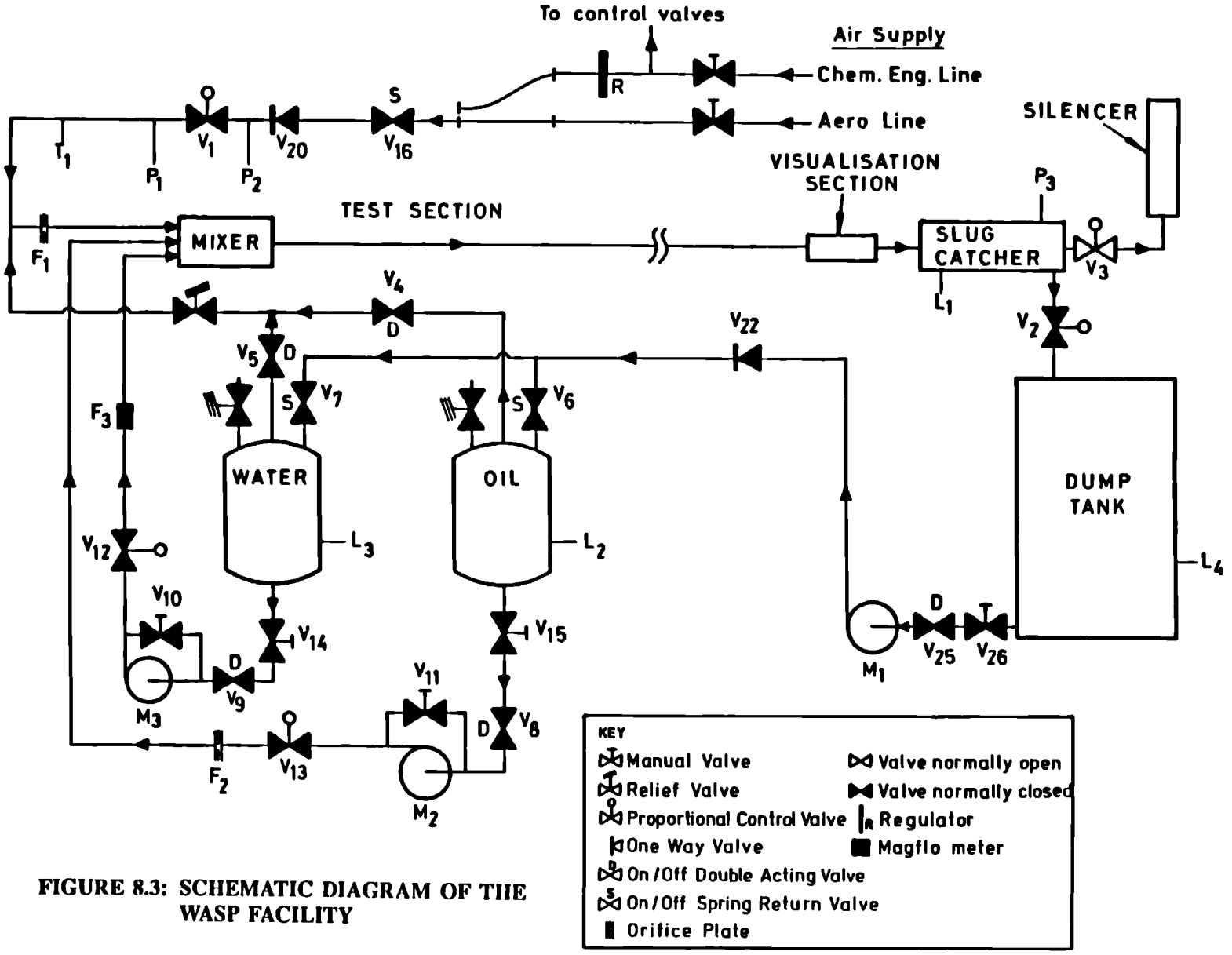


FIGURE 8.3: SCHEMATIC DIAGRAM OF THE WASP FACILITY

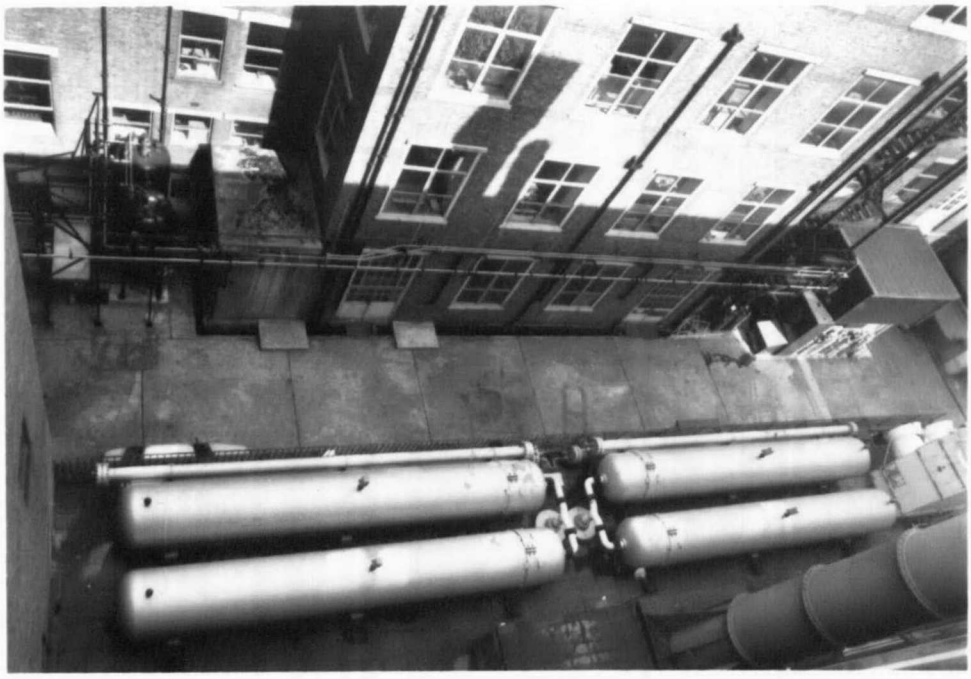


Figure 8.4: Overall view of the WASP facility

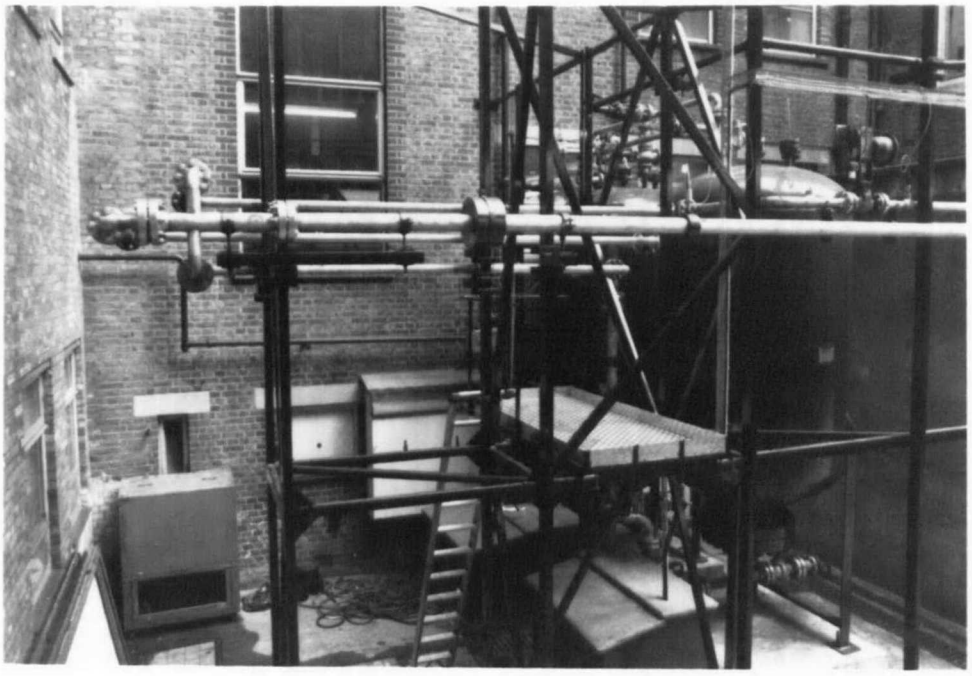


Figure 8.5: Mixer section and liquid storage tanks

AEA TECHNOLOGY
CULHAM / HARWELL
PHOTOGRAPHIC GROUP

HR 81567

UNCLASSIFIED

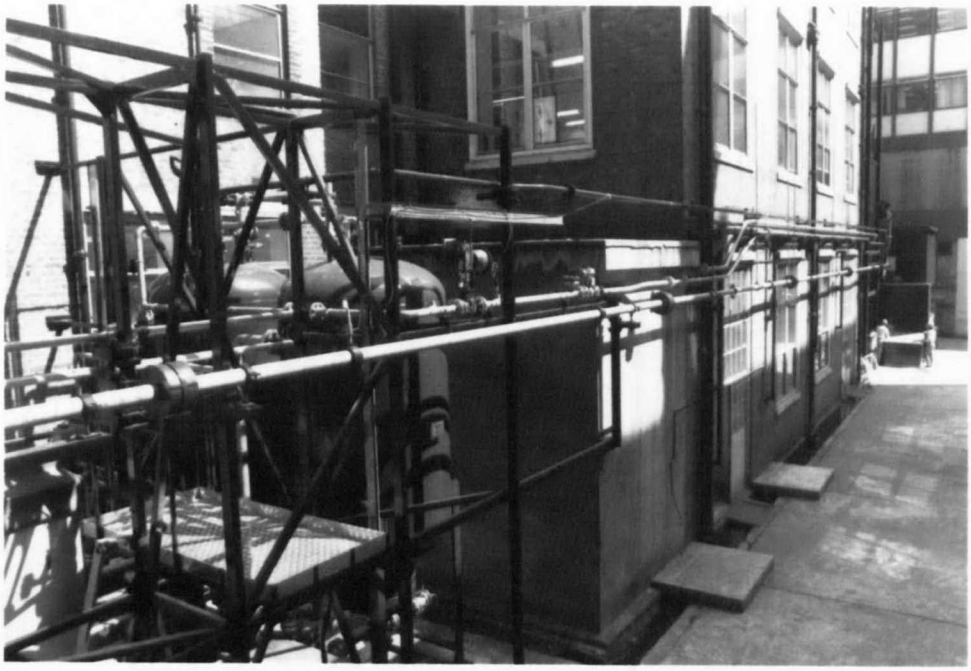


Figure 8.6: WASP test section

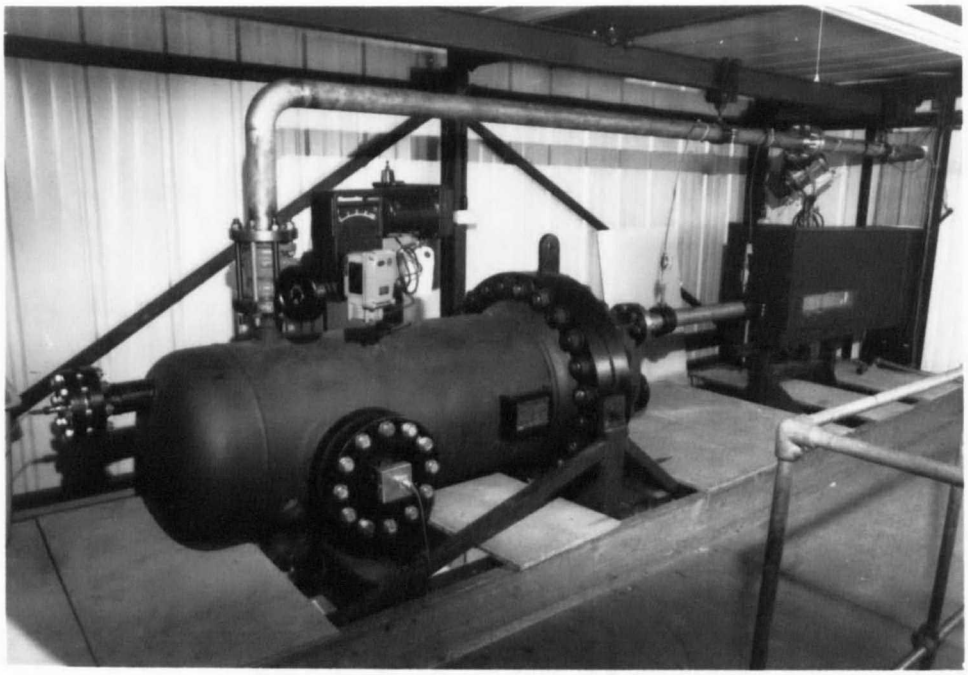
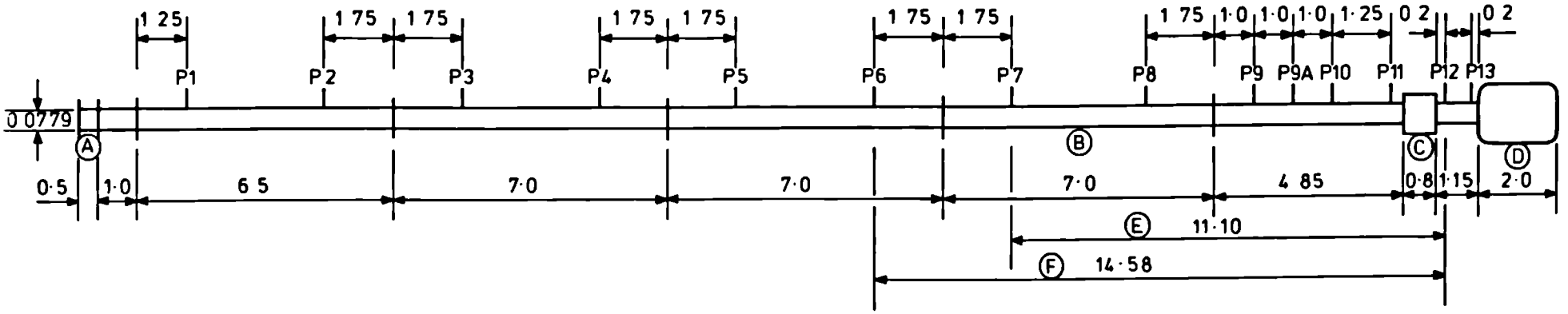


Figure 8.7: Slug catcher and visualisation section

AEA TECHNOLOGY
CULHAM / HARWELL
PHOTOGRAPHIC GROUP

HR 81568

UNCLASSIFIED



Dimensions in Metres

Notes.

(A) Mixer section

(B) This section of pipe replaced by holdup section - Length 6·98m

(C) Visualisation section

(D) Slug catcher

(E) Pressure drop measured from P7 to P12 (Before holdup section installed)

(F) Pressure drop measured from P6 to P12 (After holdup section installed)

A.R.W.HALL 27/8/92

FIGURE 8·8. WASP FACILITY TEST SECTION DETAILS

FIGURE 8.9: RISE IN UPSTREAM PRESSURE DUE TO ACTUATION OF QUICK-CLOSING VALVES
(Data Point 84)

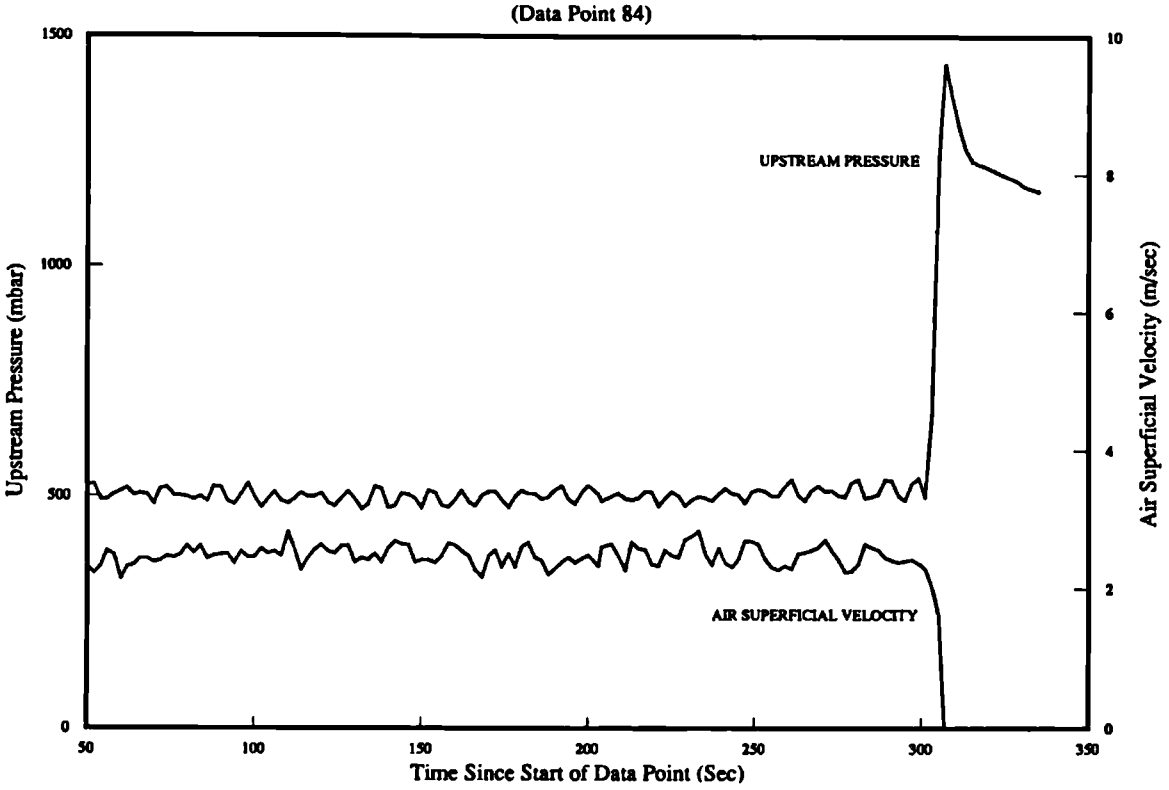


FIGURE 8.10: VISCOSITY OF SHELL TELLUS 22 OIL
(Bohlin Rheometer 30/3/92)

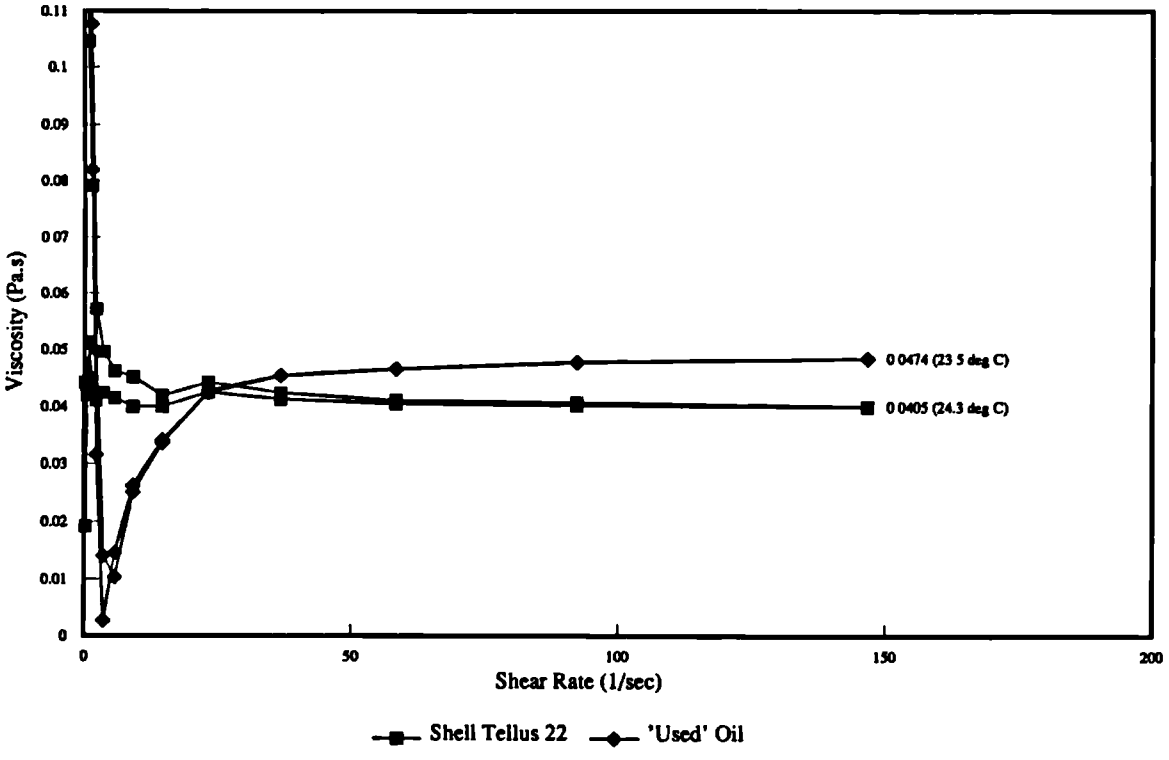


FIGURE 8.11: VISCOSITY OF SHELL TELLUS 22 OIL

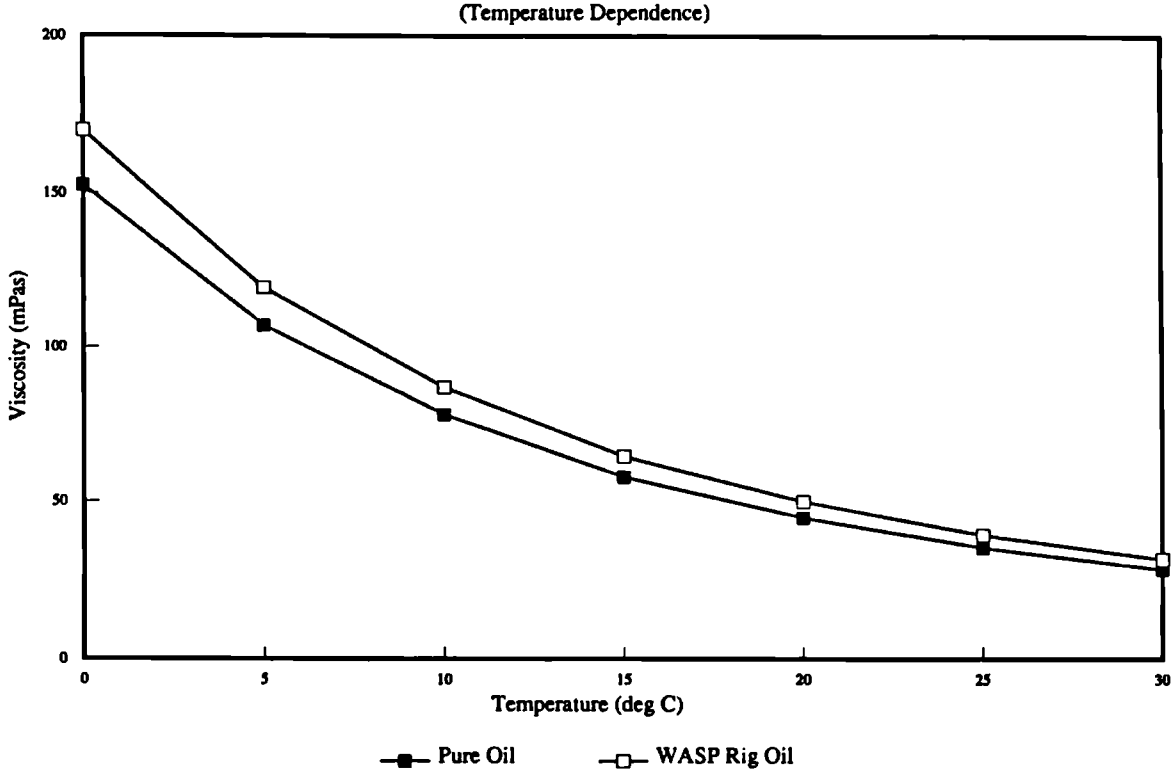


FIGURE 9.1: WASP PRESSURE GRADIENT CALCULATION

(Comparison with Beggs & Brill Correlation)

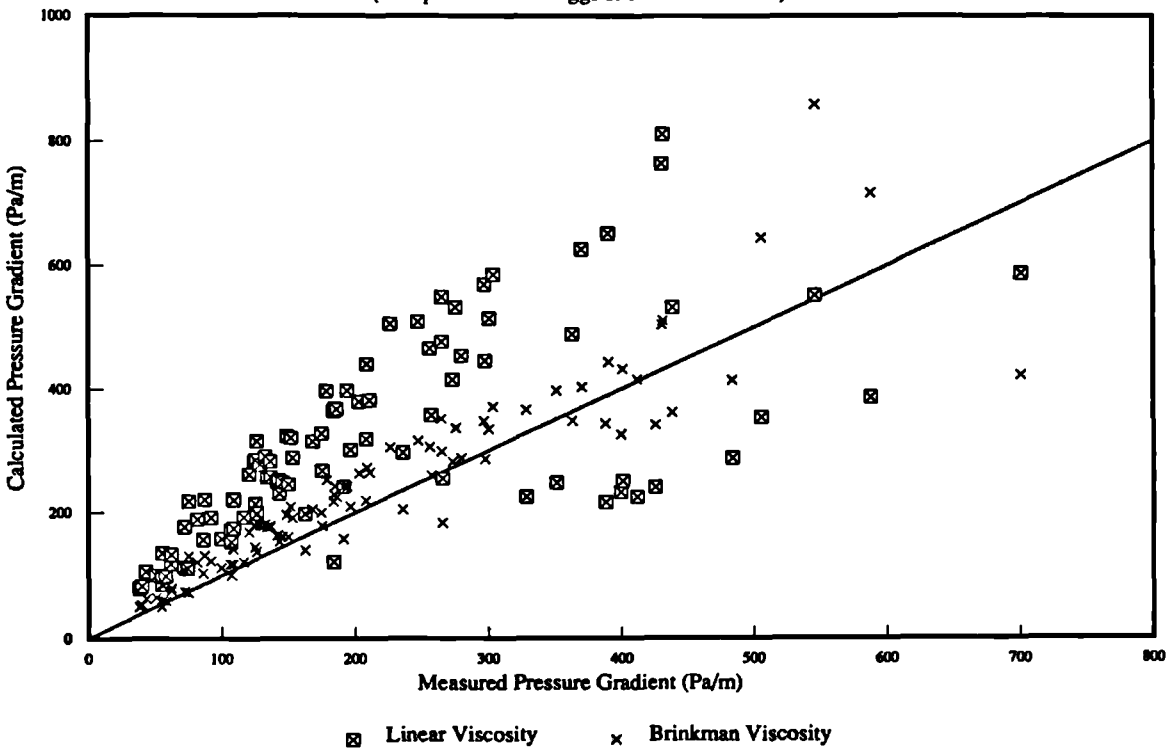


FIGURE 9.2: WASP PRESSURE GRADIENT CALCULATION

(Comparison with Beggs & Brill Correlation)

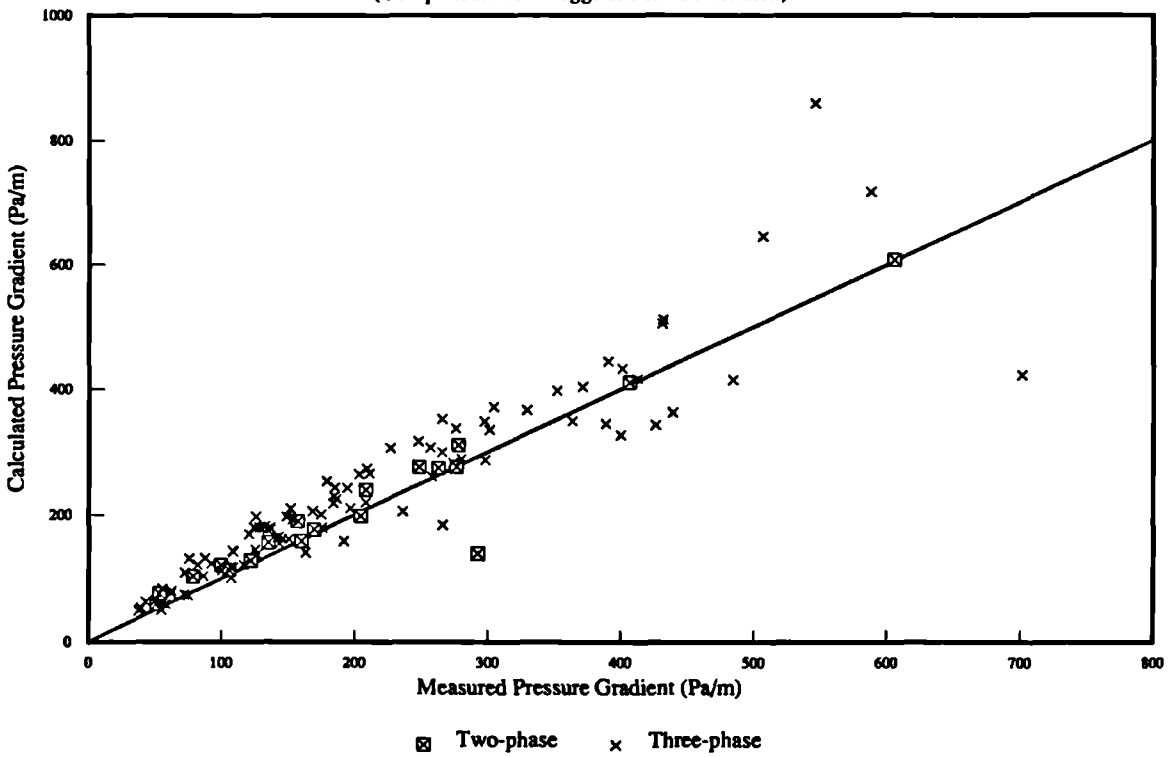


FIGURE 9.3: WASP PRESSURE GRADIENT CALCULATION

(Comparison with Beggs & Brill Correlation)

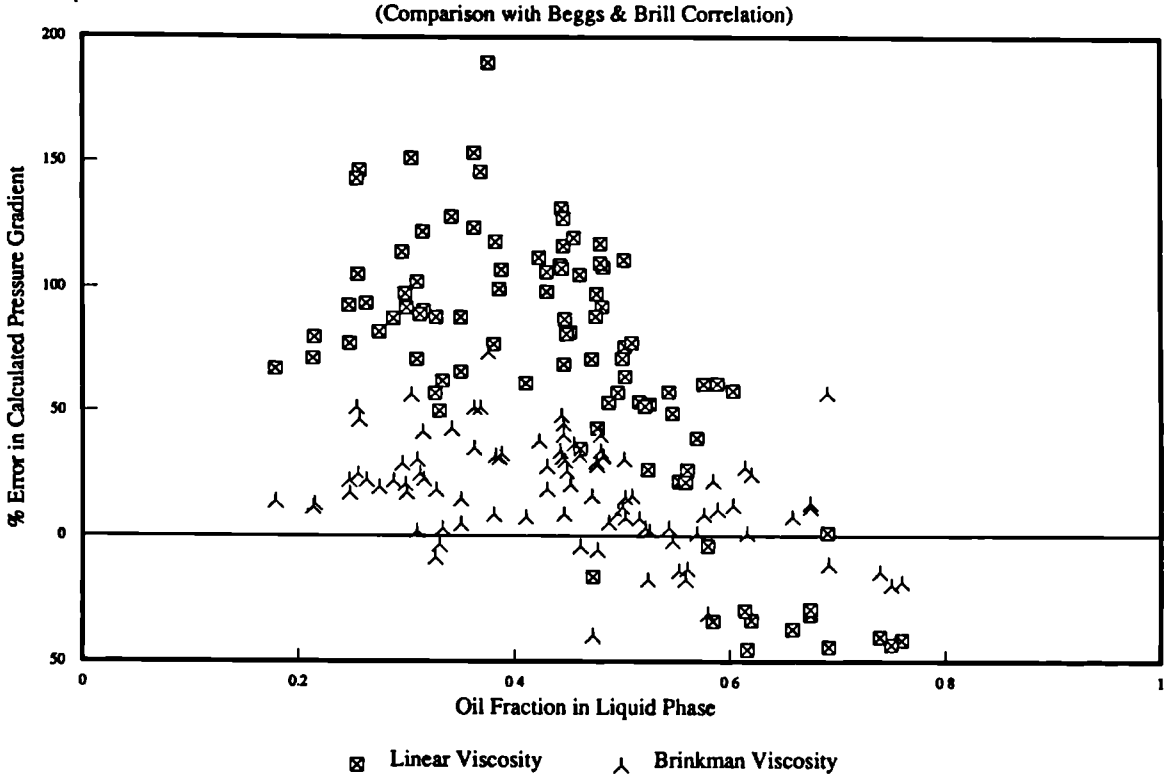


FIGURE 9.4: WASP PRESSURE GRADIENT CALCULATION

(Comparison with Beggs & Brill Correlation)

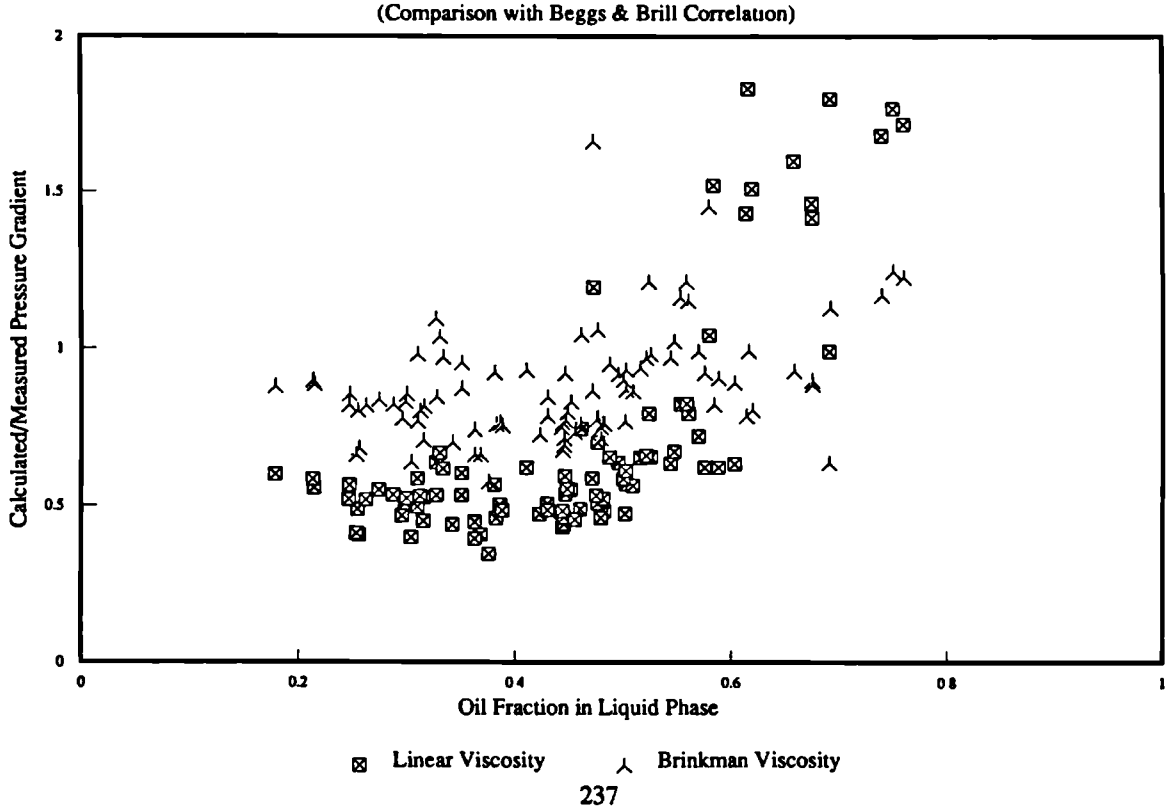


FIGURE 9.5: WASP EFFECTIVE LIQUID VISCOSITY

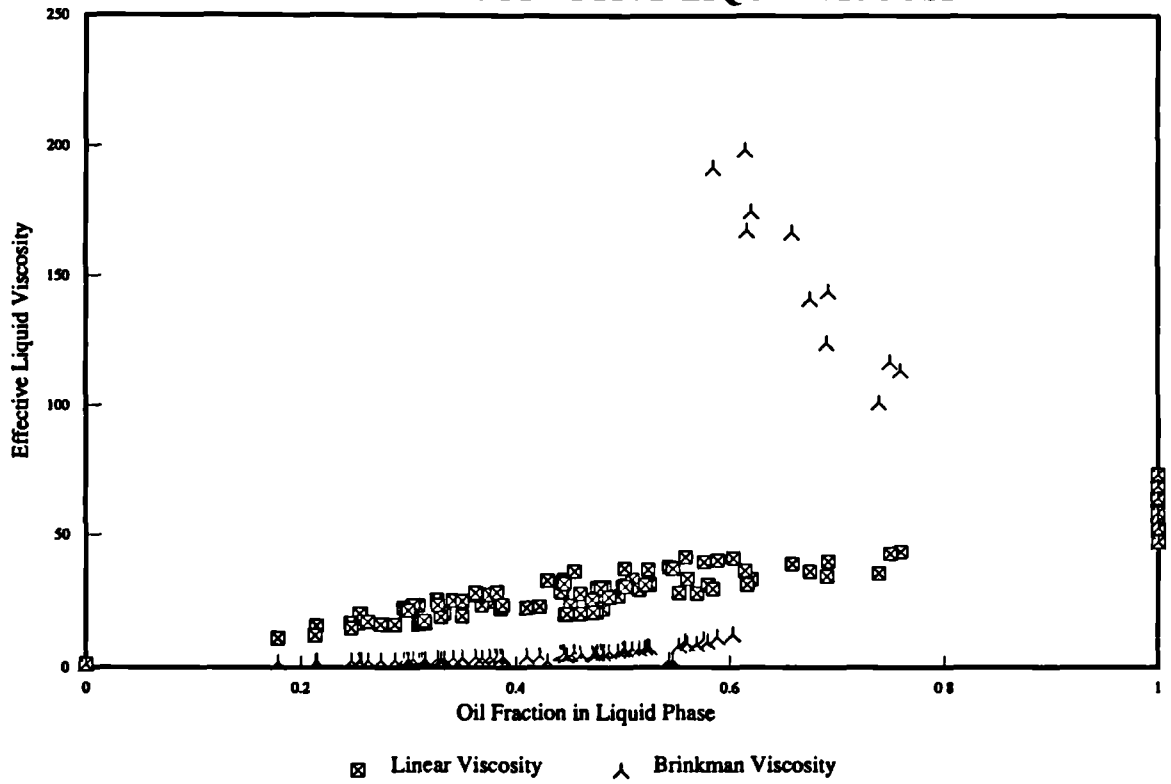


FIGURE 9.6: WASP PRESSURE GRADIENT CALCULATION

(Comparison of Correlations)

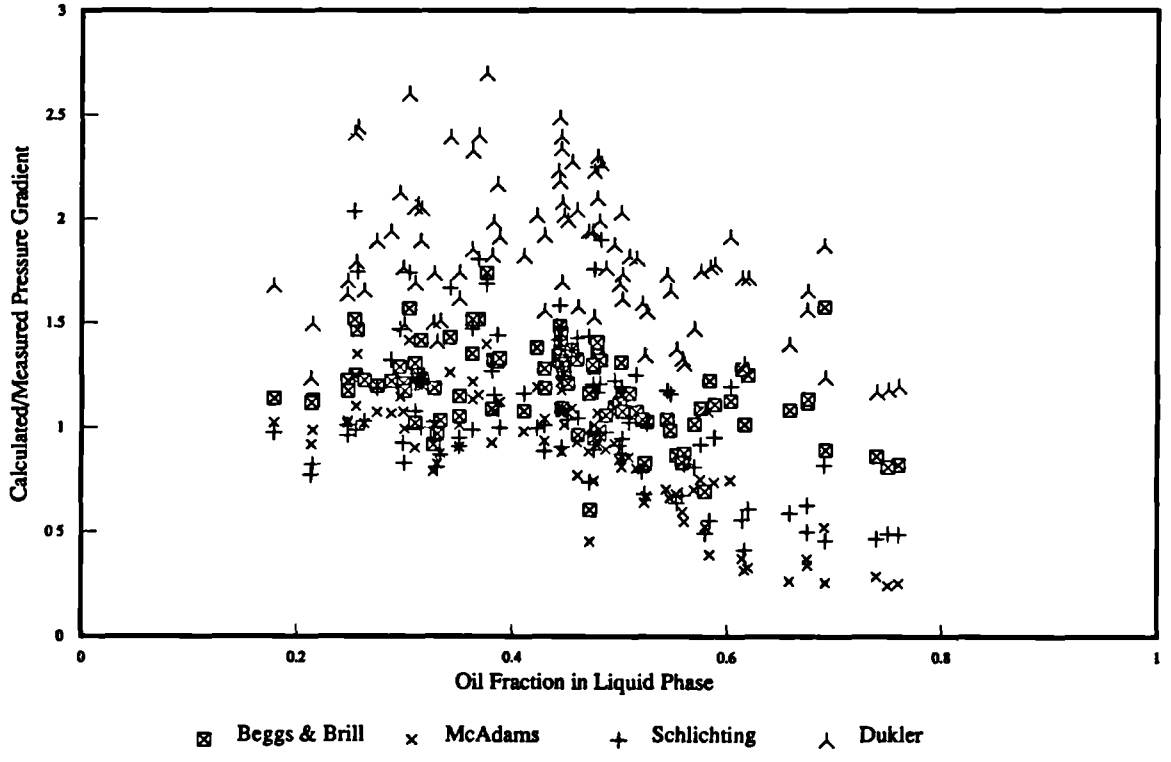


FIGURE 9.7: WASP PRESSURE GRADIENT CALCULATION

(Comparison of Correlations)

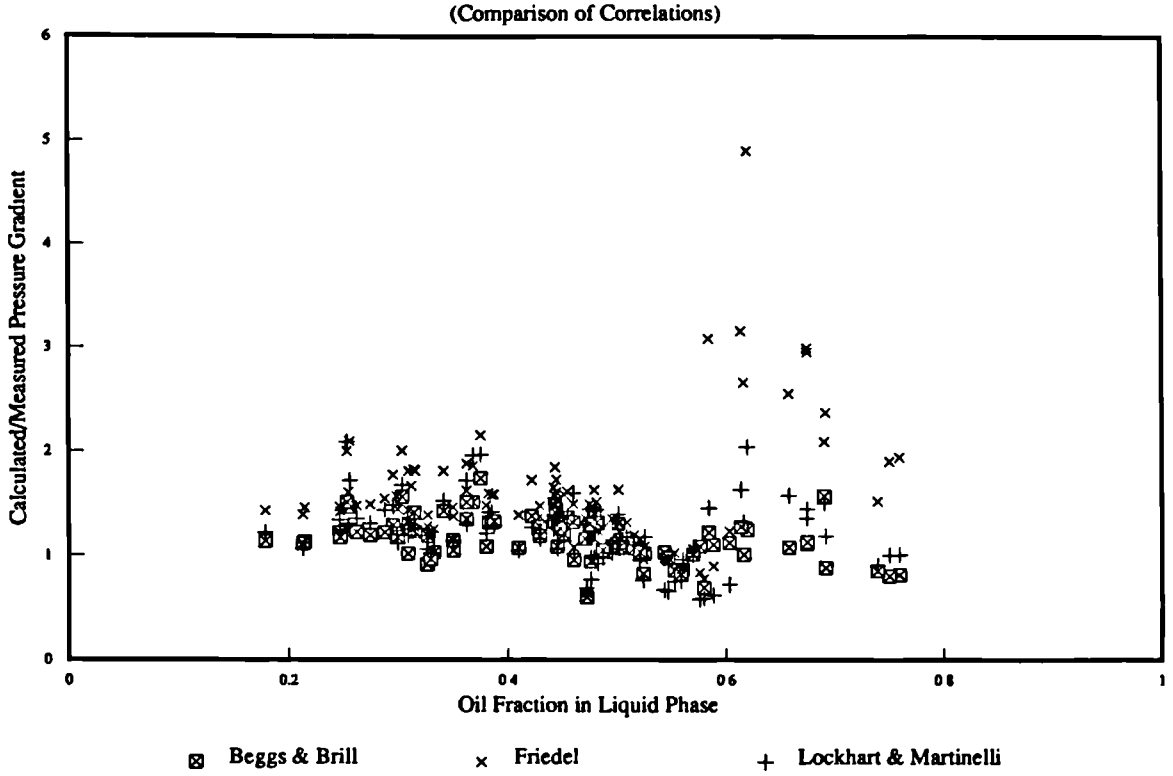


FIGURE 9.8: COMPARISON OF PRESSURE GRADIENT DATA WITH SLUG FLOW MODEL

(WASP Water-Continuous Three-Phase Flows)

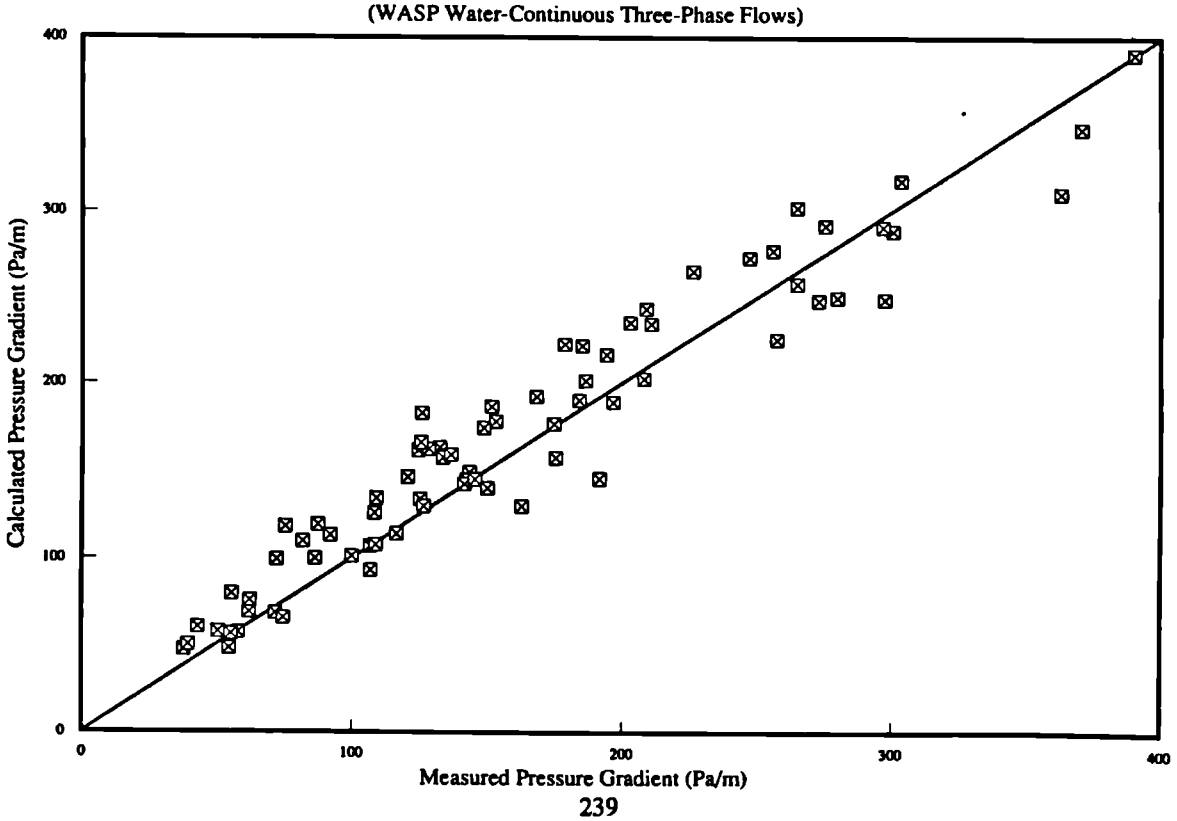


FIGURE 9.9: COMPARISON OF PRESSURE GRADIENT DATA WITH SLUG FLOW MODEL
(WASP Water-Continuous Three-Phase Flows)

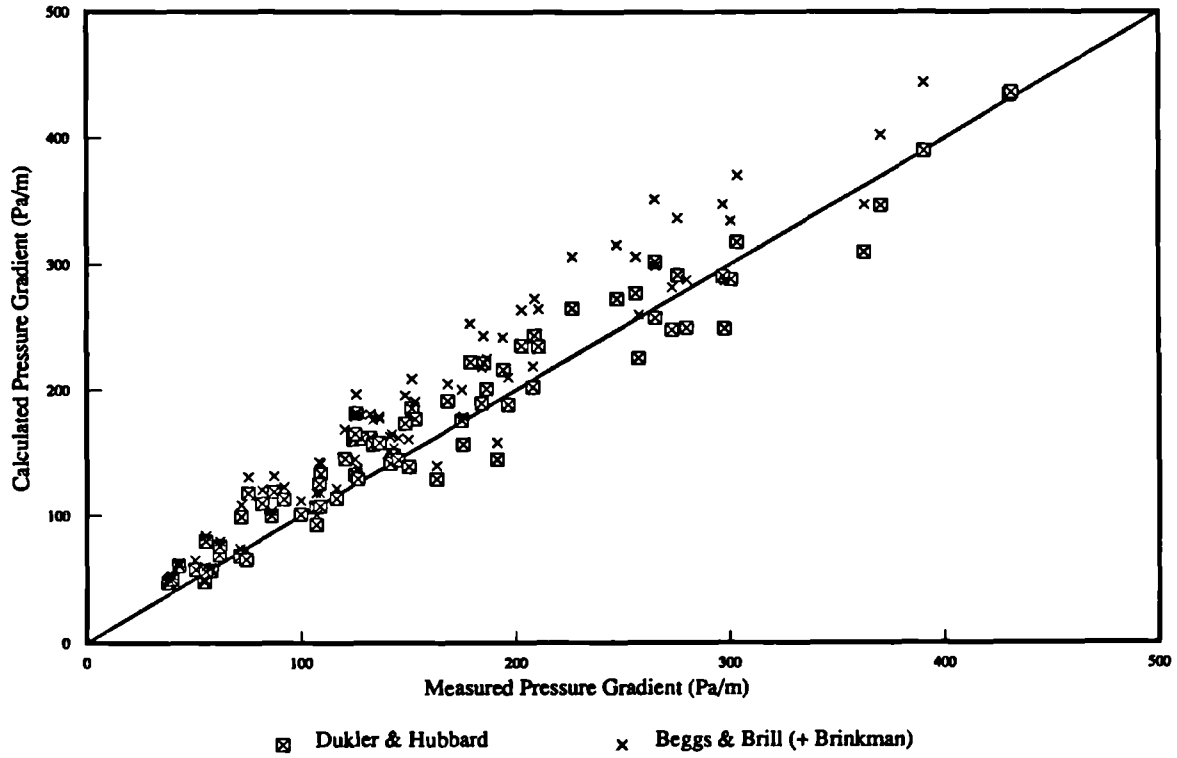


FIGURE 9.10: WASP OIL HOLDUP

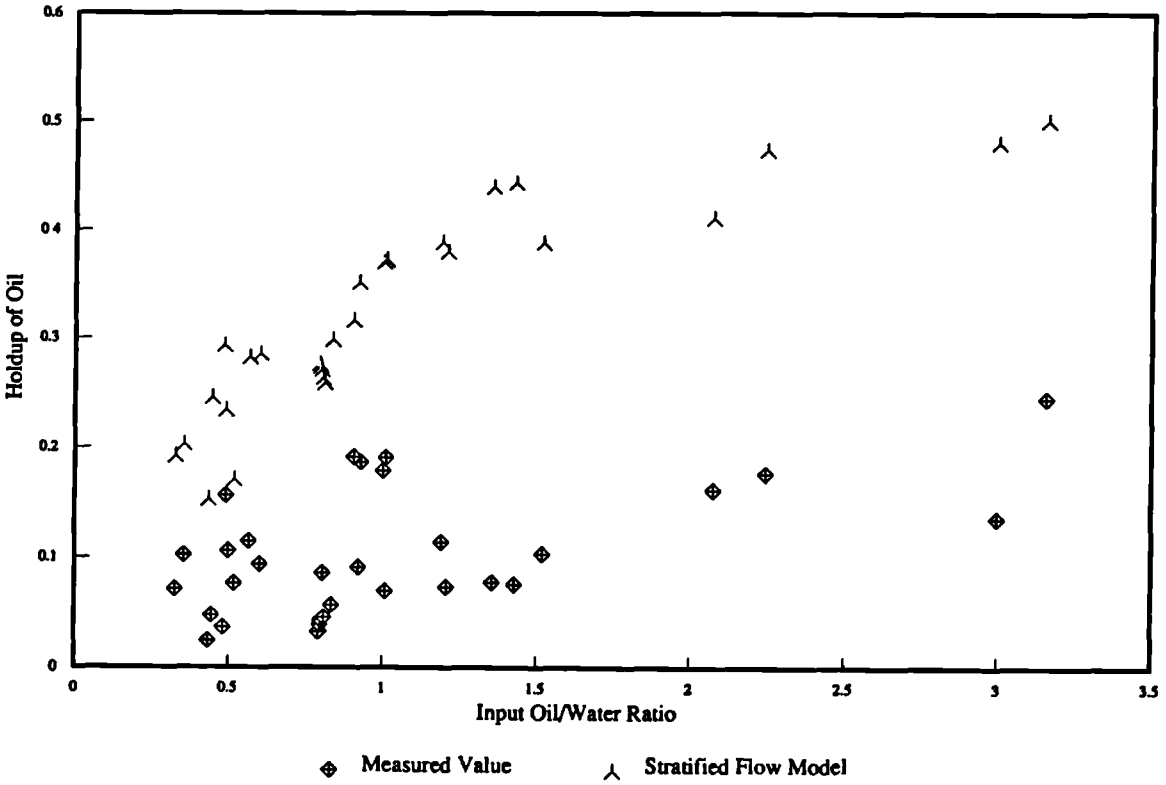


FIGURE 9.11: WASP WATER HOLDUP

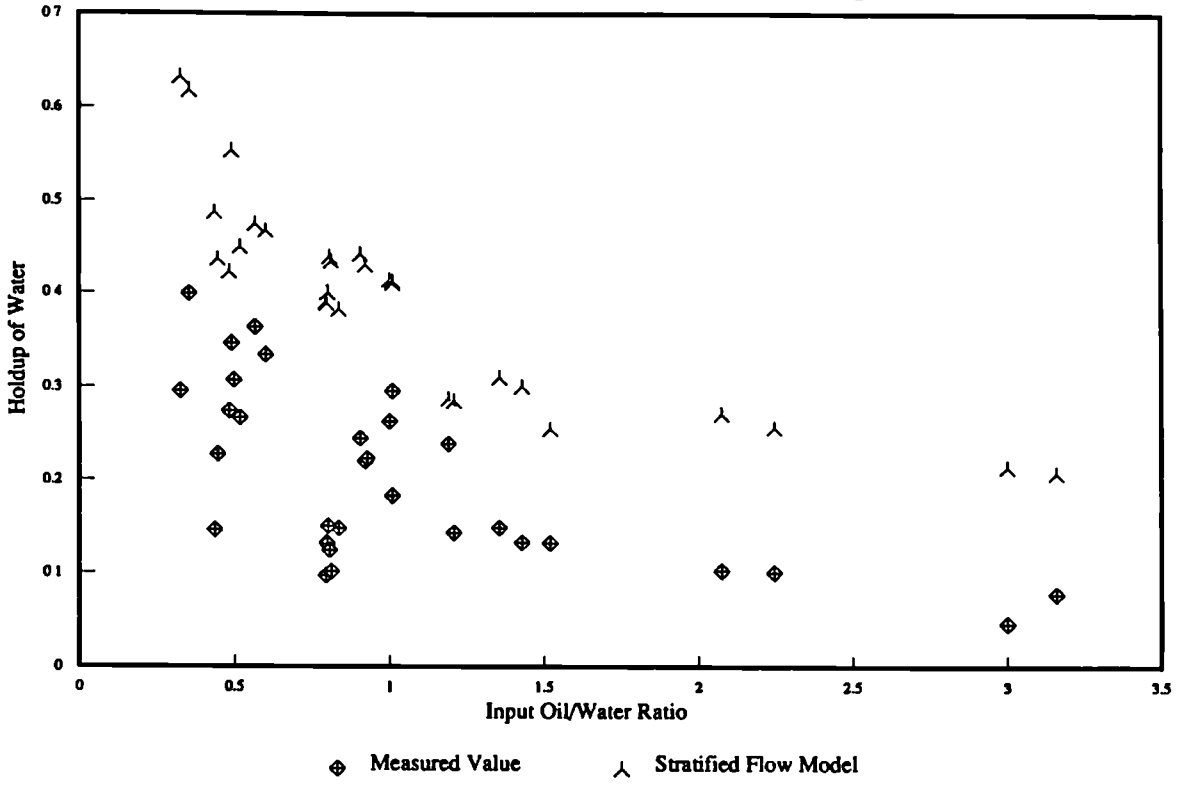


FIGURE 9.12: WASP OIL HOLDUP

(Comparison with simple slug flow models)

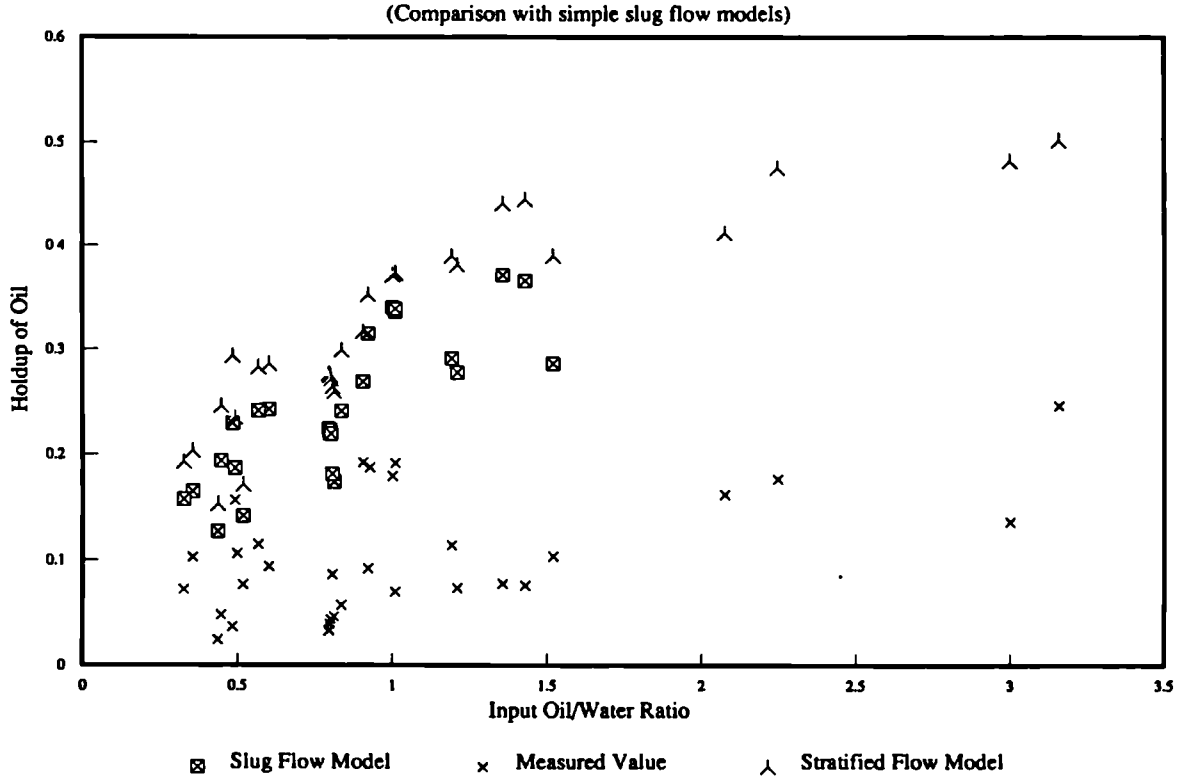


FIGURE 9.13: WASP WATER HOLDUP

(Comparison with simple slug flow models)

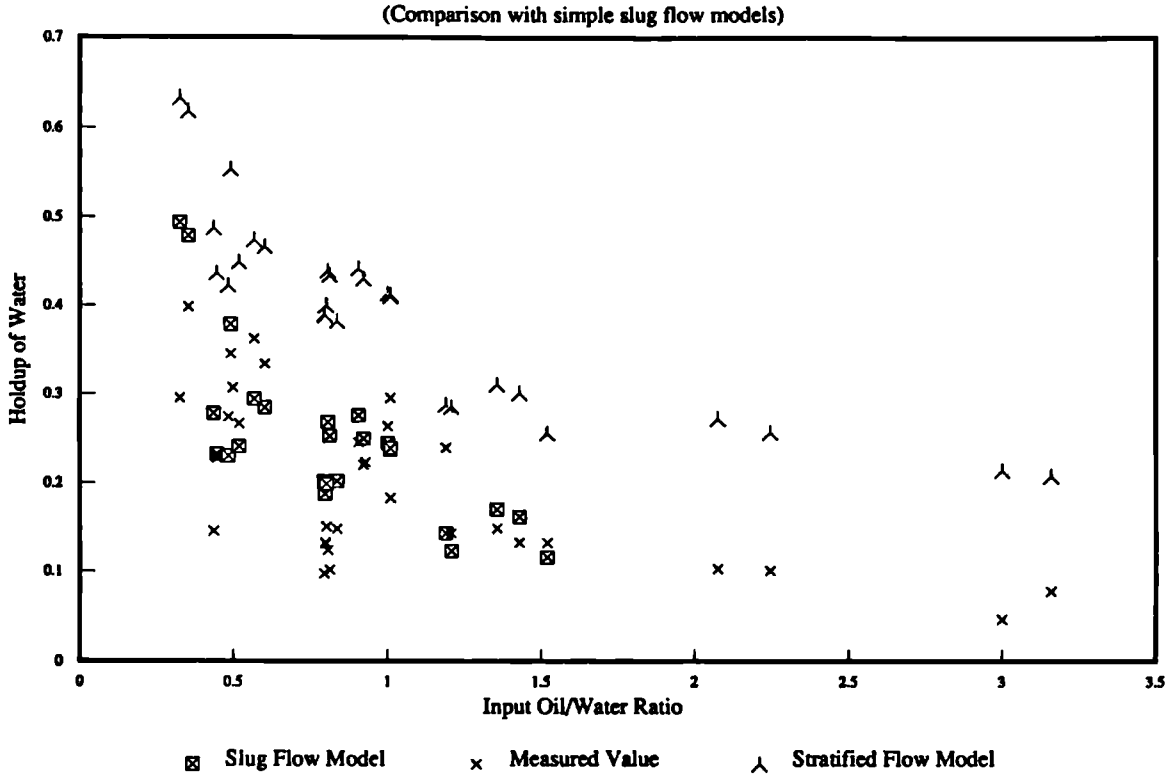


FIGURE 9.14: WASP SLUG FREQUENCY DATA

(Variation with Liquid Flowrate)

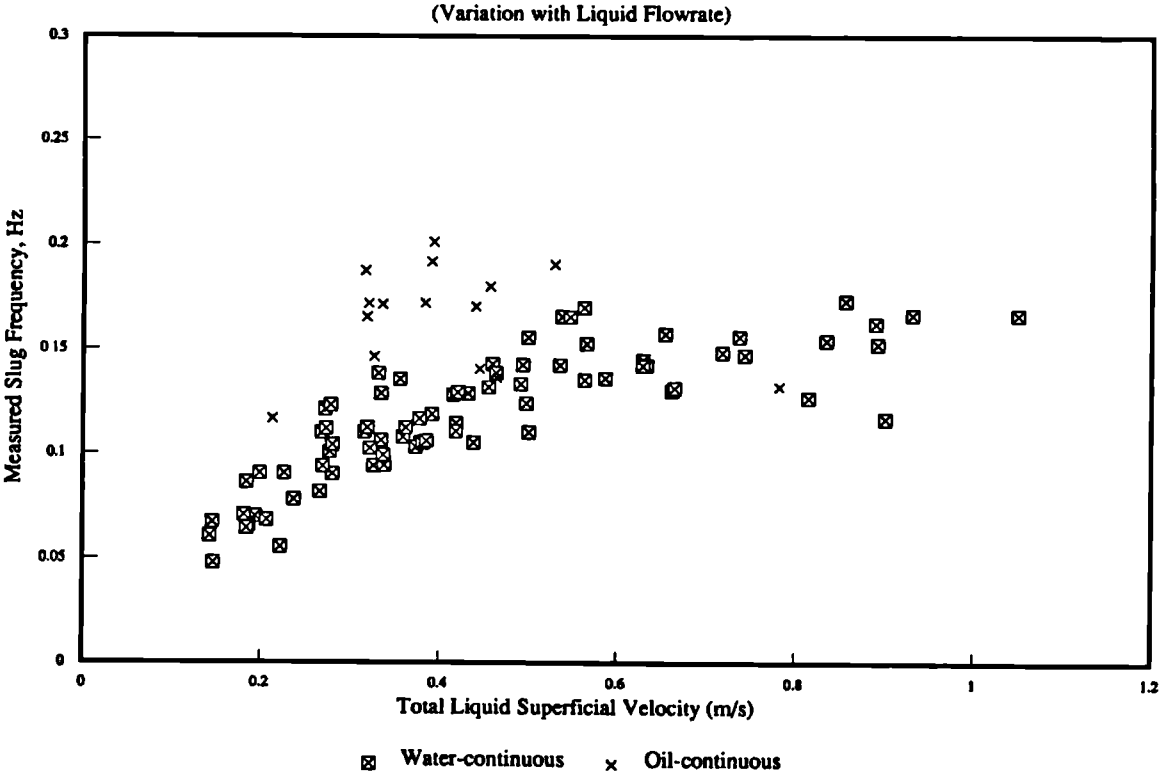


FIGURE 9.15: WASP SLUG FREQUENCY DATA

(Comparison with Correlations)

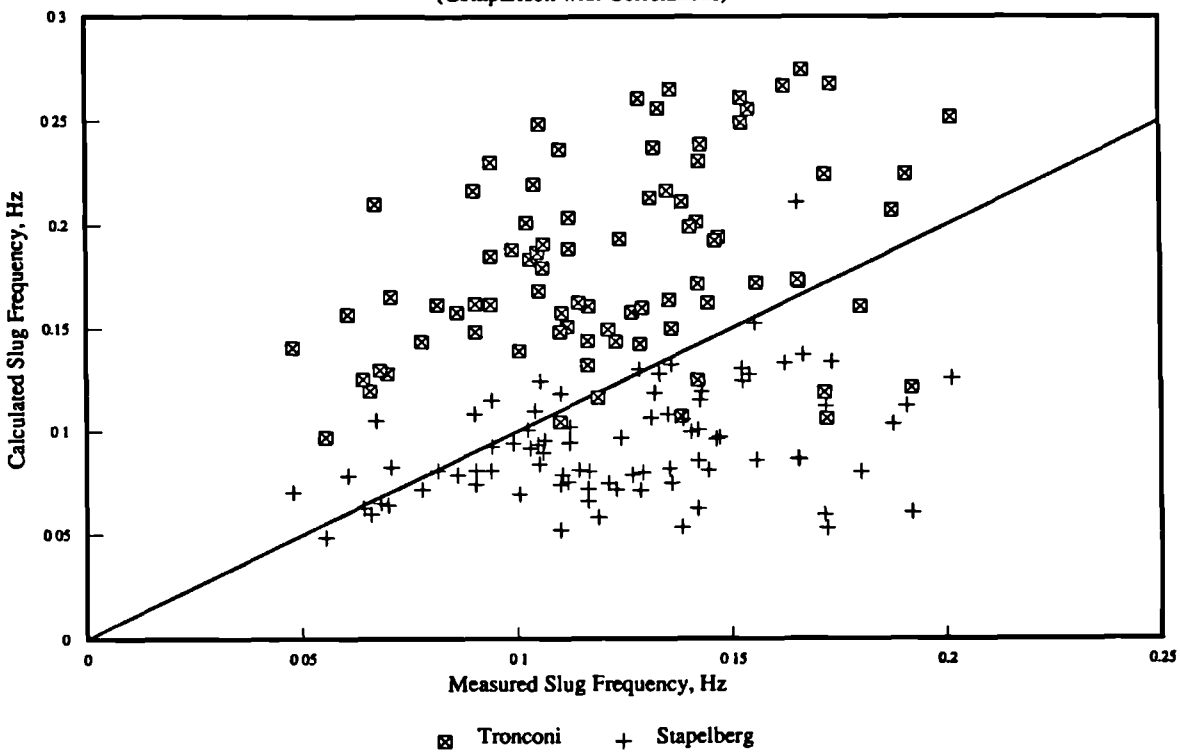


FIGURE 9.16: PREDICTION OF WATER SEPARATION

(Observations from WASP: Water-continuous flows)

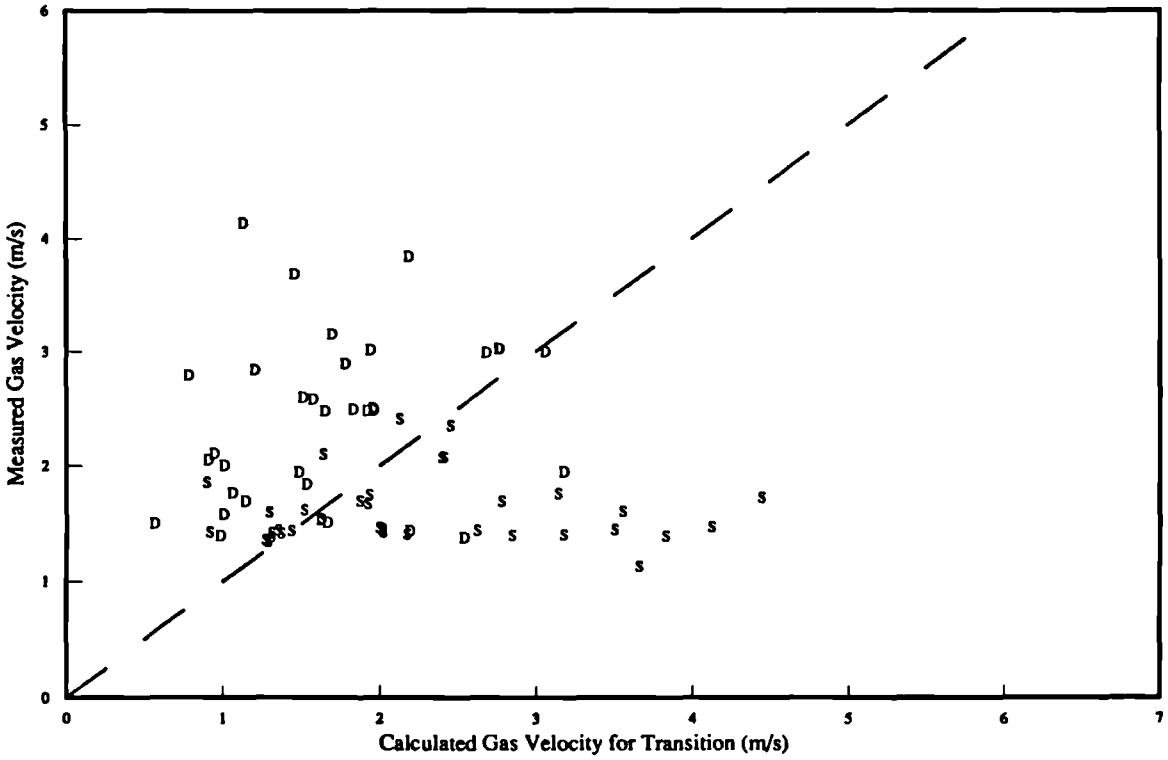


FIGURE 9.17: COMPARISON OF WASP DATA WITH TRANSITION PREDICTION
(Three-phase Water Continuous Separated Slug Flows)

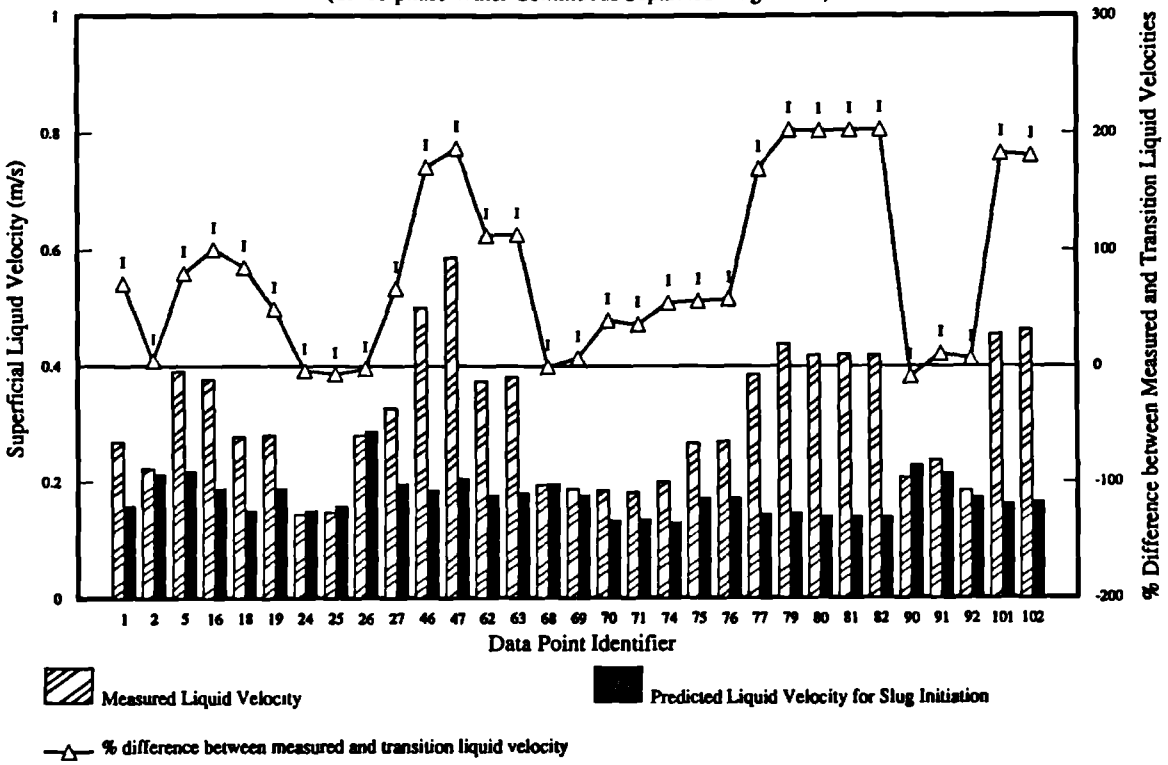
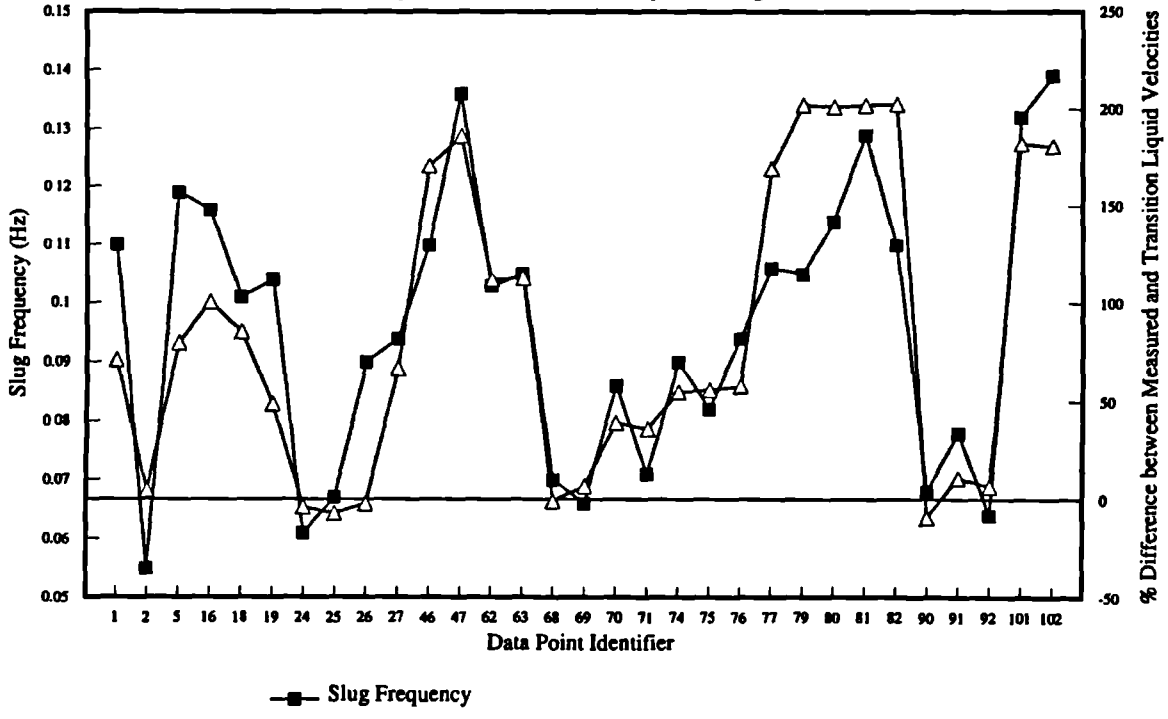


FIGURE 9.18: COMPARISON OF WASP DATA WITH TRANSITION PREDICTION
(Three-phase Water Continuous Separated Slug Flows)



Appendix A: SUMMARY OF PRESSURE GRADIENT CORRELATION EQUATIONS

A.1 Common Calculations

$$S - \pi D^2/4 \tag{A.1}$$

$$v - (V_g + V_o + V_w)/S \tag{A.2}$$

$$\rho_\ell - \phi_o \rho_o + (1 - \phi_o)\rho_w \tag{A.3}$$

$$x_g - \frac{V_g \rho_g}{V_g \rho_g + V_o \rho_o + V_w \rho_w} \tag{A.4}$$

$$\rho_h - \frac{\rho_\ell \rho_g}{x_g \rho_\ell + (1 - x_g)\rho_g} \tag{A.5}$$

$$\phi_o - \frac{V_o}{V_o + V_w} \tag{A.6}$$

A.2 McAdams-Homogeneous

$$\frac{1}{\mu_h} - \frac{x_g}{\mu_g} + \frac{(1 - x_g)}{\mu_\ell} \tag{A.7}$$

$$Re_{TP} - \rho_h v D/\mu_h \tag{A.8}$$

$$f = 0.079(Re_{TP})^{-\frac{1}{4}} \tag{A.9}$$

$$\left(\frac{dp_F}{dz}\right) - \frac{2f\rho_h v^2}{D} \tag{A.10}$$

A.3 Schlichting

$$U_g = V_g/S \tag{A.11}$$

$$U_\ell = V_\ell/S \tag{A.12}$$

$$Re_\ell = \rho_\ell U_\ell D/\mu_\ell \tag{A.13}$$

$$Re_g = \rho_g U_g D/\mu_g \tag{A.14}$$

$$f_\ell = 0.079 Re_\ell^{-\frac{1}{4}} \tag{A.15}$$

$$f_g = 0.079 Re_g^{-\frac{1}{4}} \tag{A.16}$$

$$\left(\frac{dp}{dz}\right)_\ell - \frac{2f_\ell \rho_\ell U_\ell}{D} \tag{A.17}$$

$$\left(\frac{dp}{dz}\right)_g - \frac{2f_g \rho_g U_g}{D} \tag{A.18}$$

$$X - \sqrt{\left(\frac{dp}{dz}\right)_\ell \div \left(\frac{dp}{dz}\right)_g} \tag{A.19}$$

$$\mu_r = \left(\frac{\mu_\ell}{\mu_g}\right) \times 10^{-4} \tag{A.20}$$

If $\mu_r < 10^2$

$$C_1 = 1.0; C_2 - 6.0 \tag{A.21}$$

Else

$$C_1 = \frac{1 + 0.65\mu_r^{0.8}}{(1 - \varepsilon_{wf})^{1.3}} \tag{A.22}$$

and

$$C_2 - 6 + 7.5\mu_r^{0.5} \tag{A.23}$$

$$\phi_\ell^2 = C_1 + C_2/X \tag{A.24}$$

$$\left(\frac{dp_F}{dz}\right) - \phi_\ell^2\left(\frac{dp}{dz}\right)_\ell \tag{A.25}$$

A.4 Friedel

$$\dot{m} - \frac{V_g\rho_g + V_w\rho_w + V_o\rho_o}{S} \tag{A.26}$$

$$Re_{go} - \frac{\dot{m}D}{\mu_g} \tag{A.27}$$

$$Re_{\ell o} - \frac{\dot{m}D}{\mu_\ell} \tag{A.28}$$

$$f_{go} - 0.079(Re_{go})^{-\frac{1}{4}} \tag{A.29}$$

$$f_{\ell o} - (Re_{\ell o} < 2000)?16/Re : 0.079(Re_{\ell o})^{-\frac{1}{4}} \tag{A.30}$$

$$\rho_{TP} - \left(\frac{x_g}{\rho_g} + \frac{(1-x_g)}{\rho_\ell}\right)^{-1} \tag{A.31}$$

$$We - \frac{\dot{m}^2 D}{\rho_{TP}\sigma} \tag{A.32}$$

$$Fr - \frac{\dot{m}^2}{gD\rho_{TP}} \tag{A.33}$$

$$E = (1 - x_g)^2 + x_g^2 \frac{\rho_\ell}{\rho_g} \frac{f_{go}}{f_{\ell o}} \tag{A.34}$$

$$F = x_g^{0.78}(1 - x_g)^{0.24} \tag{A.35}$$

$$H = \left(\frac{\rho_\ell}{\rho_g}\right)^{0.91} \left(\frac{\mu_g}{\mu_\ell}\right)^{0.18} \left(1 - \frac{\mu_g}{\mu_\ell}\right)^{0.7} \tag{A.36}$$

$$\left(\frac{dp}{dz}\right)_{\ell o} = \frac{2 f_{\ell o} \dot{m}^2}{D \rho_\ell} \tag{A.37}$$

$$\phi_{\ell o}^2 = E + \frac{3.24 F H}{Fr^{0.045} We^{0.035}} \tag{A.38}$$

$$\left(\frac{dp_F}{dz}\right) = \phi_{\ell o}^2 \left(\frac{dp}{dz}\right)_{\ell o} \tag{A.39}$$

A.5 Lockhart & Martinelli

$$\dot{m} = \frac{(V_g \rho_g + V_w \rho_w + V_o \rho_o)}{S} \tag{A.40}$$

$$Re_g - \frac{\dot{m} x_g D}{\mu_g} \tag{A.41}$$

$$Re_\ell = \frac{\dot{m}(1 - x_g) D}{\mu_\ell} \tag{A.42}$$

$$f_g = (Re_g < 2000)?16/Re_g : 0.079(Re_g)^{-\frac{1}{4}} \tag{A.43}$$

$$f_\ell = (Re_\ell < 2000)?16/Re_\ell : 0.079(Re_\ell)^{-\frac{1}{4}} \tag{A.44}$$

$$\left(\frac{dp}{dz}\right)_g - \frac{2 f_g \dot{m}^2 x_g^2}{D \rho_g} \tag{A.45}$$

$$\left(\frac{dp}{dz}\right)_{\ell} - \frac{2f_{\ell}\dot{m}^2(1-x_g^2)}{D\rho_{\ell}} \tag{A.46}$$

$$X^2 - \left(\frac{dp}{dz}\right)_{\ell} \div \left(\frac{dp}{dz}\right)_{g} \tag{A.47}$$

$$\phi_{\ell}^2 - 1 + \frac{C}{X} + \frac{1}{X^2} \tag{A.48}$$

where C depends on whether the gas and liquid are laminar or turbulent:

Gas	Liquid	C
Laminar	Laminar	5.0
Laminar	Turbulent	10.0
Turbulent	Laminar	12.0
Turbulent	Turbulent	20.0

$$\left(\frac{dp_F}{dz}\right) - \phi_{\ell}^2\left(\frac{dp}{dz}\right)_{\ell} \tag{A.49}$$

A.6 Beggs & Brill

$$U_{\ell} - \frac{(V_o + V_w)}{S} \tag{A.50}$$

$$U_g - \frac{V_g}{S} \tag{A.51}$$

$$v_m - U_{\ell} + U_g \tag{A.52}$$

$$\lambda_{\ell} - \frac{U_{\ell}}{v_m} \tag{A.53}$$

$$F_r - \frac{v_m^2}{gD} \tag{A.54}$$

$$L_1 = 316\lambda_\ell^{0.302} \tag{A.55}$$

$$L_2 = 0.0009252\lambda_\ell^{-2.4684} \tag{A.56}$$

$$L_3 = 0.10\lambda_\ell^{-1.4516} \tag{A.57}$$

$$L_4 = 0.5\lambda_\ell^{-6.738} \tag{A.58}$$

The position on the flow map is determined according to the following relations:

Segregated	$\lambda_\ell < 0.01$ and $Fn < L_1$
	or $\lambda_\ell \geq 0.01$ and $Fn < L_2$
Transition	$\lambda_\ell \geq 0.01$ and $L_2 < Fn \leq L_3$
Intermittent	$0.01 < \lambda_\ell < 0.4$ and $L_3 < Fn \leq L_1$
	or $\lambda_\ell > 0.4$ and $L_3 < Fn \leq L_4$
Distributed	$\lambda_\ell < 0.4$ and $Fn \geq L_1$
	or $\lambda_\ell \geq 0.4$ and $Fn > L_4$

The holdup is calculated using the formula:

$$H_\ell - \frac{a\lambda_\ell^b}{Fn^c} \tag{A.59}$$

where the values of a, b and c depend on the flow pattern as follows:

Flow Pattern	a	b	c
Segregated	0.980	0.4846	0.0868
Intermittent	0.845	0.5351	0.0173
Distributed	1.065	0.5824	0.0609

For transition flow

$$H_\ell = AH_\ell(\text{Segregated}) + BH_\ell(\text{Intermittent}) \tag{A.60}$$

where

$$A = \frac{L_3 - Fn}{L_3 - L_2} \tag{A.61}$$

$$B - 1 - A \tag{A.62}$$

$$\mu_m - \lambda_\ell \mu_\ell + (1 - \lambda_\ell)\mu_g \tag{A.63}$$

$$\rho_m - \lambda_\ell \rho_\ell + (1 - \lambda_\ell)\rho_g \tag{A.64}$$

$$Re - \frac{\rho_m v_m D}{\mu_m} \tag{A.65}$$

$$f - \left[2 \log \left[\frac{Re}{4.5223 \log Re - 3.8215}\right]\right]^{-2} \tag{A.66}$$

The two-phase friction factor multiplier, f_{TP}/f is calculated by:

$$y - \frac{\lambda_\ell}{II_\ell^2} \tag{A.67}$$

For $1 < y < 1.2$

$$S - \ln (2.2y - 1.2) \tag{A.68}$$

else

$$S - \frac{\ln y}{\left(-0.0523 + 3.182 \ln y - 0.8725(\ln y)^2 + 0.01853(\ln y)^4\right)} \tag{A.69}$$

$$f_{TP}/f - \exp (S) \tag{A.70}$$

$$\left(\frac{dp_F}{dz}\right) - \frac{f \rho_m v_m^2}{2D}\left(\frac{f_{TP}}{f}\right) \tag{A.71}$$

A.7 Dukler

$$U_\ell = \frac{(V_o + V_w)}{S} \tag{A.72}$$

$$U_g - \frac{V_g}{S} \tag{A.73}$$

$$v_m - U_\ell + U_g \tag{A.74}$$

$$\lambda_\ell = \frac{U_\ell}{v_m} \tag{A.75}$$

$$\mu_m = \lambda_\ell \mu_\ell + (1 - \lambda_\ell)\mu_g \tag{A.76}$$

$$\rho_m - \frac{\rho_\ell \lambda_\ell^2}{H_\ell} + \frac{\rho_g (1 - \lambda_\ell)^2}{(1 - H_\ell)} \tag{A.77}$$

$$Re_{TP} - \frac{v_m D \rho_m}{\mu_m} \tag{A.78}$$

$$f = 0.0056 + 0.5(Re_{TP})^{-0.32} \tag{A.79}$$

$$\frac{f_{TP}}{f} = 1.0 + \frac{-\ln \lambda_\ell}{1.281 - 0.478(-\ln \lambda_\ell) + 0.444(-\ln \lambda_\ell)^2 - 0.094(-\ln \lambda_\ell)^3 + 0.00843(-\ln \lambda_\ell)^4} \tag{A.80}$$

$$\left(\frac{dp_F}{dz}\right) = \frac{f \rho_m v_m^2}{2D}\left(\frac{f_{TP}}{f}\right) \tag{A.81}$$

A.8 Theissing

$$n_A - \frac{\ln\left[\left(\frac{dp}{dz}\right)_A / \left(\frac{dp}{dz}\right)_{At}\right]}{\ln\left[\dot{m}_A/\dot{m}_t\right]} \tag{A.82}$$

$$n_B - \frac{\ln\left[\left(\frac{dp}{dz}\right)_B / \left(\frac{dp}{dz}\right)_{Bt}\right]}{\ln\left[\dot{m}_B/\dot{m}_t\right]} \tag{A.83}$$

$$n - \frac{n_A + \left[\left(\frac{dp}{dz}\right)_B / \left(\frac{dp}{dz}\right)_A\right]^{0.1} n_2}{1 + \left[\left(\frac{dp}{dz}\right)_B / \left(\frac{dp}{dz}\right)_A\right]^{0.1}} \tag{A.84}$$

$$\varepsilon - 3 - 2\left(\frac{2\sqrt{\rho_A/\rho_B}}{1 + \rho_A/\rho_B}\right)^{\frac{0.7}{n}} \tag{A.85}$$

$$\left(\frac{dp_f}{dz}\right)_{2ph} - \left[\left(\frac{dp}{dz}\right)_{At}^{\frac{1}{n\varepsilon}} \left(\frac{\dot{M}_1}{\dot{M}_t}\right)^{\frac{1}{\varepsilon}} + \left(\frac{dp}{dz}\right)_{Bt}^{\frac{1}{n\varepsilon}} \left(\frac{\dot{M}_B}{\dot{M}_t}\right)^{\frac{1}{\varepsilon}}\right]^{\varepsilon n} \tag{A.86}$$

where

$$\left(\frac{dp}{dz}\right)_A \tag{A.87}$$

is the pressure gradient for phase A flowing alone in the pipe,

$$\left(\frac{dp}{dz}\right)_{At} \tag{A.88}$$

is the pressure gradient for phase A flowing alone in the pipe, but with the total mass flux; $\dot{M}$ is the mass flowrate.

THIS IS A BLANK PAGE

Appendix B: FINITE DIFFERENCE SOLUTION FOR STRATIFIED TWO-PHASE FLOW USING BIPOLAR COORDINATES

B.1 Finite difference equations for the upper phase

The upper phase is spanned by a grid of I+1 points in the η-direction and K+1 points in the ξ-direction, ie:

$$\xi_0 - \pi \twoheadrightarrow \xi_K - \gamma \tag{B.1}$$

and

$$\eta_0 - 0 \twoheadrightarrow \eta_I - \infty \ (\simeq 5) \tag{B.2}$$

The momentum equation for the upper phase:

$$\frac{\partial^2 u_B}{\partial \xi^2} + \frac{\partial^2 u_B}{\partial \eta^2} - \frac{1}{\mu_{B,eff}} \left(\frac{dp}{dz}\right) \frac{c^2}{(\cosh \eta - \cos \xi)^2} \tag{B.3}$$

can be expressed in finite difference form, for a variable grid spacing $\Delta\xi_k$ and $\Delta\eta_i$:

$$\frac{(v_{i,k+1} - v_{i,k})\Delta\xi_k - (v_{i,k} - v_{i,k-1})\Delta\xi_{k+1}}{\xi_d/2} + \frac{(v_{i+1,k} - v_{i,k})\Delta\eta_i - (v_{i,k} - v_{i-1,k})\Delta\eta_{i+1}}{\eta_d/2}$$

$$- \left(\frac{1}{\mu_{B,eff}}\right)\left(\frac{dp}{dz}\right) \frac{c^2}{(\cosh \eta_i - \cos \xi_k)^2} \tag{B.4}$$

where

$$\eta_d - \Delta\eta_i \Delta\eta_{i+1}(\Delta\eta_i + \Delta\eta_{i+1}) \tag{B.5}$$

and

$$\xi_d - \Delta\xi_k \Delta\xi_{k+1}(\Delta\xi_k + \Delta\xi_{k+1}) \tag{B.6}$$

Equation (B.4) can be rearranged to give:

$$v_{i,k} - Q_1 v_{i,k-1} + Q_2 v_{i+1,k} + Q_3 v_{i,k+1} + Q_4 v_{i-1,k} - Q_5 \tag{B.7}$$

where

$$v_{i,k} - u_B(\xi_k, \eta_i) \tag{B.8}$$

$$Q_1 - \frac{\Delta\xi_{k+1}\eta_d}{Q_d} \tag{B.9}$$

$$Q_2 = \frac{\Delta\eta_i \xi_d}{Q_d} \tag{B.10}$$

$$Q_3 - \frac{\Delta\xi_k \eta_d}{Q_d} \tag{B.11}$$

$$Q_4 = \frac{\Delta\eta_{i+1} \xi_d}{Q_d} \tag{B.12}$$

$$Q_5 = \left(\frac{dp}{dz}\right) \frac{\xi_d \eta_d}{2Q_d \mu_{B,eff}} \frac{c^2}{(\cosh \eta_i - \cos \xi_k)^2} \tag{B.13}$$

and

$$Q_d = \eta_d(\Delta\xi_k + \Delta\xi_{k+1}) + \xi_d(\Delta\eta_i + \Delta\eta_{i+1}) \tag{B.14}$$

B.2 Listing of the source code for the bipolar solution

```
/* LIQLIQ.c

2-phase steady-state gas-liquid or liquid liquid stratified flow numerical
solution

Written by A.R.W.Hall, Process Studies Department, APS; April 1991


Calculates the heights of the lower fluid layer and the pressure gradient
in a stratified flow of oil and  water or of liquid and gas. The superficial
velocities of the two phases plus physical properties are specified. Solution
has an inner iteration on the velocity profiles and an outer iteration  n t tal
flowrates to give lower fluid height and pressure gradient. Velocity fields are
solved using bipolar grids in both fluids. Grids are set up so that boundary
points are coincident between phases.

This file contains main(), routines to set up the grids and the IO routines.
It must be linked with LIQLIQ_FD.c and the C maths library.

Currently set up to process a file of input superficial velocity data for a
number of data points. Physical properties and pipe diameter fixed in
input2().

Note that "alpha" is the amount by which the interface is deviated from its
normal position (= pi) in order to simulate the effect of interface curvature.
Positive alpha gives an interface which is higher at the pipe axis than at the
walls. Alpha normally set to zero.

*/

# include <stdio.h>
# include "math.h"
# define I 20 /* no of eta-grid points *
# define J 20 /* no of liquid phase xi-grid p ints */
# define K 20 /* no of gas phase xi-grid points */
# define XICONST 2.5
# define MAXC 80
struct flow_variables{
 double D;
 double uls, ugs;
 double mul, mug;
 double densl, densg;
```

```
};
d uble c, gam;
double sqrt(), pow(), ac s();
d uble fabs(), exp();
d uble pdrop, hl;
double Tıg, Tıl, Twl, Twg;
struct fl w_varıables ıp;
double u[I+1  J+1], v I+1  K+1 ;
double xıL[J+1], xıG K+1], eta[I+1 ;
FILE *fle, *fın;
extern FILE *fopen();
double alpha;


maın()
{
 ınt ı, ȷ, k, count, mm;
 extern v ıd ınıtıal guess();
 extern v ıd fd();
 double hlold, pdrop old;

 hlold = 0.0;
 pdrop_old =  . ;
 alpha    . ;

 ıf(!(fın   f pen("ındata.a  ","r")))
  exıt(1);

 whıle(ınput2()){
  mu eff ınıt( ;
  ınıtıal guess();
  fprıntf(fle," n n%s t%6.4f","Pıpe d_ameter",ıp.D ;
  fprıntf(fle," n%s\t%6.3f","Water superfı ıal vel cıty",ıp.uls);
  fprıntf(fle," n%s t%6.3f","Gas superf cıal vel  ıty",ıp.ugs);
  fprıntf(fle,"\n%s\t%6.3e","Water vısc sıt ",ıp.mul);
  fprıntf(fle," n%s t%6.3e","Ga  vıs os ty",ıp.mug ;
  fprıntf(f e," n%s\t%6.1f","Water dens ty", p.dens );
  fprıntf(fle," n%s\t%6.3f","Ga  densıty", p.densg ;
  fprıntf(fle,"\n%s\t%d %d %d","I J K",I,J,K);
   fprıntf(fle,"\n\n%s n%s\t%f t%s t%f","Inıtıal Guesses","hl",hl,"Pdr p",pdr p);
  hl *  ıp.D;

 /* Inıtıalı e Vel cıty Fıeld *

  for (ı    ; ı <  I; ı++ {
   f r (     ;   <  J;  ++)
    u ı   ]   2.0 * ıp.uls;
   f r (k =  ; k <= K; k++)
    v ı  k]   2.  * ıp.ugs;
  }
  mm    ;
  whıle (((fabs((hl hl ld) hl) > 5. e 4)    (fabs  pdr p pdr p   d) pdr p)
 > 5. e 4)) && (mm < 2  )){

   c   (ıp.D   2.0) * sqrt(1.    p w((2.0*hl ıp.D   1. ),2.   ;
   gam   ac s(1.    2. *hl ıp.D);

   set grıd xıL();
   set grıd xıG();
   set grıd eta();
   fd();
   hlold = hl;
   pdrop  ld   pdrop;
   check lıquıd();
   check gas );
   shear stresses();
   ++mm;
  }
  wrıte res();
  fpr ntf(fle,"\n\n%s\t%8.4f\t%s t%8.4f","LIQ ID HE GHT",(hl  p.D),
"PRESSURE DR P",pdr p ;
  fclose(fle);
 }
 fclose(fın);
 exıt(1);
}
```

```
set_grid_xiL()
{

/* XI GRID. This is set up to be fine at the interface and the wall */
/* and coarse in the centre. The constants have been adjusted s  that */
/* xiL[J] - xiL[0] = gam, and the grid is symmetrical about j = J/2. */

 int j;
 double B = XICONST;
 double A = (gam/4.973) * pow((B/2.5),-0.8709);

 xiL[0] = M_PI;
 xiL[J] = M_PI;

 while ((fabs((xiL[J]-xiL[0])-(gam-alpha)) > 1. e-4)){
  for (j = 0; j < J; j++)
   xiL[j+1] = xiL[j] + A * exp(-fabs((j-(J/2 1)) B));
  A *= (gam-alpha)/(xiL[J] - xiL[0]);
 }
}


set_grid_xiG()
{

/* XI GRID. This is set up to be fine at the interface and the wall */
/* and coarse in the centre. The constants have been adjusted s  that */
/* xiG[K  - xiG[0] = (pi-gam), and the grid is symmetrical about k   K/2 */

 int k;
 double B = XICONST;
 double A = (gam/4.973) * pow((B/2.5),-0.8709);

 xiG[0] = M PI;
 xiG K] = M_PI;

 while ((fabs((xiG[0]-xiG K]) (M_PI + alpha   gam)) > 1.0e 4)){
  for (k = 0; k < K; k++)
   xiG[k+1] = xiG[k] - A * exp(-fabs((k-(K/2 1))/B));
  A *= (M_PI + alpha   gam)/(xiG 0] - xiG K]);
 }
}


set_grid eta()
{

/* ETA GRID. This is set up so that deta[i] increases with i (as the *
/* wall-interface junction is appr ached eta -> infinity). This is  *
/* achieved by relating the step length deta i+1  to the previ us      */
/* value of eta[i . This produces a nice even line spac ng if the  */
/* grid is drawn in x-y space      */

 int i;
 eta[0] = 0.0;
 for (i = 0; i < I; i++)
  eta[i+1] = eta[i] + eta[i]/10.0 + 0.10;
}



write_res()
{
 int i, j, k;
 printf("\n\n%s","Writing results to file");

 fprintf(fle,"\n\n%s","SHEAR STRESSES");
 fprintf(fle,"\t\t%10s\t%10s\n\n","Wall","Interface");
 fprintf(fle,"\t%10s\t%10.4f\t%10.4f\n","Gas",Twg,Tig);
 fprintf(fle,"\t%10s\t%10.4f\t%10.4f\n","Liquid",Twl,Til);

 fprintf(fle,"\n\n\t\t");
/* for (j = 0; j <= J; j++)
  fprintf(fle,"%-8.4f",xiL[j]);
 for (i = 0; i <= I; i++){
  fprintf(fle,"\n%-8.4f\t",eta i]);
```

```
  for (    0;    <= J;   ++)
    fprintf(fle,"% 8.4f",u ı [j );
 }
 fprıntf(fle,"\n\n\t t");
 f r(k = 0; k <  K; k++)
  fprıntf(fle,"%-8.4f",xıG[k );
 for (ı = 0; ı <  I; ı++){
  fprıntf(fle,"\n% 8.4f\t",eta[ı );
  f r (k     ; k <= K; k++
   fprıntf(fle,"% 8.4f",v ı  k]);
 } */
}


ınput2()
{
 char ans MAXC ;
 char *fgets(), *gets(), *strchr();
 double atof();
 ıf (!fgets(ans,MAXC,fın)) return( );
 *strchr(ans,'\n') = '\0';
 ıf(!(fle = f pen(ans,"w")))
  return(0);
 ıp.D   0. 779;
 prıntf(" n%s t","Water superfıcıal vel c ty (m s)");
 *strchr(fgets(ans,MAX ,fın),' n')   '  ';
 ıp.uls   atof(ans);
 prıntf("%f",ıp.uls);
 prıntf(" n%s\t","Oıl superfıcıal vel cıty (m s)");
 *strchr(fgets(ans,MAX ,fın),' n')   ' 0';
 ıp.ugs = atof(ans);
 prıntf("%f\n",ıp.ugs);
 prıntf("\n%s t","Water vıs  sıty (Pa.s)");
 *strchr(fgets(ans,MAXC,fın),'\n')   '\ ';
 ıp.mul   1.0e 3*at f(ans);
 prıntf("%f\n",ıp.mul);
 prıntf(" n%s t","  l vısc sıty (Pa.s " ;
 *strchr(fgets(ans,MAX ,fın),'\n')   '  ';
 ıp.mug = 1. e 3*at f(ans);
 prıntf("%f n", p.mug);
 ıp.densl = 999. ;
 ıp.densg   8  . ;
 return(1);
}
```

```
/* LIQLIQ FD.c

2 phase steady state gas lıquıd  r lıqu d lıquıd stratıfıed fl w numerıcal
s lutı n

Wrıtten by A.R.W.Hall, Process Studıes Department, APS; Aprıl 1991


Thıs fıle contaıns the subroutınes f r a fınıte dıfference solutı n  f the
m mentum equatıons f r tw  phase stratıf ed f  w ın a p pe. Als  subr utıne
to check the total fl wrate  f each phase by ıntegratı n  f the vel cıty fıelds
and calculate shear stresses and effectıve (turbulent) vısc sıtıes. These are
called fr m the maın(  ın LIQLIQ.

*/

# ınclude <stdıo.h>
# ınclude "math.h"
# defıne I 20 /* no of eta grıd poınts */
# defıne J 2   * no of lıquıd phase xı grıd p ınts *
# defıne K 2  /* no of gas phase xı grıd poınts *
struct fl w_varıables{
 double D;
 d uble uls, ugs;
 double mul, mug;
 d uble densl, densg;
};
```

```
double cosh(), cos(), pow(), sqrt(), acos(), exp(), fabs();
extern double c, gam;
extern double Tig, Til, Twg, Twl;
double utot_old, utot new, vtot_old, vtot_new;
extern double pdrop, hl;
double pdrop_g;
extern double u[I+1][J+1], v[I+1 [K+1];
extern double xilL[J+1], xiG[K+1 , eta[I+1 ;
extern struct flow_variables ip;

static double dxiL[J+1], dxiG[K+1], deta[I+1];
double xidL[J+1], xidG[K+1], etad[I+1 ;
double P1L[I+1][J+1], P2L[I+1][J+1];
double P3L[I+1][J+1], P4L[I+1][J+1];
double P5L[I+1][J+1], PDL[I+1] J+1];
double P1G[I+1][K+1 , P2G[I+1][K+1];
double P3G[I+1][K+1], P4G[I+1][K+1 ;
double P5G[I+1][K+1], PDG[I+1 [K+1];
double mu_eff_liq[I+1][J+1];
double mu_eff_gas[I+1][K+1];
extern double alpha;

fd()
{
 int i, j, k, count, mm;

/* (1) Calculate difference arrays     */
 mm = 0;
 diff_xiL();
 diff_xiG();
 diff_eta();
 Pcalc_L();
 Pcalc_G();

/* (1b) Calculate mixing-length turbulent viscosities   */

 set_mu_eff_gas();
 set mu_eff_liq();

 utot old = 0.0;
 vtot_old = 0.0;

/* (2) Set boundary conditions      *

 for (i = 0; i <= I; i++){
  u[i][J] = 0.0;
  v[i][K] = 0.0;
 }
 for (j = 0; j <= J; j++)
  u[I][j] = 0.0;
 for (k = 0; k <= K; k++)
  v[I][k  = 0.0;

/* (3) Solve main block of grids     */

 for (count = 0; count < 30000; count++){

  utot_new = 0.0;
  vtot_new - 0.0;
  for (i = 1; i < I; i++){
   for (j = 1; j < J; j++){
    u[i][j  = P1L[i] j] * u[i][j 1] + P2L[i [   * u i+1  j
      + P3L[i][j] * u[i][j+1] + P4L[i][j  * u i 1] j
      - P5L[i][j];
    utot_new += u[i]  ];
   }
   for (k = 1; k < K; k++){
    v[i][k] = P1G[i][k] * v[i][k-1  + P2G[i [k] * v i+1] k]
      + P3G[i][k  * v[i][k+1] + P4G[i][k] * v[i-1  k]
      - P5G[i][k ;
    vtot_new +- v[i  k];
   }
  }

/* (4) Solve the remaining boundary conditi ns.   */

  for (j = 1; j < J; j++)
```

```
   u[  [j]   P1L 0 [j  * u[0][j-1  + P2L 0][j  * u 1 [
  .   + P3L    j] * u    j+1  + P4L 0     * u 1
     - P5L   [j];

  f r (k   1; k < K; k++)
   v 0 [k  = P1G[0 [k] * v[ ][k 1] + P2G 0  k  * v 1  k
     + P3G 0] k] * v    k+1  + P4G    k  * v[1 [k
       P5G    k ;

  if (1p.mul <= 1p.mug)
   f r (1 = 0; 1 < I; 1++){
    v[1] 0] = v[1] 1  + (mu eff l1q 1 [   mu_eff gas 1    ) * (dx1G[1] dx1L[1])
      * (u 1 [1]   u 1] 0 );
    u[1][0  = v 1][  ;
   }

  else
   f r (1    ; 1 < I; 1++){
    u[1]  ]   u 1][1  + (mu_eff gas 1]    mu eff l1q 1    ) * (dx1L[1] dx1G 1 )
      * (v[1][1]   v[1 [0]);
    v[1][0    u 1]   ;
   }

  if (((fabs((utot new   ut t  ld)   ut t new) > 1. e 6)
   (fabs((vt t new   vtot_ ld) / vt t new) > 1. e 6))    (c unt < 10 )){
   if (mm    5   {
    printf(" n%d t%1 .6f t%1 .6f",  unt,(ut t new u+ +  ld),(vt t new vt t   d));
    mm   1;
   }
   else
    ++mm;
   utot  ld   ut t new;
   vtot  ld   vt t new;
  }

  else{
   printf(" n n%s"," atisfact ry c nvergen e  f vel city fields");
   c unt   3    ;
  }
 }
}


static diff x1L()
{
 int  ;
 for (    ;   < J; j++
  dx1L[ +1    x1L  +     x1L   ;
 dx1L 0    x1L[1    x1L   ;
 f r (    ; j < J; j++)
  x1dL j    dx1L    * dx1L  +1  * (dx1L    + dx1L  +  );
 x1dL J]   x1dL J 1 ;
}


static diff x1G()
{
 int k;
 f r (k   0; k < K; k++)
  dx1G k+1    x1G k    x1G k+1 ;
 dx1G[0    x1G[0    x1G 1 ;
 f r (k    ; k < K; k++)
  x1dG[k    dx1G k] * dx1G k+1  * (dx G k] + dx1G k+1 );
 x1d  K]   x1dG[K 1 ;
}


static diff_eta()
{
 int 1;
 f r (1    ; 1 < I; 1++)
  deta 1+1  = eta 1+1    eta 1 ;
 deta 0] = eta[1  - eta[  ;
 f r (1 =  ; 1 < I; 1++)
  etad[1    deta 1] * deta 1+1  * (deta 1  + deta 1+   ;
 etad I  = etad I 1 ;
}
```

```
static Pcalc_L()
{

/* Calculate P values. These simplify the solution of the finite  */
/* difference equation, since they do not need to be recalculated at */
/* each iteration of the grid, although since gam = f(hl~) they will */
/* need to be calculated when hl~ is updated.     */

 int i, j;
 double cosheta;
 for (i = 0; i < I; i++)
  for (j = 0; j < J; j++)
   PDL[i][j] = etad[i] * (dx1L[j] + dx1L[j+1])
      + x1dL[j] * (deta[i] + deta[i+1]);

 for (i = 0; i < I; i++){
  cosheta = cosh(eta[i]);
  for (j = 0; j < J; j++){
   P1L[i][j] = dx1L[j+1] * etad[i] / PDL[i][  ;
   P2L[i][j] = deta[i] * x1dL[j] / PDL[i][j];
   P3L[i][j] = dx1L[j] * etad[i] / PDL[i][j];
   P4L[i][j] = deta[i+1] * x1dL[j] / PDL[i][j];
   P5L[i][j] = pdrop * x1dL[j] * etad[i] * c * c / (2.0 * PDL[i][j]
       * mu_eff_liq[i][j] * pow((cosheta-cos(x1L[j])), 2.0));
  }
 }
}


static Pcalc_G()
{

/* Calculate P values. These simplify the solution of the finite  */
/* difference equation, since they do not need to be recalculated at */
/* each iteration of the grid, although since gam = f(hl ) they will */
/* need to be calculated when hl  is updated.     *

 int i, k;
 double cosheta;
 for (i = 0; i < I; i++)
  for (k = 0; k < K; k++)
   PDG[i][k] = etad[i] * (dx1G[k] + dx1G k+1 )
      + x1dG[k] * (deta[i] + deta[i+1]);

 for (i = 0; i < I; i++){
  cosheta = cosh(eta[i]);
  for (k = 0; k < K; k++){
   P1G[i [k] = dx1G[k+1] * etad[i] / PDG[i  k];
   P2G[i [k] = deta[i] * x1dG[k  / PDG[i][k ;
   P3G[i][k] = dx1G[k] * etad[i] / PDG[i][k ;
   P4G[i][k] = deta[i+1] * x1dG[k] / PDG[i] k];
   P5G[i][k  = pdrop * x1dG[k  * etad[i  * c * c / (2.0 * PDG i [k
       * mu_eff_gas[i][k  * pow((cosheta-cos(x1G[k )),2.0));
  }
 }
}


initial_guess()
{

/* Calculate initial guesses for liquid height and pressure drop using */
/* Taitel and Dukler's stratified flow model.     */

 double f(), hlold, delta;
 double ff, df;

 hl = 0.5;
 hlold = 0.0;
 delta = 1.0e-6;

 while ((fabs((hl-hlold)/hl) > 1.0e 4)){
  hlold = hl;
  ff = f(hl);
  df = (f(hl+delta)   f(hl)) / delta;
  hl = hl - ff / df;
  if (hl >= 1.0) hl = 0.99;
```

```
 if (hl <   .0) hl   0. 1;
 }

 printf(" n\n%s\n%s\t%f t%s t%f","Initial Guesses","hl",hl,"Pdr p",pdr p);
}


double f(h)
double h;
{
 double A, Al, Ag, Pi, Pl, Pg, Dl, Dg, ug, ul, X, Q, t g, fg, tol, fl, mur;
 double Reg, Rel, Cg, Cl, m, n;
 double sqrt(), p w();
 mur = ip.mug / ip.mul;
 Q - 2.  * h   1. ;
 Al = 0.25 * (M_PI   a  s(Q) + Q * sqrt(1.    Q*Q));
 Ag = 0.25 * (acos(Q)   Q * sqrt(1.0   Q*Q));
 Pi   sqrt(1.0   Q*Q);
 Pl = M PI   acos(Q);
 Pg = ac s(Q);
 A = M_PI   4. ;
 ug = A / Ag;
 ul = A / Al;

 if (mur <  1.0)
     Dl   4.  * Al   Pl;
  Dg   4.  * Ag   (Pg + Pi);
 }
 else{
  Dl   4.0 * Al / (Pl + Pi);
  Dg = 4.  * Ag   Pg;
 }

 Reg = Dg*ip.D * ug*ip.ugs * ip.densg   ip.mug;
 Rel   Dl*ip.D * ul* p.uls * ip.densl   ip.mul;

 Cg   (Reg < 2   . ) . 16.  :  . 46;
 m = (Reg < 20  .      1.  :   .2;
 Cl = (Rel < 2   .0) . 16.0 :  . 46;
 n = (Rel < 2   .0) ?  1.  :   .2;

 X - sqrt((Cl * p w((ip.uls*ip.D*ip.dens   p.mul),n)*ip.densl*ip.uls*ip.uls)
   (Cg * p w((ip.ugs*ip.D*ip.densg ip.mug ,m)*ip.densg*ip.ugs*ip.ug ));

 if (mur <  1.  {
  fg   Cg * p w(Reg,m);
  tog   fg * ip.densg * (ug*ip.ugs) * (ug*ip.ugs)   2. ;
  pdr p      tog * (Pg + Pi)   (Ag * ip.D);
  return ((X*X*p w((ul*Dl),n)*ul*ul*Pl Al)   (p w((ug Dg),m)
*ug*ug*(Pg Ag + Pi/Al + Pi/Ag) );
 }
 else{
  fl   Cl * pow(Re ,n);
  tol   fl * ip.densl * (ul*ip.ul ) * (ul*ip.uls) / 2. ;
  pdr p      tol * (Pl + Pi) / (Al * ip.D);
  return ((X*X*p w((ul*Dl),n)*ul*ul*(Pl/Al + Pi/Al + Pi Ag))
   (p w((ug/Dg),m)*ug*ug*Pg Ag));
 }
}


shear stresses()
{
 double TigPi, TilP , TwgPg, TwlPl;
 double Pi, Pl, Pg, Ag, Al;
 double atan3(), tanh(), sin();
 double A, B, Q;
 double R, S;
 double pdrop_l;
 int i;

/* Calculate gas phase mean wall shear stress (ie at xi   gam)  *

 TwgPg   0. ;
 for (i   1; i <  I; i++){
  A   sqrt((1.0 + c s(gam))   (1.    cos(gam    * tanh eta i] 2. );
  B = sqrt((1.0 + c s(gam))   (1.    c s(gam))) * tanh(eta i 1  2. );
```

```
 R = fabs(mu_eff_gas[i][1] * (cosh(eta[i]) - cos(gam))
   * ((v[i][K] - v[i][K-1]) / dxiG[K]));
 S = fabs(mu_eff_gas[i-1][1] * (cosh(eta[i 1]) - cos(gam))
   * ((v[i-1][K] - v[i-1][K-1]) / dxiG[K]));
 TwgPg += fabs(((R + S) / sin(gam)) * (atan3(A) - atan3(B)));
}
TwgPg *= 2.0;

/* Calculate gas phase mean interfacial shear stress (ie at xi = pi) */

 TigPi = 0.0;
 for (i = 1; i <= I; i++){
  A = tanh(eta[i]/2.0);
  B = tanh(eta[i-1]/2.0);
  R = fabs(mu_eff_gas[i [0] * (cosh(eta[i])   cos(M PI+alpha))
      * ((v[i][1] - v[i][0]) / dxiG[1]));
  S = fabs(mu_eff_gas[i-1][0] * (cosh(eta[i 1])   cos(M PI+alpha))
      * ((v[i-1][1] - v[i-1][0]) / dxiG[1]));
  TigPi += fabs((R + S) * (A - B) / 2.0);
 }
 TigPi *= 2.0;

/* Calculate liquid phase mean interfacial shear stress (ie at xi = pi) *

 TilPi = 0.0;
 for (i = 1; i <= I; i++){
  A = tanh(eta[i]/2.0);
  B = tanh(eta[i-1]/2.0);
  R = fabs(mu_eff_liq[i][0] * (cosh(eta[i]) - cos(M_PI+alpha))
      * ((u[i][0  - u[i][1]) / dxiL[1]));
  S = fabs(mu_eff_liq i-1][0] * (cosh(eta[i 1])   c s(M_PI+alpha))
      * ((u i-1][0  - u[i-1 [1 ) / dxiL[1]));
  TilPi += fabs((R + S) * (A   B) / 2.0);
 }
 TilPi *= 2.0;

/* Calculate liquid phase mean wall shear stress (ie at xi = pi + gam) *

 TwlPl = 0.0;
 for (i = 1; i <= I; i++){
  A = sqrt((1.0 + cos(M_PI+gam)) / (1.0 - c s(M PI+gam))) * tanh(eta i /2.0);
  B = sqrt((1.0 + cos(M PI+gam)) / (1.0   cos(M PI+gam))) * tanh(eta i 1  ∠.0);
  R = fabs(mu_eff liq i [J  * (cosh(eta[i]) - cos(M PI+gam))
    * ((u[i][J-1] - u[i][J-1]) / dxiL[J]));
  S = fabs(mu_eff_liq i-1][J-1  * (cosh(eta[i-1 )   c s(M PI+gam))
    * ((u[i-1][J-1]   u[i-1 [J )   dxiL[J]));
  TwlPl += fabs(((R + S)   sin(M PI+gam)) * (atan3(A)   atan3(B)));
 }
 TwlPl *= 2.0;

 Q = 2.0 * (hl/ip.D) - 1.0;
 Al = 0.25 * ip.D * ip.D * (M PI   acos(Q) + Q * sqrt(1.  - Q*Q));
 Ag = 0.25 * ip.D * ip.D * (acos(Q) - Q * sqrt(1.0   Q*Q));
 Pi = ip.D * sqrt(1.0   Q*Q;
 Pl = ip.D * (M_PI - acos(Q));
 Pg = ip.D * acos(Q);

 Twg = TwgPg / Pg;
 Tig = TigPi / Pi;
 Til = TilPi / Pi;
 Twl = TwlPl / Pl;

 if (ip.mug <= ip.mul){
  pdrop g = -fabs((TwgPg + TigPi) / Ag);
  pdrop_l = -fabs((TwlPl - TilPi) / Al);
 }
 else{
  pdrop_g = -fabs((TwgPg - TigPi) / Ag);
  pdrop_l = -fabs((TwlPl + TilPi)   Al);
 }

 printf("\n\n%s","SHEAR STRESSES");
 printf("\t\t%10s\t%10s\n\n","Wall","Interface");
 printf("\t%10s\t%10.4f\t%10.4f\n","Gas",Twg,Tig);
 printf("\t%10s\t%10.4f\t%10.4f\n","Liquid",Twl,Til);
 printf("\n%s\t%10.4f","Pressure drop (gas)",pdrop g);
 printf("\n%s\t%10.4f","Pressure drop (liq)",pdrop l);
```

```
}


check liquid()
{

/* checking liquid fl wrate */
 d uble hl ld;
 double QLsum, QLin, urfh;
 int i, j;
 QLsum =  .0;
 urfh   0.1 ;
 for (i = 1; i <  I; i++)
  for (j = 0; j <= J; j++)
   QLsum +  2.0 * c * c * u[i][   * dxiL    * deta i
      / p w((c sh(eta[i )   c s(xiL[j )), 2.  ;
 QLin   M PI * ip.D * ip.D * ip.uls / 4. ;
 printf("\n\n%s t%s\t%1 .4e\t%s\t%10.4e\t%6.2f","LIQUID FL WRATE","Sum",
QLsum,"Input",QLin,1 0. *(QLsum QLin) QLsum);

 /* Recalculating liquid height */
 hl ld = hl;
 hl *  QLin/QLsum;
 hl   urfh * hl + (1.    urfh) * hlold;
 printf(" n n%s t%s t%1 .4f t%s\t%1 .4f","LIQ ID HEIGHT",
" ld",hl ld ip.D,
"New",hl ip.D);
}


check gas()
{
  * checking gas fl wrate *
 d uble pdr p  ld;
 d uble Q sum, Q in, urfp;
 int i, k;

 QGsum    . ;
 urfp   0.1 ;
 f r (i   1; i <  I; i++)
  f r (k =  ; k <  K; k++)
   QGsum +  2.  * c *   * v i  k  * dxiG k  * deta
       p w((c sh(eta i     c s(xiG k  ), 2. );
 QGin   M_PI * ip.D * ip.D * ip.ugs   4. ;

  * Re alculating pressure dr p *

 pdr p  ld   pdr p;
 pdrop *= QGin Q sum;
 pdrop = urfp * pdr p + (1.    urfp) * pdr p  ld;
 printf(" n n%s t%s t%i .4e t%_ t%10.4e t%6._f","GAS FL WRA E",
"Sum",QGsum,"Input",QGir,1  . * QGsum QGin)/QGin);
 printf(" n\n%s t%s t%1 .4f t%s\t%1 .4f","PRESSURE DR P",
" ld",pdr p old,"New",pdr p);
}


set_mu eff gas()
{

 int i, k;
 double cosh(), tan(), sqrt(), exp(), c s();
 double atan3(), ac s(), fabs(), sgn();
 d uble B, lxi, lm, lxi d, lm 3 ;
 double R, S, mu t;
 double la, lb, new;
 d uble Tg;
 double Q, QQ, Al, Ag, Pi, Pg, A, ug, ul, Reg, mur, Dg, Dl;
 double bound =  . 5;

 Tg   Twg;
 mur   ip.mug / ip.mul;
 QQ   2.0 * hl   1.0;
 Ag    .25 * (ac s(QQ)   QQ * sqrt(1.    QQ*QQ));
 Pg   acos(QQ);
 Pi   sqrt(1.  - QQ*QQ);
 A = M PI / 4. ;
```

```
 ug = A / Ag;
 if (mur <= 1.0)
  Dg = 4.0 * Ag / (Pg + P1);
 else
  Dg = 4.0 * Ag / Pg;

 Reg = ip.densg * ip.ugs * ug * Dg * ip.D   ip.mug;

 lm_30 = 0.4 * 30.0 * ip.mug * sqrt(ip.densg Tg) * (1.0   exp(-3 .0/26.0)) / ip.densg;
 gam = acos(1.0-2.0*hl/ip.D);

 for (i = 1; i < I; i++){
  B = cosh(eta[i]);
  for (k = 1; k < K; k++){
   R = atan3(sqrt((B+1.0)/(B-1.0)) * tan(x1G k]/2.0));
   S = atan3(sqrt((B+1.0)/(B-1.0)) * tan(gam 2.0));
   la = R - S;
   lb = (M_PI / 2.0) - R;
   Q = (la > lb) ? lb : la;
/*   Q = la;  */
   lx1 = 2.0 * c * Q / sqrt(B*B - 1.0);
   lx1_d = lx1 * sqrt(Tg/ip.densg) * ip.densg / ip.mug;
   if (lx1_d > 30.0)
    lm = lm_30;
   else
    lm = 0.4 * lx1 * (1.0   exp( lx1_d/26.0));
   mu_t = lm * lm * ip.densg * fabs((v i [k    v[i  k 1 )
* (B - cos(x1G[k])) / (c * dx1G[k]));
   if (Reg < 2000.0)
    mu t = 0.0;
   if (mu_t < 1.0e 7)
    mu_eff_gas[i][k] = ip.mug;
   else{
    new = ip.mug + mu_t;
    if (fabs((new   mu_eff_gas[i  k]) / mu eff gas i] k]) > bound)
     new = mu eff_gas[i [k  * (1.  + b und
* sgn((new - mu_eff_gas[i] k]) / mu eff gas i  k ));
    mu_eff_gas[i] k] = new;
   }
   mu_eff_gas[0][k] = mu_eff gas 1 [k];
   mu_eff_gas[I][k] = ip.mug;
  }
  mu_eff gas[i][K]   ip.mug;
  mu_eff_gas[i [0]   ip.mug;
 }
}

set_mu_eff_liq()
{

 int i, j;
 double cosh(), tan(), sqrt(), exp(), p w();
 double cos(), fabs(), sgn(), acos(), atan3();
 double B, lx1, lm, lx1_d, lm 30;
 double R, S, gam, mu_t;
 double la, lb, new, Tw;
 double Q, QQ, Al, Ag, P1, Pl, A, ug, ul, Rel, mur, Dl, Dg;

 double bound = 0.05;
 gam = acos(1.0-2.0*hl/ip.D);
 Tw = Twl;
 mur = ip.mug / ip.mul;
 QQ = 2.0 * hl - 1.0;
 Al = 0.25 * (M_PI - acos(QQ) + QQ * sqrt(1.    QQ*QQ));
 Pl = M PI - acos(QQ);
 P1 = sqrt(1.0   QQ*QQ);
 A = M_PI / 4.0;
 ul = A / Al;
 if (mur <= 1.0)
     Dl = 4.0 * Al / Pl;
 else
  Dl = 4.0 * Al   (Pl + P1);

 Rel = ip.densl * ip.uls * ul * Dl * ip.D / ip.mul;

 lm_30 = 0.4 * 30.0 * ip.mul * sqrt(ip.densl/Tw) * (1.    exp( 3 .0/26. )) / ip.densl;
```

```
 for (i = 1; i < I; i++){
  B   cosh(eta[i]);
  for (j   1; j < J;  ++){
   R = atan3(sqrt((B+1. )/(B 1. )) * tan(xiL[j] 2.0));
   S   atan3(sqrt((B+1.0)/(B-1.0)) * tan((M PI + gam)/2. ));
   la   R   (M PI   2. );
   lb = S - R;
 *   Q   (la > lb) . lb : la; */
   Q   la;
   lxi = 2.0 * c * Q / sqrt(B*B   1. );
   lxi d = lxi * sqrt(Tw ip.densl) * ip.densl / ip.mul;
   if (lxi d > 3 .0)
    lm = lm_30;
   else
    lm = 0.4 * lxi * (1.0 - exp( lxi d 26. ));
   mu t   lm * lm * ip.densl * fabs((u i [     u i    1 )
* (B   cos(xiL[j ))   (c * dxiL[  ));
   if (Rel < 2 0 .0)
    mu t   0.0;
   if (mu t < 1. e 7)
    mu eff liq i       ip.mul;
   else{
    new   ip.mul + mu t;
    if (fabs((new   mu eff liq i    )   m  eff liq i        b und)
     new   mu_eff liq i     * (1.  + b und
* sgn((new   mu eff liq i   ])   mu eff liq i    ));
    mu eff liq i       new;
   }
   mu eff liq[0 [ ]   mu eff liq[1 [  ;
   mu eff liq I [     ip.mul;
  }
  mu eff liq i] J    ip.mul;
  mu eff liq[i]      ip.mul;
 }
}

double atan3(x)
d uble x;
{
 double y, atan( ;
 y   atan(  ;
 if (y <  . )
  y +  M PI;
 return(y);
}

mu eff init()
{
 int i,  , k, l;
 for (i    ; i <  I; i++ {
  f r (    0; j <  J;  ++
   mu eff_liq i  j     p.mul;
  f r (k   0; k <  K; k++)
   mu eff gas i  k    ip.mug;
 }
}

d uble sgn(x)
double x;
{
 d uble abs();
 return(x/abs(x );
}
```

THIS IS A BLANK PAGE

Appendix C: TABLES OF EXPERIMENTAL DATA POINTS

Table C.1: Sobocinski (University of Oklahoma, 1955)

Data Point	U_a	U_ℓ	Water fraction	Transition Velocity	Transition Velocity ("Taitel & Dukler")
51	2.548	0.051	0.569	0.235	0.352
58	2.399	0.047	0.340	0.194	0.360
64	2.660	0.047	0.787	0.327	0.346
91	2.844	0.051	0.039	0.164	0.337
41	3.115	0.076	0.645	0.263	0.339
42	5.731	0.076	0.645	0.262	0.279
43	2.671	0.070	0.614	0.249	0.349
45	4.084	0.070	0.614	0.257	0.317
49	2.838	0.064	0.422	0.209	0.349
46	2.648	0.092	0.685	0.272	0.348
52	3.811	0.051	0.569	0.244	0.324
61	3.444	0.047	0.298	0.195	0.337
92	2.844	0.061	0.164	0.178	0.350
93	4.095	0.059	0.136	0.175	0.319
50	4.174	0.064	0.422	0.213	0.319
71	3.862	0.067	0.761	0.319	0.319
47	4.007	0.092	0.685	0.282	0.317

Oil Density	841.0 kg/m^3
Oil Viscosity	3.83 mPas
Water Density	998.0kg/m^3
Water Viscosity	1.00 mPas
Air Density	1.224 kg/m^3
Air Viscosity	0.0222 mPas
Pipe Diameter	0.079 m

Table C.2: Stapelberg (University of Hannover, 1991)

Data Point	Flow Pattern	U_a	U_ℓ	Water fraction	Transition Velocity	Transition Velocity ("Taitel & Dukler")
2	I	0.604	0.431	0.471	0.054	0.069
3	S	0.386	0.107	0.604	0.064	0.100
6	I	0.386	0.181	0.511	0.055	0.093
8	I	0.823	0.177	0.521	0.061	0.085
9	I	0.386	0.169	0.219	0.036	0.067
10	S	0.604	0.083	0.615	0.071	0.093
11	S	0.386	0.112	0.579	0.061	0.100
12	I	0.604	0.114	0.569	0.064	0.081
13	I	0.823	0.113	0.571	0.065	0.086
14	I	0.386	0.181	0.511	0.055	0.092
16	I	0.823	0.185	0.500	0.058	0.080
21	I	0.495	0.241	0.498	0.058	0.098
22	I	0.604	0.250	0.479	0.058	0.088
23	I	0.823	0.249	0.482	0.060	0.094
28	I	0.495	0.313	0.471	0.055	0.085
29	I	0.714	0.319	0.463	0.057	0.072
30	S	0.386	0.072	0.515	0.056	0.099
31	S	0.386	0.086	0.593	0.064	0.110
32	S	0.386	0.100	0.650	0.072	0.121
33	S	0.495	0.072	0.515	0.059	0.094
34	S	0.495	0.086	0.593	0.068	0.106
35	S	0.604	0.072	0.515	0.061	0.091
36	S	0.604	0.086	0.593	0.071	0.102
37	S	0.714	0.072	0.515	0.063	0.087
38	S	0.714	0.086	0.593	0.073	0.097
39	S	0.823	0.072	0.515	0.064	0.103
40	S	0.823	0.086	0.593	0.074	0.113
44	S	0.823	0.078	0.654	0.081	0.113
45	S	0.386	0.091	0.709	0.082	0.127
46	S	0.495	0.059	0.856	0.134	0.151
47	S	0.604	0.078	0.656	0.079	0.104
48	S	0.714	0.059	0.858	0.141	0.136

Table C.2: (Continued) Stapelberg (University of Hannover, 1991)

Oil Density	846.3 kg/m^3
Oil Viscosity	27.8 mPas
Water Density	989.2 kg/m^3
Water Viscosity	0.984 mPas
Air Density	1.195 kg/m^3
Air Viscosity	0.018 mPas
Pipe Diameter	0.0238 m

THIS IS A BLANK PAGE

Appendix D: WASP EXPERIMENTAL DATA POINTS (THREE-PHASE FLOW)

Table D.1: WASP measured quantities

Data No	Phases	U_a	U_o	U_w	$\frac{dp}{dz}$	% error in $\frac{dp}{dz}$	Slug frequency	Flow pattern
1	aow	1.695	0.121	0.147	86.2	7	0.110	WC SLUG SEP
2	aow	1.728	0.070	0.152	61.9	13	0.055	WC SLUG SEP
3	aow	1.544	0.183	0.148	162.6	5	0.138	WC SLUG SEP (Oily Film)
4	aow	1.358	0.236	0.147	411.9	3	0.172	OC SLUG DISP
5	aow	1.760	0.121	0.270	108.8	15	0.119	WC SLUG SEP
6	aw	1.691	0.000	0.269	53.2	13	0.076	WATER SLUG
7	aw	1.346	0.000	0.673	156.9	2	0.149	WATER SLUG
8	ao	1.790	0.226	0.000	169.0	6	0.144	OIL SLUG
9	aow	1.637	0.226	0.109	328.6	10	0.171	OC SLUG DISP
10	aow	1.642	0.226	0.164	265.6	5	0.192	OC SLUG DISP
11	aow	1.535	0.226	0.309	151.4	4	0.142	WC SLUG DISP
12	aow	1.360	0.226	0.492	178.6	2	0.148	WC SLUG DISP
13	aow	0.976	0.224	0.826	300.5	2	0.167	WC SLUG DISP
14	aw	1.264	0.000	0.823	208.2	1	0.175	WATER SLUG
15	ao	1.833	0.132	0.000	78.4	9	0.105	OIL SLUG
16	aow	1.384	0.132	0.245	116.3	7	0.116	WC SLUG SEP
17	aow	1.397	0.132	0.081	184.0	7	0.116	OC SLUG DISP
18	aow	1.436	0.132	0.145	106.9	7	0.101	WC SLUG SEP
19	aow	2.405	0.132	0.148	125.0	10	0.104	WC SLUG SEP
20	aow	2.347	0.132	0.327	168.0	8	0.143	WC SLUG SEP
21	aw	2.384	0.000	0.325	99.5	11	0.104	WATER SLUG
22	ao	1.920	0.070	0.000	51.4	11	0.046	OIL SLUG
23	aow	1.948	0.070	0.077	50.6	13	0.048	WC SLUG DISP
24	aow	1.400	0.069	0.074	37.9	9	0.061	WC SLUG SEP
25	aow	1.440	0.070	0.076	39.5	14	0.067	WC SLUG SEP
26	aow	1.405	0.071	0.209	55.5	9	0.090	WC SLUG SEP
27	aow	1.412	0.120	0.206	72.0	9	0.094	WC SLUG SEP
28	aow	1.438	0.174	0.204	108.2	5	0.105	WC SLUG SEP (Oily Film)

Data No	Phases	U_a	U_o	U_w	$\frac{dp}{dz}$	% error in $\frac{dp}{dz}$	Slug frequency	Flow pattern
29	aow	1.428	0.227	0.205	175.2	4	0.129	WC SLUG SEP (Oily Film)
30	aow	1.435	0.260	0.204	235.9	3	0.136	OC SLUG DISP
31	aow	1.365	0.258	0.134	400.9	4	0.201	OC SLUG DISP
32	ao	3.156	0.112	0.000	121.8	7	0 100	OIL SLUG
33	aow	2.997	0.112	0.161	143.2	6	0.112	WC SLUG DISP
34	aow	2.986	0.112	0.114	126.4	7	0.090	WC SLUG DISP (Oily Film)
35	aow	3.038	0.112	0.247	152.9	6	0.108	WC SLUG DISP
36	aow	3.011	0.173	0.182	208.0	7	0.135	WC SLUG DISP (Oily Film)
37	aow	2.719	0.257	0.183	588.0	4	0.170	OC SLUG DISP
38	aw	2.819	0.000	0.699	292.0	4	0.164	WATER SLUG
39	aow	3.153	0.163	0.153	196.5	8	0.110	WC SLUG DISP (Oily Film)
40	aow	3.113	0.160	0 255	185.0	9	0.128	WC SLUG DISP
41	aow	3.041	0.155	0.410	255.9	6	0.153	WC SLUG DISP
42	aow	2.895	0.153	0.703	390.3	4	0.173	WC SLUG DISP
43	aow	2.842	0.230	0.701	430.7	6	0.167	WC SLUG DISP
44	ao	1.943	0.177	0.000	159.5	8	0 124	OIL SLUG
45	aow	1.842	0.175	0.159	191.4	6	0.129	WC SLUG DISP (Oily Film)
46	aow	1.751	0.175	0.325	174.5	4	0.110	WC SLUG SEP
47	aow	1.678	0.175	0.411	186.3	4	0.136	WC SLUG SEP
48	aow	1.512	0.175	0.640	265.0	2	0.127	WC SLUG DISP
49	aow	1.399	0.270	0.631	296 7	1	0 117	WC SLUG DISP
50	ao	2.256	0.290	0.000	247.7	6	0.156	OIL SLUG
51	aow	2.003	0.288	0.455	264.9	3	0.147	WC SLUG DISP
52	aow	1.966	0.280	0.176	505.9	3	0.180	OC SLUG DISP
53	aow	2.051	0.280	0.257	273.0	5	0.166	WC SLUG DISP (Oily Film)
54	aw	2.168	0.000	0.435	134.9	8	0.134	WATER SLUG
55	aw	1.646	0.000	1.504	605.5	1	0.160	WATER SLUG
56	ao	2.896	0.262	0.000	277.1	7	0.164	OIL SLUG

Data No	Phases	U_a	U_o	U_w	$\frac{dp}{dz}$	% error in $\frac{dp}{dz}$	Slug frequency	Flow pattern
57	aow	2.797	0.295	0.233	438.6	5	0.191	OC SLUG DISP
58	aow	2.844	0.291	0.362	370.5	5	0.157	WC SLUG DISP (Oily Film)
59	aow	2.790	0.291	0.599	431.5	4	0.163	WC SLUG DISP
60	aw	2.956	0.000	0.594	275.9	6	0.147	WATER SLUG
61	aw	2.794	0.000	0.870	406.0	4	0.181	WATER SLUG
62	aow	1.446	0.140	0.233	75.2	6	0.103	WC SLUG SEP
63	aow	1.424	0.138	0.243	87.2	6	0.105	WC SLUG SEP
64	aow	1.420	0.160	0.112	106.7	4	0.121	WC SLUG SEP (Oily Film)
65	aow	1.417	0.160	0.118	108.7	4	0.123	WC SLUG SEP (Oily Film)
66	aow	1.698	0.161	0.471	194.0	2	0.142	WC SLUG SEP (Borderline)
67	aow	1.585	0.267	0.470	226.4	2	0.156	WC SLUG DISP
68	aow	1.394	0.060	0.134	57.9	7	0.070	WC SLUG SEP
69	aow	1.132	0.061	0.126	54.7	8	0.066	WC SLUG SEP
70	aow	1.454	0.100	0.084	71.7	7	0.086	WC SLUG SEP
71	aow	1.466	0.099	0.082	74.5	9	0.071	WC SLUG SEP
72	aow	1.060	0.270	0.358	183.9	2	0.144	WC SLUG SEP (Borderline)
73	aow	2.106	0.270	0.358	247.3	3	0.142	WC SLUG DISP
74	aow	2.099	0.120	0.079	99.8	11	0.090	WC SLUG SEP
75	aow	2.073	0.118	0.148	81.6	11	0.082	WC SLUG SEP
76	aow	2.071	0.119	0.150	91.8	8	0.094	WC SLUG SEP
77	aow	1.597	0.196	0.189	142.2	4	0.106	WC SLUG SEP
78	aow	1.617	0.190	0.307	148.4	5	0.124	WC SLUG SEP (Borderline)
79	aow	1.386	0.210	0.228	120.4	3	0.105	WC SLUG SEP
80	aow	1.363	0.210	0.208	141.3	3	0.114	WC SLUG SEP
81	aow	1.359	0.210	0.210	145.3	3	0.129	WC SLUG SEP
82	aow	1.342	0.210	0.208	149.9	3	0.110	WC SLUG SEP
83	aow	2.491	0.152	0.182	132.3	7	0.106	WC SLUG DISP
84	aow	2.482	0.150	0.188	136.2	7	0.094	WC SLUG DISP

Data No	Phases	U_a	U_o	U_w	$\frac{dp}{dz}$	% error in $\frac{dp}{dz}$	Slug frequency	Flow pattern
85	aow	2.500	0.150	0.187	124.3	7	0.099	WC SLUG DISP
86	aow	2.475	0.160	0.159	128.3	8	0.112	WC SLUG DISP
87	aow	2.476	0.160	0.403	208.8	6	0.135	WC SLUG DISP
88	aow	3.019	0.110	0.252	125.7	8	0.112	WC SLUG DISP
89	aow	3.025	0.110	0.212	125.3	8	0.102	WC SLUG DISP
90	aow	1.471	0.053	0.154	43.0	13	0.068	WC SLUG SEP
91	aow	1.608	0.070	0.167	62.1	8	0.078	WC SLUG SEP
92	aow	1.448	0.070	0.114	55.3	8	0.064	WC SLUG SEP
93	aow	1.574	0.220	0.098	388.2	3	0.165	OC SLUG DISP
94	aow	2.006	0.220	0.106	351.2	4	0.146	OC SLUG DISP
95	aow	1.952	0.220	0.441	279.8	2	0.130	WC SLUG DISP
96	aow	1.947	0.219	0.445	297.5	2	0.131	WC SLUG DISP
97	aow	1.697	0.219	0 616	275.4	2	0.154	WC SLUG DISP
98	aow	1.768	0.220	0.672	303.6	2	0.153	WC SLUG DISP
99	aow	1.724	0.240	0.076	399.7	5	0.188	OC SLUG DISP
100	aow	1.793	0.240	0.080	425.7	3	0.172	OC SLUG DISP
101	aow	1.462	0.219	0.236	133 6	4	0.132	WC SLUG SEP
102	aow	1.445	0.220	0.243	136.4	3	0.139	WC SLUG SEP
103	aow	2.594	0.220	0.271	210.7	5	0.133	WC SLUG DISP
104	aow	2.580	0.220	0.273	202.9	5	0.142	WC SLUG DISP
105	aow	3.690	0.230	0.269	362.9	6	0.155	WC SLUG DISP
106	aow	4.135	0.258	0.288	701.0	6	0.165	WC SLUG DISP
107	ao	1.186	0.322	0.000	204.3	4	0.163	OIL SLUG
108	aow	1.440	0.329	0.116	483.8	2	0.140	OC SLUG DISP
109	aow	1.506	0.320	0.242	257 4	2	0.170	WC SLUG DISP
110	aow	1.419	0.540	0.242	545.7	2	0.132	OC SLUG DISP
111	aw	1.516	0.000	0.407	105.7	5	0.106	WATER SLUG
112	aw	1.461	0.000	0.865	262.3	1	0.130	WATER SLUG

Table D.2: WASP physical properties

Data No	Temp	Oil Density	Water Density	Air Density	Oil Viscosity	Water Viscosity	Air Viscosity	Oil Fraction	Exit Pressure
1	20	872.2	998.2	1.42	50.0	1.090	0.018	0.451	1.18
2	20	872.2	998.2	1.43	50.0	1.090	0.018	0.315	1.18
3	20	872.2	998.2	1.40	50.0	1.090	0.018	0.553	1.16
4	20	872.2	998.2	1.38	50.0	1.090	0.018	0.616	1.15
5	20	872.2	998.2	1.42	50.0	1.090	0.018	0.309	1.18
6	21	871.7	998.0	1.42	47.8	1.067	0.018	0.000	1.19
7	21	871.7	998.0	1.37	47.8	1.067	0.018	0.000	1.14
8	19	872.6	998.4	1.48	52.9	1.114	0.018	1.000	1.23
9	19	872.6	998.4	1.45	52.9	1.114	0.018	0.675	1.20
10	19	872.6	998.4	1.44	52.9	1.114	0.018	0.579	1.19
11	19	872.6	998.4	1.40	52.9	1.114	0.018	0.422	1.16
12	19	872.6	998.4	1.37	52.9	1.114	0.018	0.315	1.13
13	19	872.6	998.4	1.33	52.9	1.114	0.018	0.213	1.10
14	19	872.6	998.4	1.34	52.9	1.114	0.018	0.000	1.11
15	19	872.6	998.4	2.37	52.9	1.114	0.018	1.000	1.96
16	19	872.6	998.4	2.17	52.9	1.114	0.018	0.350	1.79
17	19	872.6	998.4	2.18	52.9	1.114	0.018	0.620	1.81
18	19	872.6	998.4	2.20	52.9	1.114	0.018	0.477	1.82
19	19	872.6	998.4	2.53	52.9	1.114	0.018	0.471	2.09
20	19	872.6	998.4	2.51	52.9	1.114	0.018	0.288	2.08
21	19	872.6	998.4	2.53	52.9	1.114	0.018	0.000	2.09
22	15	874.4	999.1	2.13	64.5	1.218	0.018	1.000	1.74
23	16	873.9	999.0	2.02	61.6	1.191	0.018	0.476	1.66
24	16	873.9	999.0	3.02	61.6	1.191	0.018	0.483	2.48
25	16	873.9	999.0	4.10	61.6	1.191	0.018	0.479	3.36
26	16	873.9	999.0	4.00	61.6	1.191	0.018	0.254	3.28
27	16	873.9	999.0	3.93	61.6	1.191	0.018	0.368	3.22
28	17	873.5	998.8	3.95	58.7	1.165	0.018	0.460	3.25

Data .No	Temp	Oil Density	Water Density	Air Density	Oil Viscosity	Water Viscosity	Air Viscosity	Oil Fraction	Exit Pressure
29	17	873.5	998.8	3.95	58.7	1.165	0.018	0.525	3.24
30	17	873.5	998.8	3.87	58.7	1.165	0.018	0.560	3.18
31	17	873.5	998.8	3.87	58.7	1.165	0.018	0.658	3.18
32	18	873.1	998.6	1.43	55.8	1.139	0 018	1.000	1.18
33	19	872.6	998.4	1.40	52.9	1.114	0.018	0.410	1 16
34	19	872.6	998.4	1.40	52.9	1.114	0.018	0.496	1.16
35	19	872.6	998.4	1.41	52.9	1.114	0.018	0.312	1.17
36	19	872.6	998.4	1.42	52.9	1.114	0.018	0.487	1.17
37	20	872.2	998.2	1.40	50.0	1.090	0 018	0.584	1.16
38	20	872.2	998.2	1.39	50.0	1.090	0.018	0.000	1.16
39	18	873.1	998.6	2.10	55.8	1.139	0.018	0.516	1.73
40	18	873.1	998.6	2.05	55.8	1.139	0.018	0.386	1.69
41	18	873.1	998.6	2.00	55.8	1.139	0.018	0 274	1 65
42	18	873.1	998.6	1.90	55.8	1.139	0.018	0 179	1 57
43	18	873.1	998.6	1.86	55.8	1.139	0.018	0.247	1.53
44	14	874.8	999.3	1.69	69.0	1.246	0.018	1.000	1.38
45	14	874.8	999.3	1.66	69.0	1.246	0.018	0.524	1.35
46	14	874.8	999.3	1.61	69.0	1.246	0.018	0.350	1 31
47	14	874.8	999.3	1.58	69.0	1.246	0.018	0.299	1 28
48	14	874.8	999.3	1.52	69.0	1.246	0.018	0.215	1 24
49	14	874.8	999.3	1.48	69.0	1.246	0.018	0.300	1.21
50	17	873.5	998.8	2.21	58.7	1.165	0.018	1.000	1.81
51	17	873.5	998.8	1.67	58.7	1.165	0.018	0.388	1.37
52	17	873.5	998.8	1.65	58.7	1.165	0.018	0 614	1.36
53	17	873.5	998.8	1.69	58.7	1.165	0.018	0.521	1.39
54	17	873.5	998.8	1.74	58.7	1.165	0.018	0 000	1.43
55	17	873.5	998.8	1.51	58.7	1.165	0.018	0.000	1.24
56	13	875.3	999.4	1.85	73.5	1.275	0 018	1.000	1.50

Data No	Temp	Oil Density	Water Density	Air Density	Oil Viscosity	Water Viscosity	Air Viscosity	Oil Fraction	Exit Pressure
57	13	875.3	999.4	1.80	73.5	1.275	0.018	0.559	1.46
58	14	874.8	999.3	1.83	69.0	1.246	0.018	0.446	1.49
59	14	874.8	999.3	1.81	69.0	1.246	0.018	0.327	1.47
60	14	874.8	999.3	1.88	69.0	1.246	0.018	0.000	1.53
61	14	874.8	999.3	1.81	69.0	1.246	0.018	0.000	1.47
62	13.6	875.0	999.3	2.69	70.8	1.258	0.018	0.375	2.19
63	13.1	875.2	999.4	2.75	73.0	1.272	0.018	0.362	2.23
64	14.3	874.7	999.2	2.21	67.7	1.238	0.018	0.588	1.80
65	14.2	874.7	999.2	2.10	68.1	1.241	0.018	0.576	1.71
66	12.6	875.4	999.5	1.77	75.3	1.287	0.018	0.255	1.44
67	12.6	875.4	999.5	1.65	75.3	1.287	0.018	0.362	1.33
68	13.3	875.1	999.4	2.31	72.1	1.266	0.018	0.309	1.87
69	12.7	875.4	999.4	2.47	74.8	1.284	0.018	0.326	2.00
70	14.1	874.8	999.3	2.67	68.6	1.243	0.018	0.543	2.17
71	14.5	874.6	999.2	2.83	66.8	1.232	0.018	0.547	2.30
72	12.8	875.4	999.4	2.07	74.4	1.281	0.018	0.430	1.68
73	12.8	875.4	999.4	1.83	74.4	1.281	0.018	0.430	1.48
74	14.3	874.7	999.2	1.98	67.7	1.238	0.018	0.603	1.62
75	15.5	874.2	999.1	1.99	62.3	1.205	0.018	0.444	1.63
76	15.3	874.3	999.1	1.98	63.2	1.210	0.018	0.442	1.62
77	15.2	874.3	999.1	2.36	63.6	1.213	0.018	0.509	1.93
78	13.4	875.1	999.4	2.35	71.7	1.263	0.018	0.382	1.91
79	16.3	873.8	998.9	2.31	60.7	1.183	0.018	0.479	1.90
80	16.4	873.8	998.9	2.26	60.5	1.181	0.018	0.502	1.86
81	16.6	873.7	998.9	2.22	59.9	1.175	0.018	0.500	1.82
82	16.7	873.6	998.9	2.21	59.6	1.173	0.018	0.502	1.81
83	12.0	875.7	999.5	1.90	78.0	1.304	0.018	0.455	1.53
84	13.7	875.0	999.3	1.87	70.4	1.255	0.018	0.444	1.52

Data No	Temp	Oil Density	Water Density	Air Density	Oil Viscosity	Water Viscosity	Air Viscosity	Oil Fraction	Exit Pressure
85	13.9	874.9	999.3	1.90	69.5	1.249	0.018	0.445	1.54
86	13.2	875.2	999.4	1.90	72.6	1.269	0.018	0.445	1.54
87	13.1	875.2	999.4	1.97	73.0	1.272	0.018	0.502	1.60
88	12.9	875.3	999.4	1.82	73.9	1.278	0.018	0.304	1.48
89	13.5	875.1	999.3	1.84	71.2	1.260	0.018	0.342	1.49
90	12.6	875.4	999.5	2.24	75.3	1.287	0.018	0.256	1.82
91	13.2	875.2	999.4	2.24	72.6	1.269	0.018	0.295	1.82
92	15.2	874.3	999.1	2.19	63.6	1.213	0.018	0.380	1.79
93	17.4	873.3	998.7	2.36	57.5	1.155	0.018	0.692	1.94
94	19.0	872.6	998.4	2.29	52.9	1.114	0.018	0.675	1.89
95	16.9	873.5	998.8	2.13	59.0	1.168	0.018	0.333	1.75
96	18.2	873.0	998.6	2.09	55.2	1.134	0.018	0.330	1.72
97	15.9	874.0	999.0	2.55	61.9	1.194	0.018	0.262	2.09
98	15.3	874.3	999.1	2.45	63.7	1.210	0.018	0.247	2.00
99	17.5	873.3	998.7	2.69	57.2	1.152	0.018	0.759	2.22
100	17.6	873.2	998 7	2.88	57.0	1.150	0.018	0.750	2.38
101	22.5	871.1	997.5	2.89	44.6	1.033	0.018	0 481	2.42
102	23.3	870.7	997.5	3.01	42.9	1.015	0 018	0.475	2.52
103	23.1	870.8	997.6	2.38	43.3	1.019	0.018	0.448	2.00
104	23.2	870.7	997.5	2.12	43.1	1.017	0.018	0.446	1.78
105	23.4	870.7	997.5	2.18	42.7	1.013	0.018	0.461	1.83
106	23.5	870.6	997.5	2.78	42.5	1.011	0 018	0.473	2.34
107	21.1	871.7	998.0	2.33	47.6	1.064	0.018	1.000	1.94
108	21.1	871.7	998.0	2.46	47 6	1.064	0 018	0.739	2.05
109	20.8	871.8	998.1	2.55	48.2	1.071	0.018	0.569	2.13
110	20.3	872.0	998.2	2.41	49.3	1.083	0 018	0.691	2.01
111	19.3	872.5	998.4	2.54	52.0	1.107	0.018	0.000	2.10
112	19.3	872.5	998.4	2.47	52.0	1.107	0 018	0.000	2.05

Table D.3: WASP holdup measurements

Data No	Water Volume	Oil Volume	Total Volume	Water Fraction	Oil Fraction	Gas Fraction	*in-situ* Oil/Water ratio	input Oil/Water ratio
62	10.81	3.05	13.86	0.334	0.094	0.572	0.282	0.601
63	11.74	3.71	15.45	0.363	0.115	0.522	0.316	0.568
64	4.28	2.46	6.74	0.132	0.076	0.792	0.575	1.429
65	4.80	2.51	7.31	0.148	0.078	0.774	0.523	1.356
68	7.37	1.54	8.91	0.228	0.048	0.725	0.209	0.448
69	8.88	1.18	10.06	0.274	0.036	0.689	0.133	0.484
70	7.75	3.68	11.43	0.240	0.114	0.647	0.475	1.190
71	4.63	2.38	7.01	0.143	0.074	0.783	0.514	1.207
74	4.26	3.35	7.61	0.132	0.104	0.765	0.786	1.519
75	4.28	1.06	5.34	0.132	0.033	0.835	0.248	0.797
76	3.15	1.05	4.20	0.097	0.032	0.870	0.333	0.793
79	7.13	2.97	10.10	0.220	0.092	0.688	0.417	0.921
80	5.92	2.26	8.18	0.183	0.070	0.747	0.382	1.010
81	8.53	5.79	14.32	0.264	0.179	0.557	0.679	1.000
82	9.56	6.17	15.73	0.296	0.191	0.514	0.645	1.010
83	4.78	1.85	6.63	0.148	0.057	0.795	0.387	0.835
84	4.24	1.26	5.50	0.131	0.039	0.830	0.297	0.798
85	4.86	1.40	6.26	0.150	0.043	0.806	0.288	0.802
88	4.71	0.78	5.49	0.146	0.024	0.830	0.166	0.437
89	8.64	2.49	11.13	0.267	0.077	0.656	0.288	0.519
93	3.26	5.71	8.97	0.101	0.177	0.723	1.752	2.245
94	3.32	5.23	8.55	0.103	0.162	0.736	1.575	2.075
95	9.94	3.43	13.37	0.307	0.106	0.587	0.345	0.499
96	11.19	5.06	16.25	0.346	0.156	0.498	0.452	0.492
97	12.89	3.32	16.21	0.398	0.103	0.499	0.258	0.356
98	9.56	2.33	11.89	0.296	0.072	0.632	0.244	0.327
99	2.51	7.96	10.47	0.078	0.246	0.676	3.171	3.158
100	1.50	4.42	5.16	0.046	0.137	0.840	2.947	3.000
101	7.23	6.05	13.28	0.223	0.187	0.589	0.837	0.928
102	7.94	6.20	14.14	0.245	0.192	0.563	0.781	0.905
103	3.29	1.49	4.78	0.102	0.046	0.852	0.453	0.812
104	4.01	2.79	6.80	0.124	0.086	0.790	0.696	0.806

Table D.4: Stratified flow equilibrium holdup and slug frequency

Data No	Water Height	Oil Height	γ	Oil Fraction	Water Fraction	Air Fraction	$\frac{dp}{dz}$	Slug Frequency (Tronconi)	Slug Frequency (Stapelberg)
1	0.432	0.240	0.024	0.301	0.414	0.285	21.0	0.105	0.052
2	0.485	0.155	0.022	0.195	0.481	0.324	15.5	0.097	0.049
3	0.398	0.314	0.026	0.391	0.371	0.238	27.8	0.107	0 054
4	0.375	0.369	0.027	0.455	0.343	0.202	33.4	0.106	0.053
5	0.543	0.160	0.018	0.196	0.555	0.249	31.7	0.116	0.058
9	0.325	0.385	0.032	0.477	0.282	0.241	31.1	0.119	0.060
10	0.391	0.329	0.025	0.408	0.362	0.229	35.5	0.121	0.061
11	0.505	0.251	0.017	0.305	0.506	0.189	50.6	0.125	0.063
16	0.514	0.196	0.017	0.241	0.518	0.241	31.4	0.144	0.072
17	0.322	0.341	0.031	0.426	0.278	0.296	18.8	0.132	0.066
18	0.418	0.258	0.023	0.323	0.396	0.281	23.0	0.139	0 070
19	0.404	0.177	0.027	0.224	0.379	0.397	26.0	0.220	0.110
20	0.529	0.125	0.017	0.156	0.537	0.307	48.2	0.239	0.119
23	0.343	0.230	0.029	0.289	0.303	0.407	13.9	0.141	0.070
24	0.344	0.253	0.026	0.318	0.305	0.377	13.0	0.157	0.078
25	0.342	0.228	0.026	0.287	0.302	0.411	13.9	0.210	0.105
26	0.520	0.114	0.015	0.143	0.525	0.331	22.9	0.217	0.108
27	0.474	0.186	0.017	0.233	0.467	0.300	29.8	0.230	0.115
28	0.442	0.233	0.019	0.292	0.426	0.282	36.1	0.249	0.124
29	0.419	0.272	0.020	0.340	0.397	0.263	43.2	0 260	0 130
30	0 406	0.294	0.021	0.367	0.381	0.252	47.4	0.265	0.133
31	0.338	0.357	0.026	0.444	0.297	0.258	40.5	0.252	0.126
33	0.432	0.151	0.027	0.192	0.414	0.395	24.4	0.151	0.075
34	0.372	0.194	0.032	0.245	0.339	0.416	21.0	0.148	0.074
36	0.420	0.196	0.027	0.248	0.399	0.354	33.4	0.164	0.082
39	0.383	0.185	0.029	0.234	0.352	0.414	32.9	0.236	0.118
41	0.539	0.121	0.017	0.151	0.550	0.300	68.9	0.249	0.125
42	0.625	0.095	0.012	0.113	0.657	0.229	121.5	0.268	0 134

Data No	Water Height	Oil Height	γ	Oil Fraction	Water Fraction	Air Fraction	$\frac{dp}{dz}$	Slug Frequency (Tronconi)	Slug Frequency (Stapelberg)
43	0.591	0.144	0.013	0.173	0.615	0.212	141.0	0.274	0.137
45	0.387	0.308	0.021	0.384	0.357	0.258	35.8	0.143	0.071
46	0.515	0.220	0.014	0.269	0.519	0.212	53.4	0.149	0.074
47	0.558	0.197	0.012	0.236	0.574	0.190	64.7	0.150	0.075
48	0.635	0.160	0.009	0.183	0.670	0.147	101.0	0.158	0.079
49	0.591	0.222	0.010	0.255	0.615	0.129	119.7	0.161	0.080
51	0.516	0.242	0.015	0.293	0.520	0.187	96.1	0.195	0.097
52	0.374	0.334	0.025	0.416	0.341	0.243	47.0	0.161	0.080
53	0.439	0.275	0.021	0.341	0.423	0.236	55.8	0.173	0.086
57	0.396	0.283	0.021	0.354	0.369	0.277	66.6	0.225	0.112
59	0.543	0.194	0.013	0.235	0.555	0.210	137.6	0.267	0.133
62	0.474	0.230	0.015	0.285	0.467	0.248	37.8	0.184	0.092
63	0.480	0.228	0.014	0.282	0.475	0.243	39.2	0.187	0.094
64	0.341	0.357	0.023	0.444	0.301	0.255	29.0	0.150	0.075
65	0.349	0.354	0.023	0.440	0.311	0.249	29.5	0.144	0.072
66	0.583	0.174	0.010	0.207	0.605	0.188	73.8	0.172	0.086
67	0.533	0.251	0.011	0.299	0.542	0.159	95.1	0.172	0.086
68	0.450	0.195	0.017	0.246	0.436	0.318	16.3	0.128	0.064
69	0.439	0.234	0.015	0.293	0.423	0.284	15.9	0.120	0.060
70	0.330	0.311	0.024	0.389	0.288	0.323	19.0	0.158	0.079
71	0.328	0.304	0.025	0.381	0.285	0.334	18.5	0.165	0.083
72	0.483	0.320	0.012	0.382	0.478	0.139	78.3	0.162	0.081
73	0.482	0.249	0.015	0.306	0.477	0.217	77.9	0.202	0.101
74	0.303	0.312	0.030	0.389	0.256	0.355	22.5	0.162	0.081
75	0.412	0.217	0.023	0.274	0.389	0.338	25.3	0.162	0.081
76	0.413	0.219	0.022	0.276	0.390	0.334	25.8	0.162	0.081
77	0.413	0.288	0.020	0.359	0.390	0.251	39.4	0.180	0.090
78	0.493	0.233	0.014	0.287	0.491	0.222	55.1	0.194	0.097

Data No	Water Height	Oil Height	γ	Oil Fraction	Water Fraction	Air Fraction	$\frac{dp}{dz}$	Slug Frequency (Tronconi)	Slug Frequency (Stapelberg)
79	0.445	0.285	0.018	0.352	0.430	0.218	43.6	0.168	0.084
80	0.429	0.301	0.019	0.372	0.410	0.218	41.4	0.162	0.081
81	0.432	0.300	0.019	0.371	0.414	0.216	41.3	0.160	0.080
82	0.431	0.302	0.019	0.373	0.412	0.214	40.9	0.158	0.079
83	0.407	0.237	0.019	0.299	0.382	0.319	39.0	0.191	0.096
84	0.421	0.218	0.020	0.275	0.400	0.325	36.6	0.185	0.093
85	0.421	0.215	0.021	0.271	0.400	0.329	36.3	0.188	0.094
86	0.385	0.253	0.022	0.319	0.355	0.327	36.4	0.189	0.095
87	0.551	0.137	0.013	0.169	0.565	0.266	64.5	0.217	0.108
88	0.490	0.121	0.017	0.153	0.487	0.360	38.9	0.204	0.102
89	0.460	0.135	0.019	0.171	0.449	0.380	34.2	0.201	0.101
90	0.482	0.161	0.015	0.202	0.477	0.320	17.0	0.130	0.065
91	0.473	0.174	0.016	0.219	0.466	0.316	20.8	0.144	0.072
92	0.417	0.220	0.021	0.277	0.395	0.328	15.3	0.125	0.063
93	0.304	0.383	0.031	0.475	0.257	0.268	32.3	0.174	0.087
94	0.317	0.330	0.034	0.412	0.272	0.316	31.7	0.193	0.096
96	0.542	0.193	0.015	0.234	0.553	0.212	79.2	0.213	0.107
97	0.593	0.172	0.011	0.203	0.618	0.179	112.0	0.256	0.128
98	0.605	0.164	0.010	0.192	0.633	0.175	124.8	0.261	0.131
99	0.261	0.407	0.038	0.502	0.208	0.290	34.1	0.208	0.104
100	0.267	0.390	0.037	0.482	0.214	0.303	34.5	0.225	0.112
102	0.454	0.255	0.022	0.317	0.442	0.242	44.1	0.212	0.106
103	0.448	0.206	0.025	0.259	0.434	0.307	55.5	0.256	0.128
104	0.452	0.210	0.025	0.264	0.439	0.297	54.6	0.231	0.115
105	0.423	0.188	0.029	0.238	0.402	0.360	64.6	0.305	0.153
106	0.409	0.182	0.029	0.230	0.385	0.385	81.0	0.423	0.211
108	0.311	0 404	0.035	0.500	0.265	0.235	39.9	0.199	0.100

Table D.5: Stratified-slug transition boundaries

				Transition Liquid Velocity	
Data No	U_a	Oil Fraction	U_ℓ	Linear Stability	Kelvin Helmholtz
1	1.695	0.549	0.268	0.157	0.301
2	1.728	0.685	0.222	0.212	0.317
5	1.760	0.691	0.391	0.218	0.318
16	1.384	0.650	0.377	0.188	0.295
18	1.436	0.523	0.277	0.150	0.279
19	2.405	0.529	0.280	0.188	0.280
24	1.400	0.517	0.143	0.149	0.249
25	1.440	0.521	0.146	0.157	0.245
26	1.405	0.746	0.280	0.286	0.282
27	1.412	0.632	0.326	0.196	0.263
46	1.751	0.650	0.500	0.185	0.266
47	1.678	0.701	0.586	0.205	0.275
62	1.446	0.625	0.373	0.176	0.248
63	1.424	0.638	0.381	0.179	0.246
68	1.394	0.691	0.194	0.196	0.260
69	1.132	0.674	0.187	0.175	0.247
70	1.454	0.457	0.184	0.132	0.224
71	1.466	0.453	0.181	0.133	0.227
74	2.099	0.397	0.199	0.129	0.223
75	2.073	0.556	0.266	0.171	0.264
76	2.071	0.558	0.269	0.171	0.262
77	1.597	0.491	0.385	0.143	0.245
79	1.386	0.521	0.438	0.145	0.255
80	1.363	0.498	0.418	0.139	0.252
81	1.359	0.500	0.420	0.139	0.254
82	1.342	0.498	0.418	0.138	0.254
90	1.471	0.744	0.207	0.228	0.268
91	1.608	0.705	0.237	0.214	0.265
92	1.448	0.620	0.184	0.173	0.265
101	1.462	0.519	0.455	0.161	0.304
102	1.445	0.525	0.463	0.165	0.310

Table D.6: Pressure gradient calculations (linear liquid viscosity)

				Pressure Gradient Correlations						Effective Liquid Viscosity
Data No	Phases	$\frac{dp}{dz}$	Oil Fraction	McAdams	Schlichting	Beggs & Brill	Dukler	Friedel	Lockhart & Martinelli	
1	aow	86.2	0.451	97	107	157	256	204	105	23.2
2	aow	61.9	0.315	81	91	118	197	149	77	16.5
3	aow	162.6	0.553	116	121	198	309	242	130	28.1
4	aow	411.9	0.616	127	129	225	334	259	144	31.2
5	aow	108.8	0.309	153	147	220	346	173	112	16.2
6	aw	53.2	0.000	80	77	76	123	126	84	1.1
7	aw	156.9	0.000	172	140	189	253	279	197	1.1
8	ao	169.0	1.000	78	109	176	282	394	155	52.9
9	aow	328.6	0.675	119	134	225	350	308	158	36.1
10	aow	265.6	0.579	144	153	255	390	287	162	31.1
11	aow	151.4	0.422	204	193	321	466	241	162	23.0
12	aow	178.6	0.315	274	243	397	529	410	331	17.4
13	aow	300.5	0.213	380	331	515	573	548	455	12.2
14	aw	208.2	0.000	209	170	239	299	339	244	1.1
15	ao	78.4	1.000	41	99	103	171	332	123	52.9
16	aow	116.3	0.350	116	139	193	294	166	118	19.2

				Pressure Gradient Correlations						Effective Liquid Viscosity
Data No	Phases	$\frac{dp}{dz}$	Oil Fraction	McAdams	Schlichting	Beggs & Brill	Dukler	Friedel	Lockhart & Martinelli	
17	aow	184.0	0.620	60	92	122	197	221	111	33.2
18	aow	106.9	0.477	82	113	153	242	196	117	25.8
19	aow	125.0	0.471	113	204	214	359	260	166	25.5
20	aow	168.0	0.288	194	269	315	505	314	171	16.0
21	aw	99.5	0.000	120	170	121	199	178	160	1.1
22	ao	51.4	1.000	23	77	59	101	357	94	64.5
23	aow	50.6	0.476	52	100	100	170	228	100	30.0
24	aow	37.9	0.483	37	81	79	131	178	90	30.3
25	aow	39.5	0.479	36	100	83	138	175	100	30.2
26	aow	55.5	0.254	74	136	135	216	126	105	16.5
27	aow	72.0	0.368	87	159	177	276	179	142	23.4
28	aow	108.2	0.460	104	187	222	338	218	175	27.6
29	aow	175.2	0.525	121	213	268	397	255	206	31.4
30	aow	235.9	0.560	132	229	298	434	277	224	33.4
31	aow	400.9	0.658	104	192	251	370	288	212	39.0
32	ao	121.8	1.000	57	142	128	218	501	142	55.8

				Pressure Gradient Correlations						Effective Liquid Viscosity
Data No	Phases	$\frac{dp}{dz}$	Oil Fraction	McAdams	Schlichting	Beggs & Brill	Dukler	Friedel	Lockhart & Martinelli	
33	aow	143.2	0.410	147	191	231	392	282	149	22.4
34	aow	126.4	0.496	119	172	199	341	312	145	26.8
35	aow	152.9	0.312	199	228	289	484	246	154	17.3
36	aow	208.0	0.487	192	234	319	531	345	193	26.4
37	aow	588.0	0.584	225	254	387	625	380	221	29.7
38	aw	292.0	0.000	302	259	311	471	443	326	1.1
39	aow	196.5	0.516	161	276	302	510	361	220	29.3
40	aow	185.0	0.386	217	314	369	612	307	220	22.2
41	aow	255.9	0.274	303	370	466	748	463	439	16.1
42	aow	390.3	0.179	472	481	652	977	682	631	10.9
43	aow	430.7	0.247	520	535	764	1122	762	707	14.6
44	ao	159.5	1.000	62	109	158	255	478	170	69.0
45	aow	191.4	0.524	127	156	242	383	332	180	36.7
46	aow	174.5	0.350	199	207	328	493	267	182	25.0
47	aow	186.3	0.299	235	232	368	536	367	181	21.5
48	aow	265.0	0.215	333	302	477	633	497	418	15.8

				Pressure Gradient Correlations						Effective Liquid Viscosity
Data No	Phases	$\frac{dp}{dz}$	Oil Fraction	McAdams	Schlichting	Beggs & Brill	Dukler	Friedel	Lockhart & Martinelli	
49	aow	296.7	0.300	372	349	569	719	559	475	21.5
50	ao	247.7	1.000	109	199	275	442	506	246	58.7
51	aow	264.9	0.388	338	347	549	786	521	458	23.5
52	aow	505.9	0.614	186	219	354	543	376	227	36.5
53	aow	273.0	0.521	231	261	415	629	356	238	31.2
54	aw	134.9	0.000	155	154	156	245	232	178	1.2
55	aw	605.5	0.000	496	426	608	690	764	614	1.2
56	ao	277.1	1.000	121	228	310	510	700	295	73.5
57	aow	438.6	0.559	268	350	533	840	532	341	41.6
58	aow	370.5	0.446	347	418	626	970	455	337	31.4
59	aow	431.5	0.327	496	536	811	1193	753	703	23.4
60	aw	275.9	0.000	268	276	276	431	382	317	1.2
61	aw	406.0	0.000	378	350	410	598	546	452	1.2
62	aow	75.2	0.375	113	161	218	332	225	160	27.4
63	aow	87.2	0.362	114	163	221	335	224	162	27.3
64	aow	106.7	0.588	80	117	172	267	282	153	40.3

				Pressure Gradient Correlations						Effective Liquid Viscosity
Data No	Phases	$\frac{dp}{dz}$	Oil Fraction	McAdams	Schlichting	Beggs & Brill	Dukler	Friedel	Lockhart & Martinelli	
65	aow	108.7	0.576	83	116	175	271	282	152	39.7
66	aow	194.0	0.255	253	259	398	571	397	348	20.1
67	aow	226.4	0.362	300	308	507	687	327	252	28.1
68	aow	57.9	0.309	55	84	99	163	159	88	23.2
69	aow	54.7	0.326	45	69	86	138	149	81	25.3
70	aow	71.7	0.543	51	95	113	183	238	120	37.9
71	aow	74.5	0.547	49	98	111	180	232	119	37.1
72	aow	183.9	0.430	194	223	365	462	285	219	32.7
73	aow	247.3	0.430	279	323	510	754	397	288	32.7
74	aow	99.8	0.603	75	131	158	263	334	152	41.3
75	aow	81.6	0.444	103	152	189	312	262	147	28.3
76	aow	91.8	0.442	104	153	192	316	265	149	28.6
77	aow	142.2	0.509	126	176	253	386	283	186	33.0
78	aow	148.4	0.382	174	222	324	479	274	205	28.2
79	aow	120.4	0.479	136	175	262	384	252	176	29.7
80	aow	141.3	0.502	128	165	249	366	255	173	31.0

				Pressure Gradient Correlations						Effective Liquid Viscosity
Data No	Phases	$\frac{dp}{dz}$	Oil Fraction	McAdams	Schlichting	Beggs & Brill	Dukler	Friedel	Lockhart & Martinelli	
81	aow	145.3	0.500	129	164	249	365	253	171	30.5
82	aow	149.9	0.502	128	161	246	360	251	169	30.5
83	aow	132.3	0.455	150	217	291	476	384	220	36.2
84	aow	136.2	0.444	152	214	283	464	347	204	31.9
85	aow	124.3	0.445	152	216	283	464	344	204	31.6
86	aow	128.3	0.445	141	209	278	456	384	215	33.0
87	aow	208.8	0.502	268	317	441	687	292	230	37.2
88	aow	125.7	0.304	190	263	316	527	307	200	23.3
89	aow	125.3	0.342	167	246	286	480	316	194	25.2
90	aow	43.0	0.256	62	91	106	174	150	87	20.2
91	aow	62.1	0.295	76	111	133	218	178	106	22.3
92	aow	55.3	0.380	53	83	98	162	171	89	24.9
93	aow	388.2	0.692	98	150	216	335	309	179	40.1
94	aow	351.2	0.675	119	186	248	397	327	192	36.1
95	aow	279.8	0.333	275	315	454	664	437	412	20.4
96	aow	297.5	0.330	277	311	446	653	435	406	19.0

				Pressure Gradient Correlations						Effective Liquid Viscosity
Data No	Phases	$\frac{dp}{dz}$	Oil Fraction	McAdams	Schlichting	Beggs & Brill	Dukler	Friedel	Lockhart & Martinelli	
97	aow	275.4	0.262	330	380	533	723	521	514	17.1
98	aow	303.6	0.247	368	414	585	789	574	563	16.6
99	aow	399.7	0.759	100	172	233	365	344	202	43.7
100	aow	425.7	0.750	102	185	241	379	346	210	43.0
101	aow	133.6	0.481	139	195	257	383	199	159	22.0
102	aow	136.4	0.475	140	197	257	381	190	156	20.9
103	aow	210.7	0.448	222	313	382	612	261	210	20.0
104	aow	202.9	0.446	228	298	380	608	261	202	19.8
105	aow	362.9	0.461	288	432	489	806	327	263	20.2
106	aow	701.0	0.473	325	582	587	971	355	326	20.6
107	ao	204.3	1.000	82	123	198	289	305	166	47.6
108	aow	483.8	0.739	136	191	288	420	296	199	35.5
109	aow	257.4	0.569	187	245	358	511	271	211	27.9
110	aow	545.7	0.691	278	353	552	716	364	295	34.4
111	aw	105.7	0.000	107	120	113	171	167	144	1.1
112	aw	262.3	0.000	236	231	274	352	366	322	1.1

Table D.7: Pressure gradient calculations (Brinkman liquid viscosity)

				Pressure Gradient Correlations						Effective Liquid Viscosity
Data No	Phases	$\frac{dp}{dz}$	Oil Fraction	McAdams	Schlichting	Beggs & Brill	Dukler	Friedel	Lockhart & Martinelli	
1	aow	86.2	0.451	92	89	104	172	137	98	4.9
2	aow	61.9	0.315	74	76	76	127	112	78	2.8
3	aow	162.6	0.553	110	103	140	223	167	122	8.2
4	aow	411.9	0.616	130	169	416	536	1097	545	167.8
5	aow	108.8	0.309	134	117	142	224	197	141	2.8
6	aw	53.2	0.000	80	77	76	123	126	84	1.1
7	aw	156.9	0.000	172	140	189	253	279	197	1.1
8	ao	169.0	1.000	78	109	176	282	394	155	52.9
9	aow	328.6	0.675	121	163	366	513	984	447	141.5
10	aow	265.6	0.579	138	130	183	287	207	156	9.7
11	aow	151.4	0.422	180	150	209	306	261	192	4.4
12	aow	178.6	0.315	220	178	253	339	326	240	2.9
13	aow	300.5	0.213	275	231	335	371	418	320	2.0
14	aw	208.2	0.000	209	170	239	299	339	244	1.1
15	ao	78.4	1.000	41	99	103	171	332	123	52.9
16	aow	116.3	0.350	105	110	122	188	160	133	3.3

				Pressure Gradient Correlations						Effective Liquid Viscosity
Data No	Phases	$\frac{dp}{dz}$	Oil Fraction	McAdams	Schlichting	Beggs & Brill	Dukler	Friedel	Lockhart & Martinelli	
17	aow	184.0	0.620	60	111	229	316	902	376	175.0
18	aow	106.9	0.477	79	95	101	163	124	105	5.6
19	aow	125.0	0.471	110	179	145	243	170	162	5.5
20	aow	168.0	0.288	179	222	205	326	260	241	2.6
21	aw	99.5	0.000	120	170	121	199	178	160	1.1
22	ao	51.4	1.000	23	77	59	101	357	94	64.5
23	aow	50.6	0.476	51	89	65	113	60	39	6.0
24	aow	37.9	0.483	36	72	50	86	47	35	6.2
25	aow	39.5	0.479	36	89	53	91	46	39	6.1
26	aow	55.5	0.254	69	113	84	134	111	116	2.5
27	aow	72.0	0.368	83	130	109	173	134	141	3.8
28	aow	108.2	0.460	100	154	143	221	162	173	5.4
29	aow	175.2	0.525	117	177	179	272	191	206	7.5
30	aow	235.9	0.560	129	193	205	307	210	227	9.1
31	aow	400.9	0.658	105	234	432	560	1024	632	167.0
32	ao	121.8	1.000	57	142	128	218	501	142	55.8

				Pressure Gradient Correlations						Effective Liquid Viscosity
Data No	Phases	$\frac{dp}{dz}$	Oil Fraction	McAdams	Schlichting	Beggs & Brill	Dukler	Friedel	Lockhart & Martinelli	
33	aow	143.2	0.410	140	166	154	261	199	150	4.2
34	aow	126.4	0.496	116	154	138	237	171	130	6.2
35	aow	152.9	0.312	183	192	191	317	255	191	2.8
36	aow	208.0	0.487	185	202	219	367	262	203	5.9
37	aow	588.0	0.584	228	323	717	1040	1813	856	191.8
38	aw	292.0	0.000	302	259	139	311	471	315	1.1
39	aow	196.5	0.516	157	245	210	356	236	217	7.0
40	aow	185.0	0.386	206	266	243	401	293	262	3.8
41	aow	255.9	0.274	274	303	306	485	382	334	2.5
42	aow	390.3	0.179	399	380	444	656	558	477	1.9
43	aow	430.7	0.247	443	413	505	733	613	526	2.3
44	ao	159.5	1.000	62	109	158	255	478	170	69.0
45	aow	191.4	0.524	122	130	158	257	184	146	8.0
46	aow	174.5	0.350	176	158	200	304	256	197	3.7
47	aow	186.3	0.299	200	172	225	329	292	223	3.0
48	aow	265.0	0.215	261	217	299	396	387	297	2.3

				Pressure Gradient Correlations						Effective Liquid Viscosity
Data No	Phases	$\frac{dp}{dz}$	Oil Fraction	McAdams	Schlichting	Beggs & Brill	Dukler	Friedel	Lockhart & Martinelli	
49	aow	296.7	0.300	294	245	348	442	428	332	3.0
50	ao	247.7	1.000	109	199	275	442	506	246	58.7
51	aow	264.9	0.388	297	264	352	507	420	340	4.0
52	aow	505.9	0.614	188	280	645	870	1598	827	198.7
53	aow	273.0	0.521	218	214	282	435	317	260	7.4
54	aw	134.9	0.000	155	154	156	245	232	178	1.2
55	aw	605.5	0.000	496	426	608	690	764	614	1.2
56	ao	277.1	1.000	121	228	310	510	700	295	73.5
57	aow	438.6	0.559	260	294	362	581	380	332	9.9
58	aow	370.5	0.446	325	334	403	628	454	394	5.4
59	aow	431.5	0.327	436	406	511	750	599	513	3.4
60	aw	275.9	0.000	268	276	276	431	382	317	1.2
61	aw	406.0	0.000	378	350	410	598	546	452	1.2
62	aow	75.2	0.375	105	127	131	203	162	148	4.1
63	aow	87.2	0.362	106	128	132	203	164	150	3.9
64	aow	106.7	0.588	78	101	118	190	96	66	11.4

				Pressure Gradient Correlations						Effective Liquid Viscosity
Data No	Phases	$\frac{dp}{dz}$	Oil Fraction	McAdams	Schlichting	Beggs & Brill	Dukler	Friedel	Lockhart & Martinelli	
65	aow	108.7	0.576	81	99	118	190	91	63	10.6
66	aow	194.0	0.255	213	191	242	348	312	249	2.7
67	aow	226.4	0.362	256	223	306	420	368	294	4.0
68	aow	57.9	0.309	52	70	59	98	83	69	1.8
69	aow	54.7	0.326	43	56	50	82	70	58	1.9
70	aow	71.7	0.543	50	84	74	124	70	48	2.7
71	aow	74.5	0.547	49	86	73	123	70	49	2.7
72	aow	183.9	0.430	171	162	218	286	253	213	2.2
73	aow	247.3	0.430	256	249	316	475	366	308	2.2
74	aow	99.8	0.603	74	119	112	191	123	72	12.5
75	aow	81.6	0.444	99	129	121	203	151	127	5.2
76	aow	91.8	0.442	100	130	123	205	152	128	5.2
77	aow	142.2	0.509	121	145	165	259	188	168	7.2
78	aow	148.4	0.382	159	171	196	295	237	210	4.2
79	aow	120.4	0.479	128	140	169	253	196	172	6.1
80	aow	141.3	0.502	121	133	163	245	187	162	6.8

				Pressure Gradient Correlations						Effective Liquid Viscosity
Data No	Phases	$\frac{dp}{dz}$	Oil Fraction	McAdams	Schlichting	Beggs & Brill	Dukler	Friedel	Lockhart & Martinelli	
81	aow	145.3	0.500	122	132	162	245	187	162	6.6
82	aow	149.9	0.502	121	130	161	242	185	160	6.7
83	aow	132.3	0.455	144	181	181	301	214	183	6.0
84	aow	136.2	0.444	146	179	179	297	215	182	5.4
85	aow	124.3	0.445	146	182	180	298	215	183	5.4
86	aow	128.3	0.445	137	178	180	300	207	178	5.5
87	aow	208.8	0.502	240	249	273	424	341	292	7.3
88	aow	125.7	0.304	178	219	197	327	252	211	3.2
89	aow	125.3	0.342	158	209	179	300	227	191	3.6
90	aow	43.0	0.256	58	75	63	105	90	74	2.7
91	aow	62.1	0.295	71	91	80	132	110	92	3.0
92	aow	55.3	0.380	51	70	60	101	82	67	4.0
93	aow	388.2	0.692	99	177	344	480	922	461	144.4
94	aow	351.2	0.675	119	219	397	581	1038	509	141.4
95	aow	279.8	0.333	244	242	288	422	351	305	3.2
96	aow	297.5	0.330	244	240	287	419	351	303	3.1

				Pressure Gradient Correlations						Effective Liquid Viscosity
Data No	Phases	$\frac{dp}{dz}$	Oil Fraction	McAdams	Schlichting	Beggs & Brill	Dukler	Friedel	Lockhart & Martinelli	
97	aow	275.4	0.262	280	283	337	456	407	373	2.6
98	aow	303.6	0.247	309	306	371	497	447	407	2.5
99	aow	399.7	0.759	100	193	326	477	776	401	113.8
100	aow	425.7	0.750	102	208	342	502	810	427	117.0
101	aow	133.6	0.481	132	161	176	266	203	193	5.3
102	aow	136.4	0.475	132	164	177	265	204	197	5.1
103	aow	210.7	0.448	212	266	265	425	307	288	4.5
104	aow	202.9	0.446	216	252	264	422	310	277	4.5
105	aow	362.9	0.461	278	378	348	571	391	370	4.7
106	aow	701.0	0.473	316	514	422	694	450	481	5.0
107	ao	204.3	1.000	82	123	198	289	305	166	47.6
108	aow	483.8	0.739	138	224	414	564	736	439	101.3
109	aow	257.4	0.569	179	207	260	378	274	256	8.8
110	aow	545.7	0.691	283	444	859	1022	1142	821	124.4
111	aw	105.7	0.000	107	120	113	171	167	144	1.1
112	aw	262.3	0.000	236	231	274	352	366	322	1.1